Pyroxene and olivine chemistry as an indicator of melt evolution. A contribution to the understanding of Somma-Vesuvius eruptive behaviour

by

Daniele Redi

B.Sc & Second Level Italian Degree at University of Siena

University of Naples "Federico II"

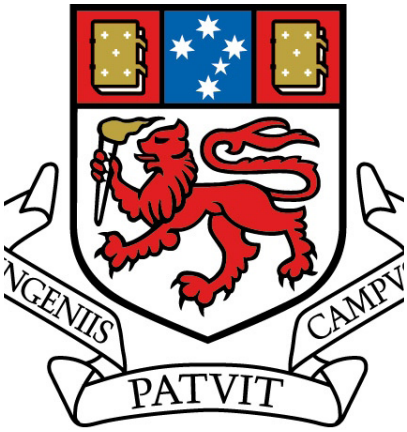

University of Tasmania

Submitted in fulfilment of the requirements for the degree of

Doctor of Philosophy

March, 2014

Declaration

This thesis contains no material which has been accepted for the award of any other degree or diploma in any tertiary institution and to the best of my knowledge and belief, contains no material previously published or written by another person, except where due acknowledgement is made in the text of the thesis.

_____ Daniele Redi

10th March 2014

Access Authority

This thesis may be made available for loan and limited copying in accordance with the Copyright Act, 1968.

_____ Daniele Redi

10th March 2014

Acknowledgements

During this long process called “PhD”, I have experienced a long series of “ups” and “downs”. It has not been easy managing the scientific expectations as well as the bureaucracy which two Universities require. At the same time, I found quite hard leaving my beloved Tuscany to live first in a different city in Italy (Naples) and after in a different continent (Australia) for the last four years.

During this roller coaster of experiences, some people within the University had played a key role to motivate me and keep me on “track” and they must be thanked. First of all, I am infinitely thankful to both my Italian supervisors the Professors Annamaria Lima and Benedetto De Vivo with who I started this amazing project on Mt. Somma-Vesuvius in 2010 at the University of Naples. I loved the Professor De Vivo’s energetic attitude and the constructive comments and feedback on the thesis which both of them carefully gave me.

I feel also very lucky that along the path I met and worked with the Professor Leonid Danyushevsky who has been my supervisor at the University of Tasmania for the past three years. I am a big believer that in our life we meet the people from whom we were meant to learn something. You are a brilliant scientist and a good man. I appreciated all the help you gave me, your efforts to improve my scientific skills and to shape my character as well as the patience with which you dealt with me and my “drama queen” personality.

I want also deeply thank all the lab stuff, Dr Sandrin Feig, Dr Karsten Goemann, Ms Sarah Gilbert and Mr Jay Thompson from the University of Tasmania for the massive help they gave me in analysing my samples at the EMP and LA-ICPMS facilities. I especially appreciated the company of Sarah and Jay. Your work attitude and your friendship have been really important and it mean a lot to me.

Many other people among academic and non-academic stuff gave me their attention and precious support during this long journey which I will never forget. These people are: Davide Ianniello, Dr Angela Doherty, Carmela Rezza, Dr. Stefano Albanese, Dr Maja Radivojevic, Tim Williamson, Hannah Johnson, Dr Jeff Steadman, Dr Anita Parbhakar-Fox, Mr JianXiang Guan, Courtney Cocks, Ashley Hanke (all my love is with you), Brielle Mason (and all the Mason family, you are such great people), Amy Dart (and all the Dart family, I love you infinitely), Skye Hamilton (whose creative personality enriched my life), Dr Anthony Brown (one of my best friends and confidant in Australia), Nawin Jinangoen (whose cookery delighted my palate and boost my work), and last but not least Minh Vo (whose infinite patience, support and yummy food kept me warm and fed).

I cannot finish this section without expressing my most deeply gratitude for all the love, time,

logistic support and motivation I received from my family (mamma, babbo e Tiziano). Vi voglio bene con tutto il mio cuore. Sono stato lontano ma ne valeva la pena e vi ringrazio per tutto il supporto che mi avete dato in tutti questi anni e durante questa esperienza.
Lastly, I have to say a big thank to a special person Ms Renée Brémond without whom I could never reached this goal; six years ago when I came to France you simply changed and I believe saved my life forever (tu a changé ma vie pour toujours).

Abstract

Explosive volcanism is commonly related to a process known as fragmentation of magma containing bubbles rich in gas phases. This process is activated by the brittle failure of the melt as its strength is overcame by viscous stresses related to bubble growth and ascending magma flow. Individual volcanoes often produce alternating effusive and explosive eruptions which cyclical dynamics remain unclear and are a subject of ongoing debate.

The Somma-Vesuvius, famous for its explosive Pompeii eruption in AD 79, generated a wide variety of eruptive events during the past 33 Ky, ranging from mild effusive (inter-Plinian) eruptions to highly disruptive (Plinian) phenomena. Over the last 3 decades, a large number of samples have been collected from the Somma-Vesuvius volcanic complex. As a result of this research effort, a large database of chemical analyses of various volcanic products from lavas to pumices and tephra is currently available. This allowed for detailed studies of magma compositions aimed at reconstructing magma differentiation processes and identifying parental and primary magma compositions. Currently there is no general consensus on whether the primary magma precursors to both eruption styles were of a similar composition.

At the same time, the compositions of mineral phases in Somma-Vesuvius volcanic products have received significantly less attention. Phenocrysts phases such as olivine and clinopyroxene occur early on the liquid line of descent and dominate fractional crystallization in the primitive magmas. At the later stages of crystallisation they are joined and/or replaced by feldspars, feldspathoids, biotite and oxides. This project aims at characterising minor and trace elements in both olivine and clinopyroxene phenocrysts from representative lava, scoriae and pumice samples from the main Plinian eruptions and a range of inter-Plinian events over the last 33 Ky. The main aim of this work is to present new constraints on the factors leading to the different Somma-Vesuvius eruptive styles.

In order to achieve this goal, 14 pumice samples from Plinian pyroclastic deposits as well as 3 scoriae and 8 lava samples from effusive flows were collected, and a representative number of olivine and clinopyroxene phenocrysts were selected under an optical microscope from each sample and analysed with an electronic microprobe and by a LA-ICP mass-spectrometry, resulting in a large database containing 2127 EMP and 1259 LA-ICP-MS analyses.

The mineral compositions obtained were examined considering the following two factors: 1) eruptive style; and 2) age of the samples. Magmas from Plinian and inter-Plinian eruptions were compared using the results of this study in conjunction with published data on lava chemistry and the compositions of melt and fluid inclusions in phenocrysts. Further, the mineral compositions have been compared with those from other volcanoes of the Roman Comagmatic

Province (RCP) and also from other tectonic settings such as Oceanic Islands, Volcanic Rifts, Mid-ocean Ridges and Supra-subduction Zones, in order to assess the extent of compositional variation among Somma-Vesuvius olivine and pyroxene phenocrysts.

The above approach led to the following main conclusions:

I) olivine and clinopyroxene phenocrysts crystallized simultaneously over a large temperature range from the earliest stages of melt evolution;

II) both olivines and clinopyroxenes display clear bimodal distribution in terms of the proportions between the Mg-rich and Fe-rich end members (Mg# = Mg/(Mg+Fe)): the primitive group has compositions $Mg\#_{92\text{-}82}$, whereas the evolved group has compositions $Mg\#_{82\text{-}72}$;

III) both Plinian and inter-Plinian clinopyroxenes and olivines populations exhibit a narrow trend of major, minor and trace elements contents as a function of their Mg#, when compared with mineral compositions from other tectonic settings, including the RCP, indicating a narrow range of melt compositions within the Somma-Vesuvius plumbing system for a given stage of differentiation regardless of the eruption style;

IV) clinopyroxene and olivine phenocrysts compositions in inter-Plinian eruption products display a narrower range compared to the Plinian eruptions;

V) as the result of a narrow compositional range of phenocrysts in inter-Plinian eruptions, there is a larger difference in phenocryst composition populations between individual inter-Plinian eruptions than between Plinian eruptions;

VI) The more evolved ($Mg\#_{82\text{-}72}$) Plinian and inter-Plinian clinopyroxene phenocrysts in rocks younger than 2.8 Ka show clear Ca enrichment (23.5-24.5 wt % CaO) in respect to the older rocks. Some of the more primitive olivine phenocrysts ($Fo\#_{92\text{-}82}$) from the inter-Plinian eruptions younger than AD 472 (CaO 0.30-0.45 wt %) are also more enriched in Ca than older olivine phenocrysts;

VII) Overall, the compositions of clinopyroxenes from the inter-Plinian eruptions display REE contents which are within the range of the Plinian clinopyroxenes.

The above results suggest:

I) a prevalently magmatic origin of olivine phenocrysts whose presence was previously mainly ascribed to magma reaction with the carbonate basement of the Campania Plain;

II) Persisting multiple sites of crystallisation where magmas of variable extent of fractionation

reside at any given time regardless of the type of eruptive activity;

III) Chemically similar sources of parental magmas feeding the Somma-Vesuvius system, which does not appear to have changed over the last 33 Ky; and

IV) A common composition of parental magmas for the Plinian and inter-Plinian eruptions of the Somma-Vesuvius.

Therefore, this study suggests that the magma residence times and the magma supply rate are the likely main factors controlling eruption style at Somma-Vesuvius. Further insights into these processes may be derived from the study of melt and fluid inclusions within the Somma-Vesuvius olivine and clinopyroxene phenocrysts, which is envisaged as a continuation to this project.

Table of Contents

Chapter 1: Introduction

Chapter 2: Regional Geology; parentage of the Italian Volcanism

Chapter 3: Somma-Vesuvius

Chapter 4: Sampling & Laboratory

Chapter 5: Clinopyroxenes Mineralogy at Somma-Vesuvius

Chapter 6: Olivines Mineralogy at Somma-Vesuvius

Chapter 7: Summary and conclusions

List of Figures

List of Tables

To Maja Radivojevic and her Balkan say
"we do not have any other way out we must win"

Through me the way is to the city dolent;
through me the way is to the eternal dole;
through me the way among the people lost.

Canto III
Inferno
Dante

Chapter 1: Introduction

1.1 Somma-Vesuvius

The Somma-Vesuvius volcano receives ongoing attention of the world-wide scientific community due to both geological and historical reasons.

As the result, Somma-Vesuvius is one of the most studied volcanoes in the world. It is best known for its historical eruption in AD 79 that led to destruction of three Roman settlements, Pompeii, Herculaneum and Stabiae as also documented by Pliny the Younger, a Roman senator who provided a detailed description of this eruption (Sigurdsson et al., 1982). Since then, the monitoring of the volcano continued during the centuries up to Lord Hamilton's systematic observation in 1766-1794, the world's first volcano observatory establishment in 1845 and Palmieri's seismographic monitoring of the 1872 eruption (Siebert et al., 2010).

There are several important features of Somma-Vesuvius: 1) its volcanic history marked by alternation of different eruptive styles, from Vulcanian to Plinian, over a period of approximately 33 Ky; 2) it is located within the Campania Plain, a sector of a tectonically complex area in Southern Italy; 3) it erupts silica under-saturated ultra potassic magma which are similar to other volcanoes of the Comagmatic Roman Province; and 3) the origin of parental magmas is a matter of ongoing debate (e.g. De Vivo et al., 2010). Another reason the volcano attracts significant attention is that there is a high population density in its proximity; currently, there are approximately 675,000 people living within 10 km from the volcano, and around 2 million within 20 km. Earthquakes, fall-out of pumices, lava flows, pyroclastic flows and nuées ardentes are only some of the volcanic hazards the population of Naples metropolitan areas would face if a Plinian eruption similar to the AD 79 even were to occur. Volcanic hazards in the area are compounded by its proximity to the Campi Flegrei volcanic field which occupies the north-western part of the city and whose activity led to the formation of pyroclastic deposits, as the widespread Neapolitan Yellow Tuff (~15 Ka), and different monogenic volcanoes as Monte Nuovo in A.D. 1538 (De Vivo et al., 2010). Furthermore, the Somma-Vesuvius is currently in an unusual state of dormancy since last eruption occurred in March 1944. Prior to that eruption, the volcano was continuously active for the last 300 years with a maximum repose time of 30 years between low-intensity Vulcanian eruptions (Rolandi et al., 1998). This current repose time of nearly 70 years opened a debate whether this is the end of the current magmatic cycle or the beginning of a much longer repose time. Such long repose times in the past always led in a high-intensity Plinian eruption, marking the start of a new magmatic cycle. The present

research project aims at providing new mineralogical constraints on the causes of the alternating effusive/explosive (Vulcanian/Plinian) behaviour of the volcano during the last 33 Ky.

1.2 Aim of the project

The main aim of this project is to provide new constraints on the possible causes of the various types of eruptive phenomena at Somma-Vesuvius.

The principal "modus operandi" of the volcano is a continuous series of Vulcanian and Strombolian events periodically alternating with single highly-disruptive Plinian eruptions, which are preceded by repose times of variable lengths (Rolandi et al., 1998; Santacroce et al., 2008). This range of eruptive styles is accompanied by different degrees of magmatic evolution. Distinctive compositions typify inter-Plinian from Plinian volcanic rocks as remarked by several studies (e.g., Ayuso et al., 1998; Joron et al., 1987; Paone, 2006), however a similar parental magma is assumed for both eruptive styles.

It is suggested that inter-Plinian eruptions operate as an "open conduit system" with an almost steady magma supply and related quiet effusive phenomena, whereas Plinian eruptions operate as an "obstruct conduit system" (Cioni et al., 1998; Lima et al., 2003) characterized by catastrophic reopening of the volcanic chimney and the beginning of a new magmatic cycle (Rolandi et al., 1998). This model implies that a different rate of magma supply and different magma residence times are the main factors controlling the eruptive behaviour of Somma-Vesuvius, rather than parental magma volatile contents as suggested by Webster et al. (2001).

In light of the above, a detailed study of major and trace elements compositions of phenocrysts aimed at constraining the chemistry of parental magmas is important for a better understanding of Somma-Vesuvius eruptive behaviour. If the composition of parental magmas is similar for Plinian and inter-Plinian eruptions, this would suggest that the different eruptive styles reflect magma supply rates and residence times instead of a different volatile content.

Chemistry of clinopyroxene and olivine phenocrysts in the Somma-Vesuvius volcanic products formed over the last 33 Ky is the focus of this study, as these minerals form early during evolution of the parental magmas of Somma-Vesuvius. It has been demonstrated that clinopyroxene and olivine compositions can be used to infer the compositions of the melt from which they crystallised (e.g., Barberi et al., 1971; Cameron and Papike, 1980; Le Bas, 1962; Leterrier et al., 1982; Nisbet and Pearce, 1977; Simkin and Smith, 1970; Thompson, 1973). Currently, the composition of Somma-Vesuvius clinopyroxenes and olivines are not well-constrained. Previous work on these phases (Barberi et al., 1981; Cioni et al., 1998; Cundari and Salviulo, 1987; Joron et al., 1987; Rahman, 1975; Trigila and De Benedetti, 1993) focused on major elements chemistry only, and covered narrow time intervals. The data obtained here will also be

used to provide further constraints on the compositions of parental magmas, magma evolution processes and magmatic plumbing system, which are a matter of debate (Piochi et al., 2006b).

1.3 Thesis structure

Chapter 2 consists of two parts. The first part presents the Western Mediterranean regional geology focusing on the Tyrrhenian Sea and the Italian Peninsula southern part, where Somma-Vesuvius is located. The second part is an overview on the Italian Quaternary magmatism with emphasis on the Roman Comagmatic Province and its genesis.

Chapter 3 describes the volcanic history, petro-chemistry and hazards at Somma-Vesuvius.

Chapter 4 is a report of the field work, sample preparation and analytical techniques.

Chapter 5 focuses on texture and major and trace elements chemistry of clinopyroxene phenocrysts from Somma-Vesuvius. A comparison is made to the compositions of clinopyroxenes from volcanic rocks erupted in other tectonic settings.

Chapter 6 describes texture and major/trace elements chemistry of olivine phenocrysts from Somma-Vesuvius. These are also compared to the compositions of olivines from other tectonic settings.

Chapter 7 presents the major conclusions of the project comparing magma compositions between Plinian and inter-Plinian eruptions using the results of this study and published data on lava chemistry.

Chapter 2: Regional Geology; parentage of the Italian Volcanism

2.1 Introduction

It is widely accepted that the present Mediterranean geological setting reflects subduction of the European-Asiatic plate beneath Africa (Rehault et al., 1984) during the final stage of a continent-continent collision as remarked by Cavazza et al. (2004). Since late Cretaceous, the northward motion of the African plate led to a progressive contraction of the Tethys ocean resulting in the Alpine orogeny (Schmid et al., 2004), associated localised extensional regimes within the main Africa-Eurasia collision zone (Dilek, 2006) and Tertiary-Quaternary magmatism (Wilson and Bianchini, 1999).The geological setting in this region is quite complex, leading to a range of geodynamic models (Carminati et al., 2012 and references therein; Turco and Schettino, 2011). The current Mediterranean structure is a by-product of regional interactions among major and minor tectonic plates whose number and geometry are still a matter of debate. Along the Italian peninsula, compressional and extensional regimes coexisted in time and space and have been accompanied by diverse volcanic activity since Oligocene (Peccerillo, 2003). The Italian Quaternary volcanism occurred both offshore and inland. Its chemistry varies from sub-alkaline tholeiitic and calcoalkaline to Na and K-alkaline and ultra-alkaline and also from mafic to sialic and from silica under-saturated to over-saturated (Peccerillo, 2003). This variable chemistry reflects this region's complex tectonics.This chapter presents an overview of the Central Western Mediterranean (CWM) geology and major Southern-Italian tectonic lineaments, followed by a description of the Italian magmatism focussed on the Roman Comagmatic Province.

2.2 Central-Western Mediterranean

2.2.1 Present-day geological lineaments

The Central-Western Mediterranean (CWM) has mostly developed in the last ~ 40 Myr. It is composed of several minor marine basins: Alboran, Algerian, Valencia, Ligure-Provencal, Tyrrhenian, Adriatic and Ionian (fig. 2.1). The age of the first 5 basins is progressively younger toward the east, whereas the Ionian and Adriatic basins are older, having formed in the Mesozoic (Bosellini, 2002; Catalano et al., 2001). All these intra-basins are differently floored, the Ligure-Provencal and Tyrrhenian basins are composed by thinned continental lithosphere and by patches of new oceanic crust (Sartori et al., 2004), the Alboran basin only by thinned continental lithosphere, while the Adriatic basin lies on thick continental lithosphere and the

Ionian basin is an unconsumed remnant of the Tethyan oceanic crust.

Nearly continuous roughly contemporaneous orogenic fold and thrust belts (Betics, Pyrenees, Alps, Dinarides, Hellenides, Apennines and Sahara Atlas) with related foreland and back-arc basins border these marine domains (Turco and Schettino, 2011). These orogenic belts are part of the Alpine Orogeny formed during the closure of the Tethys Ocean, based on the evidence from ophiolites nappes within Alps and Dinarides (Schmid et al., 2008). However, the belts differ in polarity, subduction direction, strain and stress fields, as well as age, representing different cycles within the Alpine Orogeny (Cavazza et al., 2004).

Several tomographic and seismic studies provided a more detailed view of the Mediterranean upper mantle, whereas geodetic studies allow precise estimates of the field strain acting at the lithospheric level (e.g., Agostinetti and Amato, 2009; Amato et al., 1993; Giacomuzzi et al., 2011; Grad and Tiira, 2009; Piromallo and Morelli, 2003; Serretti and Morelli, 2011; Spakman and Wortel, 2004). The depth of Moho defines three distinct domains within the CWM (e.g., Agostinetti and Amato, 2009; Amato et al., 1993; Calvert et al., 2000; Di Stefano et al., 2011; Giacomuzzi et al., 2011; Grad and Tiira, 2009; Tiberi et al., 2001) and is 40-45 km under the Alps-Dinarides-Hellenides system and the Pyrenees, approximately 25-30 km below the Adriatic Sea, Italy, Sicily, Sardinia and Corsica, down to 10-20 km under the Algero-Provencal and Tyrrhenian basins.

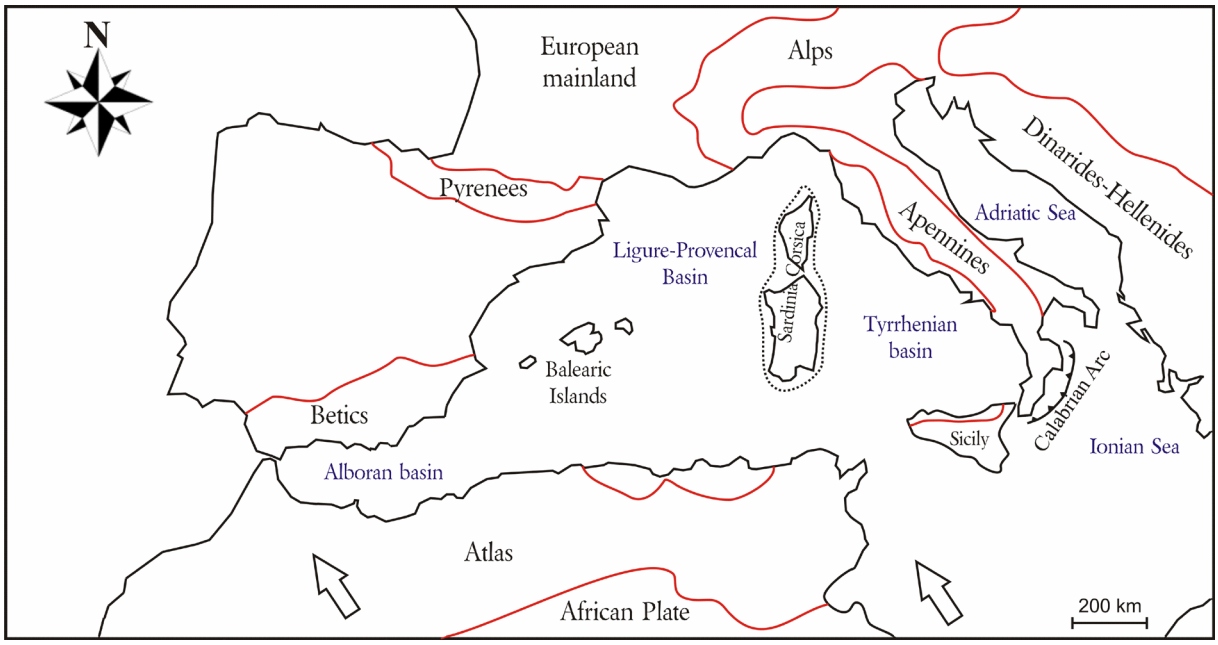

Figure 2.1 General geological lineaments of the CWM. Red lines indicate the main orogenic belts of this area. Two black arrows indicate the contemporary African Plate motion direction.

2.2.2 Geodynamic evolution

Since the early kinematic models of Smith (1971) and Dewey et al. (1973) which emphasised the role of the opening of the Atlantic Ocean as the cause of the Africa-Europe collision, several other models have been proposed in order to explain the evolution of the CWM. One of the most controversial topics about the CWM evolution is the westward extension of the Alpine belt. Alvarez (1976) supported the theory that the Western Alps crossed over Corsica, Calabria, Kabylies and Betic Cordillera. This model implied the presence of a pre-existing micro-continent (Calabria-Kabylies) which divided the Tethys Ocean in two parts, one of which was consumed by the Alpine collision, whereas the other by the Apennine orogeny. Later, this idea was supported by some (e.g., Handy et al., 2010) but rejected by others (e.g., Stampfli and Borel, 2002; Turco and Schettino, 2011). A large number of published geodynamic models of the Mediterranean over the last 3 decades (e.g., Dewey et al., 1989; Rehault et al., 1984; Rosenbaum et al., 2002; Schmid et al., 2008; Wortel and Spakman, 2000), makes it difficult to offering a succinct overview of the CWM evolution. However, the majority of these models agree on some aspects of the Tertiary CWM evolution as follow:

a) the Alpine orogeny was caused by the African tectonic plate motion towards Europe, NE-NEE directed until Eocene (52-37 Myr) and NW-NNW directed from Eocene until present (Dewey et al., 1989; Rosenbaum et al., 2002).

b) The Ligure-Provencal and Tyrrhenian basins formed as a consequence of crustal thinning. In the former, the extension occurred during late Oligocene (30 Myr), whereas the later formed during Miocene (20-17 Myr; Carminati et al., 1998a; Séranne, 1999).

c) The Corsica-Sardinia-Calabria block was part of the European plate. It was progressively detached during rifting that formed the Ligure-Provencal basin, starting at ~ 23 Ma and rotating by 30-35 degrees counter clockwise by ~ 18 Ma (Edel et al., 2001; Edel et al., 1981; Turco et al., 2006).

d) The Tyrrhenian opening started during Miocene (Rosenbaum and Lister, 2004) and culminated with the formation of two mini oceanic plateaus, Vavilov (4.3-2.6 Myr) and Marsili (ca. 1-0.1 Myr).

e) The Calabria accretionary wedge originally linked to the Sardinia-Corsica continental block, progressively migrated towards E-SE colliding with the Apulia micro-plate during the Tyrrhenian basin opening (Gasparini et al., 1982).

f) Throughout Eocene (52-37 Myr) the collisional system in the western Mediterranean involved Mesozoic Tethyan oceanic crust; the subduction system progressively moved towards south-west and is currently directed NW in the Ionian basin-Calabria Arc region (Cocchi et al., 2008 and references therein).

g) The Apulia plate, also known as Adria Plate, is broadly considered as the northern extremity of the African plate (Channell et al., 1979; Oldow et al., 2002; Stampfli et al., 1998; Wortmann et al., 2001), although many authors interpreted the Adriatic plate as a disjointed microplate, a remnant of the Liguride-Piedmontese Ocean between Cretaceous and Palaeocene (~135-55 Myr). Many authors claimed the existence of an Adriatic slab subducting beneath the Italian mainland; its existence is assumed from tomographic seismic studies (Di Stefano et al., 2011; Piromallo and Morelli, 2003; Wortel and Spakman, 2000) even if deep sited earthquakes have not been verified under the Apennine belt.

h) Igneous activity within CWM occurs at the edges of the various marine basins and is linked to the compressive orogenic and extensional regimes which alternate in time and space (Carminati et al., 2012; Lustrino et al., 2011; Wilson and Bianchini, 1999).

The causes of the extensions regime acting within the CWM are still a matter of debate, mostly concerning subduction polarity among the Adriatic-African and Eurasia plates. Zeck (1999) and others explained the existence of such extensional domains as a continuous westward directed subduction regime which progressively migrated eastward as a consequence of the Ligure-Provencal and Tyrrhenian basins formation. Their origin was attributed to a fast lithosphere uplift triggered by slab break off and sinking. More recently, Carminati et al. (2012), Spakman and Wortel (2004) and Rosenbaum et al. (2002) have developed a model in which the initial subduction direction is assumed eastward and the slab detachment with its sinking dragged down the dextral lithospheric slab causing subduction direction inversion from eastward to westward, which is still ongoing.
As the subduction system was migrating east and south-east towards its current position, different types of magmatism occurred in several locations, including the Betics (Spain), south-east coast of France, Corsica-Sardinia block, south-east Tyrrhenian, and along the western side of Italy; all these localities are characterized by volcanic rocks with different geochemical characteristics (e.g., Lustrino et al., 2011; Wilson and Bianchini, 1999).

2.3 Italian Peninsula and surrounding areas

2.3.1 Tectonic setting

In the last two decades the geological setting of the Italian mainland and surrounding basins (Tyrrhenian, Adriatic and Ionian) have been investigated mainly through regional teleseismic and tomographic studies. It is now broadly accepted that crustal thickness is variable beneath Italy. Agostinetti and Amato (2009) and Di Stefano et al. (2011) recognized different crustal regions from west to east (Fig. 2.2): the Tyrrhenian basin is underlined by a Moho located at 20- 25 km depth in the northern part and 10-20 km depth in the south-east sector with a minimum thickness at Vavilov and Marsili; proceeding toward east depth increases to 25-30 km under Italy's west coast, and 30-40 km further east. The Moho is located at 30-35 km below the Adria plate and Ionian basin. Chiarabba et al. (2005) reviewed the Italian seismicity for the last 20 years and argued for a continuous upper-crustal seismicity: under the Northern Apennines and in the South within the Calabrian Arc characterized by a Benioff zone dipping NW at an angle of 70º. The current geological setting of the Italian Peninsula is controlled by the Tyrrhenian basin opening during Miocene and migration of the Eurasia-African collision towards E/SE. The formation of new oceanic crust at Vavilov and Marsili is related to a more intense extension of the South-eastern Tyrrhenian (Rehault et al., 1987; Sartori et al., 2004; Trincardi and Zitellini, 1987). This major stretching is related to the Calabrian wedge progressive movement from the actual Sardinia-Corsica position towards SE where it encountered less resistance as a consequence of the oceanic Ionian Slab ongoing subduction (Vitale and Ciarcia, 2013). The Apennine chain formation is generally attributed to the Tyrrhenian opening and subsequent subduction of the Adriatic slab under the Italian peninsula although no subducted slab has been identified beneath the Central Apennines. Lastly, the Southern Tyrrhenian is bordered by the complex Sicilian domain which is partially formed by the Peloritani Mountains and African continental crust and is composed by a series of depositional domains oriented W-E that are usually filled by marine or lacustrine sediments (Krijgsman et al., 1999).

2.3.2 Campania Plain

The evolution of the Western Italy is closely connected to the Pleistocene Apennine motion towards the Adriatic-Ionian foreland and to the Tyrrhenian opening (Patacca et al., 1990). A series of basins with a "horst and graben" like structure broaden from north to south within continental crust beneath Tuscany, Northern Latium and Campania, which is now thinned to ~ 20-25 km (Agostinetti and Amato, 2009; Di Renzo et al., 2007) and is characterised by anomalous geothermal gradients (Mongelli et al., 1991).

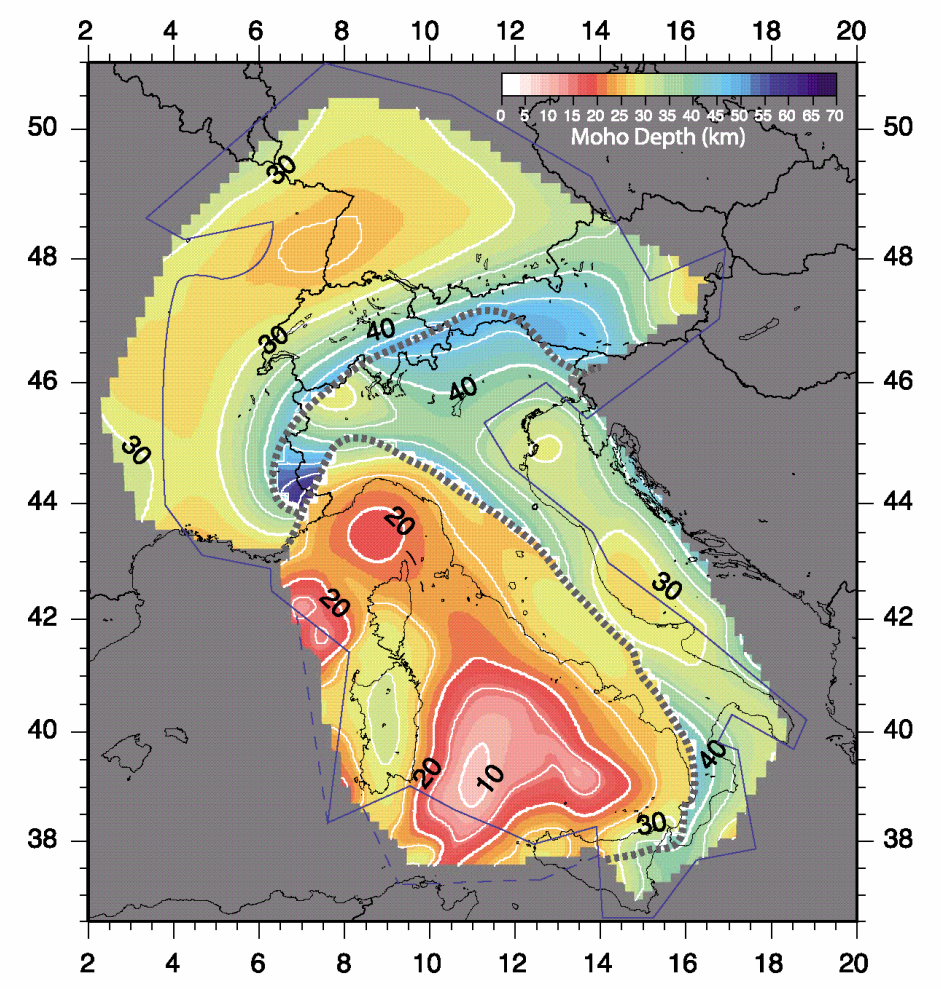

Figure 2.2 The depth of Moho under Italy and surrounding areas as reported by Di Stefano et al. (2011).

These basins are delimited by major NW-SE and NE-SW fault systems related to the Apennine belt. These are intersected by minor N-S and E-W fault systems connected to the Africa-Europe collision (Milia et al., 2003; Trincardi and Zitellini, 1987). These fault systems are related to movement of the Southern Apennines in respect to the current stationary Northern Apennines (Agostinetti and Amato, 2009; Turco et al., 2006). The two regions are separated by a left lateral lithospheric transfer discontinuity along the 41st parallel.

The Campania Plain is located between 41° and 40° N and extends from the Monte Massico to the Sorrento Peninsula (Fig. 2.3). It is bordered by the Southern Apennine chain from the NE and by the Tyrrhenian basin at the SE. Three major fault systems, NW-SE, NE-SW and E-W, cross this region inland and offshore (Berrino et al., 1998) and control its Quaternary evolution. The Campania plain is a vast graben, ~80 km long and ~ 30 km wide, formed in response to NW-SE extension active from Pliocene to Pleistocene times (5-1 Myr). This tectonic depression lies on a carbonate basement (dolostones and limestones) formed in low marine environments at the Tethys margins during Mesozoic times (e.g., Brocchini et al., 2001; Milia et al., 2003). This carbonate platform presumably lies on the crystalline Palaeozoic basement which is not

exposed within the Italian peninsula but outcrops in eastern Sardinia (Lustrino et al., 2000). Milia et al. (2003) interpreted the Campania plain as an asymmetric half-graben structure characterized by listric faults and rollover anticlines which are detached from the original basement at 10-12 km depth. The Plain is formed by alternating highs and lows filled by alluvial and marine deposits of variable thicknesses. Moreover, the Mesozoic carbonate basement is likely positioned at various depths in the different sectors of the plain as confirmed by drilling in the Campi Flegrei area (Rosi and Sbrana, 1987) where the carbonate basement is located at depth over 3 km, but it is intersected at 2 km in the Vesuvius area (Brocchini et al., 2001). The upper mantle and the continental crust beneath Southern Italy are complex (e.g., De Gori et al., 2001); the presence of a low velocity zone at around 20-22 km has been interpreted either as a thermal anomaly or a less dense material such as a crustal zone permeated by fluids likely arriving from a metamorphosed slab. The location of potassic (K) and high potassic (HK) magmatism which occurred within the last 2 Myr is controlled by the fault system within the Campania plain (Scandone et al., 1991).

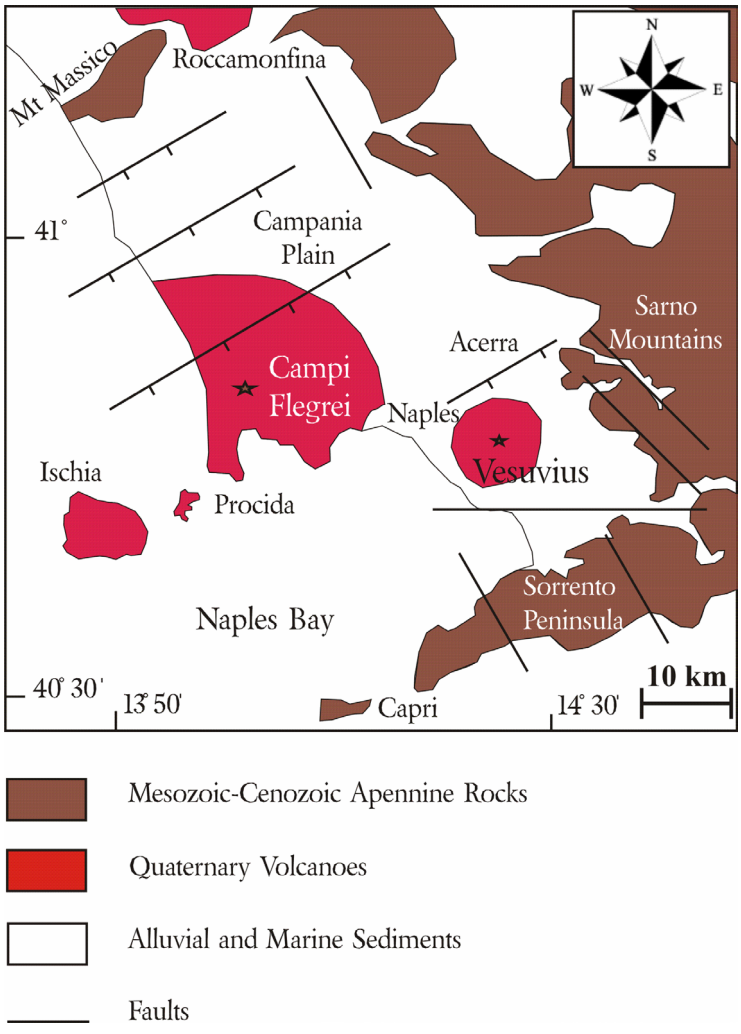

Figure 2.3 Geological sketch of the Campania Plain.

2.4 Italian volcanism

2.4.1 Magmatic domains

Several magmatic domains have been identified within Italy and surrounding areas, all formed since Pliocene (e.g., Lavecchia and Stoppa, 1996; Peccerillo, 2003; Fig. 2.4):

1) the Sardinia-Sicily domain (early Pliocene to Quaternary) is characterized by dyke intrusions of sodic basalts along N-S normal faults in Sardinia (Lustrino et al., 2000) or by hawaiitic lava flows in Sicily on Mt Etna.

2) The Tyrrhenian intra-domain has developed mostly in the south-eastern sector, where sub-alkaline to transitional MORB had floored two mini-basins, Vavilov and Marsili, during mid- Pliocene (Beccaluva et al., 1990), whereas calc-alkaline to shoshonitic magmas with rare HK series had formed the Aeolian Volcanic Archipelago during Pleistocene (Francalanci et al., 2004).

3) The Roman Comagmatic Province (RCP) is subdivided into the Tuscan and Latium-Campanian sub-domains. These sub-domains are located in the western side of Italy and were formed from Pliocene (Tuscany) until present times (Campania). The Tuscan domain is characterized by acidic peraluminous magmatism with intrusive (e.g., Mt Capanne at Elba Island) and effusive episodes (e.g., Radicofani) of anatectic origin. The southern part of this magmatic province overlaps the Latium-Campanian province that spans from Vulsini to Campi Flegrei and Vesuvius. The latter are characterized by potassic and high potassic silica-undersaturated volcanism (e.g., Lavecchia and Stoppa, 1996; Peccerillo, 2003).

4) The Intramontane Ultra-Alkaline Province (IUP) located eastward of the RCP (~ 50 km) is formed by monogenic volcanoes (i.e., San Venanzo, Cupaello, and Vulture) which produced peculiar Carbonatites-Melilites during middle Pleistocene (0.6-0.1 Myr; Lavecchia et al., 2002).

Overall, the Italian magmatism is characterized by a large compositional range (Fig. 2.5 and 2.6); alkali (Na_2O+K_2O) and LILE increase from Sardinia towards the Italian mainland where the RCP and the IUP are strongly enriched in these components (Lavecchia and Stoppa, 1996), $^{87}Sr/^{86}Sr$ increases while $^{143}Nd/^{144}Nd$ decreases from south to north within the RCP (Conticelli et al., 2002) and radiogenic Sr signature augments from the Tyrrhenian toward the IUP emphasizing strong regional variations. The Tyrrhenian basalts (T-basalts), calc-alkaline Aeolian suites and Na-series of Sardinia and Sicily are prevalently saturated in silica and exhibit lower LILE/ HFSE ratios whereas the K and HK series of the Italian inland are mostly under-saturated or slightly saturated in silica and display higher LILE/HFSE ratios. The signature of the first group is

likely associated with a non-orogenic setting and a mantle source likely containing lherzolite or harzburgite, whereas the second group has been linked to either orogenic (Conticelli et al., 2002; Peccerillo, 1985; Serri et al., 1993) or extensional environments (Lavecchia et al., 2002; Lavecchia and Stoppa, 1996).

The close spatial and temporal relationship between different magmatic provinces which were simultaneously active between 600 and 100 Ka may suggest a common regional cause of all magmatism in this area as proposed by Marra et al. (2004).

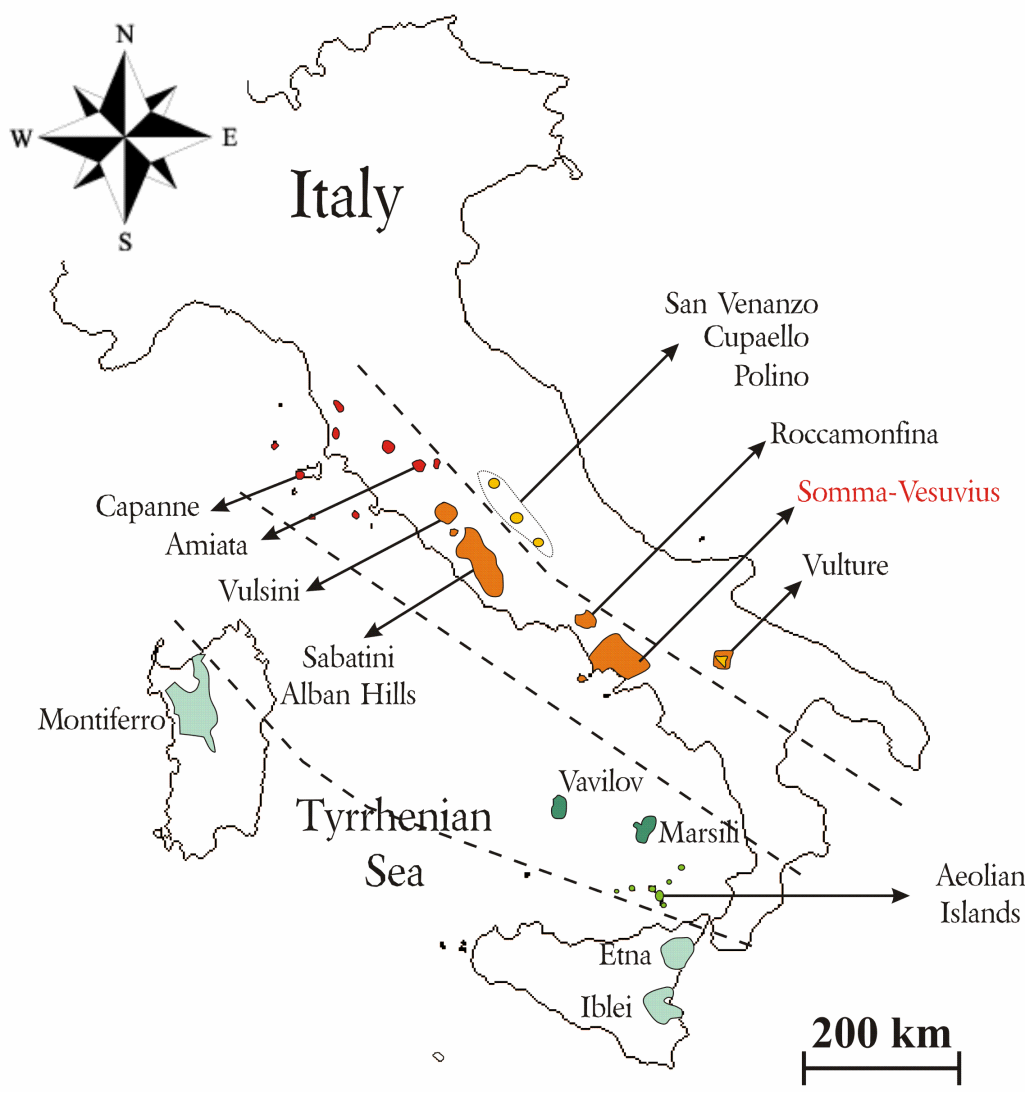

Figure 2.4 Italian mainland and surrounding areas with the related different types of magmatism. Light blue polygons = so dic basaltic magmatism (Montiferro, Etna, Iblei); dark green polygons = MORB-like magmatism (Vavilov and Marsili); light green polygons = calcalkaline-shoshonitic magmatism (Aeolian Archipelago); red polygons = acidic peraluminous anatectic magmatism (Capanne and Amiata); orange polygons = K and high-K magmatism (Vulsini, Sa batini, Alban Hills, Roccamonfina, Campi Flegrei, Vesuvius and partially Vulture); yellow polygons = ultra potassic carbonatites and melilites (San Venanzo, Cupaello, Polino, and Vulture even if not entirely).

2.4.2 Roman Comagmatic Province (RCP)

A series of monogenic volcanoes associated with large volcanic districts within the western Italy from Pliocene until present was defined at the beginning of the last century as a distinct province for its peculiar chemical and mineralogical characteristics (Washington, 1906). This volcanic province extends from northern Tuscany to the Campania Plain and presents common chemical characteristics such as enrichment in incompatible elements, a radiogenic Sr signature, and moderate to high K contents (Lavecchia and Stoppa, 1996; Peccerillo, 1985, 2003). However, based on geography, mineralogy and trace elements concentrations, different magmatic groups can be identified within the RCP. Several authors (e.g., Conticelli et al., 2002; Lavecchia and Stoppa, 1996; Peccerillo, 1985, 2003) distinguished 3 main groups;

1) A high potassic series (HKS) that is the most abundant and occurs from Vulsini (Northern Latium) to Somma-Vesuvius (Campania) and Vulture (inner side of the Apennine). It consists of under-saturated leucite bearing basanites and plagioclase leucitites to leucite phonolites and marked by a strong enrichment in K and incompatible elements. Leucite, clinopyroxene, plagioclase, mg-olivine, nepheline, biotite and phlogopite are common mineral phases of this series.

2) A potassic series (KS) which occurs mostly in Latium and Campania (Roccamonfina, Campi Flegrei, Somma-Vesuvius, and rarely at Aeolian Islands).This series is mostly formed by slightly silica under-saturated to silica saturated products. Clinopyroxene, plagioclase, sanidine, minor olivine, biotite, and magnetite are usually present.

3) A lamproitic series that occurred in Northern Corsica, Southern Tuscany and Northern Latium. This series is characterized by lower concentrations of incompatible elements in respect to the previous series and consists of ultrapotassic, silica saturated up to silica oversaturated plagioclase-free lamproites. Olivine, phlogopite, sanidine, minor clinopyroxene, apatite, and ilmenite are common.

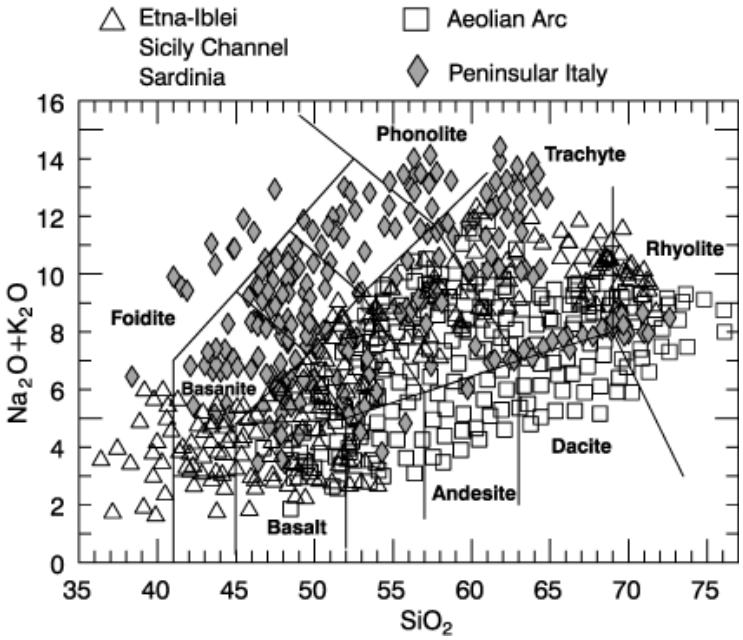

Figure 2.5 A "TAS" classification diagram for Italian Plio-Quaternary rocks from Peccerillo (2003).

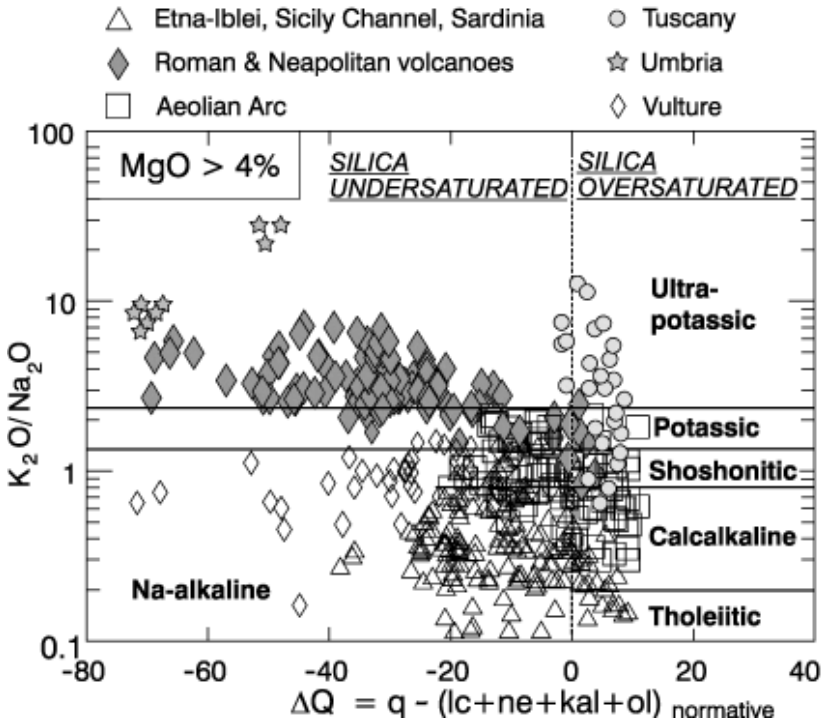

Figure 2.6 A silica discriminative ΔQ vs K_2O/Na_2O diagram for Italian Plio-Quaternary mafic rocks (MgO > 4%) from Peccerillo (2003). ΔQ = normative quartz (q) – leucite (lc) + nepheline (ne) + kalsilite (kal) + olivine (ol).

Chapter 3: Somma-Vesuvius

3.1 Introduction

Mt. Somma-Vesuvius is a stratovolcano in the southern part of the Campania plain (Fig. 2.3 of Chapter 2) at ~ 40°49'17"N and 14°25'33"E. The volcano has a conical shape, 7-8 km wide at the base and is 1279 m high. It is a composite volcano which consists of an older dissected cone, named Somma (Fig. 3.1), built on the Campania Ignimbrite deposits (Barberi et al., 1978; De Vivo et al., 2001; Rolandi et al., 2003a), a recent multiphase asymmetrical caldera, and an intra-caldera cone, named Vesuvius, which grew after the A.D. 472 Pollena eruption (Rolandi et al., 2004; Rolandi et al., 1998).

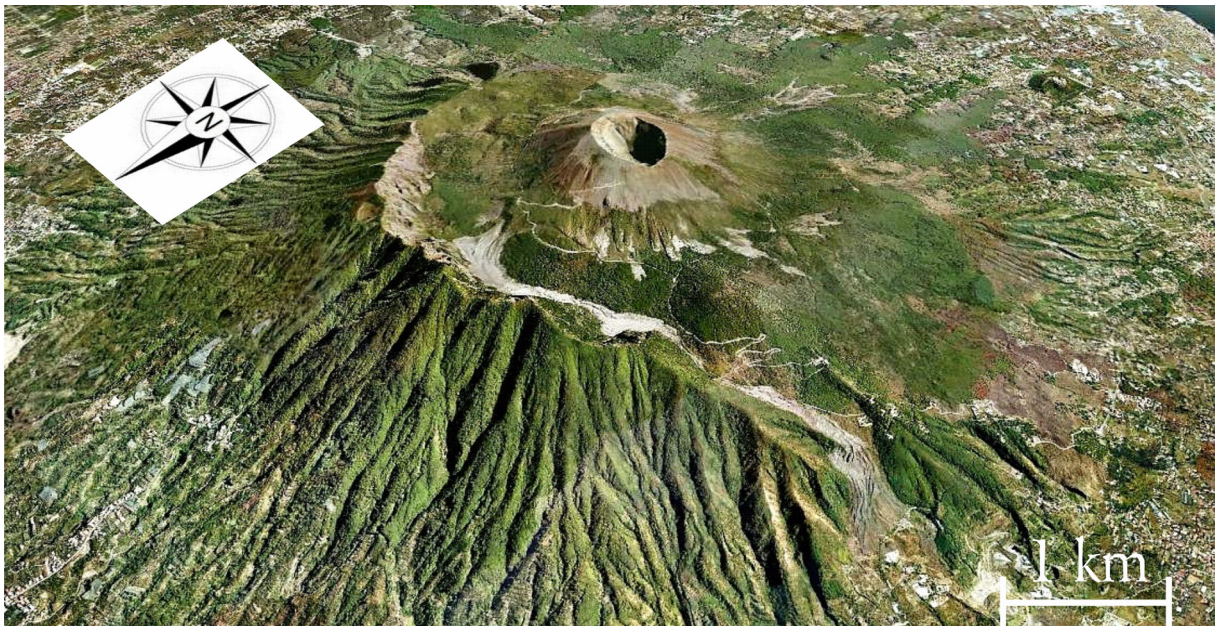

Figure 3.1 3D satellite image of the Somma-Vesuvius volcanic system. The external corona represents the remnant skeleton of the older cone named Somma that was partially destroyed by the eruption of Pollena (A.D. 472) whereas the mono cone inside the older caldera is the actual Vesuvius resulting from the more recent activity (A.D. 472-1944.; Rolandi et al. (1998)).

3.2 Volcanic history

3.2.1 Somma-Vesuvius volcanic dynamics

The Somma-Vesuvius volcanic history involves a well document period over the last 2 Ky, a relatively well-known activity between 2 and 33 Ka, and a poorly understood pre-33 Ka period. Information on the early stages of volcanism is available from a deep borehole (~ 2072 m depth) drilled on the southern slopes of the volcano in the Trecase area (Brocchini et al., 2001).

The $^{40}Ar/^{39}Ar$ dating and nanofossils studies have suggested that volcanism started at ~ 0.4 Ma. Later on, small volcanic centres and fissures developed in the area. The activity consisted of an alternating tephritic magmatic activity and repose times of variable lengths, which were characterized by marine sedimentations during sea transgressions. These sedimentation periods abruptly ended around 37 Ky ago due to the Campania Ignimbrite extensive emplacement which covered an area of 7000 km^2 (Barberi et al., 1978; De Vivo et al., 2001; Rolandi et al., 2003a).
The proper Somma-Vesuvius magmatic activity started only after the Campania Ignimbrite super-eruption. Mostly during the last 33 Ky, different eruptive styles alternated and produced the actual volcanic conical shape with lava flows and tephra. Magma flows have been erupted during both extremely disruptive Plinian eruptions and less explosive Strombolian activities, whereas fall and pyroclastic pumices erupted during Plinian phases only. The main "modus operandi" of the volcano involves prolonged periods of Strombolian-Vulcanian activity, collectively called "inter-Plinian eruptions", usually lasting several centuries, which are interrupted by explosive Plinian events commonly preceded by significant repose times. This alternation of eruptive styles results in a cyclic behaviour of the volcano with each mega-cycle beginning with a Plinian/sub-Plinian eruption followed by subsequent inter-Plianian events which in turn are followed by a repose period (Rolandi et al., 1998).
Joron et al. (1987) has shown that Plinian and inter-Plinian products display distinctive features. Plinian deposits are generally characterized by the more evolved compositions and usually exhibit chemical gradients through the stratigraphic sequences. The basal part of these deposits is usually characterized by the most sialic compositions (white pumices) and the degree of magma differentiation decreases upwards (grey pumices). Volcanic products erupted during inter-Plinian periods show a smaller extent of differentiation (Pappalardo et al., 2004; Piochi et al., 2006b).
The timing of the beginning of the activity at Somma-Vesuvius, as well as the number and type of explosive eruptions during the last 33 Ky are still a matter of debate (e.g., De Vivo et al., 2010; Santacroce et al., 2008). Rolandi (1997) considered the Codola Eruption (~ 33 Ka, Giaccio et al. (2008)) as the first Somma-Vesuvius high VEI event (Simkin and Siebert, 1984). However, the attribution of this eruption to the Somma-Vesuvius activity is still controversial. Sulpizio et al. (2003) attributed the Codola pyroclastic deposits to a Campi Phlegrei eruption.
Over the last 33 Ky, at least 4 major Plinian eruptions have occurred: "Sarno (Pomici di Base) eruption" at ~ 22.03 Ka, "Ottaviano (Pomici di Mercato) eruption" at ~ 8.9 Ka, "Avellino Eruption" at ~ 4.3 Ka, and "Pompeii Eruption" at A.D. 79 (Tab. 3.1 and Fig. 3.2; Arrighi et al., 2001; Ayuso et al., 1998; Landi et al., 1999; Rolandi et al., 1998; Santacroce et al., 2008). In between these main eruptions, 8 to 10 minor explosive events occurred (Rolandi, 1997;

Santacroce et al., 2003). Among the Plinian episodes, the Pompeii eruption is well-documented by Pliny the Younger.

The last activity of the volcano occurred in 1944, and presently the volcano is the site of fumaroles, diffuse degassing, and low magnitude seismicity characterized by up to around 100 local earthquakes per year (Berrino et al., 1998). The nomenclature for the Somma-Vesuvius eruptions is not exclusive as different eruption names have been adopted by different authors (Tab. 3.1; Ayuso et al., 1998; Delibrias et al., 1979; Rolandi et al., 1998; Santacroce et al., 2008). The adopted nomenclature and eruption ages in this work are reported in table 3.1 (after Ayuso et al., 1998; Rolandi et al., 1993a; Rolandi et al., 1993b; Rolandi et al., 1993c; Rolandi et al., 1998; Santacroce et al., 2008 and references therein). The ages correspond to those from Reimer et al. (2004) and take in account the C atmospheric fluctuations impact.

3.2.2 Plinian and Inter-Plinian eruptive history

As described above, at least four major Plinian eruptions are recorded among the Somma-Vesuvius deposits during the last 33 Ky: "Sarno" (Pomici di Base), "Ottaviano" (Pomici di Mercato), "Avellino" and "Pompeii". They represent four distinct stratigraphic intervals which are separated by well-developed paleosols. Moreover, three main sub-Plinian eruptions have been also identified: "Novelle" (Pomici Verdoline) at ~ 19.2 Ka, "Pollena" at A.D. 472, and the "Renaissance Eruption" at A.D. 1631; these events had similarities with both Plinian and inter-Plinian eruptions. All these main Plinian/sub-Plinian eruptions were followed by periods of inte-Plinian activity which consisted of numerous minor Vulcanian/Strombolian events (Fig. 3.2).

The Sarno (Pomici di Base) eruption, dated at ~ 22.03 Ka (Santacroce et al., 2008) has been unambiguously assigned to the activity of Somma-Vesuvius (Capaldi et al., 1985). As stressed by Santacroce et al. (2008), three main phases distinguished this explosive event: 1) a preliminary interval marked by thin ash and pumice fall deposition; 2) an intermediate Plinian stage controlled by abundant pumice falls and pyroclastic flows which emplaced ~ 4.4 km^3 mainly towards E-NE; 3) a phreatomagmatic phase in which surge deposits and lithic flows preceded the caldera collapse. Relatively close to Sarno (Pomici di Base), at ~ 19.2 Ka another conspicuous eruption, called "Novelle (Pomici Verdoline)", occurred at Somma-Vesuvius. It is considered among the largest sub-Plinian eruptions of Prehistoric times and was characterized by several distinct phases (Cioni et al., 2003): an initial magma discharge was followed by a main sub-Plinian phase which developed a quasi-steady eruptive column 17-20 km high. Afterwards, a more discontinuous and pulsating activity occurred and likely ended in a weak hydro-magmatic phase. Included between the Novelle (Pomici Verdoline)

and Ottaviano (Mercato) deposits, is a thick layer of pumices belonging to "Agnano Pomici Principali" produced by Phlegrean Fields activity (Di Vito et al., 1999). At ~ 8.9 Ka, another main Plinian eruption occurred, named "Ottaviano (Mercato)" (Rolandi, 1997; Rolandi et al., 1993b; Santacroce et al., 2008). It progressed, similarly to the Sarno (Pomici di Base) eruption, through three main phases: an opening phase, a high Plinian convective column (22 km) and a phreatomagmatic stage. During this eruption, around 2.40 km^3 of sorted pyroclastic products, were emplaced as a result of pyroclastic falls/flows and minor surge flows which reached a distance of up to 70 km from the volcano. Ottaviano has been one of the most destructive and explosive events among the Plinian eruptions. After this eruption, the Somma-Vesuvius underwent to a dormancy period and no evidence of volcanic activity has been found prior to the Avellino eruptions. The Avellino Plinian eruption is dated at ~ 4.3 Ka. The deposits are similar to the Pompeii eruption; however its volumes correspond to the Ottaviano (Pomici di Mercato) eruption. During this volcanic event, ~ 2 km^3 of materials were dispersed mainly toward E/ NE forming a 50 cm thick cover around Avellino (Rolandi et al., 1993c). This eruption was characterized by alternating complex phreatomagmatic and magmatic phases, followed by a main Plinian sustained convective column (24-36 km) ending in a hydro-magmatic stage. The main pyroclastic deposits show a typical gradation from the bottom up, starting with white basal pumices covered by grey pumices. The Avellino eruption was tailed by a series of explosive activity referred to as Protohistorical in Rolandi et al. (1998). Their number is still controversial; Scaillet et al. (2008) suggested 6 distinct minor events, referred to as AP1-AP6, whereas Rolandi et al. (1998) interpreted the deposits as being formed by 3 distinct eruptions named as 1st, 2nd, and 3rd Protohistoric. It is overall accepted that the Somma-Vesuvius activity during this period was characterized by strong Strombolian eruptions which produced pumices, scoria and ash deposition. After an 800 year repose time, the Plinian Pompeii eruption occurred at A.D. 79 (Sigurdsson et al., 1982). This eruption has also displayed the three-phase behaviour: an opening phase that was characterized by weak lapilli and ash falls followed by the main Plinian phase dominated by extensive pyroclastic/surge flows emplacing ~ 4 km^3 of white and grey pumices. Lastly a main phreatomagmatic stage in which extensive lithic flows were emplaced (Santacroce et al., 2008). The activity of the Somma-Vesuvius continued until late IVth Century with mostly ash emissions. After ~169 years of dormancy, the A.D. 472 Pollena sub-Plinian eruption occurred (Rolandi et al., 2004). During this event, pyroclastic falls alternated with dense pyroclastic flows which emplaced 0.6 km^3 of deposits. Strong and weak explosive events alternated, culminating in a particularly potent hydro-magmatic activity that destroyed the older Somma. The Pollena eruption is classified as sub-Plinian. The Vesuvius cone developed inside the Somma caldera during 8 distinct main Vulcanian and Strombolian events at A.D. 512, 685,

Eruption nomenclature (this project)	Alternative nomenclature	^{14}C yr Bpi	^{14}C cal yr Bpi	Other dating methods[i]	Favoured age (this project)[i]	References
AD 1631 [c & h]		470 ± 55	520 ± 40	AD 1631	AD 1631	[a] Ayuso et al. (1998)
		330 ± 55	410 ± 70			[b] Delibrias et al. (1979)
						[c] Rolandi et al. (1993)a
	AS 5[g]	545 ± 50	580 ± 50		540 ± 30 cal BP	[d] Rolandi et al. (1993)b
		475 ± 50	520 ± 40			[e] Rolandi et al. (1993)c
						[f] Rolandi et al. (1998)
	AS 4 a-b[h]	1181 ± 46	1100 ± 70		1100 ± 70 cal BP	[g] Santacroce (1987)
4th Medieval[f]	AS 4[g], PM6[h]	1165 ± 55	1100 ± 80		1160 ± 80 cal BP	[h] Santacroce and Sbrana (2003)b
		1230 ± 55	1160 ± 80			[i] Santacroce et al. (2008) and ref. therein
3th Medieval[f]	AS 3[g], PM3-4-5[h]	1265 ± 55	1200 ± 70		1270 ± 35 cal BP	[j] Scaillet et al. (2008)
		1355 ± 55	1280 ± 50		1290 ± 30 cal BP	
		1335 ± 46	1260 ± 50		1310 ± 30 cal BP	
		1370 ± 50	1290 ± 50			
		1372 ± 46	1290 ± 40			
		1340 ± 50	1270 ± 50			
		1380 ± 60	1310 ± 50			
		1425 ± 55	1350 ± 50			
2nd Medieval[f]	AS 2[g], PM2[h]	1570 ± 50	1470 ± 60			
1st Medieval[f]	AS 1[g], PM1[h]			AD 512, 1420 BP	AD 512	
Pollena[f & i]		1630 ± 50	1530 ± 70	AD 472, 1440 BP	AD 472	
		1650 ± 30	1570 ± 40			
		1630 ± 50	1530 ± 70			
Pompeii[f & i]		2085 ± 80	2080 ± 110	AD 79	AD 79	
		2120 ± 60	2140 ± 110			
		1805 ± 40	1750 ± 60			
	AP6[j]			217–216 BC		
3rd Protohistoric[f]	AP4[j]			3990		
3rd Protohistoric[f]	AP3[j]	2710 ± 60	2830 ± 50	4020	2830 ± 50	
2nd Protohistoric[f]	AP2[j]	3000 ± 200	3170 ± 240	4150	3500 ± 40 cal BP	
		3240 ± 45	3480 ± 50			
		3400 ± 160	3680 ± 190			
		3300 ± 80	3540 ± 90			
1st Protohistoric[f]	AP1[j]	3220 ± 65	3460 ± 70		3500 ± 60 cal BP	
		3420 ± 300	3671 ± 370			
		3270 ± 50	3500 ± 60			
Avellino[a & h]		3360 ± 40	3600 ± 60	4310	4365 ± 40 cal BP	
		3460 ± 65	3740 ± 90			
		3590 ± 25	3900 ± 40			
		3675 ± 57	4010 ± 80			
		3920 ± 50	4350 ± 70			
		3960 ± 60	4410 ± 60			
		3850 ± 55	4280 ± 100			
Ottaviano[d]	Pomici di Mercato[i]	7910 ± 100	8780 ± 150	9680	8890 ± 90 cal BP	
	Pomici e proietti[b]	7870 ± 50	8710 ± 90			
	Pomici Gemelle[b]	8098 ± 71	9010 ± 130			
		8010 ± 35	8890 ± 90			
Novelle[a]	Pomici Verdoline[i]	14420 ± 160	17730 ± 200	17560	19265 ±105 cal BP	
	Novelle Seggiari Formation[a]	15500 ± 170	18790 ± 140			
		16780 ± 170	20010 ± 260			
		16130 ± 110	19300 ± 150			
		16020 ± 130	19230 ± 150			
Sarno[a]	Pomici di Base[i]	17050 ± 140	20220 ± 200	22520 ± 1000	22030 ± 175 cal BP	
		19170 ± 420	23000 ± 460	19280		
		18750 ± 420	22520 ± 570			
		18300 ± 180	22030 ± 250			
		18300 ± 150	22030 ± 240			

Table 3.1 Somma-Vesuvius eruptions existing nomenclature (Ayuso et al., 1998; Delibrias et al., 1979; Rolandi et al., 2003a; Rolandi et al., 1993b; Rolandi et al., 1993c; Rolandi et al., 1998; Santacroce, 1987; Santacroce et al., 2008; Santacroce and Sbrana, 2003b; Scaillet et al., 2008) with annexed ^{14}C age determined on soil organic matter or charcoal (Santacroce et al., 2008 and references therein), and ^{14}C calibrated ages (Reimer et al., 2004).

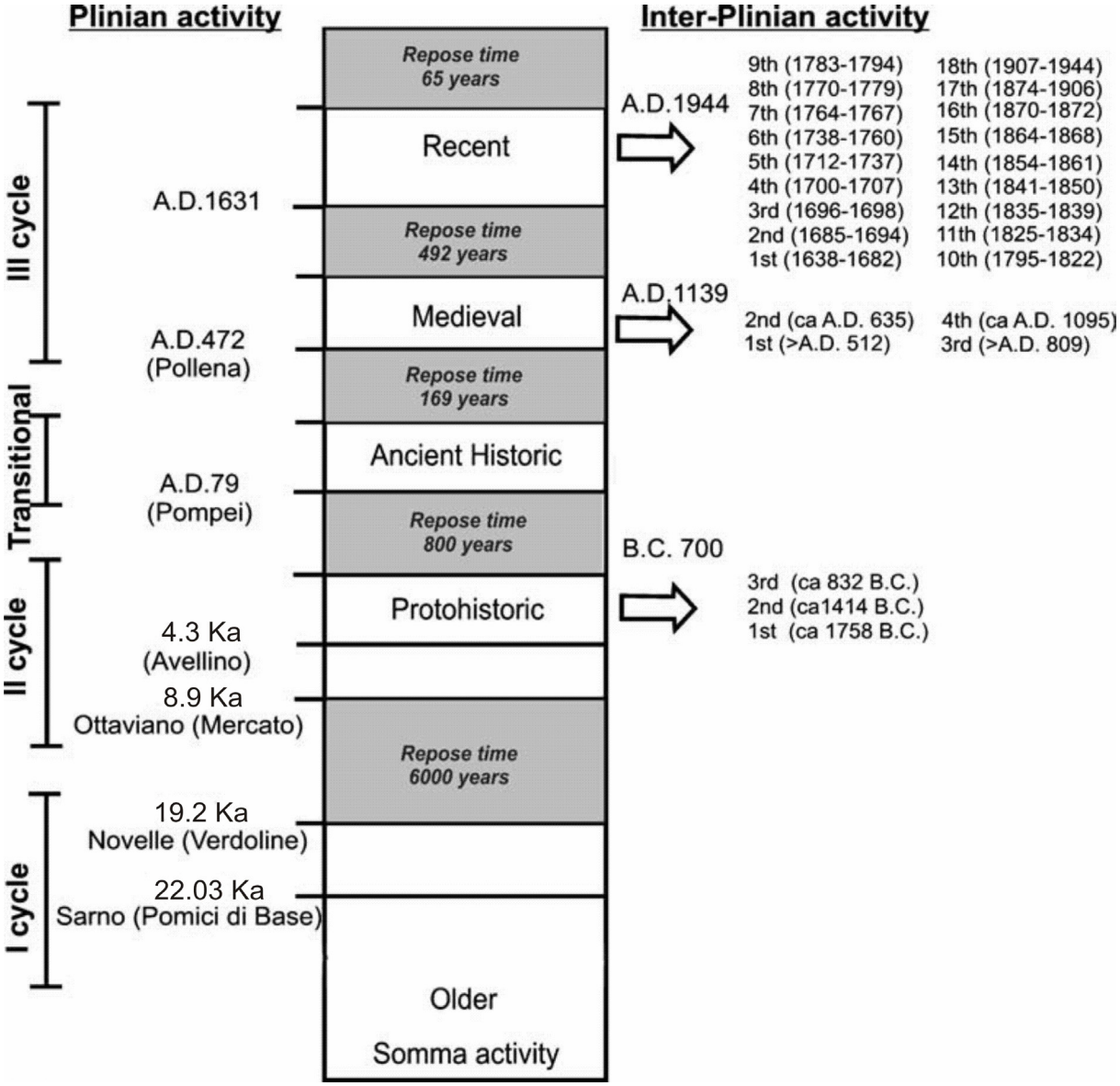

Figure 3.2 Reconstructed volcanic activity for the last 33 Ky at Somma-Vesuvius from De Vivo et al. (2010) modified.

787, 968, 999, 1007, 1037 and 1139 (Rolandi et al., 2004). These eruptions mainly produced lapilli scoria and sand deposits. They are grouped in 4 main periods of activity by Rolandi et al. (1998) who called them as "Medieval"; other authors have ordered and named them as "AS 1-2-3-4" (Santacroce, 1987) or as "PM 1-2-3-4-5-6" (Santacroce and Sbrana, 2003b). On A.D. 1631 the last major historic eruption occurred after a 500 years repose (Rolandi et al., 1993a). It was well-documented by the contemporaneous historic chronicles. The eruption consisted of preliminary sub-Plinian and Vulcanian activities followed by the main Plinian phase with a high sustained convective column which reached ~ 28 km of altitude, and ended with lava flows and superficial water-magma interaction. Overall, the eruption emplaced approximately 1.1 km^3 of tephra, pyroclastic and lava flows. After this eruption, the volcano was continuously active until 1944 producing a large number of small inter-Plinian eruptions with a maximum repose

time between them of no longer than 40 years. These events mainly produced lava flows at the summit crater or in its proximity within the Somma-Vesuvius caldera (Santacroce et al., 2008). The last activity of the volcano is dated back to 1944 and since then the volcano is in a dormancy state.

3.3 Petrochemistry

During the last 33 Ky the Somma-Vesuvius activity has been mainly characterized by the emission of lavas, pumices and scoriae. The compositions are mainly high- to ultra-high potassium (Middlemost, 1994) and silica undersaturated. The potassium content and silica-undersaturation increased with time (K_2O = 2.3- 9.6 wt %; SiO_2 = 59-47 wt %; Ayuso et al., 1998, Joron et al., 1987). The extent of silica undersaturation and potassium enrichment has been used to distinguish different magmatic series (e.g., Ayuso et al., 1998; Joron et al., 1987; Somma et al., 2001; Fig. 3.3) and three main groups have been identified.The first group (older than 8.9 Ka; Ayuso et al., 1998) consists of porphyritic slightly silica-undersaturated basic potassic rocks whose compositions correspond to the boundary between trachybasalt-trachyandesite and tephrite-phonolite fields on the total alkali vs silica classification diagram (Group 1 in fig. 3.4). The second group (from ~ 8.9 Ka to A.D. 79; Group 2 in fig. 3.4) is characterized by a mildly silica-undersaturated series with a slightly porphyritic character and comprises phonotephrites, tephriphonolites and phonolites richer in alkalis compared with Group 1. The third group (younger than A.D. 79; Group 3 in fig. 3.4) are strongly silica-undersaturated leucite tephrites, leucitites, phonotephrites, tephriphonolites, foidites and phonolites with a distinctive porphyritic texture. In terms of mineral associations, Group 1 contains clinopyroxene, biotite, plagioclase, sanidine and subordinately olivine and amphibole phenocrystals. Group 2 also comprises nepheline and garnet phenocrystals as secondary phases; whereas, Group 3 is characterized by the presence of leucite, Al-rich diopside, plagioclase and minor amphibole, olivine, biotite, sanidine, nepheline and garnet. Apatite and Ti-magnetite have also been identified in many samples (Ayuso et al., 1998; Joron et al., 1987). In each series, the above mineral phases are also commonly present in the groundmass as microlites. Leucite-free rocks usually occurred before A.D. 79 (Group 1 and 2; Piochi et al., 2006b). They are characterized by both Mg and Fe rich diopside, olivine, plagioclase, K-feldspar, magnetite and biotite. Leucite bearing rocks (Group 3) contain plagioclase, Mg poor and Fe-rich diopside, olivine and oxide with rare nepheline. A large database exists of major, trace elements and isotopic compositions of Somma-Vesuvius volcanic products (Ayuso et al., 1998; Belkin et al., 1993b; Caprarelli, 1993; Graham et al., 1993; Joron et al., 1987; Paone, 1998, 2006; Piochi et al., 2006b; Somma et al., 2001; Trigila and De Benedetti, 1993; Villemant et al., 1993).

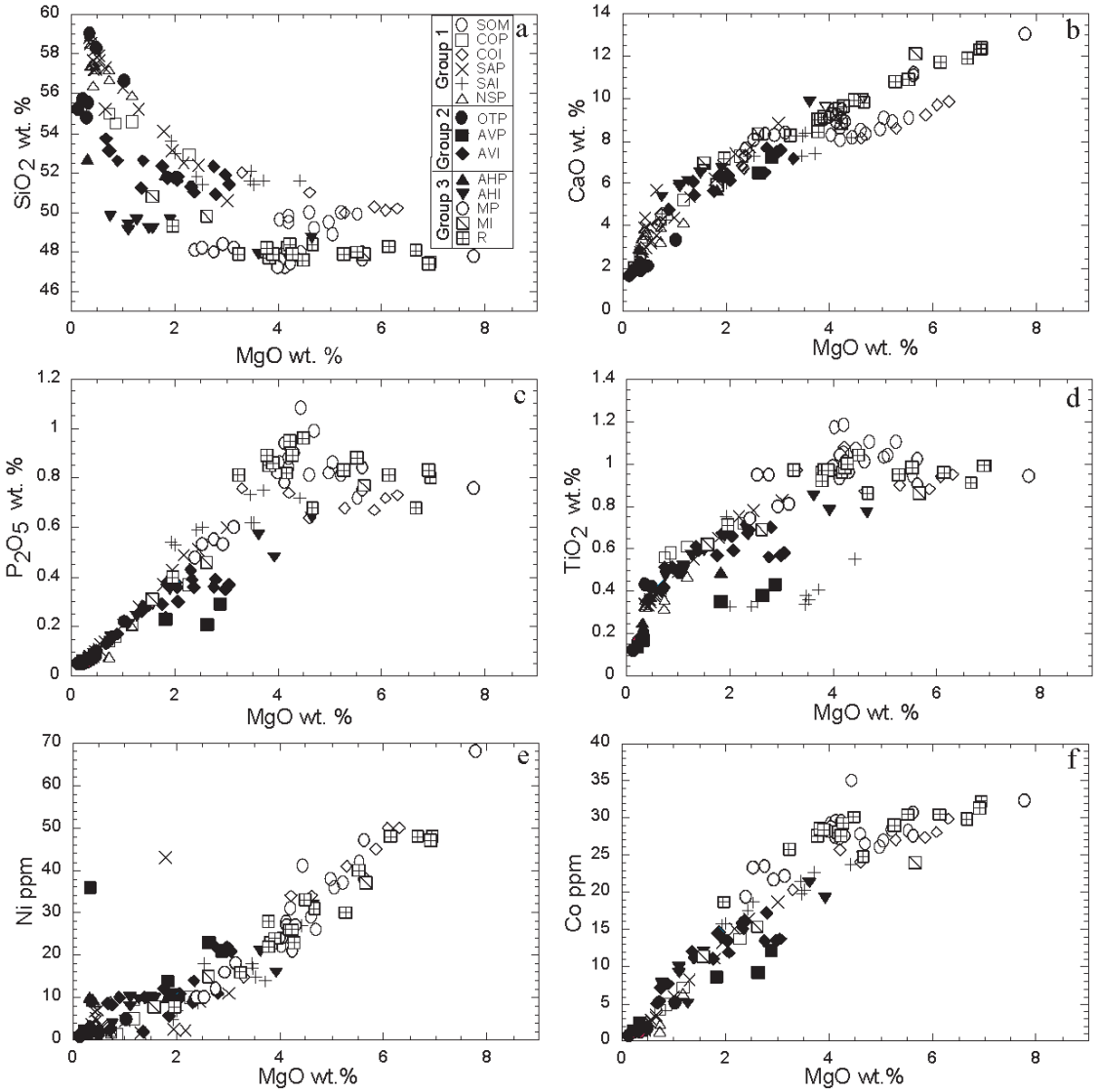

Figure 3.3 Variation diagrams for a. SiO_2, b. CaO, c. P_2O_5, d. TiO_2, e. Ni, and f. Co as a function of MgO wt% from Ayuso et al., 1998. Abbreviations are as follows, Group 1: SOM = Somma; COP = Codola formation, plinian; COI = Codola formation, interplinian; SAP = Sarno formation, plinian; SAI = Sarno formation, interplinian; NSP = Seggiari (Novelle, Bosco) formation, plinian. Group 2: OTP = Ottaviano formation, plinian; AVP = Avellino formation, plinian; AVI = Avellino formation, interplinian. Group 3: AHP =Ancient Historic (A.D. 79 formation), plinian; AHI = Ancient Historic 213 (A.D. 472 formation), interplinian; MP = Medieval (1631), plinian; MI = Medieval (1631) interplinian; R =Recent (post-1631). In the Seggiari formation, samples from Lagno Amendolare plot as part of Group 1 and Ottaviano as Group 2. Formations and names in parentheses according to Rolandi et al. 1993a,b.; Rolandi et al. 1998. and Rolandi unpublished data.

Overall, the degree of silica and the incompatible elements contents decrease over time while the alkalis contents (Na_2O+K_2O) increases; Group 1 has the highest and the broadest range of silica contents but the lowest alkalis concentrations, whereas Group 3 is formed by the most silica-undersaturated and alkaline members of the entire Vesuvius series. Somma et al. (2001) suggested that the distinct major, trace and isotope compositions shown by the three magmatic series can be related to significant variations in the magma evolution paths but they also may reflect an increase in the primary magma alkalinity. Decreasing contents of major elements as Fe_2O_3*, CaO, P_2O_5, TiO_2, and the correspondent increase in Al_2O_3, Na_2O and K_2O observed within each series reflects clinopyroxene, subordinately olivine and Fe-Ti oxide fractionation. Within each series, pumices are the most evolved, having the lowest Mg# values and are usually emitted during explosive events (Plinian and sub-Plinian eruptions). Lavas and scoriae represent less evolved magmas and are usually produced by less explosive inter-Plinian eruptions. Pumice fall deposits are commonly isotopically zoned (mostly $^{87}Sr/^{86}Sr$) suggesting

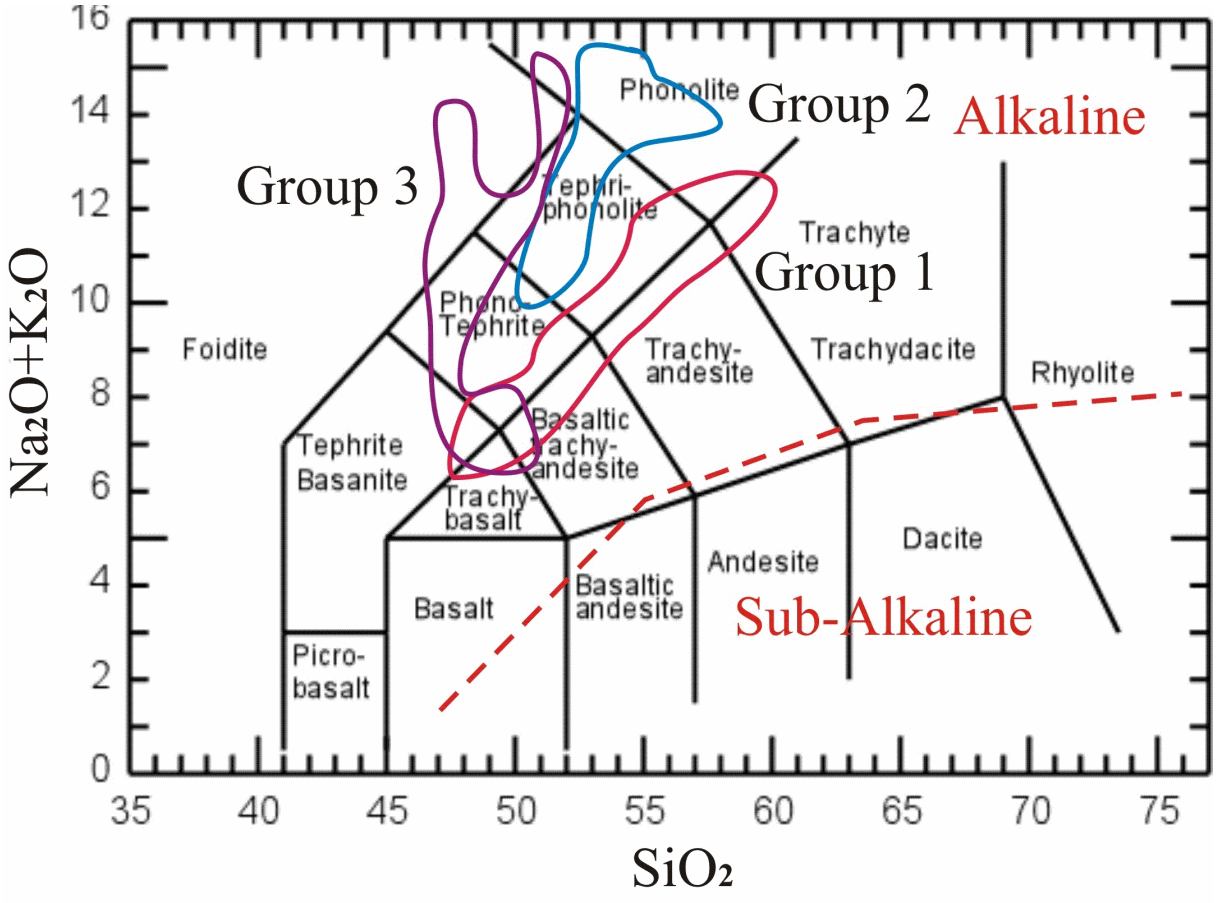

Figure 3.4 Total alkali (Na_2O+K_2O) vs SiO_2 (wt %) of Vesuvius rocks for the last 33 Ky. Group 1 (older than 8.9 Ka), Group 2 (between 8.9 Ka and A.D. 79) and Group 3 (from A.D. 79 until recent times) are respectively delineated with the red, blue and purple polygons.

a differentiation occurring inside shallow magmatic chambers (Cioni et al., 1998); Avellino, Pompeii, and Pollena show a large range of $^{87}Sr/^{86}Sr$ whereas Ottaviano is more homogeneous and Novelle does not display variations in Sr isotopes.

The first pumices that are deposited in each eruption are typically more sialic containing a minor amount of lithic fragments (Joron et al., 1987). The extent of fractionation decreases toward the top of the deposits which are usually more enriched in the lithic fraction, and as a result, Plinian deposits are usually capped by a grey pumice cover on top of a "more evolved" white-pumice layer.

3.4 Possible magmatic origin: an overview

In regard to the nature of Somma-Vesuvius parental magmas, a range of hypothesis has been proposed, based mainly on geochemical studies of lava compositions (Ayuso et al., 1998; Joron et al., 1987; Paone, 2006; Piochi et al., 2006b; Somma et al., 2001). Clinopyroxene and feldspar were considered the main crystallizing phases at Somma (< AD 472); instead, clinopyroxenes and olivines drive the crystallization while plagioclase, leucite and nepheline appear later in the crystallization sequence at Vesuvius (> AD 472). The Mg contents only rarely exceed > 6 wt%. Concentrations of incompatible elements are dissimilar to other lavas from the Roman Comagmatic Province and potassic series worldwide. The overall chemical signature of Vesuvius lavas described above suggests a rather evolved nature of erupted products (Joron et al., 1987).

Geochemical studies (Ayuso et al., 1998; Joron et al., 1987; Somma et al., 2001 and references therein) provided information on the nature of the magmatic source at Somma-Vesuvius. Initially, it has been observed that overall trace elements showed quite similar distribution patterns when plotted on MORB and OIB multi-elements normalized diagrams (Fig. 3.5). However, the least evolved products (with MgO > 3wt %) which are usually considered chemically closer to the original pristine magma compositions, revealed an enrichment in LILE (Large Ion Lithophile Elements as K, Rb, Sr and Ba) and HFSE (High Field Strength Elements as Zr and Nb) relative to MORB and OIB (Piochi et al., 2006b).

In light of the above, a heterogeneous mantle has been taken as the likely original melt source which matches well the complex tectonic history of the Italian Peninsula where the subducting Ionian and the Adriatic plates possibly produced melting and metasomatism of the mantle wedge (Beccaluva et al., 1991; Peccerillo., 1999). Several petrogenetic processes have been invoked in the Vesuvius magma genesis and evolution: 1) melting of a metasomatize mantle; 2) multi-stage fractional crystallization; and 3) crustal contamination taking place in different magmatic reservoirs which formed as a consequence of the magma ponding at different depth

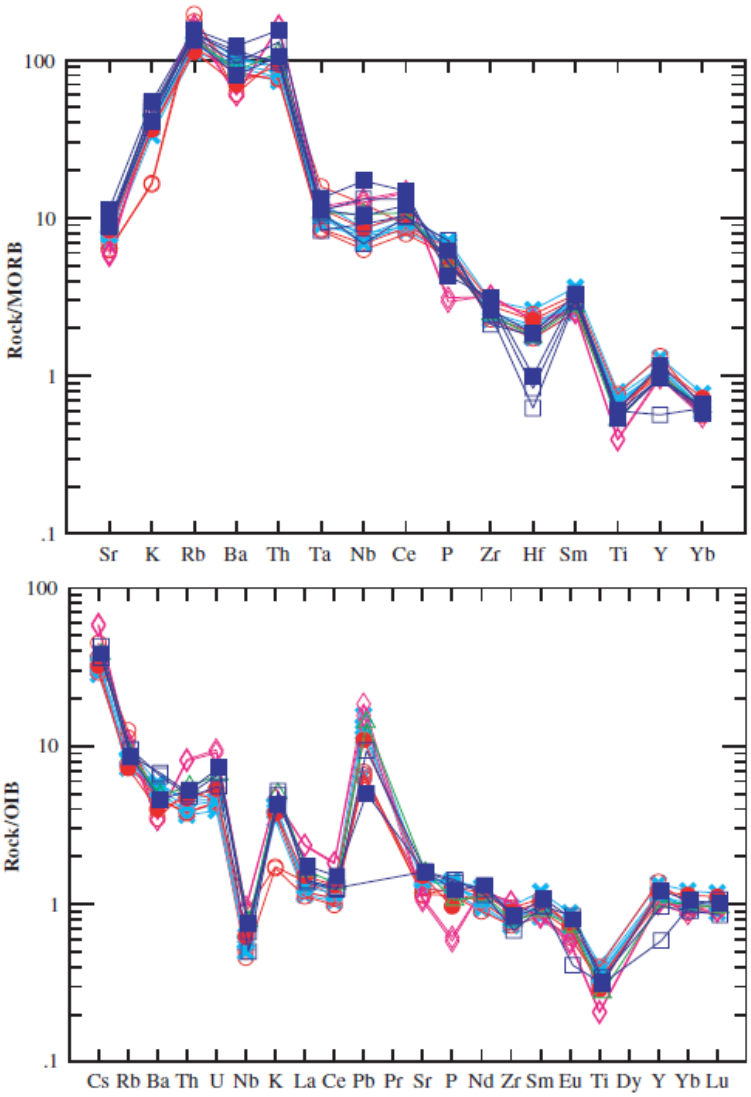

Figure 3.5 Spider diagrams for selected Somma-Vesuvius rocks with MgO > 3 wt% from Piochi et al., 2006b. Bold crosses are dykes from Somma activity; closed symbols are rocks from Plinian and sub-Plinian events; and open symbols rocks from inter-Plinian periods. Circles, first magmatic cycle; rhombus second magmatic cycle; triangles, transitional magmatic cycle; squares, third magmatic cycle.

within the crust.

Fractional crystallization is the main factor controlling 1) the range of erupted lava compositions (Ayuso et al., 1998; Paone, 2006; Piochi et al., 2006b; Piochi et al., 2004), 2) the low Mg#; 3) the low contents of compatible elements such as Cr, Co and Ni; and 4) the chemical trends of Sr, CaO-Al_2O_3 vs. K_2O which suggest clinopyroxene-olivine crystallization associated with plagioclase and marginally k-feldspar.

Crustal contamination is inferred from both mineralogical and chemical data. Garnet and phlogopite present among mineral phases are usually interpreted as by-products of interaction between the alkali magmas and the crust; Ce/Pb and Nb/U values of Somma-Vesuvius lavas are remarkably close to those ones in the upper continental crust ≈ 3.5 (Taylor and McLennan, 1985). However, the strongest evidence supporting crustal contribution comes from the strong

enrichment in radiogenic isotopes $^{87}Sr/^{86}Sr$, $^{143}Nd/^{144}Nd$ and $^{207}Pb/^{204}Pb$ which are scarcely impacted by fractional crystallization processes.

Some authors (e.g., Civetta et al., 2004; Paone, 2006) suggested that crustal contamination occurred mainly in the Hercynian basement based on high $^{87}Sr/^{86}Sr$, lower $^{43}Nd/^{144}Nd$ and $^{207}Pb/^{204}Pb$, which are close to the values of the Hercynian basement outcropping in Sardinia. In contrast, other authors (Pappalardo et al., 2004; Piochi et al., 2006a; Rolandi et al., 2003a) proposed carbonates as the main contaminant, considering that several Ca-Mg metamorphic carbonate ejecta have been recovered inside the Somma-Vesuvius pyroclastic deposits (e.g., Barberi and Leoni, 1980; Del Moro et al., 2001). Carbonate assimilation has also been suggested at Somma-Vesuvius through an experimental study in Marziano et al., 2008 in which an increasing amount of carbonate assimilation from Group 1 to Group 3 was accounted to explain the observed variations in mineral assemblages and bulk rock compositions through the time.

Variability in Nb/Ta, La/Yb, and Hf/Th vs. MgO, among the three main magmatic cycles and the increasing degree of silica-undersaturation combined with the increase in alkalinity, suggest variation degree in the parental magma compositions (Somma et al., 2001).

3.5 Plumbing system

Despite of numerous studies on Somma-Vesuvius, the plumbing system structure is still a matter of debate. Geophysical studies (e.g., Agostinetti and Amato, 2009; Auger et al., 1999; Berrino et al., 1998; Milia et al., 2003; Nunziata, 2011; Zollo et al., 1996) and chemistry of lavas and melt/ fluid inclusions (e.g., Belkin and De Vivo, 1993a; Belkin et al., 1985; Belkin et al., 1993b; Cioni et al., 1998; Lima et al., 2003; Lima et al., 2007; Marianelli et al., 1999; Piochi et al., 2006b) have addressed this issue.

In line with the geophysical studies and according to the Trecase well drilled by the Agip S.p.A. in 1980 along the Southern flank of the volcano (Brocchini et al., 2001) the structure of the crust under the Somma-Vesuvius has been depicted as illustrated in fig. 3.6. The first 0.5 km is almost entirely formed by terrigenous alluvial deposits alternated to volcanic tuff, lava and tephra; underneath, only marine and volcanogenic deposits are found testifying periods of volcanic activity alternating with marine transgressions.This lithology well matches the density of 2000- 2400 kg/m^3 reported by geophysical measurement (e.g., Berrino et al., 1998).

Underneath these volcanic deposits, a main discontinuity in the shallow crust has been suggested at around 2 km depth from gravity anomalies, also confirmed by the Trecase drill- hole. Below this discontinuity, at depths from 1.5-2.5 km in various parts of the Campania Plain, the Mesozoic Carbonate basement occurs mostly characterized by dolostones and limestones which match

the gravity data and the suggested density of 2600 kg/m³. At around 11-13 km depth another marked discontinuity has been confirmed using a DSS survey, seismic tomography, and by TOMOVES and BROADVES seismic experiments (De Natale et al., 2001; Ferrucci et al., 1989; Zollo et al., 1996). This discontinuity likely indicates the contact between the Mesozoic carbonate basement and the Palaeozoic crystalline (possibly Hercynian) basement and it is also marked by a decrease in seismic velocity of 5-6 % (De Natale et al., 2001; Nunziata, 2011), usually referred to as "Low Velocity Zone" (LVZ). Moreover, this discontinuity coincides with the presence of a sill-like magmatic reservoir whose lateral limits are not well constrained (e.g., Zollo et al., 1996). Underneath, this LVZ, high velocity regions for P waves are consistent with a crystalline basement of the Campania Apennine. At depth below 15 km, teleseismic tomography studies pointed to the occurrence of a "low velocity body" down to the Mohorovic discontinuity at 30- 35 km depth. However, it is still unclear if the sill-like magma body hypothesized at depth 10-15 km is a disjoint body fed by a deeper reservoir extending from 15 down to 30-35 km, where the Moho has been located, or if it is the top of a separate magmatic body intruded in the crust and directly fed by the upper mantle. Remarkably, geophysical studies did not reveal the presence of shallow magmatic chamber/s. Instead, an "axial velocity body" below the volcanic structure, where all the seismic activity is usually clustered, has been suggested by De Natale et al. (2001) and interpreted as a lava body solidified inside the magmatic conduit.
A further refinement on the volcanic plumbing system structure has been introduced through geochemical studies. Firstly, it was suggested through geobarometrical studies on FI in ejected nodules belonging to Plinian and non-Plinian eruptions (Belkin and De Vivo, 1993a; Belkin et al., 1985) that the magma likely ponded at different depths within the crust, between 3.5 and 12 km. More recently, in line with the previous melt and fluid inclusions studies, Lima et al. (2003) proposed that the magma was residing at several depths and it was speculated that the more superficial reservoirs are likely small, and thus are not resolvable in geophysical data. It was proposed that a small, probably < 1-2 km in diameter magma chamber is located at ~ 3.5-4 km depth and another modest magmatic reservoir is situated at ~ 8-10 km whereas a bigger reservoir is seated at depth > 12 km (Fig. 3.6). The authors suggest that the plumbing system likely appears as a complex feeding column formed by small magma chambers, where crystallization processes occur at different P-T conditions, cooling rates and magma supply rates.
The existence of magma chambers at different levels is also inferred from the presence of carbonate thermo-metamorphic and skarn ejecta (Barberi and Leoni, 1980). Cioni et al. (1998), through a detailed study of diopsidic pyroxenes and their MI, suggested that the volcanic system for both Plinian and non-Plinian episodes consisted of, shallow small magma chambers which

are periodically replenished by mafic magma batches leading to changes in their volume and in aspect ratio. Scaillet et al. (2008), based on experimental studies on four main Vesuvius eruptions proposed that magmatic reservoirs migrated from 7-8 km depth to 3-4 km depth between the Pompeii and the Pollena eruptions. They emphasised that mineral phase equilibria and the pre-eruptive water contents indicate different crystallization pressure for different eruptions. The migration of magma ponding could be produced by local stress field changes or different buoyancy due to different volatile content and chemical composition of the magma (Webster et al., 2001).

3.6 Volcanic hazards

The Somma-Vesuvius is located in one of the most densely populated areas of Italy with around 2605 inhabitants per km². Two million people leave in the Naples province and around 675,000 within 10 km from the summit crater (data available on http://www.urbistat.it/). In its past volcanic history, the Somma-Vesuvius manifested a polyhedral behaviour alternating high explosive and less disruptive Strombolian-Vulcanian events. Around 7 main eruptions, Plinian to sub-Plinian, occurred in the last 33 Ky, but up to 40 explosive eruptions have been recognized in a recent geological mapping of the volcano (Santacroce and Sbrana, 2003a) depicting a broad range of volcanic episodes which vary from high to low VEI (Fig. 3.7). Last volcanic eruption occurred during World War II on March 1944 (Fig. 3.8) when the population in the area was significantly smaller than it is now. Since 1944, the Somma-Vesuvius entered a dormant period which lasts until now. The 1944 eruption could potentially represent the end episode of the last magmatic cycle which started in the A.D. 79, or the current 69 years-long repose time could be an anomalous interval inside the last magmatic cycle. Considering the first case, in the next few centuries, a Plinian explosive eruption could be expected, whereas in the latter case, a new Strombolian-Vulcanian episode may occur. In both scenarios, considering the extent of urbanisation over the last 69 years, the volcanic hazards are dramatically high (Chester et al., 2002; Lirer et al., 2001; Marzocchi et al., 2004; Santacroce et al., 2005; Zuccaro et al., 1998). In 1995, as a consequence of the perceived high risk and in response to several studies aimed at quantification of the volcanic hazards at Somma-Vesuvius, the Italian Department of Civil Protection published a hazard and risk evaluation-evacuation plan, DPC 1995. The evacuation plan considers the eruption of A.D. 1631 as worst possible scenario which is the last sub-Plinian eruption in historic times.

Moreover, the Commission, taking in account the vulcanological dynamics reconstructed by some authors for this eruption (e.g., Rolandi et al., 1993a; Rosi et al., 1993), assumed that any future volcanic eruption will generate precursory signals such as ground-deformation (uplifting),

increasing superficial seismicity, and modification in the degassing activity (fumaroles) and that these precursor events will take place sometime before the eruption. However, another possible scenario could involve a disruptive eruption with high VEI (~ 4-5) that would strike with little warnings (De Vivo and Rolandi, 2012; Rolandi, 2010).
Additionally, the commission produced a territorial subdivision of the Somma-Vesuvius surroundings; three risk zones were created as follows (Fig. 3.9):

1. the “Red Zone” with the highest volcanic risk since susceptible to pyroclastic and tephra falls;

2. the “Yellow Zone” with intermediate risk and subject to tephra falls which are dangerous for population health and infrastructures (Zuccaro et al., 1998);

3. the “Blue Zone” which can be potentially affected by the same hazards as the Yellow Zone, but also by debris flows.

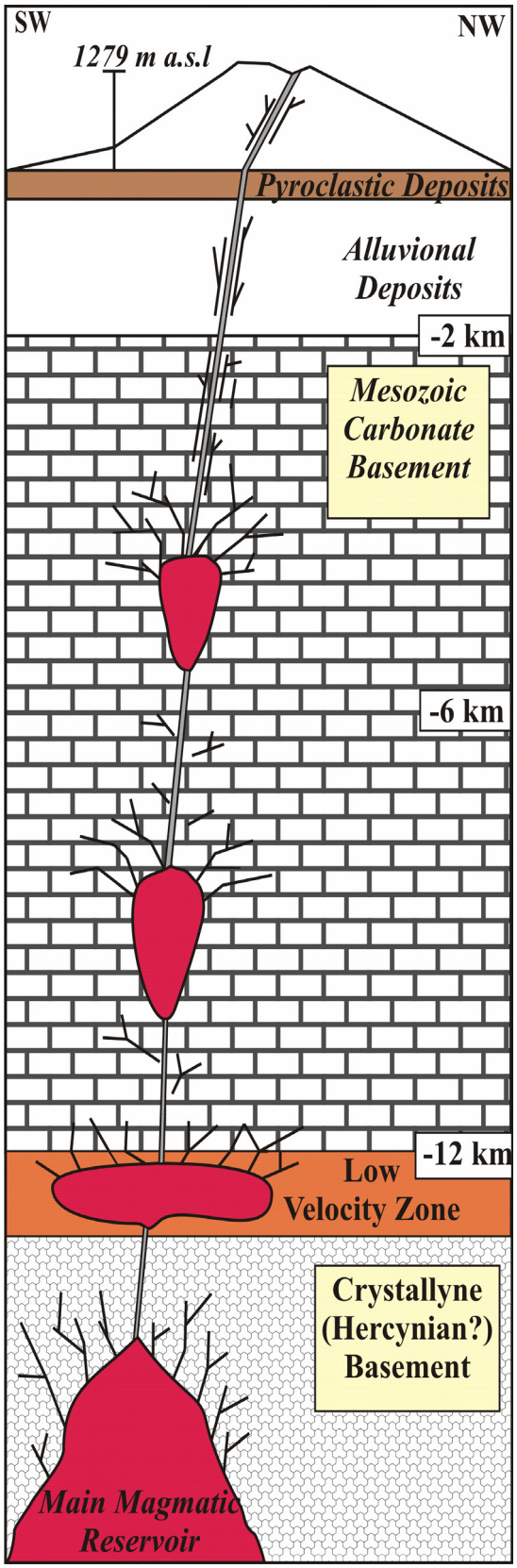

Figure 3.6 Reconstructed tectonic settings of the "plumbing system" which underlines the Somma-Vesuvius edifice as deduced from several authors (e.g., Auger et al., 1999; Bel kin and De Vivo, 1993a; Belkin et al., 1985; Berrino et al., 1998; De Natale et al., 1998; De Natale et al., 2001; Lima et al., 2003; Lima et al., 2007; Zollo et al., 1996).

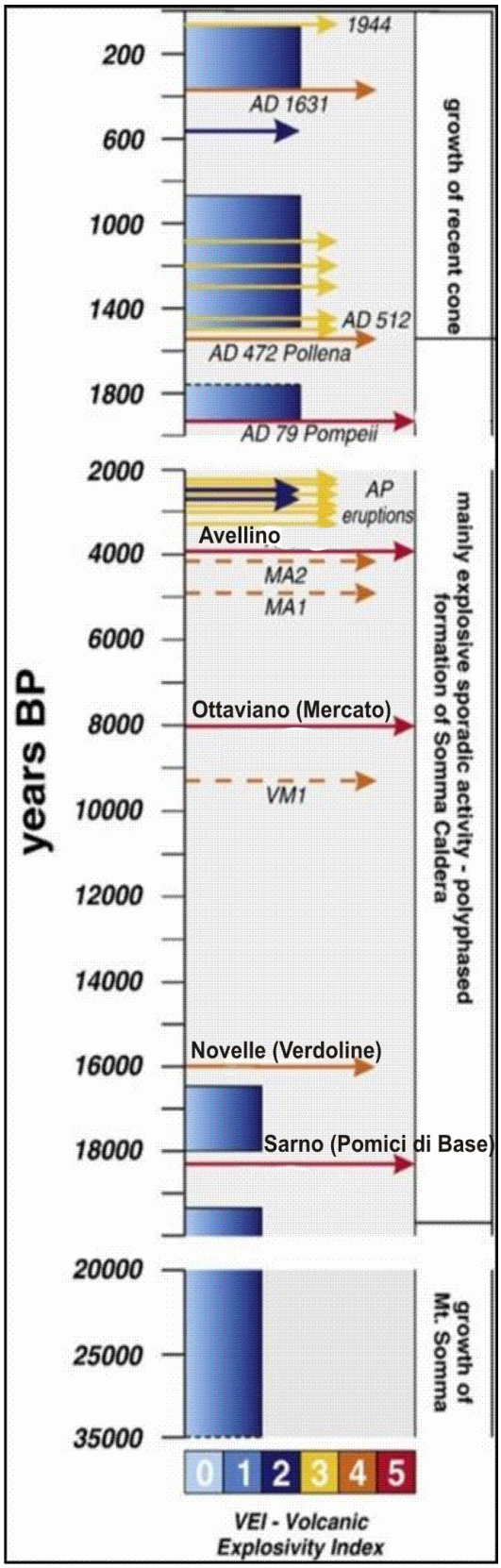

Figure 3.7 Reconstructed activities at Somma-Vesuvius for the last 33 Ky associated with the Volcanic Explosivity Index from Cioni et al. (2008) modified.

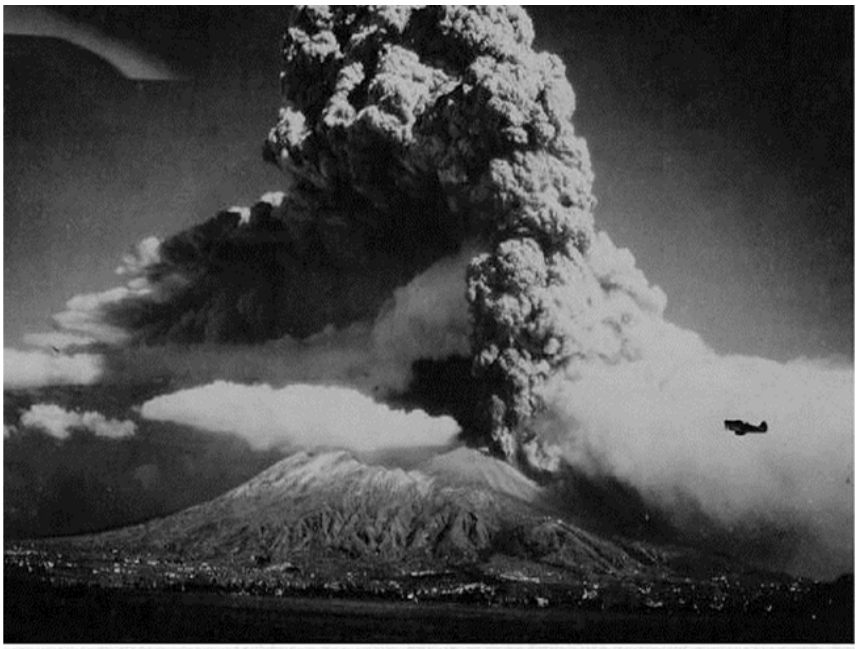

Figure 3.8 A suggestive photo of the 1944 Mt. Somma-Vesuvius Strombolian eruption which was took by the USA aviation during World War II.

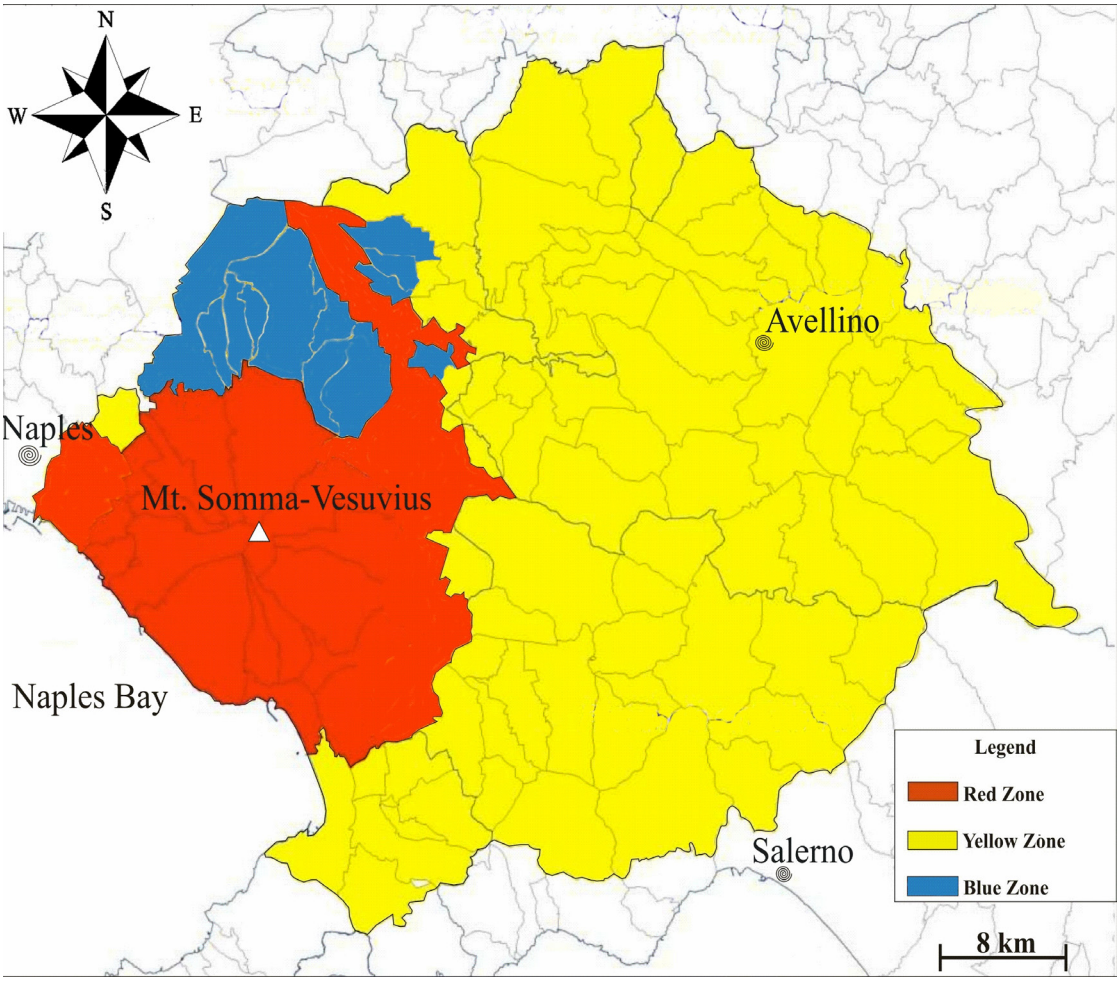

Figure 3.9 A hazards map from the Civil Protection Evacuation Plan redacted in 1995 and recently updated (2013).

Chapter 4: Sampling & Analytical Techniques

4.1 Introduction

A large number of samples have been collected on the Somma-Vesuvius over the last decades. Joron et al. (1987) report that between 1975 and 1985 approximately 500 rock samples have been collected. Belkin et al. (1993b) sampled all the recent lavas from AD 1631 to 1944 and Ayuso et al. (1998) studied additional 150 rock samples from the volcano.

All these specimens have been analysed in a number of studies by several authors and a large geochemical dataset is now available for almost the entire Vesuvius eruptive history (e.g.; Ayuso et al., 1998; Belkin et al., 1993b; Joron et al., 1987; Paone et al., 2001; Somma et al., 2001; Vaggelli et al., 1992; Villemant et al., 1993).

At the same time, mineralogy of Vesuvius eruptive products has received significantly less attention. Some analyses of clinopyroxenes and olivines have been published, (Barberi et al., 1981; Cioni et al., 1998; Cundari, 1982; Marianelli et al., 1995; Marianelli et al., 1999; Rahman, 1975; Rosi and Santacroce, 1983; Trigila and De Benedetti, 1993) but they do not cover the entire Somma-Vesuvius history and mostly are not statistically robust.

In light of the above and considering the scarce availability of material remaining from the previous campaigns, it was decided to organize and lead a new sampling.

4.2 Fieldwork

4.2.1 Sampling

Fieldwork within the Italian National Park of Vesuvius focused on collecting samples from the main Plinian pyroclastic deposits and some of the minor inter-Plinian lava deposits over the last 33 Ky. Sampling was undertaken in June - July 2010 under the supervision of the Dr Paola Petrosino. The samples have been collected from the base of the volcano where the majority of the pyroclastic Plinian deposits and lava flows from minor inter-Plinian events are located.

The sampling has been carried out using GPS (Global Positioning System), orthoimages of the interested areas, a geologic map of the Somma-Vesuvius volcanic complex (Santacroce and Sbrana, 2003b) and a topographic map (TAV. N° 448 III; Quadrante 184 I-SE, Pomigliano d'Arco; scale 1:25.000). GPS coordinates have been recorded for each sample. In total, 14 samples were collected from different localities as reported in figure 4.1 and table 4.1 ; 11 samples are from Plinian eruptions and 3 from minor inter-Plinian events. Below is a brief description of the main sampled eruptive deposits, based on our observations and also published

data (Lirer et al., 1993; Rolandi et al., 1993b; Rolandi et al., 1993c; Rolandi et al., 2004; Rolandi et al., 2008; Rolandi et al., 1998; Rosi et al., 1993; Rosi and Santacroce, 1983).

The Sarno (Pomici di Base) eruption (~ 22.03 Ka) is formed at the base by a series of fall deposits mainly constituted by white pumices and dark scoriae with subordinate surge deposits overlaid by volcanic avalanches, pyroclastic and surge flows enriched in the lithic components. Two samples from this eruption, "Lm5" and "Lm6", were collected from the top and bottom layer, respectively, of a ~ 50 cm thick pumiceous deposit prevalently formed by minor lithic fragments and consolidated pumices which evolve from dark grey at the base to light-grey in the upper part (Fig. 4.2a).

The Novelle (Pomici Verdoline) eruption (~ 19.2 Ka) generated a deposit formed at the base by a main fall pumice layer covered by a series of minor pyroclastic surge flows. The earliest fraction of this fall deposit evolves from grey to brown and green; these layers are rich in angular scoriae and pumice fragments which are variably vesicular with variable amounts of crystals. The lithic fragment fraction, prevalently formed by lava shards and carbonates, varies as a function of the stratigraphic position and distance from the volcanic conduit. Thin cineritic layers are interbedded to more coarse-grain fall deposits which display a planar stratification and are moderately sorted. The pyroclastic flows present only in the upper half of the stratigraphic sequence with the proximal deposits, are rich in the fine-grained fraction and in lithic clasts. Two samples, "Lm3" and "Lm4", were taken from a ~ 70 cm thick heterogeneous outcrop formed by coarse grained pumices and lava lithic clasts, all normally graded and lying on a well-developed paleosol (Fig. 4.2b).

The Ottaviano (Mercato) eruption (~ 8.9 Ka) is mainly characterized by fall deposits which are constituted of highly vesiculated pumice fragments (81-83%) and lava clasts that never exceed 40%. From this eruption, two samples, "Lm1" and "Lm2" were collected from the bottom and the top layer of a ~ 80 cm thick pyroclastic flow deposit, respectively. The deposit displays an inverse grading and is made up of pumice fragments and dark lithic clasts. The lithic fraction is responsible for the range of colours in the outcrop which varies from light grey in the base to rose-grey towards the top where the lithic clasts are more concentrated (Fig. 4.2d). The entire outcrop overlies a ~ 50 cm paleosol and is covered by thick flow deposits (~ 8-9 m) belonging to the same eruption.

The Avellino Eruption (~ 4.3 Ka) emitted prevalently fall deposits which resemble those from the Pompeii Eruption (A.D. 79). Overall, they are grey pumices (~ 20 %) and white pumices (~ 80 %) with subordinate lava fragments, carbonate and metamorphosed carbonate clasts abundant in every stratigraphic layer (Fig. 4.2c). Within 1 m thick deposit, two samples "Lfl1" and "Lfl2", have been taken from the base (white pumices) and the upper layer (grey pumices),

respectively.

The Pompeii Eruption (A.D. 79) emplaced fall and pyroclastic deposits as flows or surges. Similarly to the Avellino eruption, the majority of these deposits is formed by highly vesiculated white pumices (~ 80 %) at the base and by moderately vesiculated (~ 30-60 %) grey pumices in the upper part. From an ~ 80 cm thick outcrop located in the archaeological site "Villa 6 of the Renieri quarry" near Terzigno Village, two samples, "P1" and "P2", have been collected from the basal layer, mainly characterized by white pumices and rare lava lithic fragments, and the upper layer, formed by grey pumices and more abundant lithic components, prevalently lava clasts and carbonate fragments.

The Pollena sub-Plinian Eruption (A.D. 472) formed fall deposits on a large scale, distinguished by the emplacement of pyroclastic deposits alternated with debris and surge flows. The fall deposits vary in thickness across the volcano edifice from proximal to distal facies. Overall, four fall grey pumice layers rich in lithic clasts are distinguishable, superimposed by laminated flow materials with associated dry surges. These products are mostly constituted by juvenile or lava lithic fragments (> 70 wt %) and rare carbonate or metamorphic carbonate clasts. These clasts from the basal layers display a high degree of vesiculation, whereas the dark scoriae usually found at the top are less vesiculated. Considering the lack of compositional variations within this eruption, only one sample, "Lm8", has been collected from a ~ 3 m thick outcrop that is particularly rich in dark grey pumices with a minor lithic component (Fig. 4.2e).

In order to have a representative set of samples for the entire Vesuvius eruptive history, some rock samples were obtain from earlier collections (Ayuso et al., 1998; Belkin et al., 1993b). Their numbers and locations are reported in Table. 4.2 and Figure 4.3.

4.2.2 Mapping at ex-quarry Traianello

Geological mapping was conducted in order to better understand the relationships between the sampled volcanic stratigraphic units, their chronology and lithological characteristics, as well as the eruptive history of Somma-Vesuvius. The ex-quarry Traianello is located on the NE flank of the volcano between 200 and 300 m a.s.l. near the Somma-Vesuviana village. This location contains several well-exposed outcrops with clear relationships between different volcanic units. Mapping was conducted on a 1:5000 scale topographic map (Fig. 4.4). Outcrops labelled A, B, C, D, and E and the overall stratigraphic column are described below (Fig. 4.5).

Outcrop A is approximately ~ 3.5 m thick and is entirely formed by a massive flow deposit belonging to the Ottaviano (Mercato) eruption (~8.9 Ka). This deposit is made of centimetre-sized sub-rounded pumice clasts and massive lava lithic fragments (~ 1 m); these pumice clasts are mainly aphyric and, non-vesicular, seated in a cineritic matrix with a 1:1 ratio.

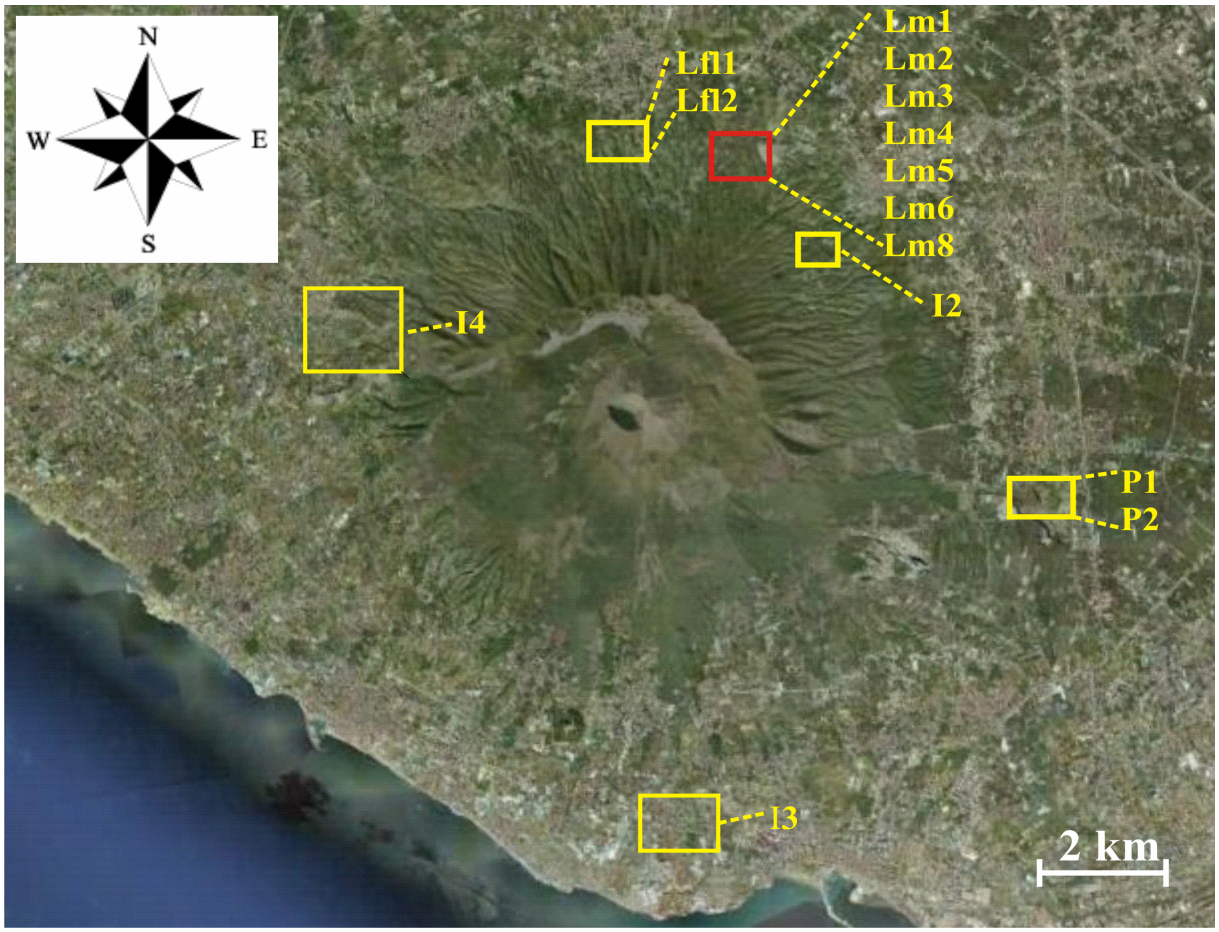

Figure 4.1 Satellite image of Mt. Somma-Vesuvius showing sampling locations.

Sample	*Locality*	*Coordinates*	*Age*	*Formation Name*	*Lithotype*
I3	Torre Annunziata - Lido Azzurro	40 °45′34′′ N - 14° 27′ 52′′ E	AD 472-1139	Medioeval ("AS")	Lava
Lm8	Traianello quarry - Somma-Vesuviana Village	40° 51′32′′ N - 14° 27′ 06′′ E - 270 m a.s.l.	AD 472	Pollena	Pumices
P1	Villa 6 - Terzigno Village	40° 51′54′′ N - 14° 26′ 29′′ E - 255 m a.s.l.	AD 79	Pompeii	White Pumices
P2	Villa 6 - Terzigno Village	40° 51′54′′ N - 14° 26′ 29′′ E - 255 m a.s.l.	AD 79	Pompeii	Grey Pumices
Lfl1	Madonna delle Grazie - Lagno Fossa dei Leoni	40° 51′54′′ N - 14° 26′ 29′′ E - 255 m a.s.l.	~ 4.3 Ka	Avellino	White Pumices
Lfl2	Madonna delle Grazie - Lagno Fossa dei Leoni	40° 51′54′′ N - 14° 26′ 29′′ E - 255 m a.s.l.	~ 4.3 Ka	Avellino	Grey Pumices
Lm1	Traianello quarry - Somma-Vesuviana Village	40° 51′26′′ N - 14° 27′ 05′′ E - 260 m a.s.l.	~ 8.9 Ka	Ottaviano (Mercato)	White Pumices
Lm2	Traianello quarry - Somma-Vesuviana Village	40° 51′26′′ N - 14° 27′ 05′′ E - 260 m a.s.l.	~ 8.9 Ka	Ottaviano (Mercato)	Grey Pumices
Lm3	Traianello quarry - Somma-Vesuviana Village	40° 51′31′′ N - 14° 26′ 59′′ E - 273 m a.s.l.	~ 19.2 Ka	Novelle (Verdoline)	Pumices
Lm4	Traianello quarry - Somma-Vesuviana Village	40° 51′31′′ N - 14° 26′ 59′′ E - 273 m a.s.l.	~ 19.2 Ka	Novelle (Verdoline)	Pumices
I2	Vallone San-Severino Zerrillo	40° 50′51′′ N - 14° 27′ 32′′ E - 250 m a.s.l.	22.03-19.2 Ka	Interplinian	Lava
Lm5	Traianello quarry - Somma-Vesuviana Village	40° 51′28′′ N - 14° 27′ 00′′ E - 256 m a.s.l.	~ 22.03 Ka	Sarno (Pomici di Base)	Grey Pumices
Lm6	Traianello quarry - Somma-Vesuviana Village	40° 51′28′′ N - 14° 27′ 00′′ E - 256 m a.s.l.	~ 22.03 Ka	Sarno (Pomici di Base)	Dark Grey Pumices
I4	San Sebastiano Village	40° 50′06′′ N - 14° 22′ 41′′ E	> 33 Ka	Pre-Codola	Lava

Table 4.1 List of samples collected during the present campaign.

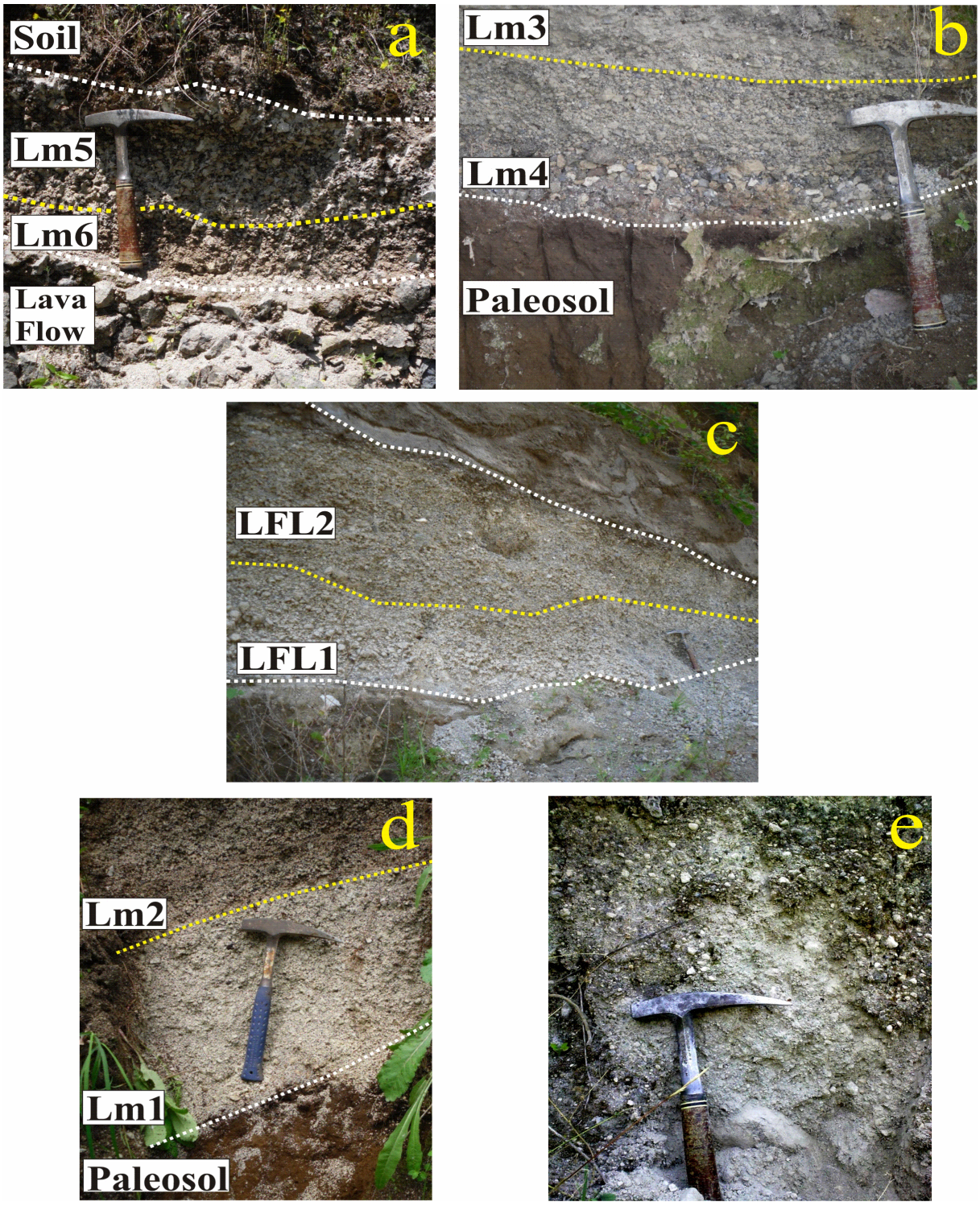

Figure 4.2 Representative outcrops. a) ~ 80 cm outcrop characterized by dark grey highly vesiculated lavas (> 33 Ka) at the bottom and ~ 50 cm of consolidated dark grey and white pumices at the top (Sarno-Pomici di Base eruption; ~ 22.03 Ka); samples, "Lm6" and "Lm5" were respectively collected from the two distinct pumiceous levels. b) A ~ 70 cm tick and heterogeneous outcrop composed by coarse pumices (Novelle-Pomici Verdoline eruption; ~19.2 Ka) normally graded; samples "Lm4" and "Lm3" belong correspondingly to the coarser and the finer pumiceous level. c) A ~ 1 m thick normally graded deposit (Avellino eruption, ~ 4.3 Ka); samples "Lfl1" is representative of the white pumice layer at the bottom, whereas "Lfl2" is from the grey pumice level. d) a ~80 cm thick pyroclastic flow deposit (Ottaviano-Mercato eruption; ~ 8.9 Ka); sample "Lm1" was collected from the finer white pumices layer at the base and sample "Lm2" from the coarser white pumices layer at the top. e) Basal part of a ~ 3 m thick deposit of dark grey pumices (Pollena Eruption; A.D. 472) from which sample "Lm8" was collected.

Sample	*Locality*	*Age*	*Formation name*	*Lythotype*
V61	Quarry 600 m NW Boccia al Mauro; 6.3 km ESE Grand Cone	AD 1834	Recent historic	Lava
V31	Torre Annunziata; C. Ranieri; 7 km S Gran cone	AD 1760	Recent historic	Lava
R6	San Pietro (200 m.a.s.l.); Terzigno	AD 1631	Renaissance Eruption (1631 A.D.)	Pumices
R1(1)	San Pietro (200 m.a.s.l.); Terzigno	AD 472-1139	Medieval ("AS")	Scoria
S20(1)	Case Pompili (200m.a.s.l.); S. Giuseppe Vesuviano	AD 79-472	Historic	Scoria
S16	Stone quarry (180 m. a.s.l.). Pozzelle; Boscoreale	~ 2.8 Ka	3rd Protohistoric (AP3)	Grey scoria
S12(1)b	Lagno Zabatta	~ 3.5 Ka	2nd Protohistoric (AP2)	Grey scoria
Scl12	Atrio del Cavallo; Valle del Gigante	> 33 Ka	Pre-Codola	Lava
Scl14	Atrio del Cavallo; Valle del Gigante	> 33 Ka	Pre-Codola	Lava

Table 4.2 List of samples from previous studies. (Ayuso et al., 1998; Belkin et al., 1993b).

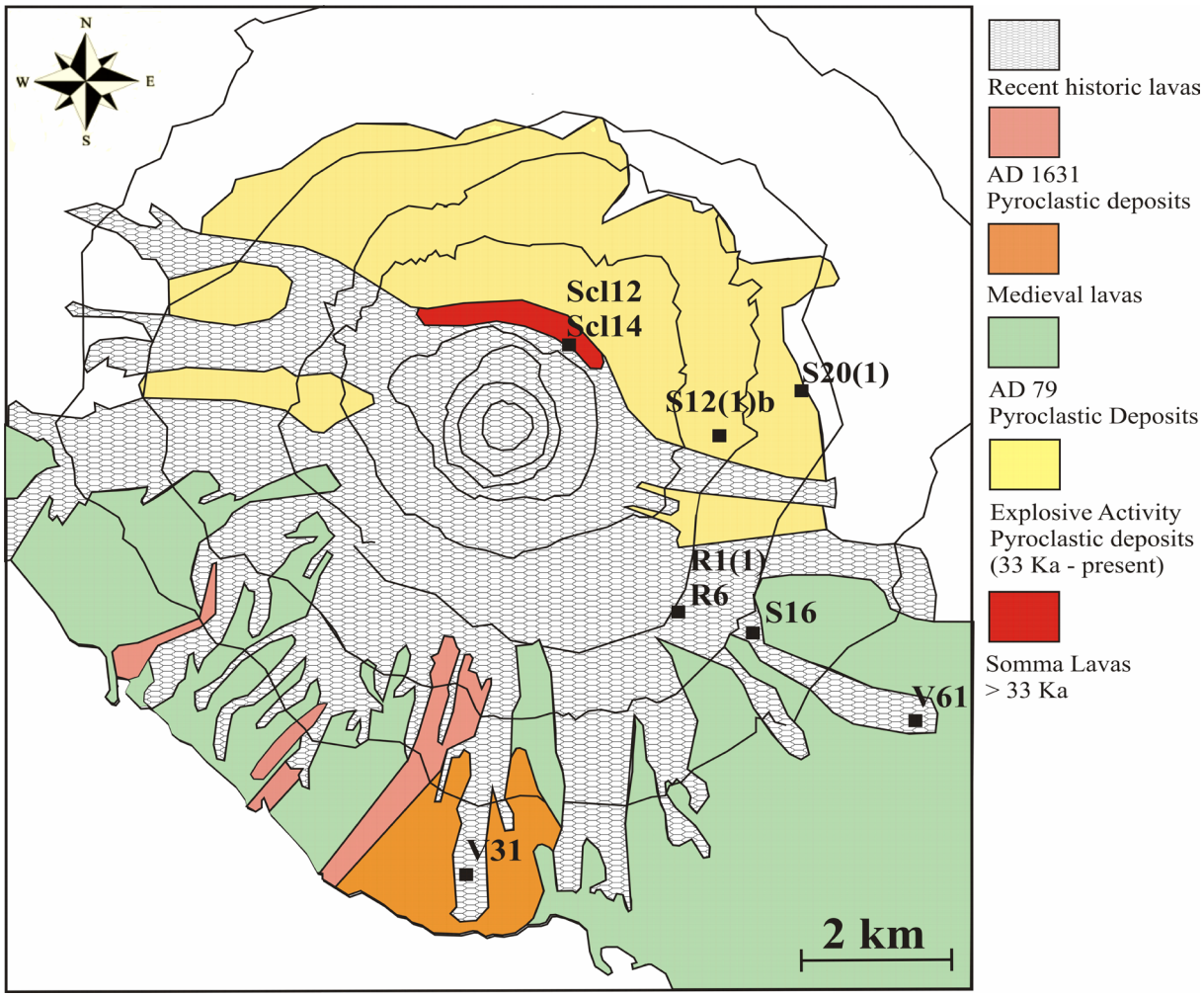

Figure 4.3 A simplified geological map of Mount Somma-Vesuvius from Ayuso et al. (1998) with the localities reported for the samples used in the present project (Ayuso et al., 1998; Belkin et al., 1993b).

Outcrop B is a ~ 3 m thick deposit produced by the Pollena eruption (A.D. 472). A ~ 2 m thick pyroclastic flow layer characterized by a cineritic matrix with a plane-parallel laminated structure and similar features to a surge, overlays a dark grey pumice fall deposit ~1 m thick.

Outcrop C is a massive deposit (~ 10-12 m) formed by the Ottaviano (Mercato) eruption (~ 8.9 Ka). From the base to the top it is formed by a ~ 30 cm paleosol, a ~ 80 cm fall pumice layer, and several flow deposits. Angular siliceous and lithic lava fragments 2 - 0.5 cm are particularly abundant in the pyroclastic layers (Fig. 4.2d).

Outcrop D (Fig. 4.6) is a ~18-20 m volcanic sequence which reveals the main Vesuvius eruptions deposits clearly juxtaposed from the base to the top, separated by paleosols. Approximately 10 m in the bottom part belong to the Novelle (Pomici Verdoline) eruption (~ 19.2 Ka). They are formed by coarse grained pumice layers < 30 cm thick alternated with coarse grained tuff layers also usually < 30 cm thick. In the central part of the sequence, there are 2 m of a volcanic breccia in which the lithic fraction is remarkably copious. Overall, the stratigraphic succession exhibits a plane-parallel laminated structure. Above, a ~ 80 cm layer of rosy angular and inversely graded pumices from the Phlegrean Fields eruption called "Pomici Principali" (~ 9-10 Ka) is separated from the underlying strata by a well-developed paleosol (~ 50 cm). In turn, this pumice layer is covered by another paleosol which is heavily eroded in the eastern part suggesting a relief inversion in the flank morphology. In the upper part, other fall and flow deposits which are related to the Ottaviano (Mercato) eruption (~ 8.9 Ka) characterized by coarse grained pumice and lithic clast lenses. Finally, the outcrop is sealed at the top by another paleosol and by ~ 1 m thick white and grey pumices deposits that are linked to the Avellino eruption (~ 4.3 Ka).

Outcrop E is ~ 1.5 m thick. This is the top part of a pyroclastic flow deposit from the Ottaviano (Mercato) eruption (~ 8.9 Ka). The base is not exposed. The deposit contains mainly coarse grained pumices (~ 2-5 cm) and lithic clasts lenses (~ 10-20 cm) at the base, whereas at the top only coarse angular pumices (~ 1) are observed, characterised by a double "inverse-normal" grading and without any matrix in the top part. This pyroclastic flow is not exposed in other sites within the area and it is a part of a pyroclastic current that likely interrupted the initial fall phase and was a product of a pulsating eruptive column. Overall, thickness and grain size is constant.

4.3 Sample preparation and analytical techniques

4.3.1 Sample preparation

All lava and pumice samples from both Plinian and inter-Plinian eruptions have been crushed in a metal mortar at the School of Earth Science (UTAS).The crushed material has been sifted obtaining 5 granulometric fractions:

- d > 2mm;
- 2 > d > 1 mm;
- 1 > d > 0.5 mm;
- 0.5 > d > 0.25;
- d < 0.25.

The two fractions between 2-0.5 mm have been examined under a binocular microscope. A total of 30-50 grains of clinopyroxenes and olivines were selected from each sample and mounted in epoxy using a double-sided sticky tape. The mounts were grinded to expose the crystals and then polished. The polished mounts were examined under an optical microscope to select crystals suitable for analyses. Individual crystals, as opposed to crystal aggregates, were selected. After that the samples where cleaned with methanol and carbon coated (25 nm) at the Central Science Laboratory (CSL) of the University of Tasmania.

4.3.2 Analytical techniques

The selected crystals were analysed by an electron microprobe (EMPA) and a laser ablation inductively couple plasma mass spectrometer (LA-ICP-MS). Major elements were measured on Cameca SX100 EPMA housed at the CSL. The instrument is fitted with 5 WDS spectrometers with LiF, PET, TAP, and PC0 to PC2 analysing crystals, also integrated with a Röntec X-Flash 1204 Be-window SDD EDS with Bruker Quantax 200 Esprit software (elements Na-U), Cameca SE, BSE and CL detectors as well as an optical microscope (reflected/transmitted light, zoom, polariser). Samples were probed with a beam size of 5 μm at 15 keV – 20-30 nA. Kakanui Augites, New Zeland (USNM 122142) and San Carlos Olivine, Arizona (USNM 111312/444) were used as calibration standards (Tab. 4.3); Jarosewich et al. (1979)) and they were analysed twice at the beginning and end of each session. The following major elements were analysed in clinopyroxenes: SiO_2, TiO_2, Al_2O_3, FeO, MnO, MgO, CaO, Na_2O, Cr_2O_3, and NiO whereas only SiO_2, FeO, MnO, MgO, CaO, Cr_2O_3 and NiO in olivines. The data were normalized following the procedure of Melson et al. (1976) which allows for reducing the session by session drift from the ideal standard values. Trace elements were analysed at the CODES analytical facility, University of Tasmania, equipped with a Resonetics Resolution

Ar-F Excimer laser ablation system and a S155 large format cell. The instrument is coupled to an Agilent 7500cs ICP-MS. Samples were ablated at spots sizes of 44-110 μm with energy at the sample of ~3.5 J/cm^2, in a He atmosphere (flow rate 0.35 L/min) and the aerosol mixed with Ar carrier gas (flow rate 0.95 L/min) for transport to the ICP-MS. NIST612 was used as the primary standard for calibration and drift correction, and GSD-1G (USGS, USA) was used as a secondary standard (Max Planck Institut (2013); tab. 4.4). Both NIST612 and GSD- 1G were analysed at the beginning and after every ~ 25 analyses in order to minimize the instrumental drift. Ca from clinopyroxene and Mg from olivine probe analyses were used for the internal standardisation; this method which combines internal standards with external reference materials was separately developed by several authors (e.g., Jackson et al., 1992; Ludden et al., 1995) and is currently considered the standard approach (Longerich et al., 1996). The following isotopes were measured: Li^{7}, K^{39}, Sc^{45}, Ti^{51}, V^{51}, Cr^{53}, Co^{59}, Ni^{62}, Cu^{63}, Cu^{65}, Zn^{66}, Sr^{88}, Y^{89}, Zr^{90}, Nb^{93}, Ba^{137}, La^{139}, Ce^{140}, Nd^{146}, Sm^{147}, Eu^{153}, Gd^{157}, Dy^{163}, Er^{166}, Yb^{172}, Lu^{175}, Hf^{178}, Ta^{181}, Pb^{208}, Th^{232} and U^{238} with counting times of 0.01 0.04 seconds for each mass and a total sweep time of 0.82 sec. Depending on the range of mineral compositions as revealed by EMPA analyses, among 10 to 40 crystals of each mineral were analysed from each sample. At least two analyses were performed on each crystal, one in the core and the other in the rim, to assess the internal chemical crystal heterogeneity. In addition, mineral inclusions exposed on the surface were also analysed measuring the following elements: SiO_2, TiO_2, Al_2O_3, FeO, MnO, MgO, CaO, K_2O, Na_2O, Cr_2O_3, NiO, P_2O_5, SO_3, SrO, BaO and Cl. A series of representative backscattered high resolution images were collected at 15 KeV for each sample using the Hitachi SU-70 field emission scanning electron microscope (FESEM) at the CSL, equipped with a Schottky thermal field emission source, Hitachi in-chamber and in-lens scintillation detectors, super ExB filter, beam deceleration, a Hitachi in-chamber 5-segment solid state BSE detector, retractable, and in-column Faraday cup. The technique was used to assess zoning patterns in major elements (Blundy and Cashman, 2008).

Stoichiometry was used to assess the quality of EMP analyses. For clinopyroxene, only analyses with the sum of cations of 3.95 to 4.05 (per 6 oxygen) were accepted, whereas for olivine the acceptable range was 2.95 – 3.05 (per 4 oxygens).

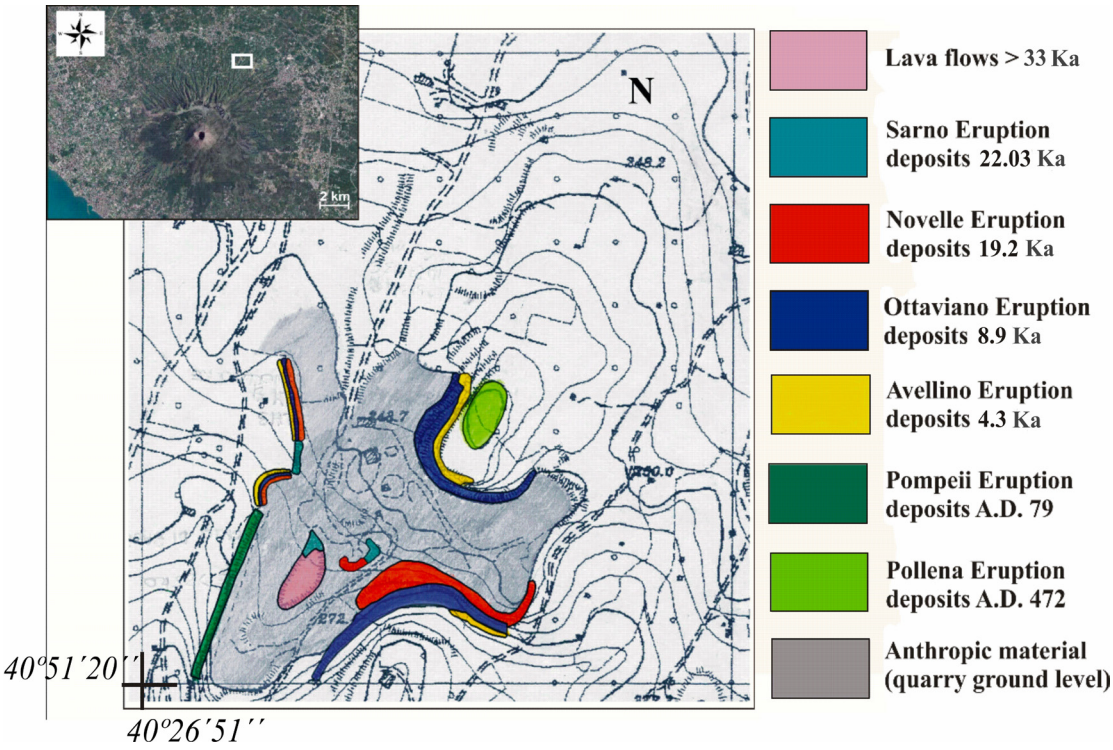

Figure 4.4 A geologic map of the ex-quarry Traianello (1:5000).

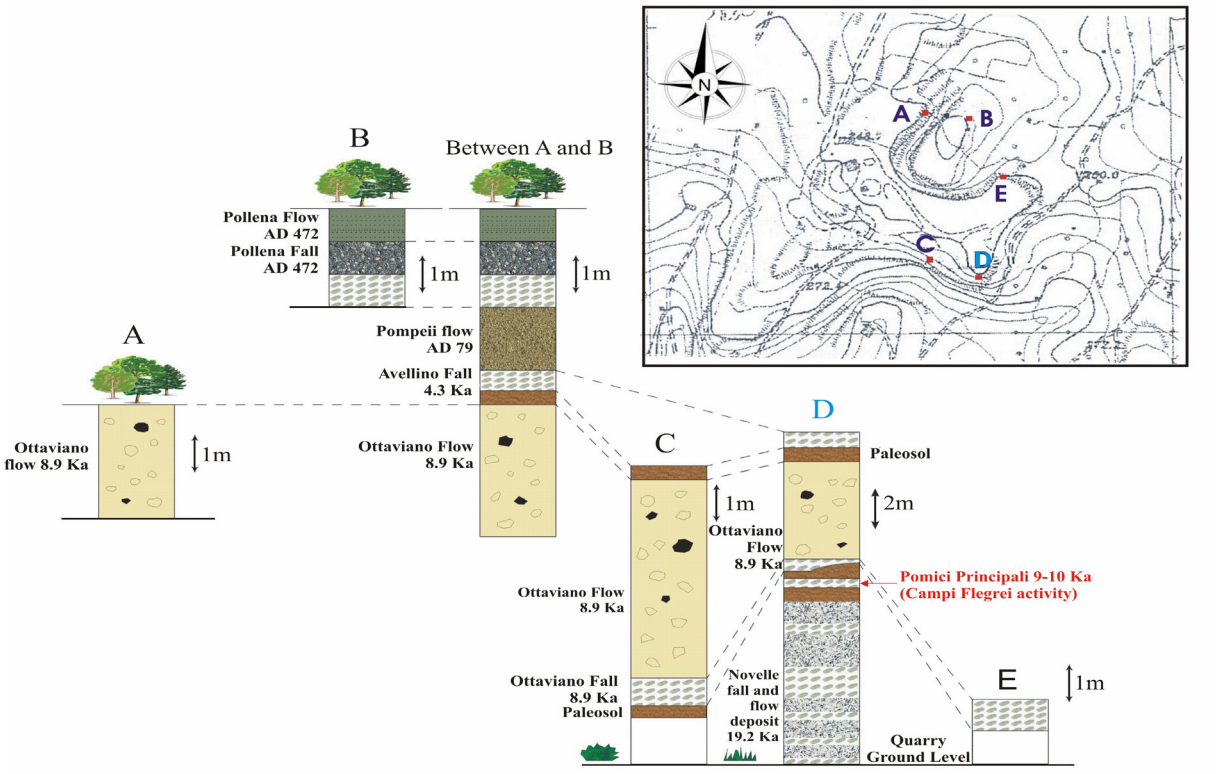

Figure 4.5 Five stratigraphic columns are referred to as many outcrops whose location is reported in the map (1:5000) on the right top and are respectively labelled as A, B, C, D, and E.

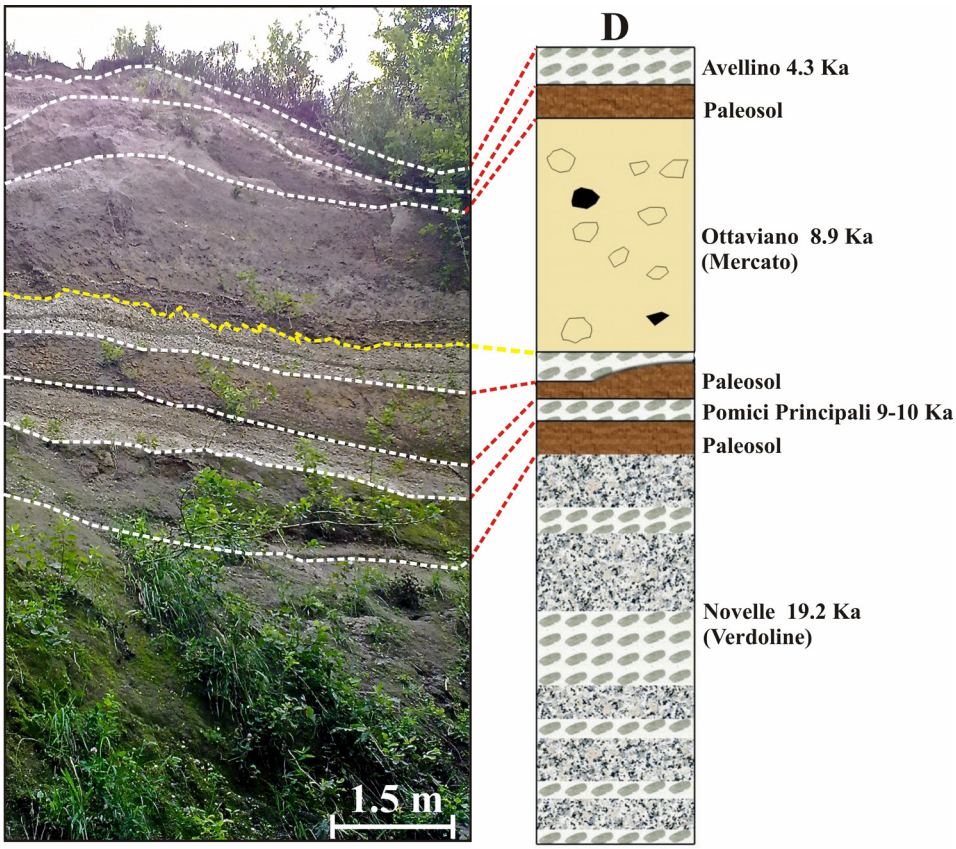

Figure 4.6 A photo of the outcrop D is reported on the left side of this figure; dotted lines distinguish different stratigraphic layers belonging to the same eruptive event (yellow line) or to different eruptions (white lines); whereas, on the right there is the related stratigraphic column.

Element	Augite *KANZ*	Olivine *SCOL*
Al_2O_3	8.73	
CaO	15.82	0.1
Cl		
CoO		
Cr_2O_3		
F		
FeOTot	6.37	9.55
H_2O	0.04	
K_2O		
MgO	16.65	49.42
MnO	0.13	0.14
Na_2O	1.27	
NiO		0.37
P_2O_5		
SO_3		
SiO_2	50.73	40.81
TiO_2	0.74	
V_2O_5		
ZnO		
Tot	100.48	100.39

Table 4.3 EMPA Augite (KANZ) and Olivine (SCOL) standard elements values from Jarosewich et al. (1979) expressed in wt %.

Element	Nist-612	Gsd-1G	Element	Nist-612	Gsd-1G
Li^{7}	42.00	43.00	Ba^{137}	39.70	67.00
Na^{23}	103704	26707	La^{139}	35.77	39.10
Mg^{25}	64.00	21709	Ce^{140}	38.70	41.40
K^{39}	66.26	25300	Nd^{146}	35.90	44.70
Ca^{43}	85264	51457	Sm^{147}	38.10	47.80
Sc^{45}	41.05	52.00	Eu^{153}	35.00	41.00
Ti^{49}	44.00	7431.85	Gd^{157}	36.70	50.70
V^{51}	39.22	44.00	Dy^{163}	36.00	51.20
Cr^{53}	36.00	42.00	Er^{166}	38.00	40.10
Co^{59}	35.26	40.00	Yb^{172}	39.20	50.90
Ni^{62}	38.80	58.00	Lu^{175}	37.18	51.50
Cu^{65}	37.00	42.00	Hf^{178}	37.90	39.00
Zn^{66}	37.92	54.00	Ta^{181}	35.90	40.00
Sr^{88}	78.40	69.40	Pb^{208}	38.57	50.00
Y^{89}	38.25	42.00	Th^{232}	37.79	41.00
Zr^{90}	37.72	42.00	U^{238}	37.40	41.00
Nb^{93}	40.00	42.00			

Table 4.4. LA-ICP-MS standard primary (NIST612) and secondary (GSD-1G) elements values reported in ppm (Jochum et al., 2005).

Chapter 5: Mineralogy of clinopyroxene at Somma-Vesuvius

5.1 Introduction

This chapter provides a detailed description of the mineralogy and chemistry of clinopyroxene from the Somma-Vesuvius volcanic products. The chapter consists of four sections; the first two describe the distinctive properties which characterize these phenocrystals, such as macroscopic appearance and zoning, whereas the other two sections are focused on mineral composition/ phenocrystals distribution, and compositional variations in major, minor and trace elements within the three mega-magmatic cycles (Ayuso et al., 1998; Joron et al., 1987; Somma et al., 2001). Within each of these sections, a sub-section is dedicated to a comparison between the Somma-Vesuvius clinopyroxenes with those from other tectonic settings and especially the RCP. Mineral inclusions in Somma-Vesuvius clinopyroxene phenocrysts are also discussed.
Discussion on major, minor and trace elements in Somma-Vesuvius clinopyroxenes is based on a database of 1162 EMPA analyses for major elements and 624 LA-ICPMS analyses for trace elements.

5.2 Pyroxenes: a brief overview

Pyroxenes are widespread terrestrial rock-forming minerals (inosilicates) which are present in almost every type of igneous rock; their structure involves alternating "tetrahedral" and "octahedral" layers that are arranged parallel to the {100} plane. In each tetrahedral layer, every SiO_4 is bonded to the adjacent tetrahedra sharing an oxygen anion (Deer et al., 1966), and long chains are formed by the repetition along the c axis of a two tetrahedra cell unit which is ~ 5.2 Å in length. The octahedral layer is composed by M1 and M2 sites; M1 is a 6 coordinated site whereas M2 can be either 6 or 8 coordinated. The general formula of pyroxenes is usually expressed as "$M2M1T_2O_6$" where M2 and M1 are respectively distorted and regular octahedral sites whereas T is tetrahedral. Several cations can be allocated in M2 and M1; in general, M2 is occupied by Na, Ca, Mn^{2+}, Fe^{2+}, Mg^{2+} and Li whereas M1 by Al, Fe^{3+},Cr^{3+}, Ti^{4+}, Mg, Fe^{2+} and Mn; the T site normally accommodates Si or Al which is a common substitution (Cameron and Papike, 1980). However, the cations repartition among the three crystallographic sites is partly temperature dependent and as a consequence the exact site occupancy must be verified by structural analysis (Morimoto, 1988). Pyroxenes belong to both orthorhombic and monoclinic crystallographic groups; typically their composition falls inside the so-called "pyroxenes

quadrilateral" whose end-members are $CaMgSi_2O_6$ (Diopside), $CaFeSi_2O_6$ (Hedenbergite), $Mg_2Si_2O_6$ (Enstatite) and $Fe_2Si_2O_6$ (Ferrosilite). Orthorhombic pyroxenes have essentially a restricted composition with $Ca_2Si_2O_6$ molecule < 5 wt % and the cations which occupy the M2 site are only in coordination IV. Instead, monoclinic pyroxenes that are more commonly referred as clinopyroxenes (usually abbreviated as cpxs) are formed by three main space groups which are reported in literature as C2/c, P2/c and P2/n. The stability field of these phases is temperature and pressure dependent; Diopside and Hedenbergite form a complete solid solution series both at atmospheric pressure and at P > 1 atm (e.g. Huebner, 1980; Lindsley, 1980). Clino-enstatite and clino-ferrosilite are very rare in terrestrial rocks and compositions between the two series are partially occupied by Pigeonite and Augite which forms a complete solid solution with Diospide and Hedembergite.

5.3 Clinopyroxenes at Somma-Vesuvius

5.3.1 Distinguishing features

Clinopyroxene is an omnipresent mineral phase in all lava, scoriae and pumices samples investigated in the present project; this is a common feature of all Somma-Vesuvius products (e.g., Joron et al., 1987; Rahman, 1975; Santacroce, 1987).

Overall, these phenocrystals have a vitreous texture, a prismatic euhedral or sub-euhedral habit, with some specimens totally anhedral. They occur in the entire sample collection both as phenocrystals ranging in size between 0.5 mm and > 2 mm and micro-crystals in the groundmass with dimensions < 0.5 mm. Two common types of clinopyroxenes are present, a translucent pale-green richer in Mg, and an opaque dark-green richer in Fe. The latter is common in all lava, pumice and scoriae samples from Somma-Vesuvius (Barberi et al., 1981; Cioni et al., 1998; Joron et al., 1987; Thompson, 1973). Both types are present in the volcanic products younger than 19.2 Ka which are significantly more phyric (Joron et al., 1987). Both types are characterized by complex zoning which is an indication of their intricate crystallization history (Cioni et al., 1998). Fluid, melt and mineral inclusions are common in all pyroxenes (e.g., Belkin and De Vivo, 1993a; Belkin et al., 1998; Lima et al., 2003; Vaggelli et al., 1992; Vaggelli et al., 1993; Webster et al., 2001).

5.3.2 Zoning: a common feature of Somma-Vesuvius clinopyroxenes

Zoning is a common phenomenon occurring in many different mineral phases in volcanic rocks (e.g., Barton and Bergen, 1981; Barton et al., 1982; Dobosi, 1989; Duda and Schmincke, 1985; Shore and Fowler, 1996). At Somma-Vesuvius zoning in clinopyroxenes was documented in several studies (Cioni et al., 1998; Cundari and Salviulo, 1987; Thompson, 1973).

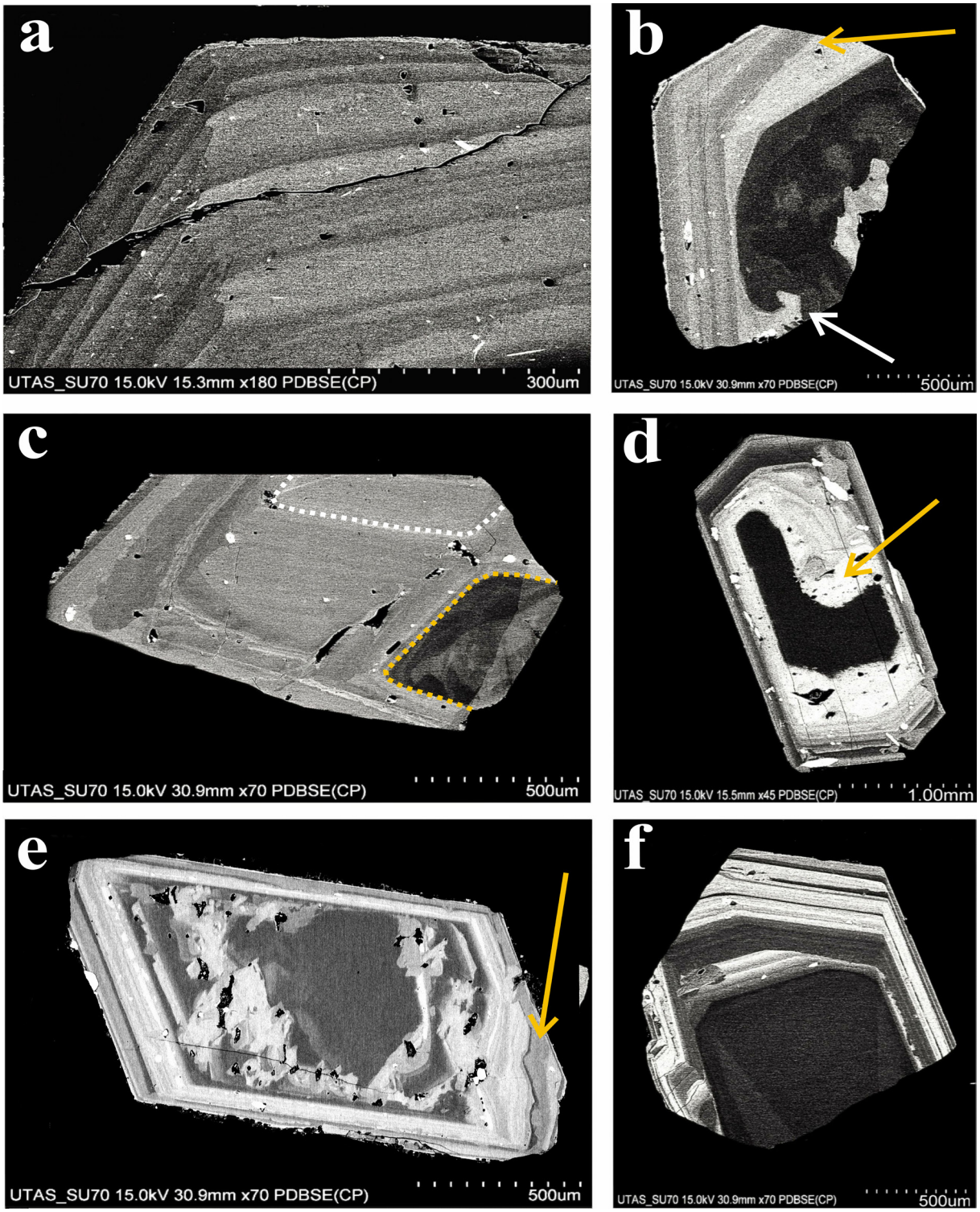

Figure 5.1 a-f. SEM-BSE images of strongly zoned diopside phenocrysts from representative Somma-Vesuvius lava, scoriae and pumice samples covering the last 33 Ky. a) Rounded corners and single grown-layers varying in thickness and composition in a cpx from the lava sample SCL12 (> 33 Ka). b) Example of a localized angular unconformity between grown-layers (yellow arrow) and dissolution-resorption phenomena (white arrow) within a cpx from the pumice sample LM3 (Novelle Plinian eruption, ~19.2 Ka). c) Two pre-individual cpx crystals that merged within a single phenocryst which belongs to the pumice sample LM2 (Ottaviano Plinian eruption, ~8.9 Ka) and whose presumed original nuclei are respectively underlined by white and yellow dash-lines; these two crystals fused together at a certain time during their volcanic history within the volcanic plumbing system likely through a synneusis process. d) An euhedral prismatic cpx crystal from the grey scoria, S12(1)b (Protohistoric period, ~ 3.5 Ka) which shows changing in thickness of grown-layers and a massive nucleus resorption phenomenon (yellow line). e) Embayed grown-layers within an euhedral parallelogram-like clinopyroxene from the scoria sample, R1(1) (A.D. 472-1139) f) A strongly zoned clinopyroxene crystal belonging to the scoria sample S20(1) (A.D. 79-472) characterized by layers with different thickness and a partially homogeneous core contoured by rounded corners.

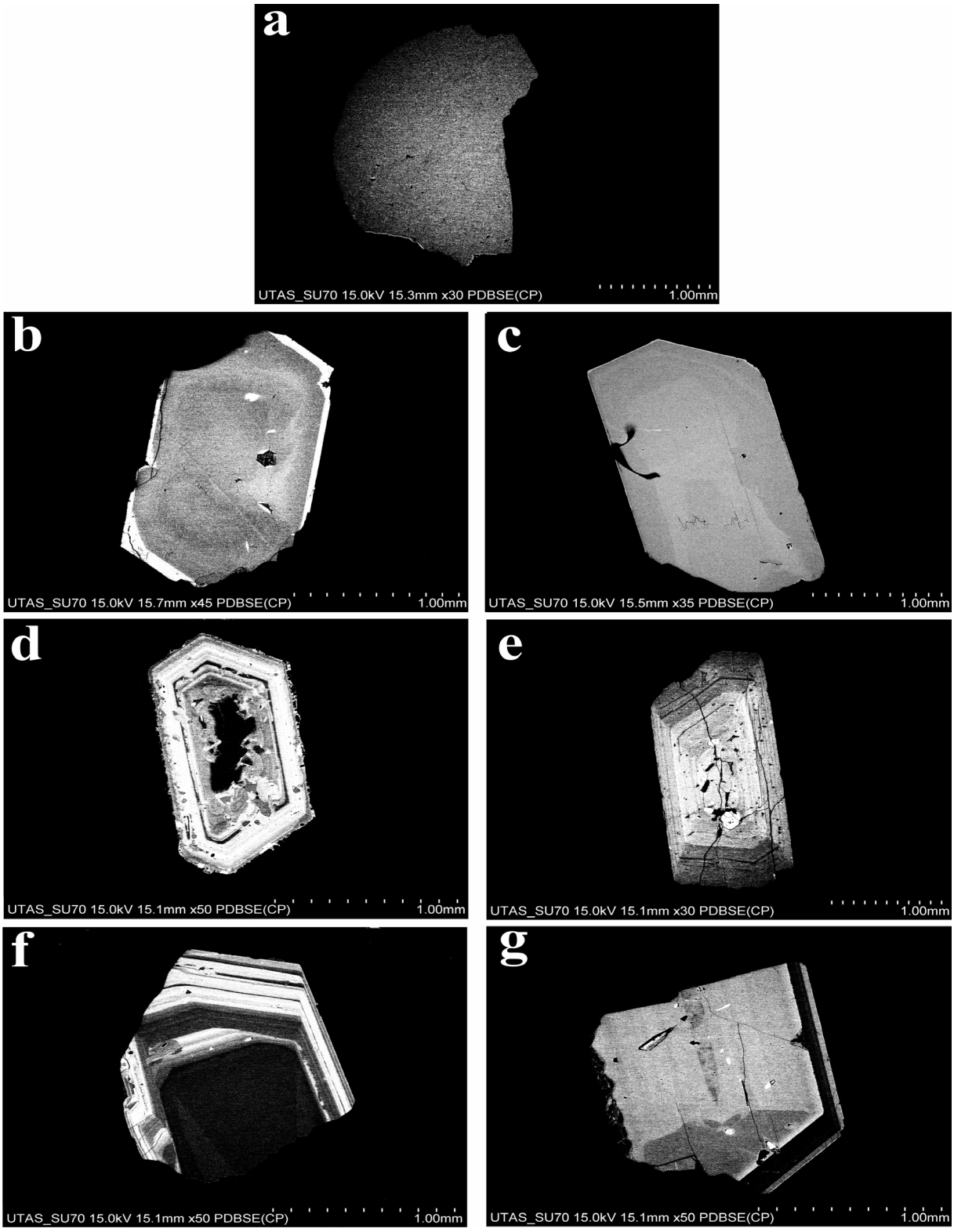

Figure 5.2 a-g SEM-BSE images of representative zoning types in clinopyroxene phenocrysts at Somma-Vesuvius for the last 33 Ky. a) Reverse diffuse zoning in a sub-ehuedral phenocryst from the Avellino Plinian eruption top layer (~ 4.2 Ka) b) and c) Normal and reverse zoning in euhedral prismatic phenocrysts from the Novelle Plinian eruption (~ 19.2 Ka). d) and f) Normal and reverse complex oscillatory zoning in euhedral prismatic crystals respectively belonging to the ancient Somma-Vesuvius non-Plinian activity (> 33 Ka) and to an historic inter-Plinian eruption (A.D. 79-472); the specimen "e" is also a clear example of a superimposed hour-glass zoning along the (I00)-sector (Ferguson, 1973). f) and g) Roughly-monotematically cores sorrounded by complex oscillatory zoned margins in normally and reversely zoned crystals from the Plinian Sarno eruption (~ 22.03 Ka) and a historic inter-Plinian eruption (A.D. 79-472), respectively.

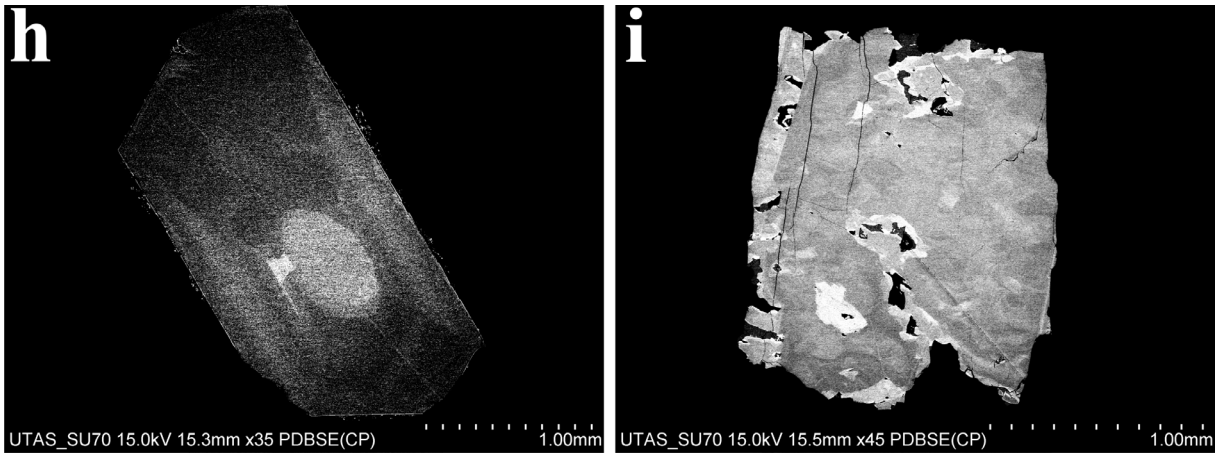

Figure 5.3 h-i. SEM-BSE images of minor zoning types in clinopyroxene phenocrysts at Somma-Vesuvius. h) Euhedral clinopyroxene specimen characterized by hour-glass zoning oriented along the b-axis, parallel to (0I0) section, from the Avellino Plinian eruption (~ 4.2 Ka). i) Sub-euhedral clinopyroxene specimen interested by a widespread patchy zoning which affects both core and rim, from the lava sample V31 (A.D. 1760).

Several zonation types were recognized within each sample studied from all eruptions. This likely points to common mechanisms governing their crystallization history (Shore and Fowler, 1996). The interpretation is complicated by the occurrence of minor structures such as embayed faces, single growth-layers that vary in thickness, rounded corners, angular "unconformities", dissolution cross-bedding among layers, as well as crystals aggregates produced by synneusis, which were also observed over the entire clinopyroxene phenocrysts set (Fig. 5.1). Such minor structures are commonly connected to changes in the magmatic conditions such as pressure or compositional variations due to magma mixing (Vernon, 2004).

Different types of clinopyroxene zoning are present at Somma-Vesuvius. The main type is normal zoning from diopsidic towards more salitic compositions, as confirmed by chemical analyses. However, albeit rare, reversely zoned phenocrysts were found in all eruptions. Within the 18 investigated eruptions, 4 main types of zoning were recognized. Although these zoning types were described by Cioni et al. (1998), some significant differences in their characteristics and occurrence were found in the present project.

The "a" type cpx crystals (Fig. 5.2) are present in both Plinian and inter-Plinian Somma-Vesuvius products younger than 19.2 Ka. They display diffused reverse zoning from "Fe-Salite to Salite". No normally zoned crystals of this type were found, contrarily to what was reported by Cioni et al. (1998). Such reversely zoned phenocrysts are commonly found within alkaline magmas and are often reported in the literature as "green cores" (Barton and Bergen, 1981; Brooks and Printzlau, 1978; Dobosi, 1989; Duda and Schmincke, 1985).

The "b" and "c" types (Fig. 5.2) were found mainly in the pumice samples from Plinian activity, and in only two Medieval scoriae samples (I3 and R1(1)). More common is the normally zoned "b" type which is formed by a roughly homogeneous diopsidic core and a salitic margin, referred

to as monotonous “textureless” zoning (Streck, 2008). Instead, the “c” type which consists of a salitic core and a diopsidic margin occurs more rarely.

The “e” and “d” types (Fig. 5.2) display a complex oscillatory zoning that involves two alternating compositional end-members, diopside and salite, whose compositions gradually shift towards more iron-rich compositions in normally zoned crystals, or towards more Mg-rich compositions in the reversely zoned specimens. Each growth-shell is usually parallel to the crystallographic planes of low Miller indices and varies in thickness from tens of nanometers to several tens of micrometers, (“fine banding” and “coarse banding”, respectively). The origin of fine banding is possibly kinetically controlled whereas coarse banding may be related to magmatic dynamics (Downes, 1974). Both normal and reverse complex oscillatory zoning patterns were commonly found in all inter-Plinian lava and scoriae samples whereas they are less common in Plinian pumice samples. In the Pompeii (A.D. 79) and in the Renaissance (A.D. 1631) eruptions such pyroxenes were not found.

The last main zoning type is represented by clinopyroxene phenocrysts with a largely homogeneous core surrounded by an outer complex oscillatory zoned rim, the “f” and “g” types of figure 5.2. They are present in all Plinian rock samples but are scarce in Plinian and sub-Plinian products < 4.2 Ka. This type is also present in the inter-Plinian scoria and lava samples of the last 2000 years, but was not found in older inter-Plinian products.

In addition, 2 other minor zoning types were found in the Somma-Vesuvius clinopyroxene population: sector “hour-glass” zoning and patchy zoning. The first type is a common feature of clinopyroxene from silica-undersaturated lavas (Ferguson, 1973; Downes, 1974; Hollister and Gancarz, 1971; Leung, 1974; Nakamura, 1973). It consists of opposite sectors with identical optical and chemical properties which are visibly distinct from the other pair of sectors within the same phenocryst. At Somma-Vesuvius this type is frequently superimposed on the zoning types described above (Fig. 5.3h), and was found in the Plinian clinopyroxenes only.
The patchy zoning is an irregular distributed zoning pattern which may form during crystal growth or diffusive re-equilibration (Stewart and Pearce, 2004; Streck et al., 2007; Tomiya and Takahashi, 2005). At Somma-Vesuvius, this zoning type is present in all samples from every eruption styles. It occurs as different patches separated by sharp compositional transitions as, for example, on Figures 5.2g and 5.3i (Streck, 2008; Vance, 1962). As evident from the above images, different zoning types are frequently superimposed within a crystal, which a common phenomenon in volcanic systems.

Unzoned clinopyroxene phenocrystals were found over the entire range of crystal compositions,

however not in every eruption. They are commonly found in pumice samples from Plinian eruptions < ~ 22 Ka, but were not found in lavas > ~ 19.2 Ka, and are rare in the younger scoria samples associated with inter-Plinian activity (< 19.2 Ka).

5.3.3 Mineral compositions and population distributions

Overall, clinopyroxene phenocrysts from Somma-Vesuvius reveal a major element compositional range spanning from $Mg\#_{93.4\text{-}71.4}$, $Wo_{44.2\text{-}51.5}$, $En_{34.7\text{-}50.4}$, $Fs_{3.4\text{-}14.6}$ (Fig. 5.4); according to the Commission on New Minerals and Minerals Names of the International Mineralogical Association (Morimoto, 1988) these phenocrysts are all classified as "Diopside" belonging to the Diopside-Hedenbergite series ($CaMgSi_2O_6$- $CaFeSi_2O_6$); although, some specimens lie above the CaMg-$CaFe^{2+}$ node. Following Poldervaart and Hess (1951) these clinopyroxenes are classified as "Diopside", "Aluminian Salite" and "Fassaite" (Fig. 5.5). Phenocrysts from the lava samples older than 22.03 Ka are restricted to the Salite field whereas the few fassaitic specimens come prevalently from the Somma-Vesuvius activity younger than 4.3 Ka, suggesting to some extent Ca enrichment within the more Fe-rich clinopyroxenes over the time.

The range of clinopyroxene compositions in terms of Mg# (Mg/(Mg+Fe)) is presented as histograms on Figures 5.6, 5.7 and 5.8.

In lava flows from inter-Plinian eruptions older than 19.2 Ka (the first compositional cycle of Somma-Vesuvius activity after Ayuso et al., 1998; lava samples SCL12, SCL14, I4 and I2; Fig. 5.6) a single clinopyroxene population is present with compositions $Mg\#_{83\text{-}72}$. The clinopyroxenes in these samples are dark-green phenocrystals. However, clinopyroxenes in pumices of the two Plinian eruptions which occurred during that time, Sarno (~22.03 Ka) and Novelle (~ 19.2 Ka), are characterised by a modal distribution of clinopyroxene Mg# (Fig. 5.6). The first population is similar in composition to the lavas, whereas the second population is much more magnesian, with $Mg\#_{93\text{-}84}$. The two populations are present in approximately equal proportions.

The two Plinian eruptions with the 2nd geochemical cycle of Ayuso et al., (1988), the Ottaviano (~ 8.9 Ka) and Avellino (~ 4.3 Ka) eruptions are also characterized by a bimodal distribution of clinopyroxene compositions (pumice samples LM1, LM2, LFL1, and LFL2; Fig 5.7). In terms of their compositional range, the two populations are essentially identical to those in the older Plinian eruptions. The two samples from the Ottaviano eruption display similar distribution patterns characterised by a larger proportion of crystals from the more evolved population. The two samples from the Avelino eruption display different distribution. Within the basal layer, corresponding to the onset of eruption, the two populations are present in approximately

equal proportions, whereas in the sample from the top of the layer almost all clinopyroxene phenocrysts belong to the more primitive population. It is also worth noting that within the high-Mg# population in this sample the most common phenocrystals are those with the highest Mg# values.

The inter-Plinian period which follows the Avellino eruption, the so-called "Protohistoric" period (4.3 Ka – A.D.79) is represented by two scoriae samples (S12(1)b, ~ 3.5 Ka and S16, ~ 2.8 Ka; Fig 5.7) which are also characterised by the two population of clinopyroxene with the same compositional range. In both samples, the more primitive population is clearly more abundant, constituting ~ 70% of the phenocrysts.

The Plinian and sub-Plinian eruptions within the 3rd geochemical cycle of Ayuso et al., (1988), the Pompeii (A.D. 79), Pollena (A.D.472) and Renaissance (A.D. 1631) eruptions (samples P1 and P2, Fig. 5.7; samples LM8 and R6, Fig. 5.8) are also characterised by bimodal distributions of clinopyroxene compositions. However, unlike in the older Plinian eruptions, clinopyroxene in all pumice samples from these younger eruptions is clearly dominated by the high-Mg# population. Similar to the Avellino eruption, at the top of the Pompeii pumice layer only the high-Mg# population of clinopyroxene is present

The inter-Plinian activity during the 3rd geochemical cycle (samples S20(1) (pumice; A.D.79-472); R1(1), I3 (both scoriae; A.D.472-1139); V31 (lava; A.D.1760), and V61 (lava; A.D.1834); Fig. 5.8) is characterised by the presence of two clinopyroxene populations. The high Mg# population is clearly more abundant.

In summary, all samples studied are characterised by a significant range of Mg# of clinopyroxene phenocrysts. The range of phenocryst compositions remains effectively the same over the time span of the Somma-Vesuvius activity studied here.

In order to ensure that the samples we studied are representative, their compositions are compared to the compositions of Somma-Vesuvius eruption products on figure 5.9. As demonstrated previously (Ayuso et al., 1998; Joron et al., 1987, see Chapter 4), there is a clear change in rock compositions over the last 30,000 years. The oldest rocks (Group 1) are the least silica under-saturated, having the highest SiO_2 contents and the lowest alkali contents. The most evolved rocks of this group (< 3 wt% MgO) are also characterised by lower Al_2O_3 contents compared to the younger lavas, likely reflecting late fractionation of feldspars, which has not occurred in younger lavas. Major element compositions of all groups at MgO > 3 wt% are dominated by crystallisation of clinopyroxene, magnetite and apatite. Apatite appeared on the liquidus at MgO 4-4.5 wt% as indicated by decreasing P_2O_5 values, whereas Magnetite appeared at MgO 3.5-4 wt% as indicated by simulataneously decreasing Fe and Ti contents. Very high CaO contents in rocks with high MgO reflect accumulation of clinopyroxene (e.g., Danyushevsky

and Lima, 2001).

As can be seen on the figure 5.9, the studied samples cover a wide range compositions and are representative for the entire Vesuvius range. Importantly, the range of clinopyroxene phenocryst compositions is the same regardless of the sample compositions, i.e., in highly evolved pumices and realtivlely high-MgO lavas, the same range of mineral compositions is present. The difference is only in the abundance of the phenocrysts. The implications of this observations will be discussed in Chapter 7.

The average composition of clinopyroxene phenocrysts in each sample are presented in table 5.1.

Figure 5.10 compares the average composition of clinopyroxene phenocrysts with the rock MgO content. The following observations can be made. Despite all rocks studied having overall a very similar range of pyroxene compositions, there is a general trend of increasing average Mg# of clinopyroxene phenocrysts with decreasing eruption age, i.e., in Group 3 rocks the pyroxenes are on average more magnesian that in Group 1 rocks. Based on the data obtained, no relationship is observed between the average composition of clinopyroxenes and either MgO content of the rocks (a reflection of the amount of clinopyroxene accumulation), or the eruption style. The implications of this observations will be also discussed in Chapter 7.

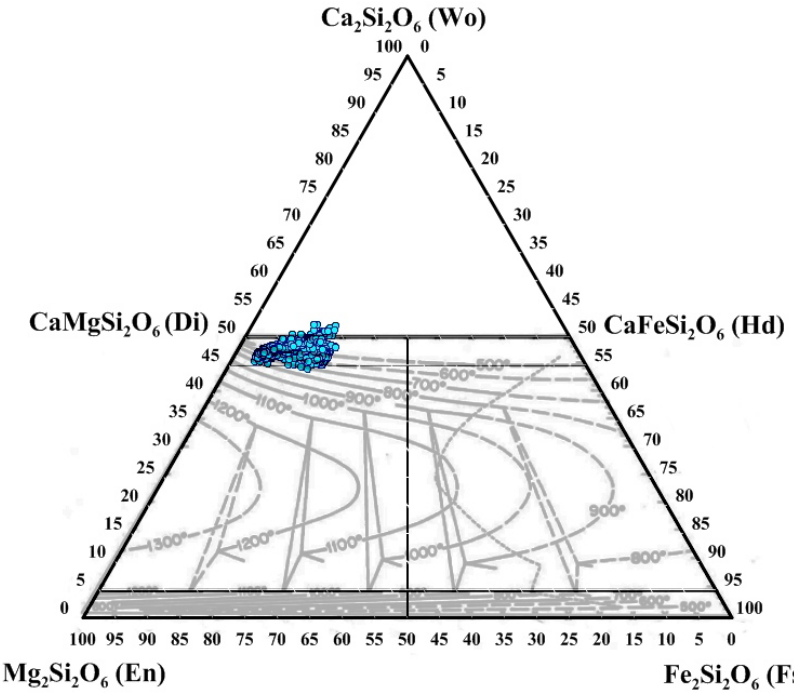

Figure 5.4 Clinopyroxene compositions dislpayed as light-blue circles within the Wo-En-Fs system ($Ca_2Si_2O_6$-$Mg_2Si_2O_6$-$Fe_2Si_2O_6$); the quadrilateral subdivisions are inferred from Morimoto (1988) whereas the background isotherm lines are derived from Lindsley (1980) and referred to atmospheric pressure (1 atm).

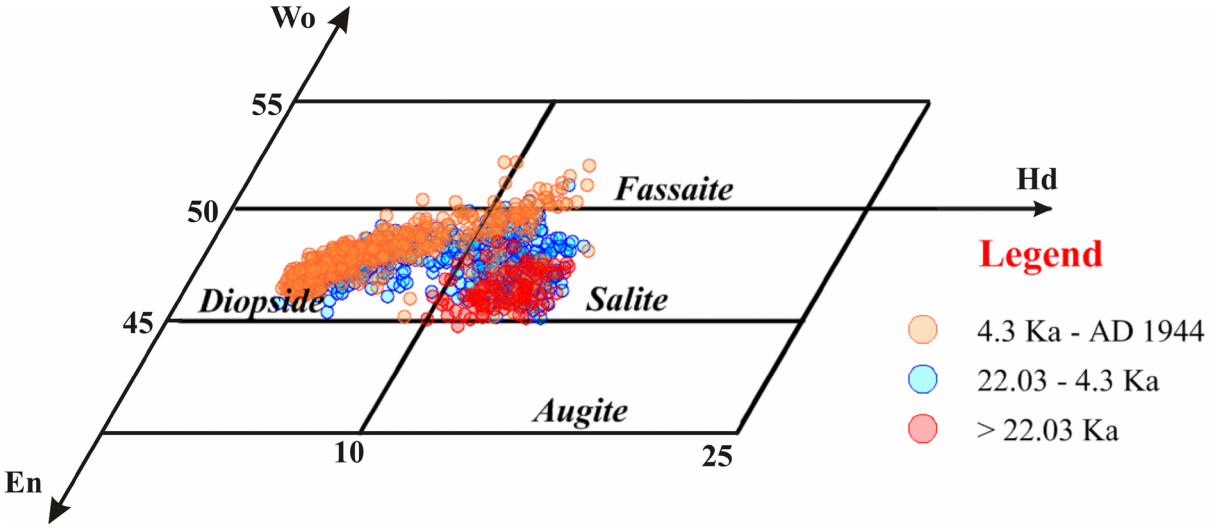

Figure 5.5 Somma-Vesuvius clinopyroxene compositions plotted on a Wo-En-Fs diagram following the old nomenclature suggested by Poldervaart and Hess (1951) which subdivides the Diopside field of Morimoto (1988) in two sectors, Diopside and Salite, and also allows naming clinopyroxenes slightly richer in Wo molecule as Fassaites.

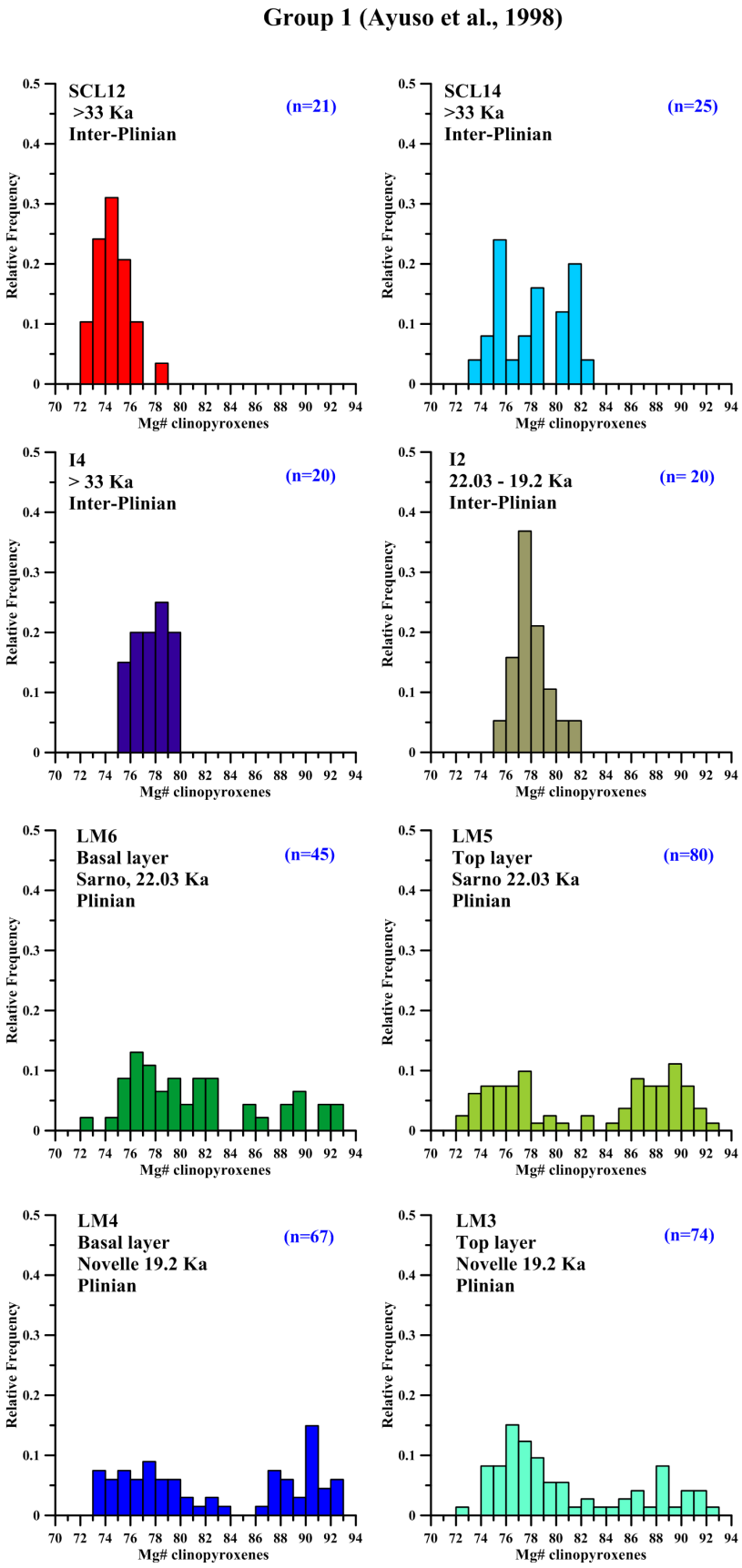

Figure 5.6 Histograms of Somma-Vesuvius clinopyroxene phenocrysts compositions for samples which belong to the geochemical Group 1 following Ayuso et al. (1998) Somma-Vesuvius rocks subdivision (Mg# = MgO/40.3/(MgO/40.3 + FeO/71.85)*100).

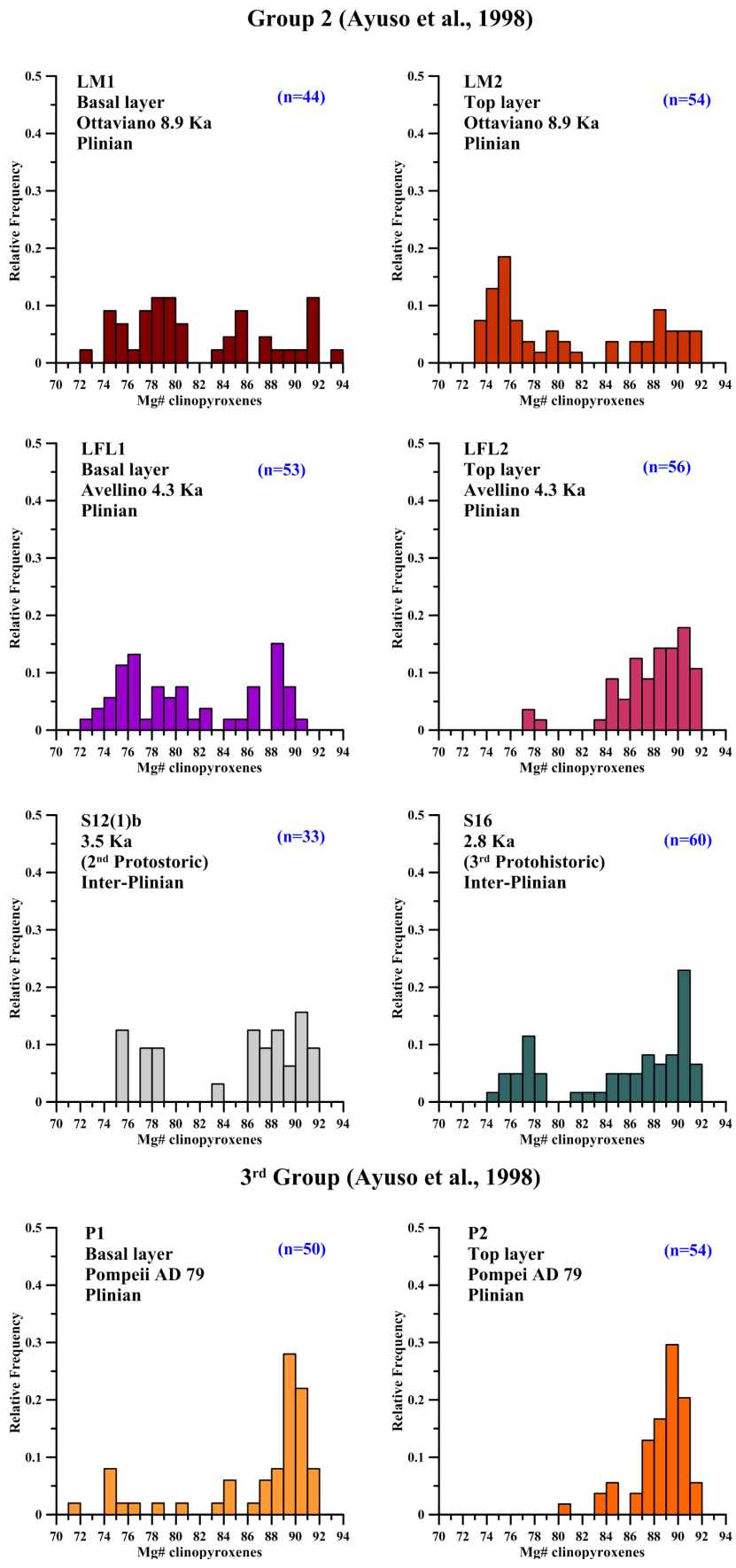

Figure 5.7 Histograms displaying Somma-Vesuvius clinopyroxene phenocrysts distribution as relative frequencies for samples which belongs respectively to geochemical Groups 2 and 3 following Ayuso et al. (1998) Som ma- Ve suvius rocks subdivision.

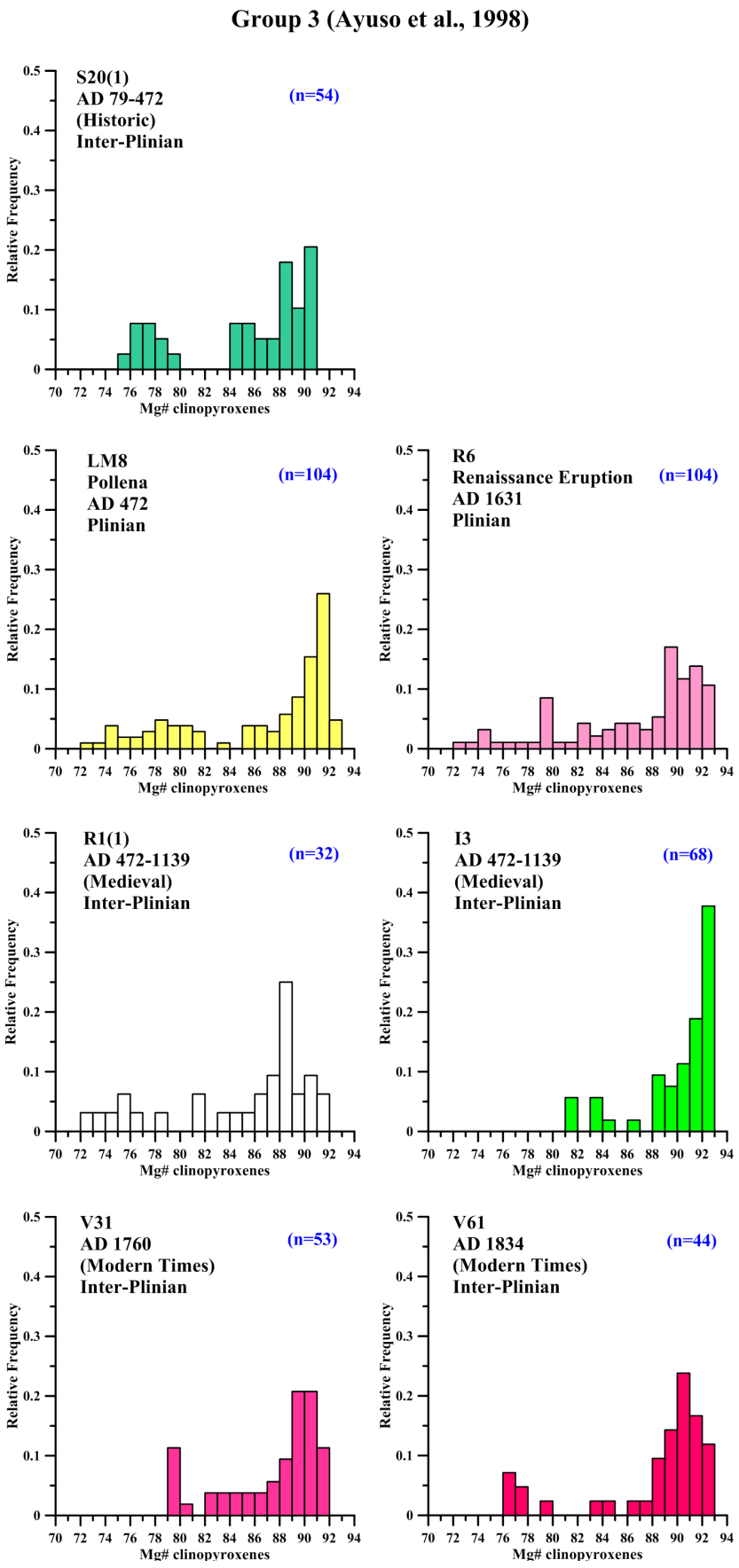

Figure 5.8 Histograms displaying Somma-Vesuvius clinopyroxene phenocrysts distribution as relative frequencies for samples which belong to geochemical Group 3 following Ayuso et al. (1998) Somma-Vesuvius rocks subdivision.

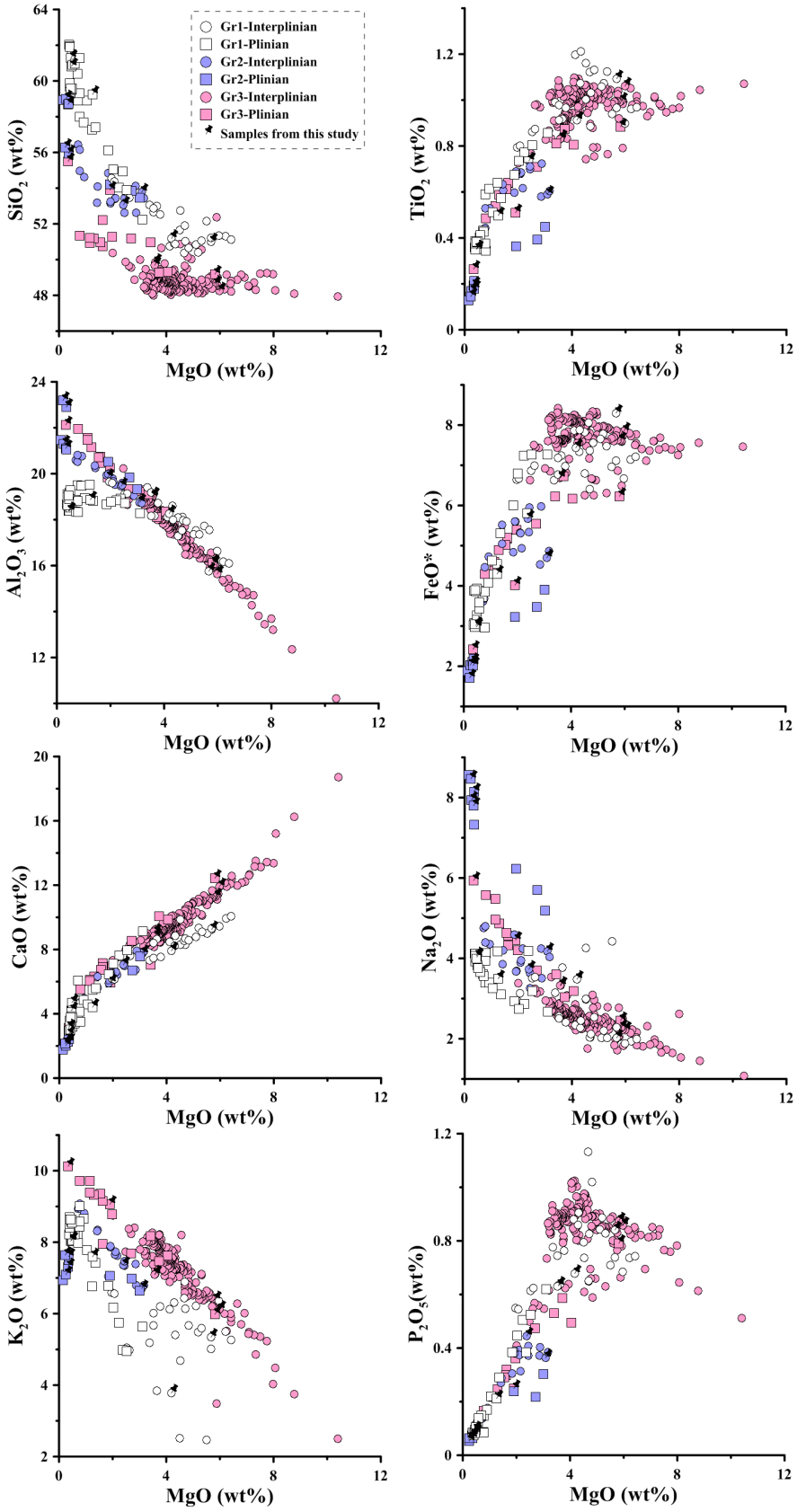

Figure 5.9 Major/minor elements composition of Somma-Vesuvius eruptive products belonging to the last 33 Ky. The black pin symbols represent samples studied in the present project. The data-set is available from De Vivo et al. (2003).

sample	SCL12	SCL14	I4	I2	LM6	LM5	LM4	LM3
age	> 33 Ka	> 33 Ka	> 33 Ka	22.03-19.2 Ka	22.03 Ka	22.03 Ka	19.2 Ka	19.2 Ka
group	Group 1	Group 1	Group 1	Group 1	Group 1	Group 1	Group 1	Group 1
eruptive style	Inter-Plinian average	Inter-Plinian average	Inter-Plinian average	Inter-Plinian average	Plinian average	Plinian average	Plinian average	Plinian average
SiO_2	49.06	49.69	49.15	50.46	50.02	50.74	50.54	50.16
TiO_2	1.20	0.82	1.02	0.84	0.88	0.77	0.82	0.89
Al_2O_3	5.01	4.94	5.19	4.07	4.44	4.03	3.86	4.40
FeO	8.28	7.27	7.30	7.33	6.15	5.65	5.61	6.16
MnO	0.22	0.15	0.15	0.15	0.16	0.15	0.15	0.16
MgO	13.63	14.56	14.30	14.85	14.86	15.35	15.27	14.87
CaO	22.15	22.21	22.50	22.00	23.16	22.90	23.33	22.95
Na_2O	0.33	0.28	0.30	0.24	0.23	0.24	0.23	0.25
Cr_2O_3	0.09	0.07	0.08	0.06	0.09	0.15	0.18	0.13
NiO	0.02	0.01	0.01	0.01	0.02	0.02	0.02	0.02
Tot	100.00	100.00	100.00	100.00	99.99	100.01	100.00	100.00
Mg#	75	78	78	78	81	83	83	81
sample	LM1	LM2	LFL1	LFL2	S12(1)b	S16	P1	P2
age	8.9 Ka	8.9 Ka	4.3 Ka	4.3 Ka	3.5 Ka	2.8 Ka	AD 79	AD 79
group	Group 2	Group 2	Group 2	Group 2	Group 2	Group 2	Group 3	Group 3
eruptive style	Plinian average	Plinian average	Plinian average	Plinian average	Inter-Plinian average	Inter-Plinian average	Plinian average	Plinian average
SiO_2	50.11	50.08	50.33	52.27	51.81	51.38	51.71	52.76
TiO_2	0.86	0.91	0.85	0.38	0.51	0.48	0.58	0.40
Al_2O_3	4.42	4.43	4.27	2.56	3.01	3.21	2.96	1.98
FeO	6.30	6.22	6.05	3.90	5.02	4.64	4.45	3.60
MnO	0.17	0.16	0.15	0.11	0.11	0.10	0.10	0.08
MgO	14.92	14.81	14.92	16.67	16.08	15.78	16.13	16.80
CaO	22.83	23.02	23.10	23.70	23.04	24.07	23.71	24.09
Na_2O	0.24	0.24	0.22	0.15	0.20	0.19	0.19	0.15
Cr_2O_3	0.12	0.11	0.09	0.24	0.19	0.14	0.14	0.10
NiO	0.02	0.02	0.01	0.02	0.02	0.02	0.02	0.02
Tot	100.00	100.00	100.00	100.00	100.00	100.00	100.00	100.00
Mg#	81	81	81	88	85	86	87	89
sample	S20(1)	LM8	R1(1)	I3	R6	V31	V61	
age	AD 79-472	AD 472	AD 472-1139	AD 472-1139	AD 1631	AD 1760	AD 1834	
group	Group 3	Group 3	Group 3	Group 3	Group 3	Group 3	Group 3	
eruptive style	Inter-Plinian average	Plinian average	Inter-Plinian average	Inter-Plinian average	Plinian average	Inter-Plinian average	Inter-Plinian average	
SiO_2	51.49	52.07	52.18	53.13	51.73	51.89	52.22	
TiO_2	0.47	0.46	0.41	0.33	0.52	0.51	0.45	
Al_2O_3	3.11	2.60	2.47	1.67	3.06	2.85	2.39	
FeO	4.49	4.03	3.99	3.09	4.17	4.13	3.84	
MnO	0.12	0.11	0.11	0.09	0.11	0.10	0.10	
MgO	16.03	16.41	16.60	17.35	16.07	16.28	16.61	
CaO	23.93	23.88	23.94	23.74	23.91	23.89	24.01	
Na_2O	0.19	0.18	0.16	0.14	0.17	0.16	0.15	
Cr_2O_3	0.15	0.24	0.13	0.42	0.25	0.19	0.21	
NiO	0.02	0.02	0.02	0.03	0.02	0.02	0.02	
Tot	100.00	100.00	100.00	100.00	100.00	100.01	100.00	
Mg#	86	88	88	91	87	88	89	

Table 5.1 Major/minor elements average composition of clinopyroxene phenocrysts in each studied sample.

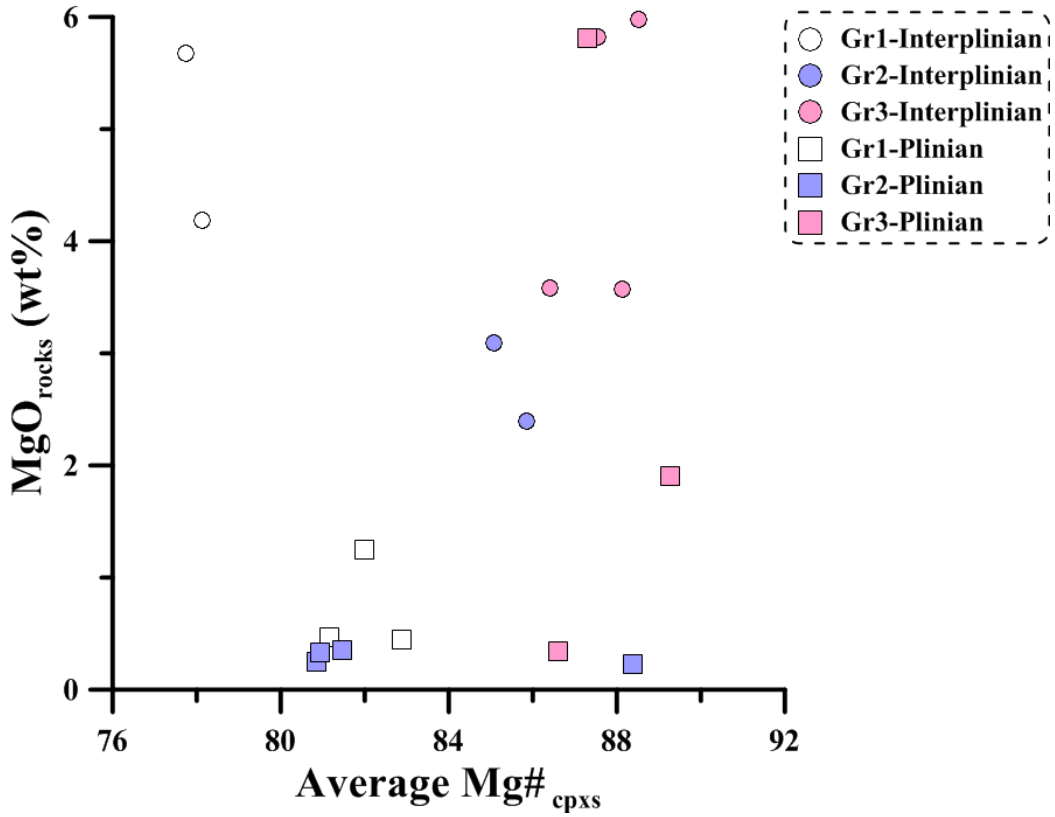

Figure 5.10 A comparative plot of clinopyroxene average compositions with MgO content of Somma-Vesuvius rocks.

5.4 Somma-Vesuvius clinopyroxenes: compositional variations

5.4.1 Major elements

Representative EMPA analyses of major and minor elements in Somma-Vesuvius clinopyroxene phenocrysts are reported in table 5.2 and all data are shown on figure 5.11. Primitive high-magnesian clinopyroxene phenocrysts have effectively identical major element compositions between the three groups, and do not display any age-dependent variations. The pyroxene compositions show well-defined trends of increasing TiO_2, Al_2O_3 and Na_2O contents with decreasing Mg#.

Cr_2O_3 contents decreases rapidly with decreasing Mg#, whereas CaO show larger variations in more evolved, lower Mg# phenocrysts. All Group 1 clinopyroxenes show a continuous decrease in CaO content with decreasing Mg#. A similar trend is observered in ~ 50% of Group 2 pyroxenes and in a small proportion of Group 3 phenocrysts. Most of Group 2 clinopyroxenes have a constant CaO content, regardless of the Mg#, and this trend is also present in ~ 50% of Group 3 phenocrysts. Moreover, some of the evolved Group 1 and Group 2 pyroxenes have higher SiO_2 and lower Al_2O_3 contents compared to the majority of Somma-Vesuvius clinopyroxenes, but none of Group 3 phenocrysts display such compositions. The observed difference in CaO contents are not related to the differences between core and rim compositions, which both show

identical patterns (Fig. 5.12 and 5.13).

Overall, there is little difference between clinopyroxene major element compositions from Plinian and inter-Plinian eruptions (Fig. 5.14). Al_2O_3, SiO_2 and all other elements, but CaO, display a complete overlap between the Plinian and inter-Plinian eruptions. CaO is the only exception. In Group 1, both Plinian and inter-Plinian clinopyroxenes show a consistent trend of decreasing CaO with decreasing Mg#. Within Group 2, all Plinian pyroxenes show the same trend as the Group 1 phenocsyrsts, whereas an inter-Plinian sample S12(1)b (2.7 Ka) shows the same trend, but sample S16 does not show a decrease in CaO (Fig. 5.14). In Group 3, most Plinian and inter-Plinian clinopyroxenes are similar to S16, showing no decrease in CaO, however the first Plinian deposits in this cycle (sample P1 from the base of Pompeii deposits), shows the same trend as Plinian clinopyroxenes from Group 2 and all clinopyroxenes from Group 1.

In order to put the extent of variations in clinopyroxene compositions at a given Mg# into perspective, the compositions of Somma-Vesuvius pyroxenes are compared with published pyroxene compositions from other volcanoes in the Roman Province and other major tectonic settings (fig. 5.15 and 5.16). As seen on these figures, overall, Somma- Vesuvius clinopyroxenes display a tight trend with little variations, suggesting that the parental magmas have not changed significantly over the last 33 Ky.

age	> 33 Ka		> 33 Ka		> 33 Ka		22.03-19.2 Ka		~22.03 Ka - basal Sarno			~ 22.03 Ka - top Sarno		
sample	SCL12	SCL12	SCL14	SCL14	I4	I4	I2	I2	LM6	LM6	LM6	LM5	LM5	LM5
mount/grain	D8/47	D8/67	D91/158	D91/164	D84/43	D84/48	D87/83	D87/86	D27/110	D28/154	D28/152	D1/67	D1/96	D1/55
SiO_2	48.7	50.38	48.19	50.45	48.13	50.72	50.5	51.27	47.83	49.72	53.27	48.52	51.16	53.33
TiO_2	1.22	0.97	1.14	0.68	1.39	0.80	0.86	0.67	1.55	0.80	0.24	1.22	0.87	0.30
Al_2O_3	5.73	3.93	6.10	4.68	6.65	3.72	3.85	3.33	6.05	4.03	1.47	6.00	4.42	2.06
FeO	8.78	7.67	8.50	6.09	7.77	7.09	7.89	6.71	8.67	6.07	3.03	8.73	6.43	3.00
MnO	0.23	0.25	0.17	0.13	0.14	0.17	0.15	0.16	0.24	0.14	0.11	0.22	0.18	0.12
MgO	13.61	14.27	13.57	15.16	13.6	15.16	14.44	15.51	13.08	14.48	17.66	13.18	14.84	17.22
CaO	21.69	22.36	22.08	22.70	22.62	22.71	22.05	22.03	22.39	23.53	23.85	21.97	22.43	23.38
Na_2O	0.33	0.29	0.37	0.22	0.31	0.28	0.26	0.24	0.35	0.21	0.15	0.38	0.26	0.20
Cr_2O_3	0.10	0.17	0.03	0.15	0.16	0.11	0.02	0.05	0.06	0.08	0.11	0.03	0.19	0.73
NiO	0.02	0.01	n.d.	0.04	0.04	0.01	0.01	0.04	n.d.	0.05	0.03	n.d.	0.02	0.02
total	100.41	100.30	100.15	100.30	100.81	100.77	100.03	100.01	100.22	99.11	99.92	100.25	100.80	100.36
cations*6/O	4.034	4.023	4.044	4.025	4.039	4.034	4.022	4.020	4.029	4.032	4.020	4.034	4.011	4.007
Mg#	73.43	76.84	74.00	81.61	75.73	79.22	76.54	80.47	72.90	80.96	91.22	72.91	80.45	91.10
Wo	45.7	46.4	46.4	46.8	47.5	46.0	45.6	45.1	47.3	48.6	47.0	46.6	46.6	47.1
En	39.9	41.2	39.7	43.5	39.8	42.8	41.6	44.2	38.4	41.6	48.4	38.9	42.9	48.2
Fs	14.4	12.4	13.9	9.8	12.7	11.2	12.7	10.7	14.3	9.8	4.7	14.5	10.4	4.7
class	Salite	Salite	Salite	Diopside	Salite	Salite	Salite	Salite	Salite	Diopside	Diopside	Salite	Salite	Diopside
age	~ 19.2 Ka - basal Novelle			~ 19.2 Ka - top Novelle			~ 8.9 Ka - basal Ottaviano			~ 8.9 Ka - top Ottaviano			~ 4.3 Ka - basal Avellino	
sample	LM4	LM4	LM4	LM3	LM3	LM3	LM1	LM1	LM1	LM2	LM2	LM2	LFL1	LFL1	LFL1
mount/grain	D16/76	D17/108	D17/112	D11/81	D11/80	D12/114	D24/52	D24/62	D24/94	D31/36	D31/22	D33/46	D39/119	D40/155	D40/175
SiO_2	47.13	49.65	53.58	47.27	50.20	53.59	47.61	50.02	53.50	47.38	49.31	53.35	49.26	50.86	53.27
TiO_2	1.83	0.88	0.19	1.64	0.87	0.17	1.44	0.70	0.32	1.56	0.81	0.30	1.43	0.80	0.35
Al_2O_3	6.71	4.86	1.35	6.79	4.77	1.10	7.00	4.70	1.97	6.43	5.42	1.79	4.84	3.93	2.18
FeO	8.32	6.27	2.55	8.06	6.25	2.42	8.41	5.61	3.15	8.49	6.30	2.97	8.51	6.30	3.53
MnO	0.16	0.15	0.10	0.18	0.15	0.09	0.19	0.15	0.10	0.21	0.19	0.09	0.22	0.19	0.13
MgO	12.77	14.41	17.72	12.95	14.88	18.68	13.17	15.02	17.63	13.19	14.39	17.59	13.54	14.96	17.26
CaO	22.53	23.59	23.72	22.54	22.83	23.44	21.98	23.58	23.70	22.10	23.39	24.27	22.20	22.83	23.96
Na_2O	0.39	0.22	0.19	0.38	0.28	0.15	0.35	0.20	0.16	0.35	0.24	0.16	0.36	0.24	0.13
Cr_2O_3	0.08	0.16	0.67	0.02	0.05	0.33	0.02	0.01	0.20	0.11	0.02	0.31	0.01	0.10	0.09
NiO	n.d.	0.02	0.04	0.02	0.01	0.02	0.01	0.01	0.03	0.01	0.02	n.d.	0.01	0.02	0.04
total	99.92	100.21	100.11	99.85	100.29	99.99	100.18	100.00	100.76	99.83	100.09	100.83	100.38	100.23	100.94
cations*6/O	4.04	4.03	4.01	4.04	4.03	4.02	4.04	4.03	4.02	4.04	4.04	4.02	4.03	4.02	4.02
Mg#	73.24	80.38	92.53	74.12	80.93	93.23	73.63	82.68	90.89	73.47	80.29	91.349	73.94	80.89	89.71
Wo	48.1	48.6	47.1	48.1	47.2	45.7	46.9	48.3	46.8	46.9	48.4	47.5	46.6	47.0	47.2
En	38.0	41.3	49.0	38.5	42.8	50.6	39.1	42.8	48.4	39.0	41.4	47.9	39.5	42.9	47.3
Fs	13.9	10.1	4.0	13.4	10.1	3.7	14.0	9.0	4.9	14.1	10.2	4.5	13.9	10.1	5.4
class	Salite	Salite	Diopside	Salite	Salite	Diopside	Salite	Diopside	Diopside	Salite	Salite	Diopside	Salite	Salite	Diopside
age	~ 4.3 Ka - top Avellino			3.5 Ka - Protohistoric		2.8 Ka - Protohistoric		AD 79 - basal Pompeii			AD 79 - top Pompeii			AD 79-472	
sample	LFL2	LFL2	LFL2	S12(1)b	S12(1)b	S16	S16	P1	P1	P1	P2	P2	P2	S20(1)	S20(1)
mount/grain	D42/40	D42/20	D42/55	D81/103	D82/136	D78/40	D78/27	D45/80	D45/78	D46/103	D48/51	D47/18	D48/60	D75/102	D76/125
SiO_2	51.65	52.34	53.37	49.98	52.73	47.94	53.64	47.44	49.86	52.86	51.28	52.77	53.05	48.25	53.30
TiO_2	0.48	0.43	0.22	0.99	0.31	0.91	0.31	1.30	0.80	0.29	0.61	0.43	0.32	0.82	0.34
Al_2O_3	3.32	2.85	1.45	4.03	2.30	6.56	1.69	6.68	5.12	1.53	3.20	2.49	1.65	6.04	1.24
FeO	5.03	4.14	2.91	8.19	3.68	7.73	3.16	8.12	4.87	2.90	5.33	3.95	2.96	7.22	3.15
MnO	0.16	0.10	0.11	0.18	0.08	0.13	0.08	0.15	0.08	0.09	0.14	0.06	0.07	0.15	0.10
MgO	15.81	16.40	17.81	14.06	17.13	12.84	17.43	13.37	14.99	17.57	15.11	16.18	17.58	13.43	18.04
CaO	23.73	24.03	23.66	22.10	23.33	24.03	24.26	22.57	23.77	24.14	24.23	24.21	23.79	24.18	24.11
Na_2O	0.14	0.15	0.12	0.37	0.15	0.27	0.13	0.32	0.21	0.16	0.18	0.20	0.12	0.26	0.14
Cr_2O_3	0.00	0.15	0.29	0.01	0.41	0.01	0.17	0.03	0.09	0.43	0.02	0.09	0.15	0.06	0.22
NiO	0.01	0.02	0.01	n.d.	0.06	0.03	0.01	0.02	0.02	0.03	0.01	0.01	0.04	0.02	0.04
total	100.33	100.61	99.95	99.89	100.17	100.45	100.88	100.00	99.82	100.00	100.11	100.39	99.73	100.42	100.67
cations*6/O	4.02	4.02	4.02	4.03	4.02	4.05	4.02	4.05	4.03	4.03	4.02	4.01	4.02	4.05	4.03
Mg#	84.86	87.59	91.60	75.37	89.25	74.75	90.78	74.59	84.58	91.53	83.48	87.96	91.37	76.83	91.07
Wo	47.8	48.0	46.7	46.0	46.6	50.1	47.6	47.5	49.1	47.5	49.0	48.6	47.0	49.9	46.7
En	44.3	45.6	48.9	40.7	47.6	37.3	47.6	39.2	43.1	48.1	42.5	45.2	48.4	38.5	48.6
Fs	7.9	6.5	4.5	13.3	5.7	12.6	4.8	13.3	7.9	4.5	8.4	6.2	4.6	11.6	4.8
class	Diopside	Diopside	Diopside	Salite	Diopside	Salite	Diopside	Salite	Diopside	Diopside	Diopside	Diopside	Diopside	Salite	Diopside
age	AD 472 - Pollena			AD 472-1139		AD 472-1139		AD 1631 - Renaissance Erup			AD 1760		AD 1834		
sample	LM8	LM8	LM8	I3	I3	R1(1)	R1(1)	R6	R6	R6	V31	V31	V61	V61	
mount/grain	D55/124	D55/110	D56/117	D66/184	D66/150	D69/9	D69/25	D51/44	D51/71	D52/77	D61/171	D62/155	D59/66	D59/63	
SiO_2	47.92	50.29	52.75	50.04	53.97	49.15	51.85	46.94	49.62	53.96	49.81	52.69	47.63	53.55	
TiO_2	1.35	0.88	0.31	0.94	0.19	1.07	0.53	1.08	0.96	0.18	0.91	0.31	1.10	0.22	
Al_2O_3	6.28	4.99	2.01	4.49	1.10	5.34	3.18	7.15	5.61	1.25	5.11	1.71	6.31	1.27	
FeO	8.28	5.83	2.86	5.94	2.24	8.24	4.75	7.80	5.52	2.52	6.36	3.33	7.40	2.68	
MnO	0.21	0.16	0.09	0.14	0.06	0.19	0.11	0.17	0.12	0.10	0.14	0.10	0.15	0.08	
MgO	13.47	14.28	17.47	14.61	18.00	13.93	15.84	11.87	14.33	17.86	13.91	17.20	13.48	17.82	
CaO	22.01	24.11	23.44	23.89	24.01	22.15	24.45	24.51	24.17	23.73	23.76	24.22	23.37	24.20	
Na_2O	0.40	0.24	0.19	0.21	0.19	0.30	0.17	0.27	0.18	0.14	0.25	0.10	0.27	0.12	
Cr_2O_3	0.04	0.02	0.99	0.05	0.82	0.04	0.12	0.01	0.24	0.65	0.04	0.14	0.01	0.42	
NiO	0.02	0.00	0.03	0.00	0.03	0.02	n.d.	0.02	0.02	0.04	0.01	0.04	0.01	0.01	
total	99.98	100.81	100.14	100.31	100.61	100.43	100.99	99.81	100.77	100.43	100.30	99.84	99.73	100.37	
cations*6/O	4.04	4.03	4.02	4.03	4.01	4.03	4.03	4.05	4.03	4.01	4.03	4.02	4.05	4.02	
Mg#	74.36	81.37	91.59	81.43	93.48	75.09	85.60	73.07	82.22	92.67	79.59	90.20	76.46	92.22	
Wo	46.6	49.7	46.9	48.9	47.3	46.2	48.7	52.0	49.9	46.9	49.4	47.7	48.8	47.4	
En	39.7	40.9	48.6	41.6	49.3	40.4	43.9	35.1	41.2	49.2	40.3	47.2	39.2	48.5	
Fs	13.7	9.4	4.5	9.5	3.4	13.4	7.4	12.9	8.9	3.9	10.3	5.1	12.1	4.1	
class	Salite	Diopside	Diopside	Diopside	Diopside	Salite	Diopside	Fassaite	Diopside	Diopside	Salite	Diopside	Salite	Diopside	

Table 5.2 Representative (EMPA) major/minor elements compositions of Somma-Vesuvius clinopyroxene phenocrysts.

.

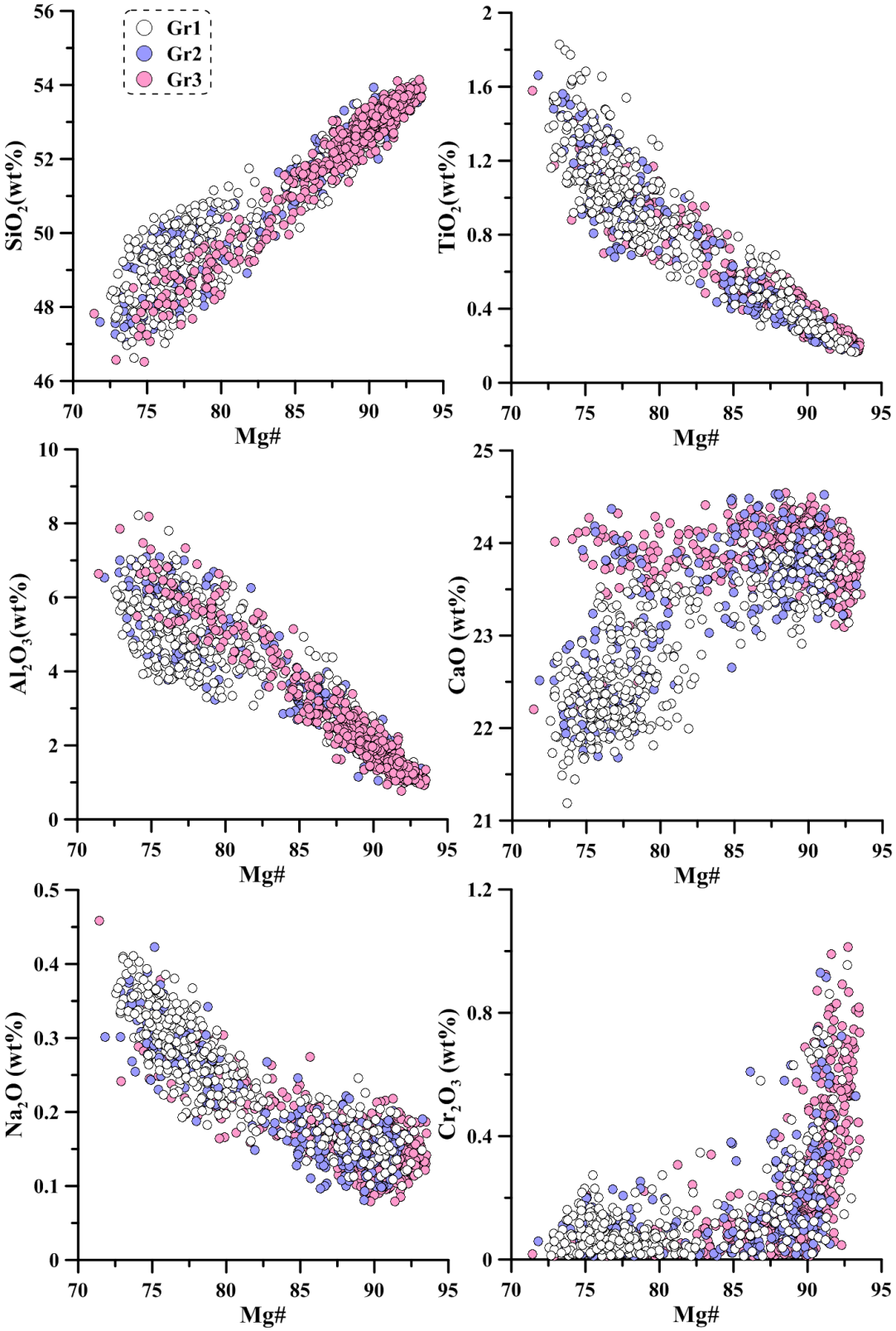

Figure 5.11 Representative plots of major/minor elements (oxides in weight % versus Mg#) in clinopyroxene phenocrysts.

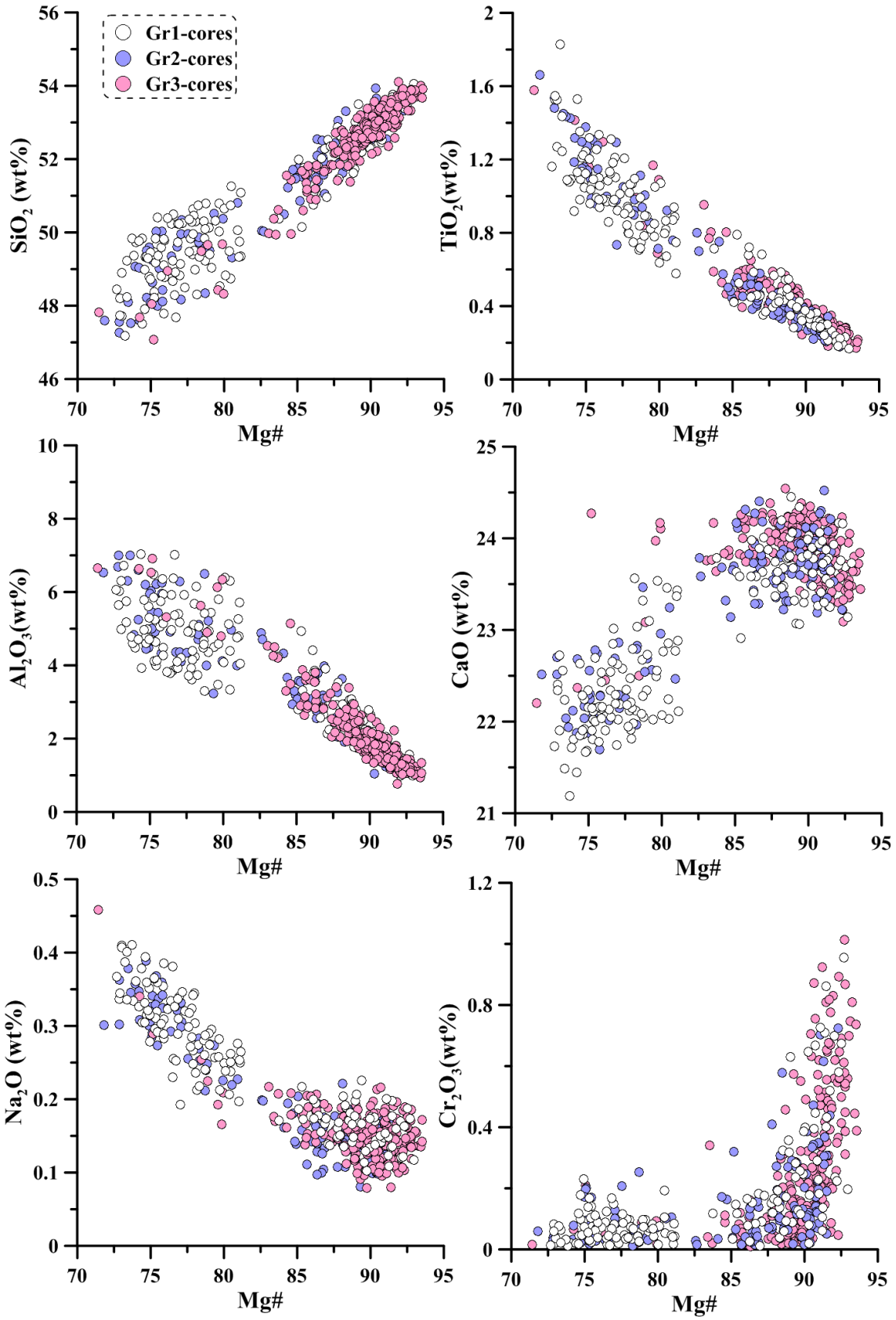

Figure 5.12 Representative plots of major/minor elements in clinopyroxene phenocryst cores.

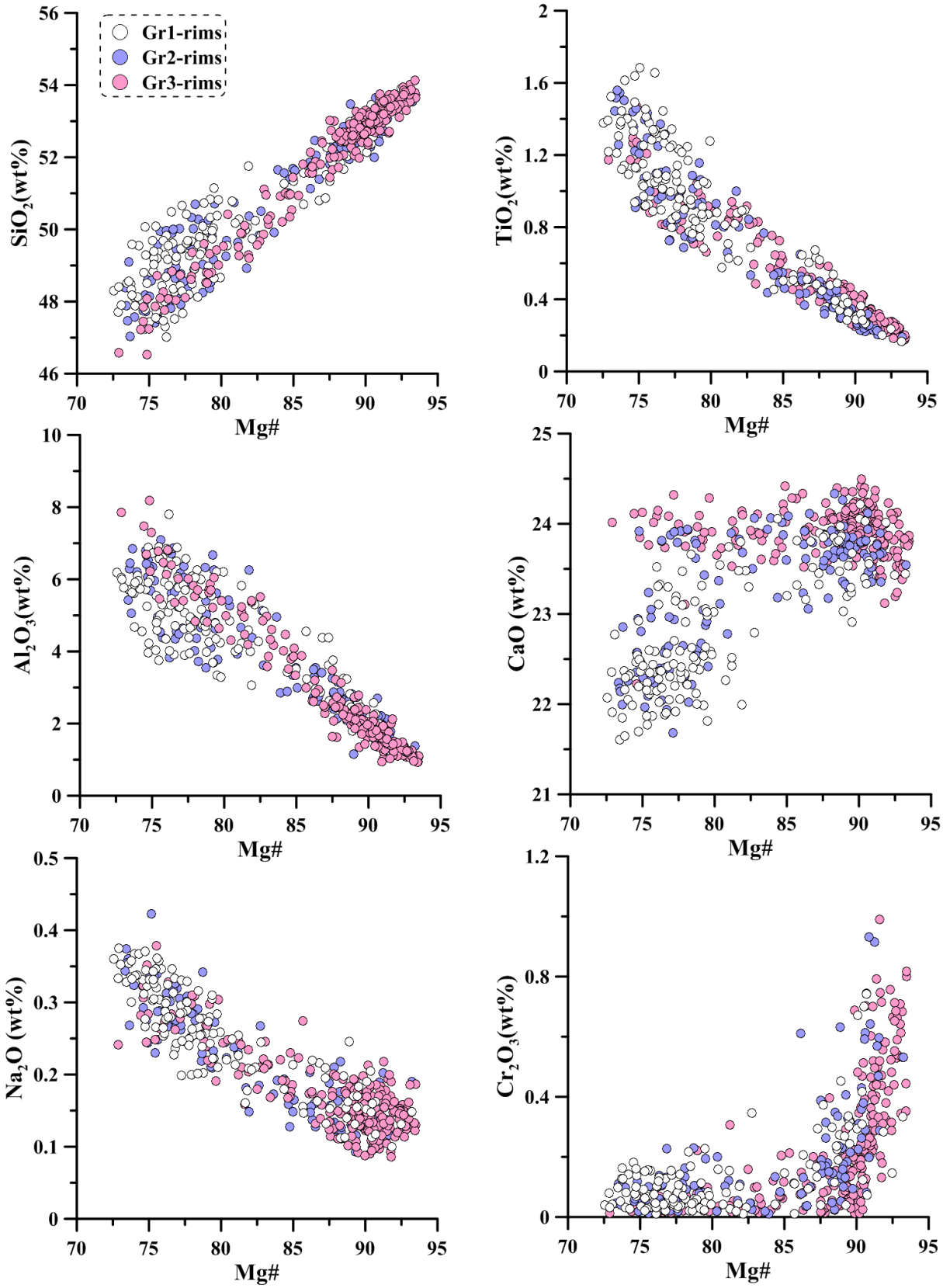

Figure 5.13 Representative plots of major/minor elements in clinopyroxene phenocryst rims.

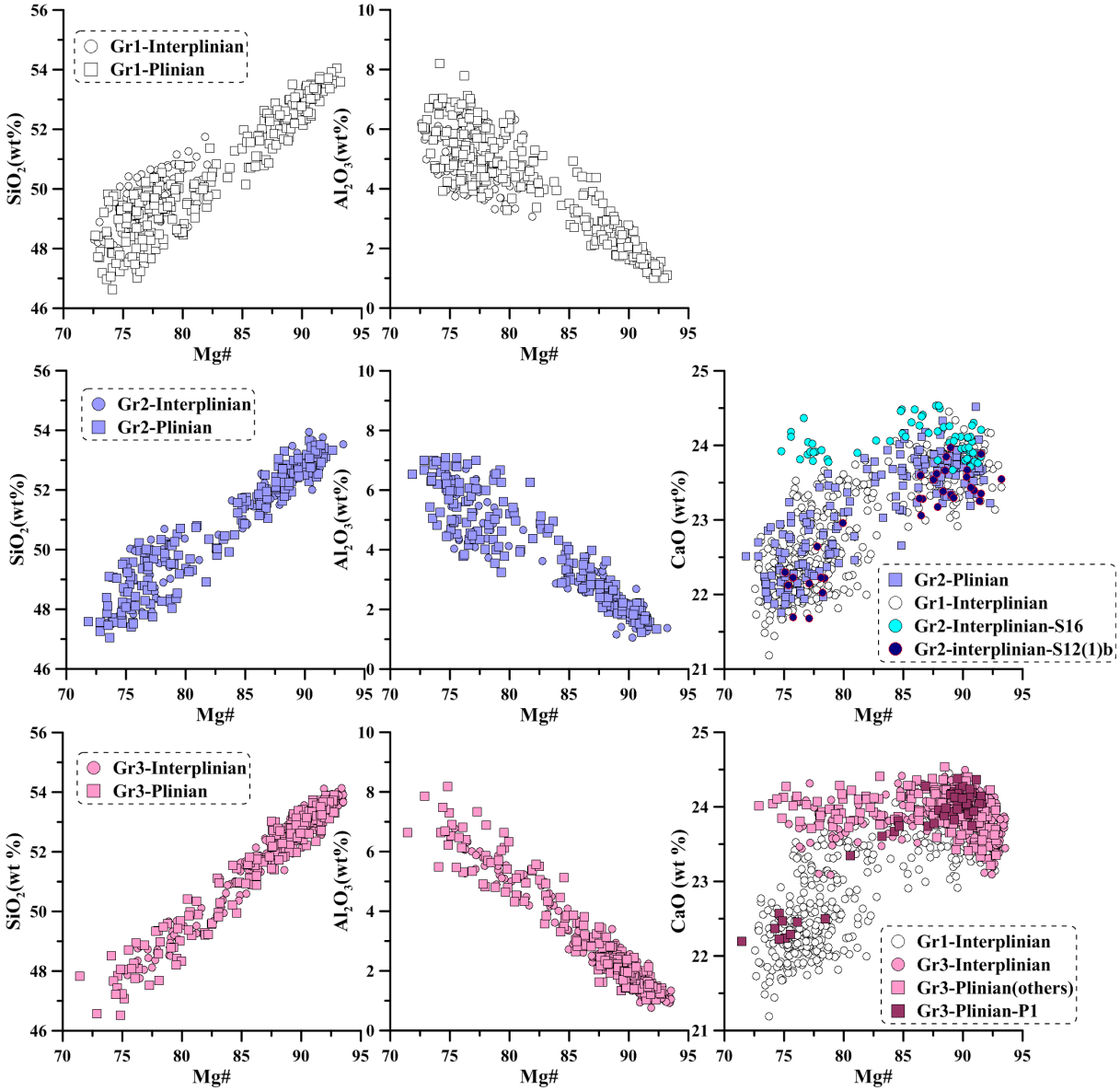

Figure 5.14 Comparative plots of major elements in Plinian and inter-Plinian clinopyroxene phenocrysts.

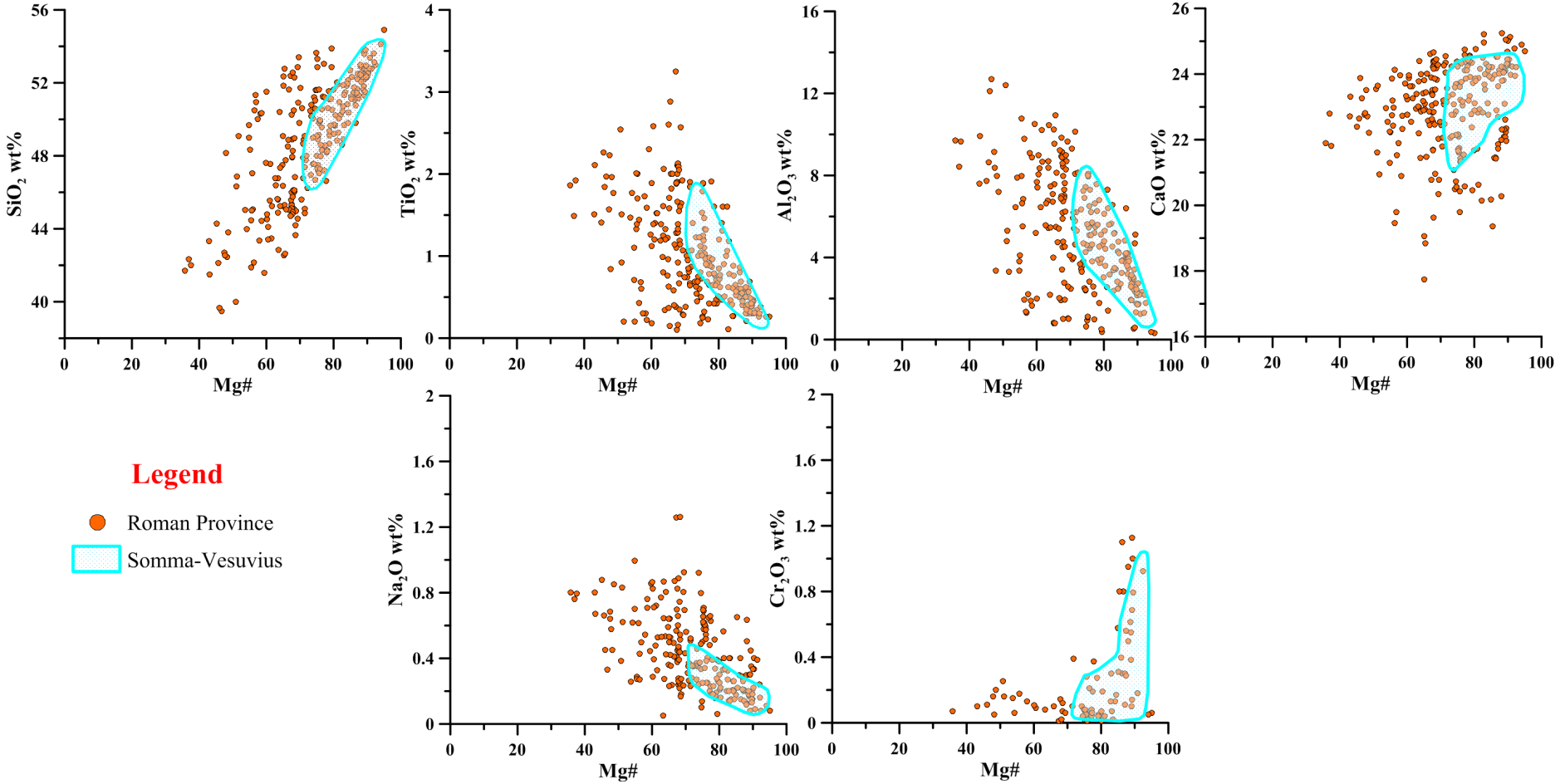

Figure 5.15 Major/minor elements plots (oxides in weight % versus Mg#) of Somma-Vesuvius clinopyroxene phenocrysts (light blue polygons) compared with those from other vol ca noes of the Roman Comagmatic Province. Major and minor elements data for clinopyroxene phenocrysts belonging to the RCP were collected from different authors (Aurisicchio et al., 1988; Barnekow, 2000; Barton et al., 1982; Bertagnini et al., 1995; Bindi et al., 1999; Carbonin et al., 1984; Carmela et al., 2006; Cellai et al., 1994; Conticelli, 1998; Conticelli et al., 2007; Cundari, 1975; Dal Negro et al., 1985; Dallai et al., 2004; De Astis et al., 1997; De Fino et al., 1986; Di Battistini et al., 1998; Faraone et al., 1988; Fedele et al., 2009; Francalanci et al., 1987; Gaeta et al., 2006; Gioncada et al., 2005; Holm, 1982; Kamenetsky et al., 1995; Melluso et al., 1996; Pasqual et al., 1998; Perini and Conticelli, 2002; Perini et al., 2000; Santo, 2000).

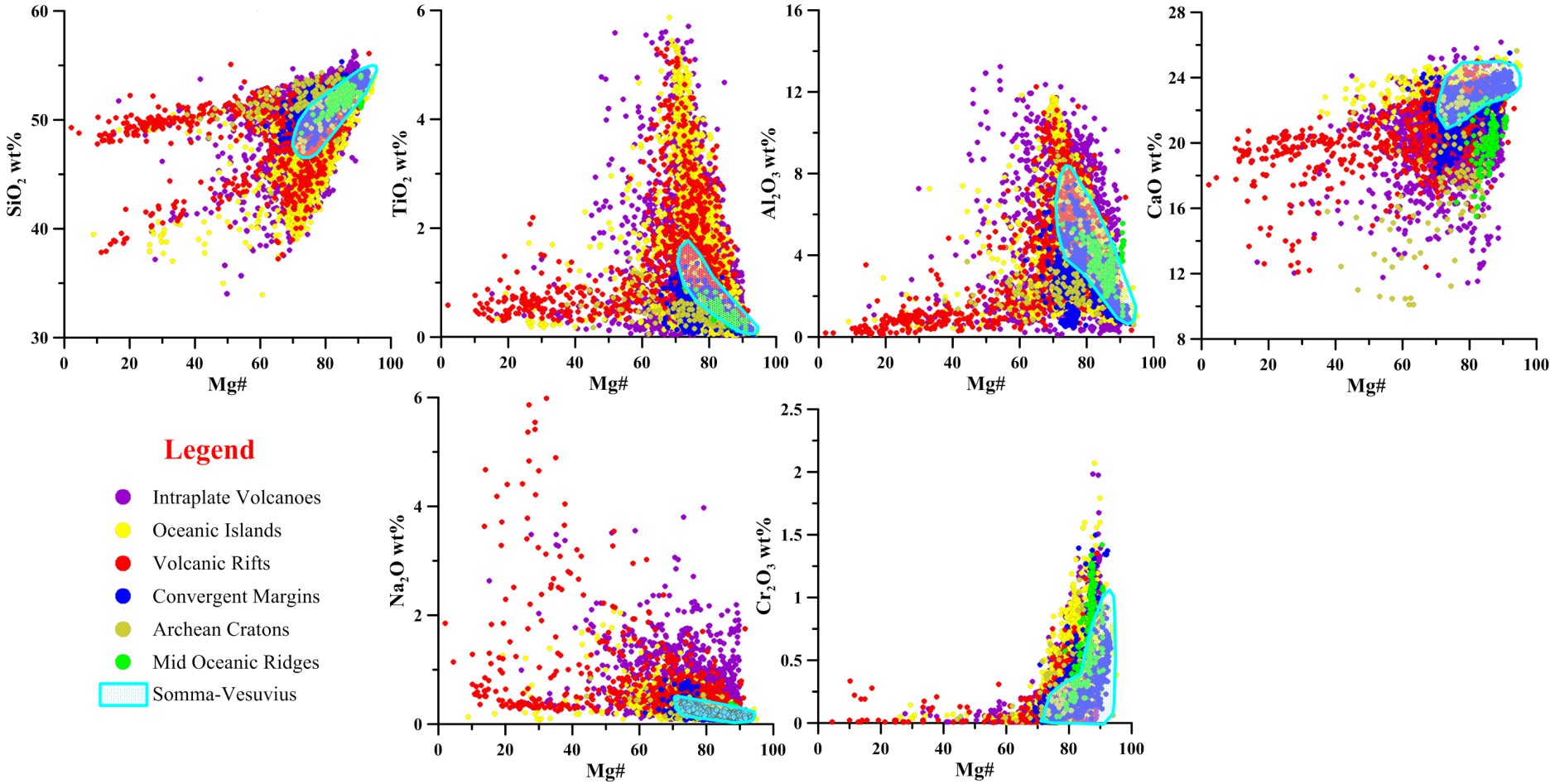

Figure 5.16. Major/minor elements plots (oxides in weight % versus Mg#) of Somma-Vesuvius clinopyroxene phenocrysts (light blue polygons) compared with those from other tectonic settings (symbols differently coloured, see legend) The ma jor/minor elements data for clinopyroxenes belonging to different tectonic settings are prevalently from database of the Max Planck Institute of Chemistry Mainz (1999) (available on line in the mineral section at http://georoc.mpch-mainz.gwdg.de/georoc/ with the name "CLINOPYROXENES 2"); however, those data relative to Mid - Oce anic Ridges and Con ver gent Margins are also from Danyushevsky (unpublished) data, and Pe-Piper (1984) as well as other Pe-Piper (unpublished) data from clinopyroxenes belonging to the Lesbos Island shoshonites.

5.4.2 Statistical assessment of compositional variations

Compositional variations are assessed using concentrations of TiO_2, Al_2O_3, CaO and Cr_2O_3 as examples. One sigma errors for each value in each analyses were taken in consideration when evaluating the significance of the observed chemical variations among the different samples. In this regard, it is worth mentioning that two measurements (e.g., x and y) may be considered the same within error at 95% confidence level if they satisfied the following equation:

$$ABS(x-y) \leq 2*\sqrt{(\sigma x^2+\sigma \gamma^2)}$$

where ABS is their absolute difference value and σx^2-$\sigma \gamma^2$ are the respective errors.

Overall, all compositions of inter-Plinian clinopyroxene phenocrysts are within the range defined by Plinian clinopyroxenes. However, the major and minor elements variability observed among clinopyroxene populations from different inter-Plinian samples appears to be significantly broader than among Plinian populations. Plinian clinopyroxenes are usually characterized by similar ranges of TiO_2, Al_2O_3 and Cr_2O_3, forming distinct trends against Mg# (Fig. 5.11), from which only few specimens deviate consistently. Instead, the compositions of inter-Plinian clinopyroxenes vary much more from sample to sample.

Clinopyroxene phenocrysts from Groups 1 and 2 are characterized by very similar major minor elements ranges. The largest deviations are represented by the Novelle clinopyroxene population which exhibits higher TiO_2 and Al_2O_3 values, up to 1.8 and 8.2, respectively, between ~ 80 and 73 Mg#, and by a few Sarno clinopyroxene phenocrysts that display slightly higher Al_2O_3 values at ~ 87.5-85 Mg# (yellow-line polygon in Fig. 5.17 A). Moreover, Avellino top layer pumices contain only clinopyroxene phenocrysts with low TiO_2 (0.2-0.8), low Al_2O_3 (1.4-4.9) and high CaO (23.2-24.2) values at primitive Mg# intervals (92-84) (dotted yellow line polygons in Fig. 5.17 B). Then, the Plinian clinopyroxenes from the Group 3 present the highest major/minor elements variability among the three geochemical groups. In fact, the Pompeii eruption is prevalently populated by primitive and by only few more evolve clinopyroxenes, ~ 82-72 Mg# (dotted yellow line polygons in Fig. 5.17 C); the latter still fall within the typical Plinian clinopyroxenes composition. Concerning the Pompeii clinopyroxenes population, Cr_2O_3 contents are between 0.05 and 0.55, with higher values, common in other Plinian eruptions, lacking completely. However, as in the Avellino eruption, the top layer is populated by clinopyroxenes with low TiO_2 (0.3-0.6), low Al_2O_3 (1.3-3), and high CaO (23.5-24.5) (yellow-line polygons in Fig. 5.17 C), even though the ranges are narrower than in the Avellino clinopyroxenes. The Pollena and the Renaissance (A.D. 1631) eruptions are formed by clinopyroxenes with a very distinct compositions; in fact, at 82-72 Mg# they exhibit lower TiO_2, up to a maximum of 1.3, higher Al_2O_3, up to 8.2 in the Renaissance eruption (A.D. 1631), lower Cr_2O_3 (0.1-0.05), and remarkably higher CaO (23.7-24) (Fig. 5.17 C). Lastly, both these eruptions are also populated

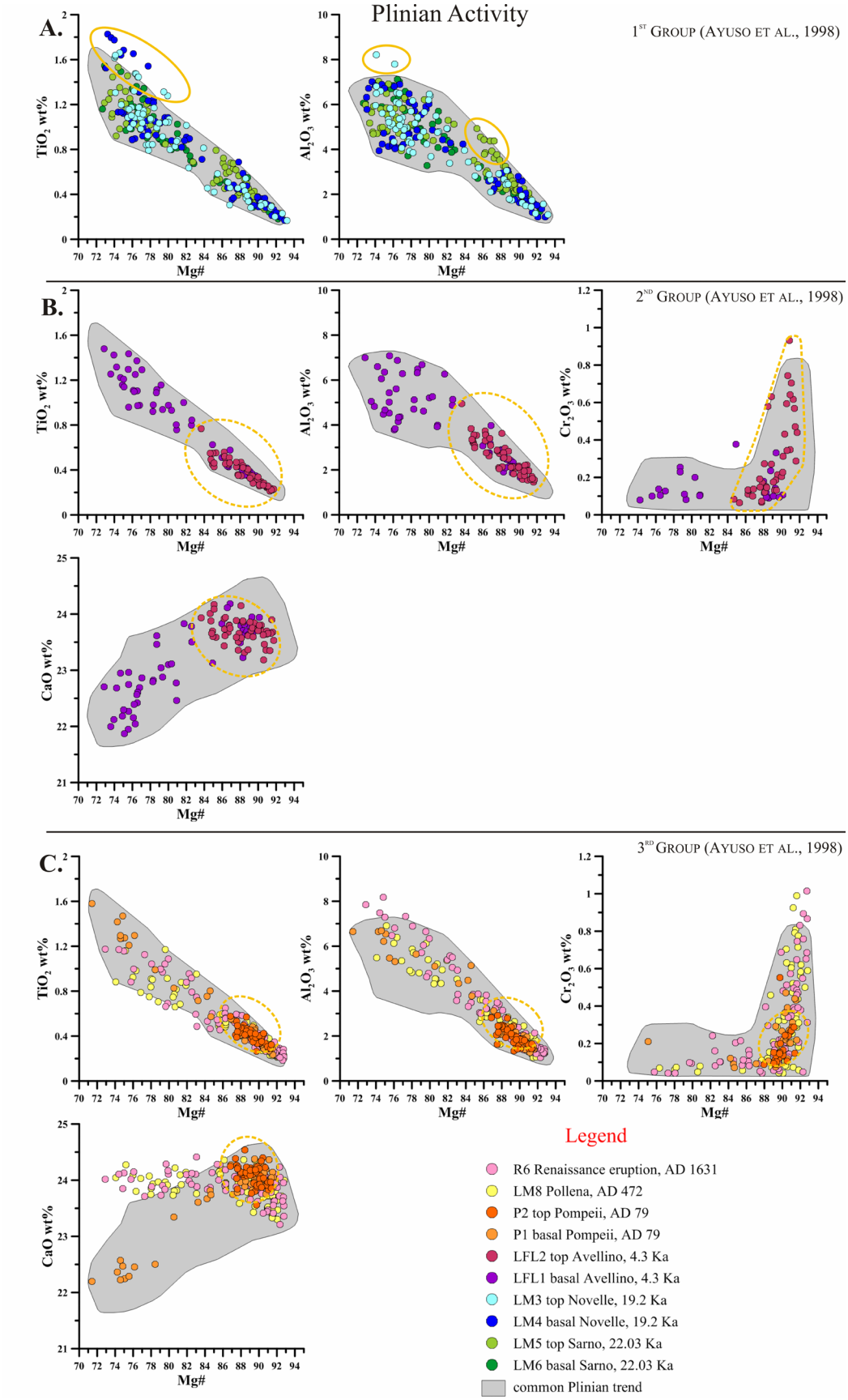

Figure 5.17 A-C Selected plots (major and minor elements vs Mg#) which display variations within/among the different Somma-Vesuvius Plinian clinopyroxenes populations subdivided in three geochemical groups following Ayuso et al. (1998). Grey polygons represent the compositional range defined by the majority of Plinian clinopyroxenes; whereas, yellow lines highlight some internal discrepancies.

by few cpxs specimens that have higher Cr_2O_3 up to 1.01 in R6 (A.D. 1631) at ~ 93-90 Mg#. Within inter-Plinian clinopyroxenes, phenocrysts from four samples from Group 1 are characterized by high TiO_2 (0.6-1.5), high Al_2O_3 (3-6.6), low Cr_2O_3 (0.03-0.2), and low CaO (21.6-23.1) at 82-72 Mg# (Fig. 5.18 A). Some clinopyroxenes from these samples display higher TiO_2, up to 1.5 in SCL12, and lower Al_2O_3 when compared with those from other inter-Plinian samples (yellow-line polygons in Fig. 5.18 A). Then, within the Group 2 and the Group 3 the inter-Plinian clinopyroxenes populations are defined by more similar chemical ranges, even if there are still some clear deviations. In fact, the more evolve phenocrysts in S12(1) b (Group 2) is characterized by alumina values falling just below the common inter-Plinian trend (yellow-line polygon in Fig. 5.18 B) similarly to those from samples SCL12, SCL14 and I4 (Group 1), whereas clinopyroxenes from S16 (Group 2) are overall richer in CaO (23.7-24.6) and are defined by a calcium trend which diverges from those characterizing S12(1)b (Fig. 5.18 B). Within Group 3, clinopyroxenes from samples I3, V31 and V61 exhibit roughly higher TiO_2 in respect of the main common inter-Plinian trend at around 85-77.5 Mg# (yellow-line polygon in Fig. 5.18 C); additionally, samples I3 and V61 contain clinopyroxene phenocrysts with Cr_2O_3 between ~ 0.3 and 0.8 at higher Mg# values (~ 93) (yellow-line polygon in Fig. 5.18 C). Then, clinopyroxenes from the Group 3 are characterized by higher Ca values, usually comprised within 23.1 and 24.6 quite similarly to those in S16, and are defined by almost identical intervals. In these two geochemical groups other minor differences are represented by few phenocrysts with lower calcium values in R1(1) at 76-75 Mg# and some in I3 at 93-91 Mg# (yellow-line polygons in Fig. 5.18 C).

5.4.3 Trace elements

Transitional and base metals. All clinopyroxenes display a consistent trend of decreasing Ni contents with decreasing Mg# (Fig. 5.19). No significant differences are observed between the three age Groups and between phenocrysts from the Plinian and inter- Plinian eruptions (not shown). However some of the high-magnesian Group 3 phenocrysts have lower concentrations of Ni compared to pyroxenes from groups 2 and 3. Other metals (Co, Sc, V, Zn) also display generally consistent trends, however, unlike Ni, their concentration increase with decreasing Mg#. Sc shows a rapid increase between Mg# 95 and 87, but remains relatively constant at Mg# < 87. Similarly to Ni, some of the Group 3 high-magnesian phenocrysts differ from the older phenocrysts by having higher values of Co, Sc , Zn and V. Also, a relatively larger scatter is observed at lower Mg# compositions for Sc and Ni. Cu contents are low and do not show any systematic pattern, likely due to significant errors.

Rare-earth elements. All clinopyroxene display a consistent trend of increasing REE contents

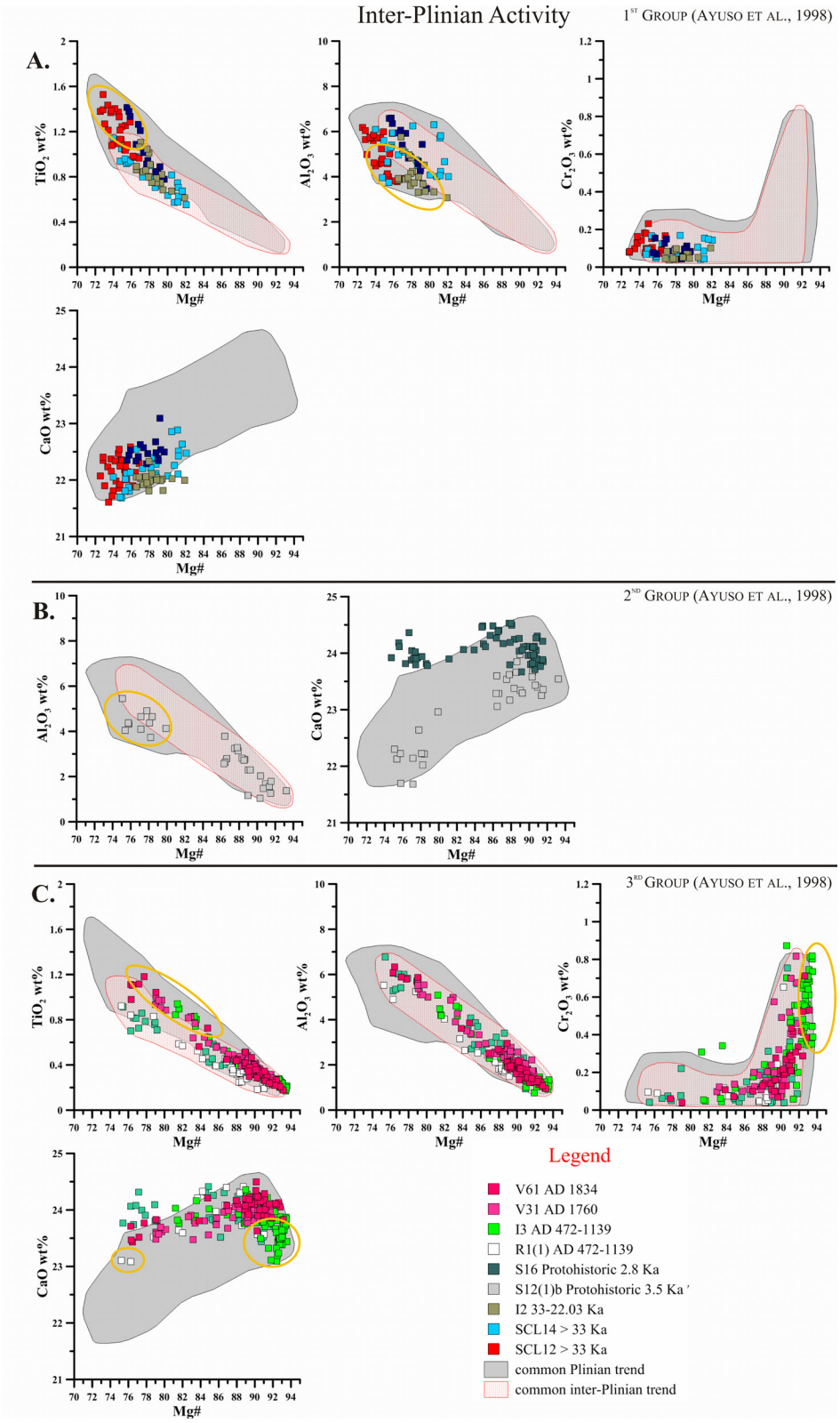

Figure 5.18 A-C Selected plots (major and minor elements vs Mg#) which display significant varia tions within/among the different Somma-Vesuvius inter-Plinian clinopyroxenes populations subdivided in three geochemical groups following Ayuso et al. (1998). Grey and red polygons represent the compositional ranges defined respectively by the majority of Plinian and inter-Plinian clinopyroxenes; whereas yellow lines highlight some internal discrepancies.

with decreasing Mg# (Fig. 5.20). When plotted normalised to the Primitive Mantle (McDonough and Sun, 1995), the REE contents display a humped pattern with a maximum at Nd and Sm, which is typical for clinopyroxenes from incompatible-element enriched magmas (Barnekow, 2000; Francalanci et al., 1987; Freda et al., 2006; Gioncada et al., 2005).

Despite this general similarity of the REE patterns, indicating that all clinopyroxenes crystallised from a similar magma, some subtle differences are observed. Pyroxenes from Group 3 eruptions are characterised by a higher, on average, Sm/Lu values, compared to the older clinopyroxenes, and there is a clear overall trend of more fractionated heavy REE patterns with decreasing age (Fig. 5.21). Note that the subtle but consistent decrease in Sm/Lu values with decreasing Mg# reflects changes in $D_{cpx/melt}$ values as a function of clinopyroxenes composition, with heavy REE Ds increasing faster than the middle REE Ds at lower Mg# values.

In order to assess in more detail the range of variation in REE contents in clinopyroxene, the compositions of representative pyroxenes from all three age Groups, both from Plinian and inter-Plinian eruptions, are compared to the compositions of a magnesian Plinian clinopyroxene from each Group (Fig. 5.22 and 5.23). Within each Group, there are clinopyroxenes which have REE patterns roughly parallel to the patterns of magnesian phenocrysts chosen for normalisation (Fig. 5.22 A, B, C, and 5.23 G, H, I). However, inside each Group there are also clinopyroxenes from both Plinian and inter-Plinian eruptions, which have fractionated patterns compared to the normalisation clinopyroxenes (Fig. 5.22 D, E, F, and 5.23 J, K). There are three general fractionated patterns, which are present in all Groups: patterns enriched in light REE, patterns depleted in light REE, and V-shaped patterns with a minimum at Eu.

The largest range of variations in the REE patterns (differences in La/Sm and Sm/Lu values) is observed in the high-magnesian phenocrysts from Group 3. The implications of these observations will be discussed in Chapter 7.

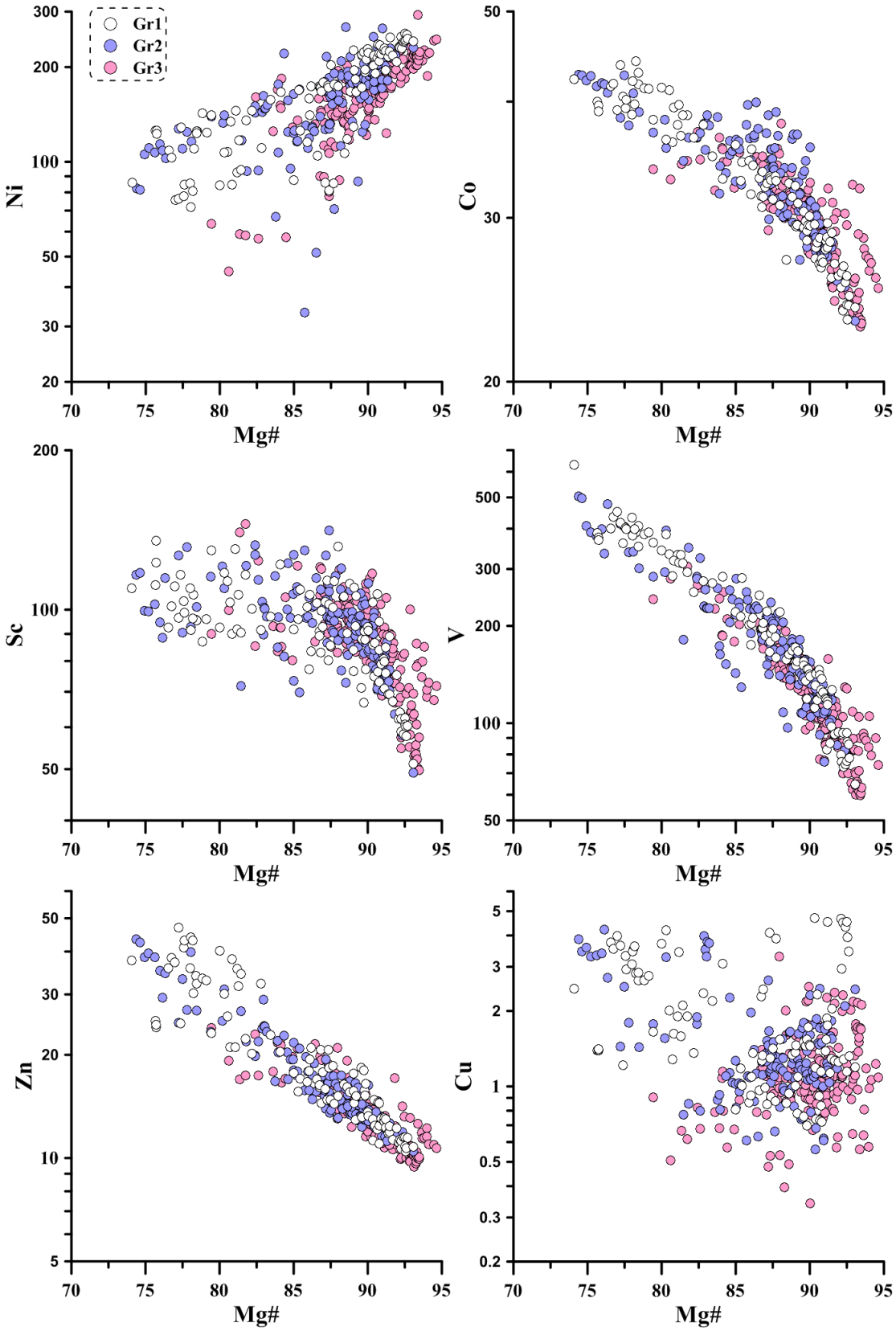

Figure 5.19 Selected trace elements plots (compatible trace elements in ppm vs Mg#) of Somma-Vesuvius clinopyroxene phenocrysts.

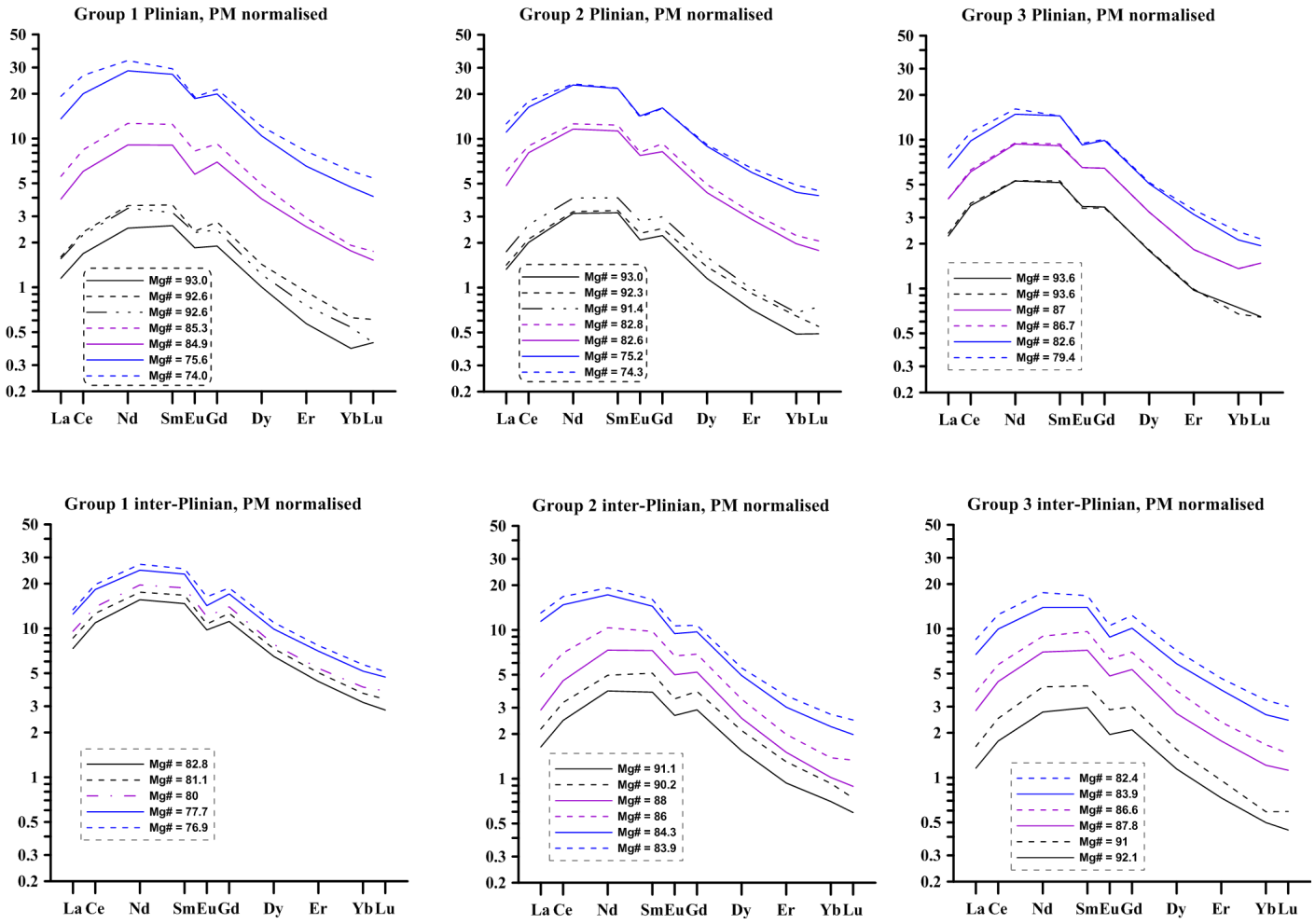

Figure 5.20 REE normalized diagrams (PM = primitive mantle; McDonough and Sun, 1995) of representative Plinian and inter-Plinian clinopyroxene phenocrysts from each geochemical group

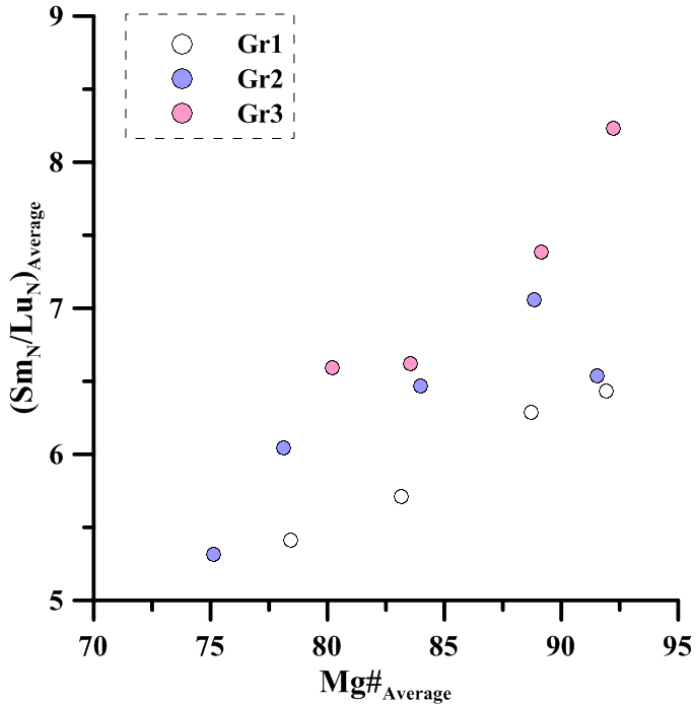

Figure 5.21 Compositions of clinopyroxene phenocrysts averaged between Mg# values of 75-80, 80-85, 85-90, 90-95. The plot demonstrate progressively more fractionated heavy REE patterns with decreasing eruption age. Note that the subtle but consistent decrease in Sm/Lu values with decreasing Mg# reflects changes in $D_{cpx/melt}$ values as a function of clinopyroxene composition, with heavy REE Ds increasing faster than the middle REE Ds at lower Mg# values.

5.5 Mineral inclusions

A common feature of the Somma-Vesuvius clinopyroxenes is the presence of mineral inclusions within their structure. Among the latter, 134 were analysed at the electronic microprobe; around 65 % of these inclusions has been identified as apatites. Within Somma-Vesuvius clinopyroxenes, they occur as micro-crystals, 10-30 μm in size, frequently with prismatic elongated habit, sometimes acicular-like, or in hexagonal sections with a weak cleavage that is scarcely visible under the optic microscope. Alongside these apatites, olivine and clinopyroxene mineral inclusions represent the second most abundant phases; both habitually appear as euhedral crystals with similar sizes to apatites, and respectively with prismatic and squat habit. The clinopyroxenes inclusions exhibit a Mg# interval between 68.0 and 78.5, and their major/ minor element compositions fall within the trends defined by the phenocrysts. Olivine inclusions are characterised by Fo between 89.5 and 71.0, and their major/minor elements chemistry is also similar to Somma-Vesuvius olivines phenocrysts composition (Chapter 6). Rare spinel inclusions are also present, with compositions of titano-magnesio magnetite. They occur as tiny square/lozenge-shaped crystals ~ 10-15 μm in size. Representative inclusion analyses are reported in table 5.3.

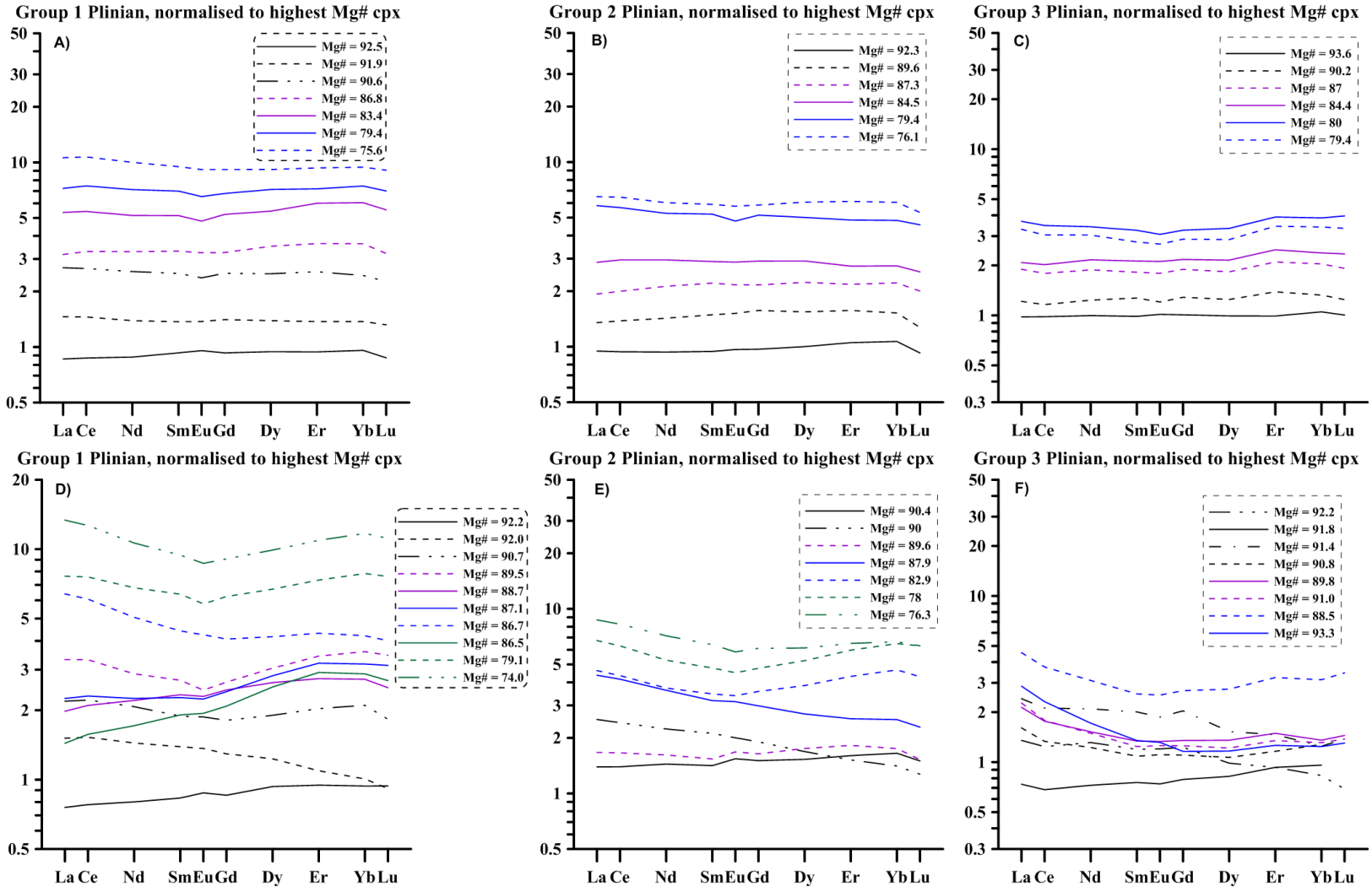

Figure 5.22 Representative REE contents of Plinian clinopyroxene phenocrysts from the three age Groups, normalised to a representative high-magnesian Plinian phenocryst from each group.

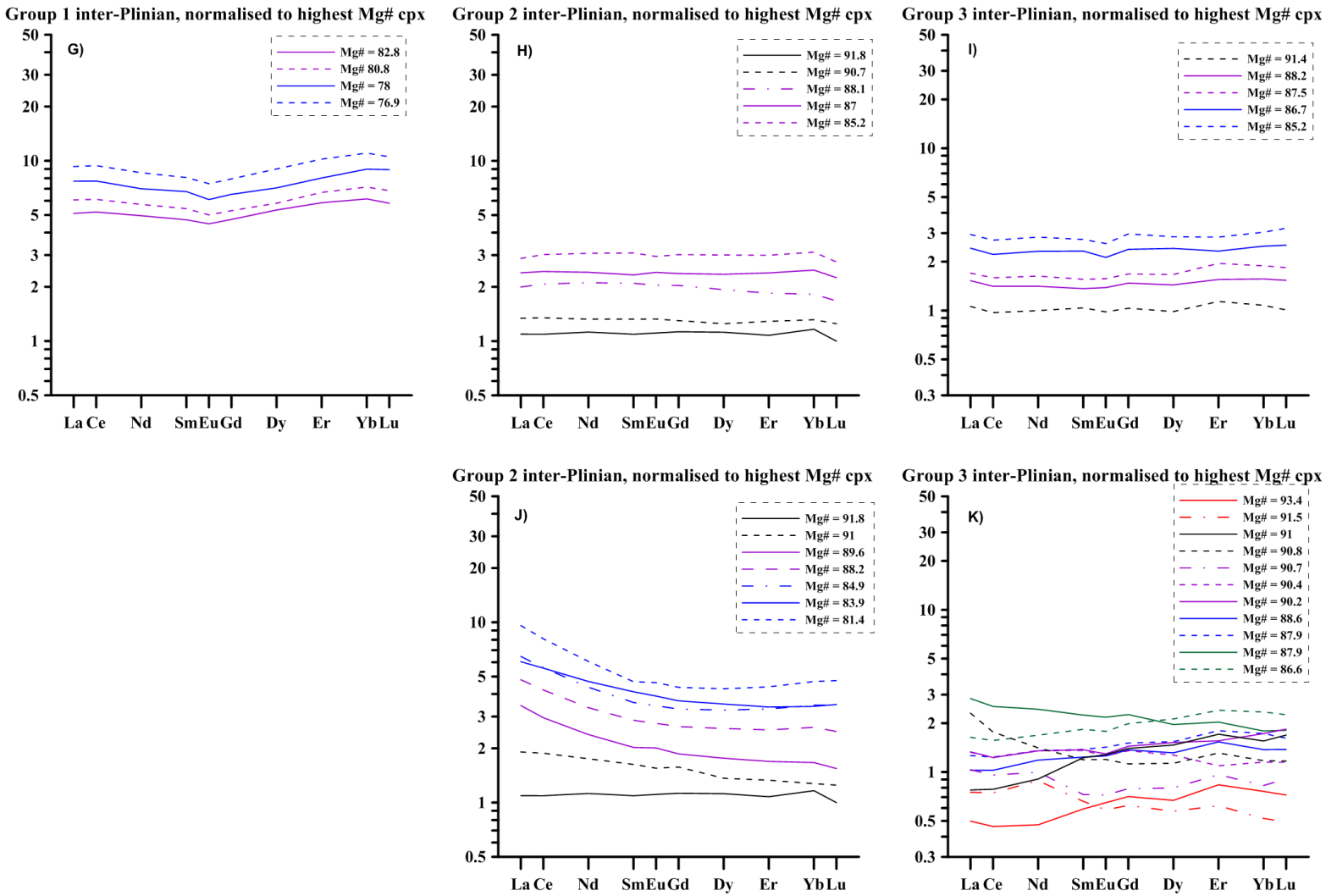

Figure 5.23 Representative REE contents of inter-Plinian clinopyroxene phenocrysts from the three age Groups, normalised to a representative high-magnesian Plinian phenocryst from each group.

sample	LM3	I4	LM1	LM2	LM5	LM2	P2	LM8	LM5	I4
mount/grain	D11/65	D84/41	D24/69	D31/37	D1/75	D33/50	D48/43	D55/119	D1/84	D84/64
SiO_2	0.36	0.35	0.09	0.11	36.33	38.88	40.30	45.68	48.25	49.12
TiO_2	0.02	0.00	13.20	6.93	0.02	0.00	0.03	1.24	1.19	0.88
Al_2O_3	0.00	0.02	7.04	10.75	0.02	0.01	0.02	7.62	6	3.72
FeO*	0.42	0.31	70.76	62.37	25.52	18.72	10.42	9.28	7.7	7.14
MnO	0.04	0.02	0.51	0.37	0.50	0.39	0.22	0.2	0.17	0.24
MgO	0.42	0.38	5.54	6.18	36.16	41.52	49.97	10.79	13.43	14.46
CaO	54.50	54.77	0.11	0.21	0.41	0.39	0.34	24.03	21.99	22.18
K_2O	0.02	0.01	0.02	0.02	0.03	0.01	0.00	0.47	0.33	0.00
Na_2O	0.00	0.06	0.03	0.03	0.00	0.04	0.01	0.01	0.03	0.25
Cr_2O_3	0.00	0.00	0.12	10.40	0.01	0.01	0.04	0.01	0.09	0.16
NiO	0.02	0.00	0.09	0.06	0.08	0.08	0.21	0.03	0.00	0.01
P_2O_5	41.44	41.35	0.01	0.00	0.04	0.11	0.03	0.02	0.07	0.05
SO_3	0.01	0.13	0.01	0.03	0.01	0.00	0.00	0.00	0.01	0.03
SrO	0.19	0.46	0.02	0.00	0.00	0.00	0.00	0.01	0.00	0.00
BaO	0.12	0.00	0.04	0.13	0.00	0.01	0.00	0.00	0.07	0.00
Cl	0.72	0.75	0.00	0.01	0.00	0.00	0.01	0.00	0.00	0.00
total	98.28	98.61	97.59	97.59	99.13	100.17	101.60	99.39	99.33	98.24
class	apatite	apatite	magnetite	magnetite	olivine	olivine	olivine	salite	salite	salite
Mg#			18.47*	21.13*	71.64	79.82	89.53	67.46	75.67	78.31
Mg# host			72.44	74.23	75.80	79.97	88.27	77.81	75.94	78.63
$Fe^{2+}O$			43.55	41.10						
$Fe^{3+}{}_2O_3$			31.57	25.39						
Wo								51.9	47.1	46.3
En								32.4	40.0	42.0
Fs								15.6	12.9	11.6

Table 5.3 Representative (EMPA) major/minor elements compositions of mineral inclusions in clinopyroxene phenocrysts from Somma-Vesuvius eruptive products. The starred Mg# for the two magnetite inclusions is calculated using only $Fe^{2+}O$.

Chapter 6: Olivines Mineralogy at Somma-Vesuvius

6.1 Introduction

This chapter presents a detailed description of the mineralogical and geo-chemical features of Somma-Vesuvius olivine phenocrysts. This section is divided in 4 main subsections describing mineralogical and compositional features of olivine phenocrysts. Olivine phenocryst compositions from the Somma-Vesuvius are compared to compositions of olivines from other tectonic settings and to other volcanoes within the Roman Comagmatic Province (RCP). Mineral inclusions in Somma-Vesuvius olivine phenocrysts are also described.
This chapter is based on 965 EMPA analyses for major elements and 635 LA-ICPMS analyses for trace elements. Some of the LA-ICPMS analyses, those which ablated melt and/ or fluid inclusions inside phenocrysts, had to be excluded from considerations as elemental concentrations in such analyses are compromised. All data are presented in Appendix.

6.2 Olivines: a brief overview

Olivine belongs to the nesosilicates class. It commonly occurs in intrusive and effusive igneous rocks both as phenocrysts and as microlites. The majority of olivines are solid solutions; the end-members of the olivine group are: Forsterite (Mg_2SiO_4), Fayalite (Fe_2SiO_4), Tephroite (Mn_2SiO_4), Monticellite ($CaMgSiO_4$), Kirschteinite ($CaFeSiO_4$), Glaucochroite ($CaMnSiO_4$), and Picrotephroite ($(MgMn)_2SiO_4$).
Between Mg_2SiO_4 and Fe_2SiO_4 (and Fe_2SiO_4-Mn_2SiO_4) there is complete solid solution, and the most abundant natural members of the olivine group belong to this series. The different members of the series are named based on their composition in terms of proportion of Forsterite (Fo): forsterite (Fo_{100-90}), chrysolite (Fo_{90-70}), hyalosiderite (Fo_{70-50}), hortnolite (Fo_{50-30}), ferrohortonolite (Fo_{30-10}), and fayalite (Fo_{10-0}) (e.g., Peccerillo and Perugini, 2003).
Olivines are the first silicate phase to crystallize from ultramafic and mafic magmas (Donaldson, 1981) and are the main constituent of mantle peridotite, with compositions from Fo_{94} to Fo_{87}. Olivines are also common in ultramafic nodules, basalts and kimberlites ranging in composition between Fo_{91}-Fo_{86} and commonly in gabbroic rocks with Fo_{80}- Fo_{50} (Deer et al., 1966). The fosteritic olivines appear in mafic and ultramafic melts; the magnesium rich olivines never in equilibrium with silica with which they react producing Enstatite ($Mg_2SiO_4+SiO_2 = 2MgSiO_3$) whereas iron-rich olivines are widely found in acidic and alkaline igneous rocks as granites,

obsidians, rhyolites, trachytes and phonolites. Olivines crystallize in the orthorhombic system (space group Pbnm) and their structure is formed by independent SiO_4 tetrahedra which are bonded usually by Mg and Fe atoms to the six closest oxygens. The SiO_4 tetrahedra are alternatively directed either way along both x and y directions and the oxygens lie in sheets parallel to the {100} plane. As remarked by Birle et al. (1968) one-half of the available octahedral voids are occupied by M atoms and one-eighth of the available tetrahedral voids by T atoms. Olivine general formula is $(M1M2)_2TO_4$; Mg^{2+} and Fe^{2+} seat in M1 and M2 sites with different degrees of ordering even though the larger Fe^{2+} cation exhibits an unexpected preference for the smaller M1 (Deer et al., 1966). Chemically, in many natural olivines Mn and Ca substitute to some extent both Mg and Fe; however, the Ca amount is commonly not above 1 wt%. Moreover, in magnesium rich olivines Ni and Cr are commonly present but chromium usually exsolves in micro chromite plates.

6.3 Olivines at Somma-Vesuvius

6.3.1 Distinguishing features

Olivine is an omnipresent but very rare phase in all lava, scoriae and pumice samples investigated in the present project (see also Barberi et al., 1981; Joron et al., 1987).

Overall, these crystals have a glassy lustre and a massive/granular habit; also, they are commonly euhedral or sub-euhedral with slightly elongated hexagonal profile in section, and exhibit a very brittle fracture with a tendency to produce small conchoidal fragments. Under the microscope, some specimens display a good cleavage along {001} and also along {010} , especially in the less Mg-rich specimens. In the majority of the Somma-Vesuvius products, olivine occurs both as phenocrysts, (1 - 0.5 mm in size), and micro phenocrysts in the groundmass (< 0.5 mm); within both populations, the majority appears yellowish-green and only few Fe-richer oxidized specimens have reddish-brown colour. Lastly, as it was previously noted for clinopyroxenes, many olivine phenocrysts are broadly zoned and contain numerous fluid, melt and mineral inclusions. However, only melt inclusions in a few Somma-Vesuvius samples were studied (e.g., Brocchini et al., 2001; Marianelli et al., 1999; Marianelli et al., 1995; Lima et al., 2003; Vaggelli et al., 1992; Vaggelli et al., 1993). Several studies have suggested that olivine phenocrysts in Somma-Vesuvius magmas form in responce to the interaction between the melt and the Mesozoic carbonate basement at shallow depths (e.g., Barberi et al., 1981; Joron et al., 1987).

6.3.2 Zoning: a common feature of Somma-Vesuvius olivines

Zoning occurs widely within olivine crystals and it is a phenomenon which is usually deciphered as a response to disequilibrium conditions in the magmatic system. Preservation of zoning patterns in solid solution minerals is a function of the time the phenocrysts spend in the magmatic system at high temperature, as diffusion would lead to levelling any compositional gradients. As diffusion rates in olivine are among the fastest among all main silicate minerals (e.g., Costa et al., 2008; Donaldson, 1990), the fact that zoning patterns are preserved indicates that they were formed not long before the eruption. Overall, zoning provides important information on the precesses within the magmatic system such as fractional crystallization or magmatic recharge (Streck, 2008). Homogeneous olivine crystals were observed in all the lava, scoriae and pumice samples considered in the present project, being the most abundant type within the entire Somma-Vesuvius olivine population (type a and b in figure 6.1).

Zoned olivine crystals were also found in every sample, although they most common in the Plinian and inter-Plinian samples older than 19.2 Ka. Different zoning types were recognized and they correspond approximately to those previously observed within clinopyroxenes (c-g in figure 6.1). The majority of the zoned olivine crystals exhibit normal zoning with more forsteritic olivine in the core and progressively more fayalitic olivine towards the rim (c, e and f in figure 6.1). In some rare cases reverse zoning, oscillatory zoning and patchy zoning patterns were also observed.

6.3.3 Mineral composition and population distribution

Overall, olivine phenocrysts from Somma-Vesuvius reveal a major element compositional range which spans from $Fo_{91.4}$ to $Fo_{68.2}$; according to Donaldson (1981), the vast majority of Somma- Vesuvius olivines from both Plinian and inter-Plinian activity can be classified as "Chrysolite" (Fo_{90-70}) with subordinate "Forsterite" (Fo_{100-90}) and rare "Hyalosiderite" (Fo_{70-50}). In many samples, similar to clinopyroxene, olivine compositions display bimodal distribution of their Fo contents.

The obtained Fo values are displayed as relative frequencies on a series of histograms in figures 6.2, 6.3 and 6.4, with the intent to visually display the variations in distribution patterns between individual eruptions and/or between the two main eruptive phenomena occurring at Vesuvius, Plinian and inter-Plinian eruptions.

In the lava samples, SCL12, SCL14, I4 and I2 which belong to the non-Plinian activity older than 19.2 Ka, the main olivine population has compositions between 78 and 68 Fo (Fig. 6.2); however, in sample I2, there are also several phenocrysts which have higher Fo# values (~ 91-90). Unlike the inter-Plinian, the Plinian samples Sarno (~22.03 Ka) and Novelle (~ 19.2

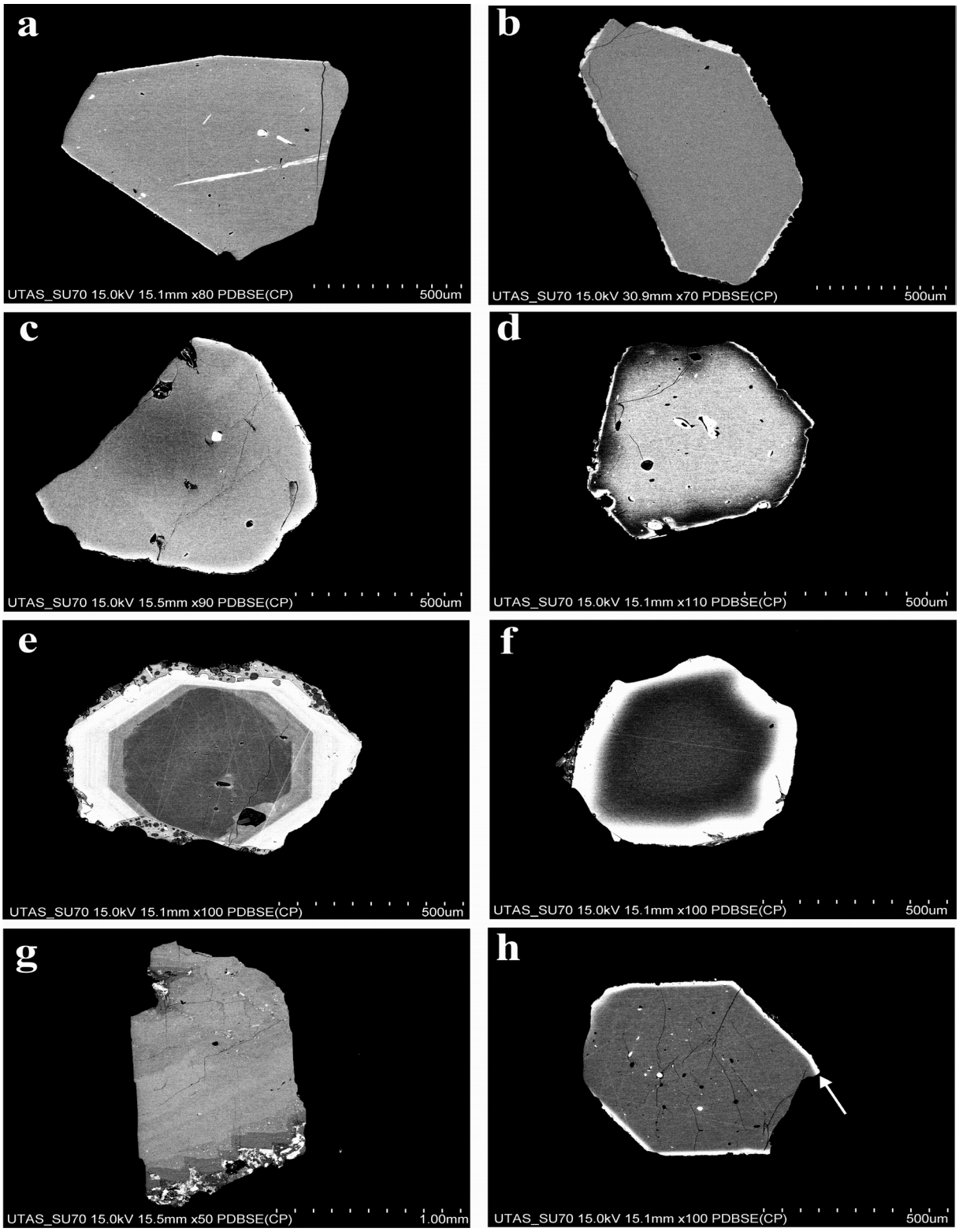

Figure 6.1 a-h. SEM-BSE images of representative zoning types in olivine phenocrysts at Somma-Vesuvius for the last 33 Ky. a) and b) Homogeneous sub-euhedral/euhedral phenocrysts which belong to two pumices samples from the basal layers of the Novelle (~ 19.2 Ka) and Ottaviano (~ 8.9 Ka) eruptions, respectively. c) and d) Normal and reverse zoning in sub-euhedral/euhedral phenocrysts; "c" is from a pumice sample from the top layer of the Novelle eruption (~ 19.2 Ka); "d" is from an old Somma lava sample (22.03-19.2 Ka). e) Roughly homogeneous core surrounded by zoned margin in a euhedral hexagonal phenocryst from a scoria sample of historic times (AD 79-472). f) Roughly homogeneous forsteritic core surrounded by a fayalitic margin from an old lava sample (22.03-19.2 Ka). g) Complex forsterite-fayalite oscillatory zoning in an elongated sub-euhedral crystal from a scoria sample of Protohistoric times (~ 3.5 Ka). h) Hex agonal euhedral phenocryst with a typical narrow faylite-rich outer zone formed on during eruption (white arrow) from a scoria sample of Medieval Times (AD 472-1139).

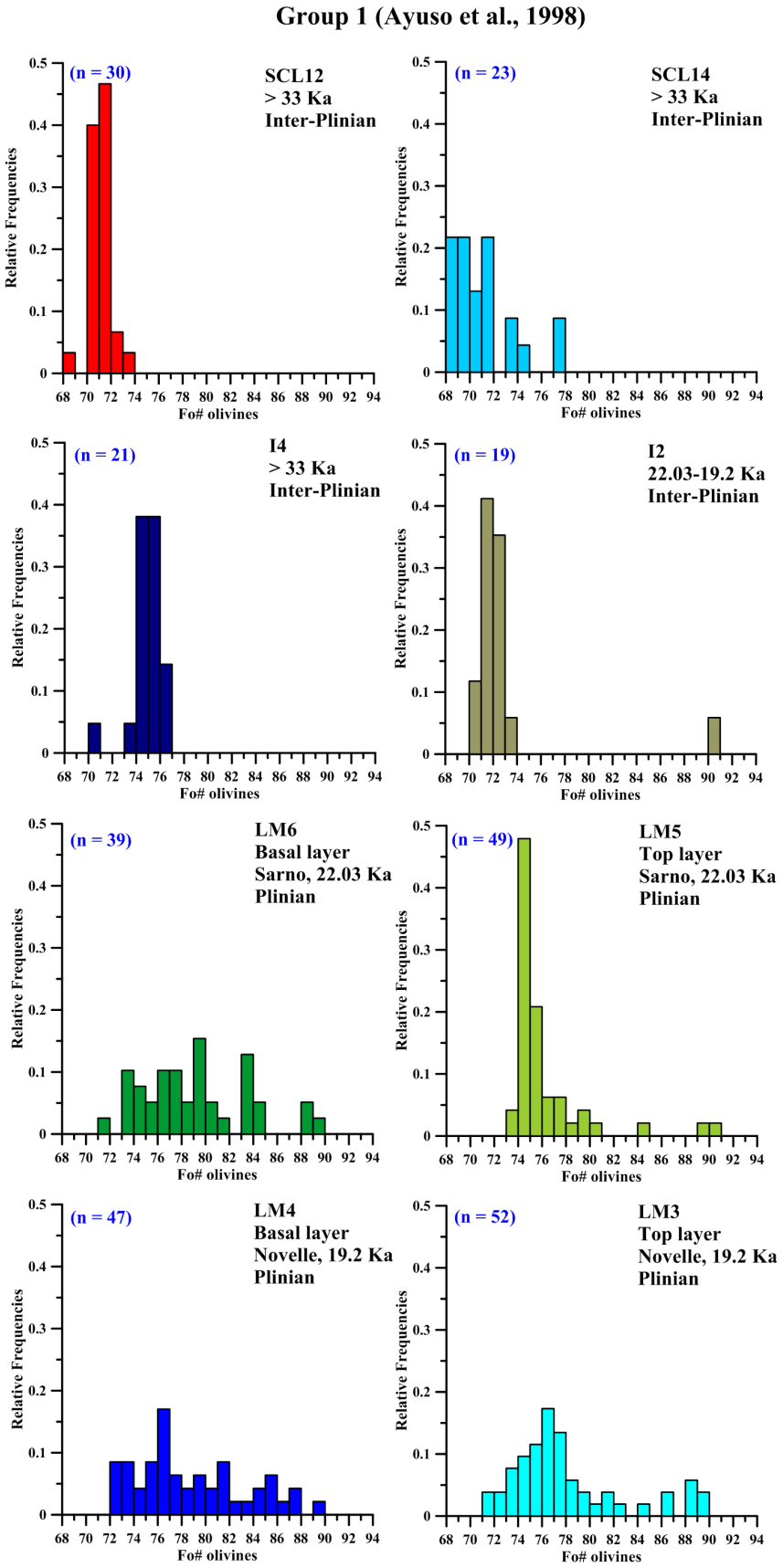

Figure 6.2 Histograms displaying Somma-Vesuvius olivine phenocrysts distribution as relative frequencies for samples which belong to the geochemical Group 1 following Ayuso et al. (1998) Somma-Vesuvius rocks subdivision (Fo# = MgO/40.3/(MgO/40.3 + FeO/71.85).

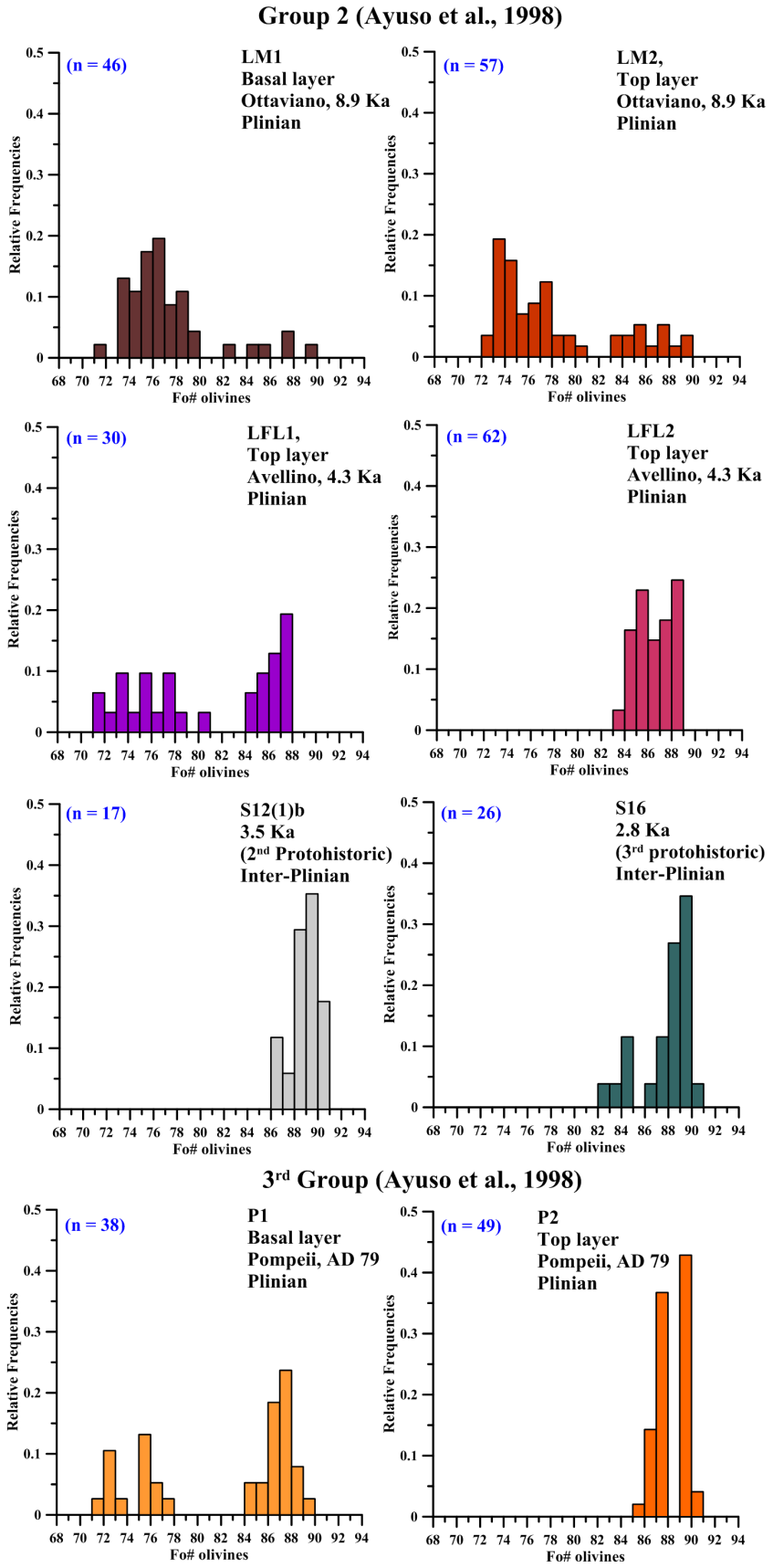

Figure 6.3 Histograms displaying Somma-Vesuvius olivine phenocrysts distribution as relative frequencies for samples which belongs respectively to the geochemical Groups 2 and 3 following Ayuso et al. (1998) Somma-Vesuvius rocks subdivision.

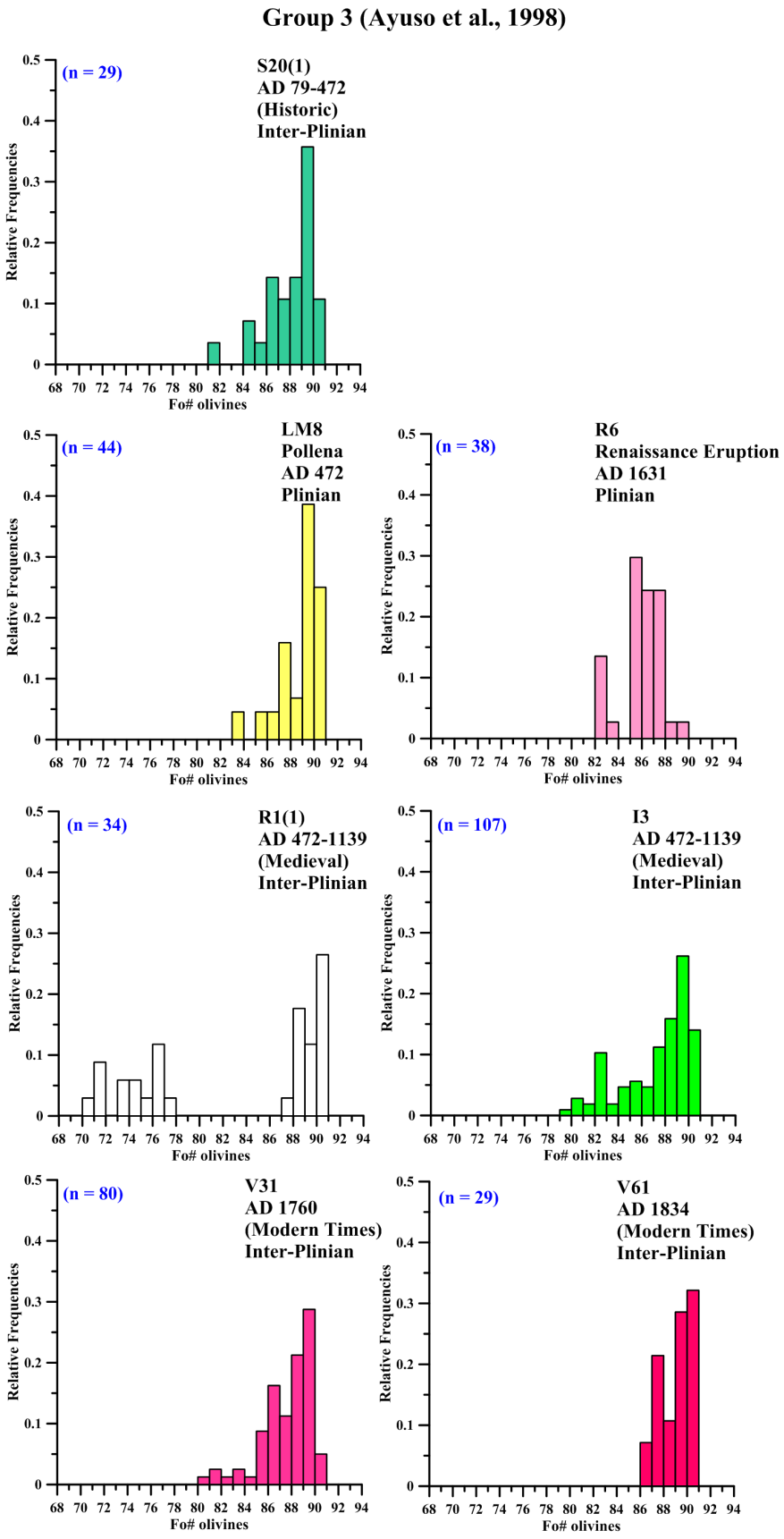

Figure 6.4 Histograms displaying Somma-Vesuvius olivine phenocrysts distribution as relative frequencies for samples which belong to the geochemical Group 3 following Ayuso et al. (1998) Somma-Vesuvius rocks subdivision.

Ka) Plinian eruptions from Group 1 (Ayuso et al., 1998), pumice samples LM5, LM6, LM3, and LM4, are characterised by a wider Fo range between ~ Fo 91 and 71 (Fig. 6.2). Bimodal distribution is observed in the top layer of Novelle eruption in which a smaller and more primitive population at Fo_{90-84} is present. In all Plinian samples from Group 1, more evolved compositions are more abundant.

Similarly, the younger Ottaviano (~ 8.9 Ka) and Avellino (~ 4.3 Ka) Plinian eruptions, samples LM1, LM2, LFL1, and LFL2, are similar to the older Plinian activity (Fig. 6.3); two olivine populations with similar Fo intervals, Fo 71-80 and Fo 83-90, are present. In the Ottaviano eruption, the majority of olivine phenocrysts (~80%) are within the lower Fo group, whereas in Avellino the more magnesian group dominates (~ 84%). The Avellino top layer (sample LFL2) contain only one population at Fo_{89-83}. The inter-Plinian period which follows this Plinian activity, the so-called "Protohistoric" period (4.3 Ka – A.D.79) is represented by two scoriae samples S12(1)b (~ 3.5 Ka) and S16 (~ 2.8 Ka), which contain only one primitive olivine population between ~ 82 and 91 Fo.

Within Group 3, the Pompeii eruption (A.D. 79), pumice samples P1 and P2, contain olivine phenocrysts with distribution patterns remarkably similar to the Avellino eruption (Fig. 6.3). Overall there are two distinct olivine populations: the more primitive, Fo_{90-84} is the more abundant (83 %) than the more evolved (Fo_{78-71}). Similarly to Avellino, the top layer of the Pompeii eruption contains the primitive population only. All younger Plinian and inter-Plinian eruptions within Group 3, with the exception of one Medieval scoria sample R1(1), are characterized by only one more primitive population at Fo_{91-80} (Fig. 6.4). Sample R1(1) (A.D. 472-1139) has two populations, similar to most Plinian samples.

In summary, similarly to the compositions of clinopyroxene phenocrysts, all samples studied are characterised by a significant range of Mg# of olivine phenocrysts. The range of phenocryst compositions remains effectively the same over the time span of the Somma-Vesuvius activity studied here. Average compositions of olivine phenocrysts from each sample are presented in table 6.1. Figure 6.5 compares average compositions of olivine and clinopyroxene from each sample with the rock compositions. Similarly to the clinopyroxene compositions, the average olivine phenocryst compositions become progressively more magnesian with decreasing eruption age, and there is no relationship between the average phenocryst compositions and the MgO content of the rocks (a reflection of the amount of olivine and clinopyroxene accumulation), or the eruption style. The implications of this observations will be discussed in Chapter 7.

For samples dominated by the high-magnesian phenocryst populations, the average compositions of olivine and clinopyroxene are effectively identical, whereas in samples with more evolved average compositions, clinopyroxene is more magnesian than olivine. As shown by experimental

sample	SCL12	SCL14	I4	I2	LM6	LM5	LM4	LM3
age	> 33 Ka	> 33 Ka	> 33 Ka	22.03-19.2 Ka	22.03 Ka	22.03 Ka	19.2 Ka	19.2 Ka
group	Group 1	Group 1	Group 1	Group 1	Group 1	Group 1	Group 1	Group 1
eruptive style	Inter-Plinian	Inter-Plinian	Inter-Plinian	Inter-Plinian	Plinian	Plinian	Plinian	Plinian
	average	average	average	average	average	average	average	average
SiO_2	37.62	37.85	37.87	37.62	38.62	38.26	38.70	38.57
FeO	25.70	25.95	22.73	25.55	19.49	21.17	19.52	19.87
MnO	0.53	0.48	0.39	0.42	0.40	0.44	0.40	0.41
MgO	35.75	35.36	38.59	36.06	41.03	39.67	40.92	40.69
CaO	0.33	0.31	0.32	0.29	0.33	0.35	0.32	0.33
NiO	0.06	0.05	0.08	0.05	0.12	0.10	0.12	0.11
Tot	100.00	100.00	99.99	100.00	99.99	99.99	99.99	99.99
Mg#	71	71	75	72	79	77	79	78
sample	LM1	LM2	LFL1	LFL2	S12(1)b	S16	P1	P2
age	8.9 Ka	8.9 Ka	4.3 Ka	4.3 Ka	3.5 Ka	2.8 Ka	AD 79	AD 79
group	Group 2	Group 2	Group 2	Group 2	Group 2	Group 2	Group 3	Group 3
eruptive style	Plinian	Plinian	Plinian	Plinian	Inter-Plinian	Inter-Plinian	Plinian	Plinian
	average	average	average	average	average	average	average	average
SiO_2	38.43	38.44	39.00	39.81	40.32	40.54	39.35	40.16
FeO	20.99	20.16	18.05	12.92	10.86	11.50	16.39	11.22
MnO	0.44	0.42	0.36	0.23	0.19	0.23	0.30	0.22
MgO	39.69	40.53	42.17	46.61	48.18	47.24	43.52	47.91
CaO	0.34	0.34	0.30	0.25	0.24	0.28	0.31	0.29
NiO	0.10	0.11	0.11	0.16	0.18	0.20	0.13	0.18
Tot	100.00	99.99	100.00	99.99	99.98	99.98	99.99	99.98
Mg#	77	78	80	87	89	88	82	88
sample	S20(1)	LM8	R1(1)	I3	R6	V31	V61	
age	AD 79-472	AD 472	AD 472-1139	AD 472-1139	AD 1631	AD 1760	AD 1834	
group	Group 3	Group 3	Group 3	Group 3	Group 3	Group 3	Group 3	
eruptive style	Inter-Plinian	Plinian	Inter-Plinian	Inter-Plinian	Plinian	Inter-Plinian	Inter-Plinian	
	average	average	average	average	average	average	average	
SiO_2	40.16	40.32	39.51	40.12	39.86	39.93	40.54	
FeO	11.31	10.93	15.53	12.06	13.34	11.84	10.63	
MnO	0.22	0.20	0.28	0.25	0.27	0.23	0.21	
MgO	47.80	48.04	44.18	47.00	46.06	47.47	48.10	
CaO	0.29	0.30	0.31	0.36	0.28	0.337	0.342	
NiO	0.20	0.19	0.16	0.20	0.18	0.17	0.16	
Tot	99.98	99.98	99.98	99.98	99.99	99.98	99.98	
Mg#	88	89	83	87	86	88	89	

Table 6.1 Major/minor elements average compositions of olivine phenocrysts in each studied sample.

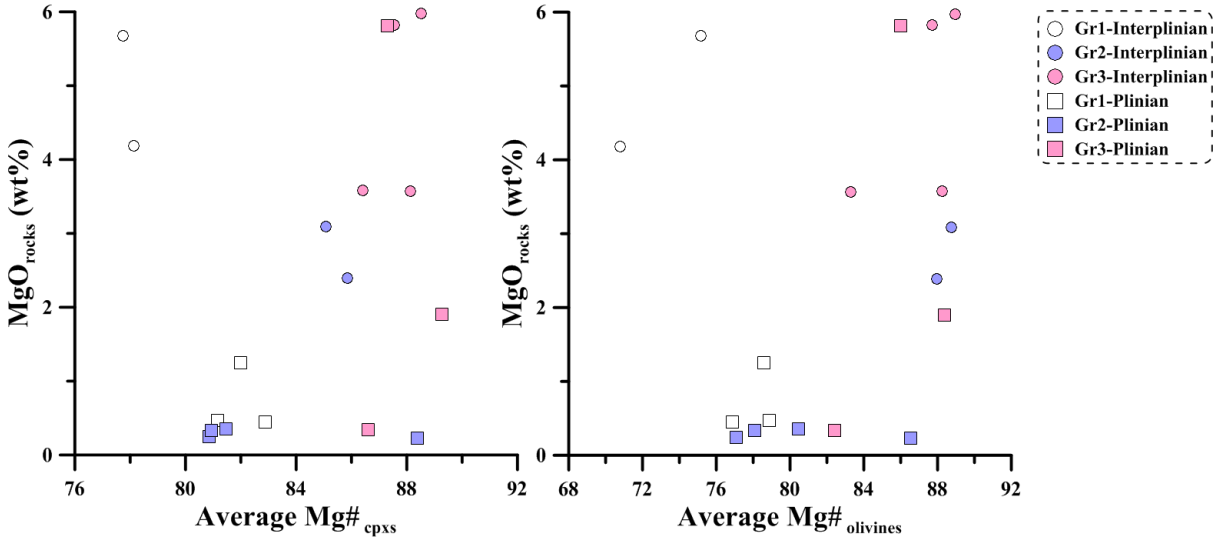

Figure 6.5 Comparative plots of olivine and clinopyroxene average compositions with MgO content of Somma-Vesuvius rocks.

studies (i.e., *Vrnr-zrur, 1992*), at temperatures around 1200 °C, co-crystallising olivine and clinopyroxene would have very similar Mg#; whereas, at lower temperatures clinopyroxene is progressively more magnesian than co-existing olivine. Thus the observed relationships between average compositions of olivine and clinopyroxene phencrysts are consistent with their formation during cotectic olivine-clinopyroxene crystallisation. Co-crystllisation of olivine and clinopyroxene has been suggested for Somma-Vesuvius magmas in many studies (i.e., Cigolini, 2007; Joron et al., 1987; Lima et al., 2003, Marianelli et al., 1999; Pappalardo et al., 2010; Piochi et al., 2006a).

6.4 Somma-Vesuvius olivines: major and minor elements

6.4.1 Major and minor elements

Representative EMPA analyses of major and minor elements in Somma-Vesuvius olivine phenocrysts are reported in table 6.2; overall, minor elements content in olivines from different eruptions of Somma-Vesuvius are similar (Fig 6.6). MnO concentration in olivine from all samples form a tight trend. No clear differences is observed between olivines from the three Groups, however the relatively low MnO contents in low-Fo olivines have not been found in our Group 2 samples. CaO contents show a general increase with decreasing Fo, however the variations are significant at any given Fo. It appears that on average, Group 3 samples have somewhat higher CaO contents, although the differences are not statistically meaningful based on the number of analyses collected in this study. NiO contents decrease with decreasing Fo, forming an overall tight trend for all samples. In all three Groups, there are high-Fo samples that have somewhat lower Ni contents than the main trend.

When different eruption styles are compared (Fig. 6.7), it is clear that the observered deviations from the main trend are found in olivines from both Plinian and inter-Plinian eruptions. For example, the low-Fo, low-MnO group is represented by olivines from both Plinian and inter- Plinian eruptions in samples from Groups 1 and 3, whereas within Group 3, the low-Ni, high-Fo olivines are also present in both Plinian and inter-Plinian eruptions. The high-CaO olivines are more common in the inter-Plinian samples from Group 3, but in the Plinian samples from Groups 1 and 2. This is likely to reflect sampling bias rather than being an indication of systematic differences between Somma-Vesuvius geochemical cycles and/or eruption styles.

In order to better understand the significance of the observed variations in the composition of Somma-Vesuvius olivine phenocrysts at a given Fo, their compositions are compared to the published olivine compositions from other volcanoes within the Roman Comagmatic Province and from other tectonic settings (Figs 6.8 and 6.9). Compared to other volcanoes

within the RCP, Somma-Vesuvius olivines have a significantly narrow range of CaO and similar ranges of NiO and MgO. The relatively narrow range of minor elements concentrations in Somma- Vesuvius olivines is highlighted even stronger when their compositions are compared to olivines from other tectonic settings. It can be thus concluded that, similar to clinopyroxene, olivine compositions show little variations, clearly indicating that they are formed by a single magma type.

age	> 33 Ka		> 33 Ka		> 33 Ka		22.03-19.2 Ka		~22.03 Ka - basal Sarno			~22.03 Ka - basal Sarno		
sample	SCL12	SCL12	SCL14	SCL14	I4	I4	I2	I2	LM6	LM6	LM6	LM5	LM5	LM5
mount/grain	D7/17	D7/12	D92/144	D92/137	D86/34	D86/14	D89/17	D89/27	D30/72	D30/61	D30/95	D4/14	D4/28	D3/8
SiO_2	37.45	37.75	37.42	38.23	37.78	38.34	37.29	37.59	37.63	38.40	39.36	38.10	37.96	41.25
FeO	26.06	24.83	27.55	24.05	23.22	22.07	26.71	24.38	23.91	20.40	14.90	22.84	20.33	9.05
MnO	0.54	0.50	0.52	0.43	0.39	0.39	0.44	0.42	0.47	0.42	0.34	0.48	0.43	0.20
MgO	35.58	36.35	33.99	36.99	38.24	39.47	34.99	36.98	36.90	40.23	44.67	38.15	40.39	50.10
CaO	0.33	0.34	0.33	0.28	0.35	0.25	0.28	0.29	0.36	0.34	0.40	0.35	0.28	0.29
Cr_2O_3	0.00	0.00	0.00	0.01	0.00	0.01	0.00	0.01	0.00	0.01	0.00	0.01	0.01	0.03
NiO	0.07	0.06	0.05	0.08	0.06	0.14	0.07	0.05	0.08	0.13	0.14	0.07	0.13	0.24
total	100.01	99.82	99.86	100.07	100.03	100.66	99.78	99.72	99.35	99.92	99.82	100.01	99.53	101.16
cations/4*O	3.01	3.00	3.00	3.00	3.01	3.01	3.00	3.01	3.00	3.01	3.01	3.00	3.01	3.00
Mg#	70.88	72.30	68.75	73.27	74.60	76.12	70.02	73.00	73.35	77.86	84.24	74.86	77.98	90.80
class	crysolite	crysolite	hyalosiderite	crysolite	crysolite	crysolite	crysolite	crysolite	crysolite	crysolite	crysolite	crysolite	crysolite	fayalite
age	~ 19.2 Ka - basal Novelle			~ 19.2 Ka - top Novelle			~ 8.9 Ka - top Ottaviano			~ 8.9 Ka - basal Ottaviano			~ 4.3 Ka - basal Avellino	
sample	LM4	LM4	LM4	LM3	LM3	LM3	LM1	LM1	LM1	LM2	LM2	LM2	LFL1	LFL1	LFL1
mount/grain	D19/23	D20/51	D20/39	D15/21	D15/26	D14/7	D23/133	D23/106	D21/33	D35/84	D35/98	D35/80	D38/25	D38/34	D38/17
SiO_2	37.71	38.16	40.61	37.23	38.50	40.24	37.55	38.62	39.84	37.74	38.36	40.34	37.87	38.38	40.03
FeO	24.85	21.50	11.89	24.84	20.61	10.54	23.99	20.71	11.64	24.06	20.68	11.37	24.99	20.35	11.59
MnO	0.51	0.50	0.26	0.49	0.41	0.23	0.50	0.45	0.26	0.53	0.47	0.25	0.48	0.44	0.23
MgO	36.38	39.13	47.40	36.12	39.87	48.44	37.15	39.64	47.10	36.92	39.79	47.75	36.03	40.13	47.59
CaO	0.32	0.44	0.27	0.44	0.28	0.31	0.33	0.45	0.32	0.31	0.46	0.30	0.32	0.44	0.28
Cr_2O_3	0.00	0.00	0.02	0.01	0.00	0.03	0.01	0.00	0.01	0.00	0.01	0.03	0.00	0.00	0.01
NiO	0.06	0.09	0.18	0.06	0.11	0.21	0.07	0.08	0.18	0.06	0.09	0.19	0.08	0.07	0.19
total	99.82	99.81	100.64	99.18	99.79	99.99	99.58	99.95	99.36	99.62	99.85	100.22	99.76	99.80	99.92
cations/4*O	3.00	3.01	3.00	3.01	3.00	3.01	3.01	3.00	3.01	3.00	3.01	3.00	3.00	3.01	3.01
Mg#	72.30	76.44	87.66	72.17	77.52	89.12	73.41	77.34	87.82	73.23	77.43	88.22	71.99	77.86	87.99
class	crysolite	crysolite	crysolite	crysolite	crysolite	crysolite	crysolite	crysolite	crysolite	crysolite	crysolite	crysolite	crysolite	crysolite	crysolite
age	~ 4.3 Ka - basal Avellino			3.5 Ka - Protohistoric		2.8 Ka - Protohistoric		AD 79 - basal Pompeii			AD 79 - top Pompeii			AD 79-472	
sample	LFL2	LFL2	LFL2	S12(1)b	S12(1)b	S16	S16	P1	P1	P1	P2	P2	P2	S20(1)	S20(1)
mount/grain	D44/98	D44/52	D44/44	D83/49	D83/43	D77/110	D77/89	D50/75	D49/48	D50/98	D53/72	D53/78	D53/65	D73/39	D73/52
SiO_2	39.25	40.00	40.22	40.15	40.69	39.72	40.98	37.51	38.50	40.49	40.03	39.90	40.45	39.29	40.91
FeO	14.75	12.66	11.19	12.62	9.72	15.14	9.83	24.68	20.92	10.60	12.49	11.82	9.78	14.69	9.79
MnO	0.29	0.20	0.19	0.20	0.17	0.36	0.18	0.44	0.43	0.17	0.23	0.23	0.19	0.32	0.17
MgO	44.88	46.56	47.86	47.16	49.68	44.34	48.55	36.36	39.73	48.24	46.79	47.69	49.70	45.20	49.45
CaO	0.24	0.24	0.27	0.23	0.25	0.28	0.28	0.33	0.30	0.24	0.27	0.28	0.29	0.28	0.28
Cr_2O_3	0.00	0.02	0.03	0.01	0.03	0.00	0.04	-0.01	0.02	0.02	0.00	0.01	0.03	0.01	0.02
NiO	0.14	0.19	0.20	0.16	0.21	0.15	0.22	0.08	0.12	0.20	0.16	0.18	0.21	0.15	0.22
total	99.55	99.87	99.97	100.53	100.75	99.99	100.08	99.39	100.02	99.96	99.97	100.09	100.65	99.94	100.84
cations/4*O	3.01	3.00	3.01	3.01	3.01	3.00	3.00	3.00	3.00	3.00	3.00	3.01	3.01	3.01	3.00
Mg#	84.44	86.77	88.41	86.95	90.11	83.92	89.80	72.43	77.20	89.03	86.98	87.80	90.06	84.59	90.00
class	crysolite	crysolite	crysolite	crysolite	crysolite	crysolite	crysolite	crysolite	crysolite	crysolite	crysolite	crysolite	fayalite	crysolite	fayalite
age	AD 472 - Pollena			AD 472-1139		AD 472-1139		AD 1631 - Renaissance Erup			AD 1760		AD 1834		
sample	LM8	LM8	LM8	I3	I3	R1(1)	R1(1)	R6	R6	R6	V31	V31	V61	V61	
mount/grain	D57/30	D90/137	D57/11	D67/87	D67/83	D71/83	D71/67	D54/114	D54/89	D54/97	D63/15	D63/24	D60/145	D60/163	
SiO_2	39.49	40.10	40.66	39.00	40.67	37.40	40.23	39.02	39.73	40.25	38.95	40.34	40.22	40.64	
FeO	14.11	12.19	9.32	16.32	9.18	25.47	9.60	16.63	12.90	12.07	17.26	9.74	12.15	9.36	
MnO	0.25	0.23	0.17	0.35	0.16	0.46	0.17	0.34	0.25	0.25	0.35	0.20	0.25	0.20	
MgO	45.38	46.86	49.18	43.30	49.46	35.48	49.38	43.46	46.42	47.37	43.20	49.29	46.68	49.13	
CaO	0.30	0.28	0.37	0.37	0.35	0.33	0.28	0.28	0.29	0.28	0.34	0.34	0.34	0.34	
Cr_2O_3	0.01	0.01	0.02	-0.01	0.05	0.00	0.04	0.02	0.02	0.01	0.01	0.04	0.02	0.06	
NiO	0.09	0.16	0.19	0.15	0.22	0.07	0.21	0.17	0.16	0.19	0.09	0.18	0.15	0.20	
total	99.63	99.84	99.91	99.48	100.09	99.21	99.91	99.92	99.75	100.42	100.19	100.14	99.79	99.94	
cations/4*O	3.01	3.00	3.00	3.01	3.00	3.00	3.01	3.01	3.01	3.01	3.01	3.01	3.00	3.00	
Mg#	85.16	87.26	90.40	82.55	90.57	71.29	90.17	82.33	86.52	87.49	81.69	90.02	87.26	90.35	
class	crysolite	crysolite	fayalite	crysolite	fayalite	crysolite	fayalite	crysolite	crysolite	crysolite	crysolite	fayalite	crysolite	fayalite	

Table 6.2 Representative (EMPA) major/minor elements composition of Somma-Vesuvius olivine phenocrysts.

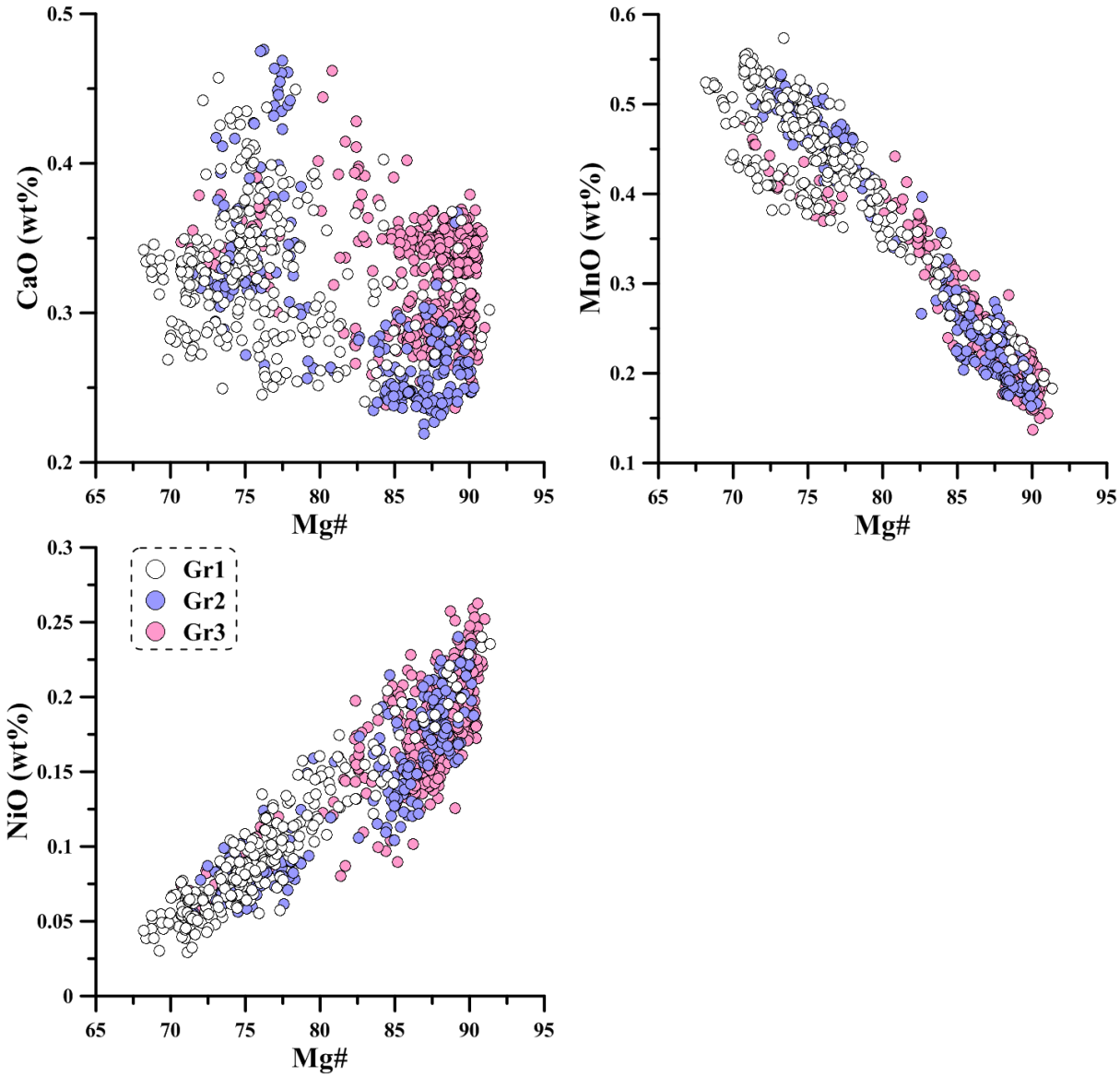

Figure 6.6 Representative plots of minor elements (oxides in weight % versus Mg#) in olivine phenocrysts.

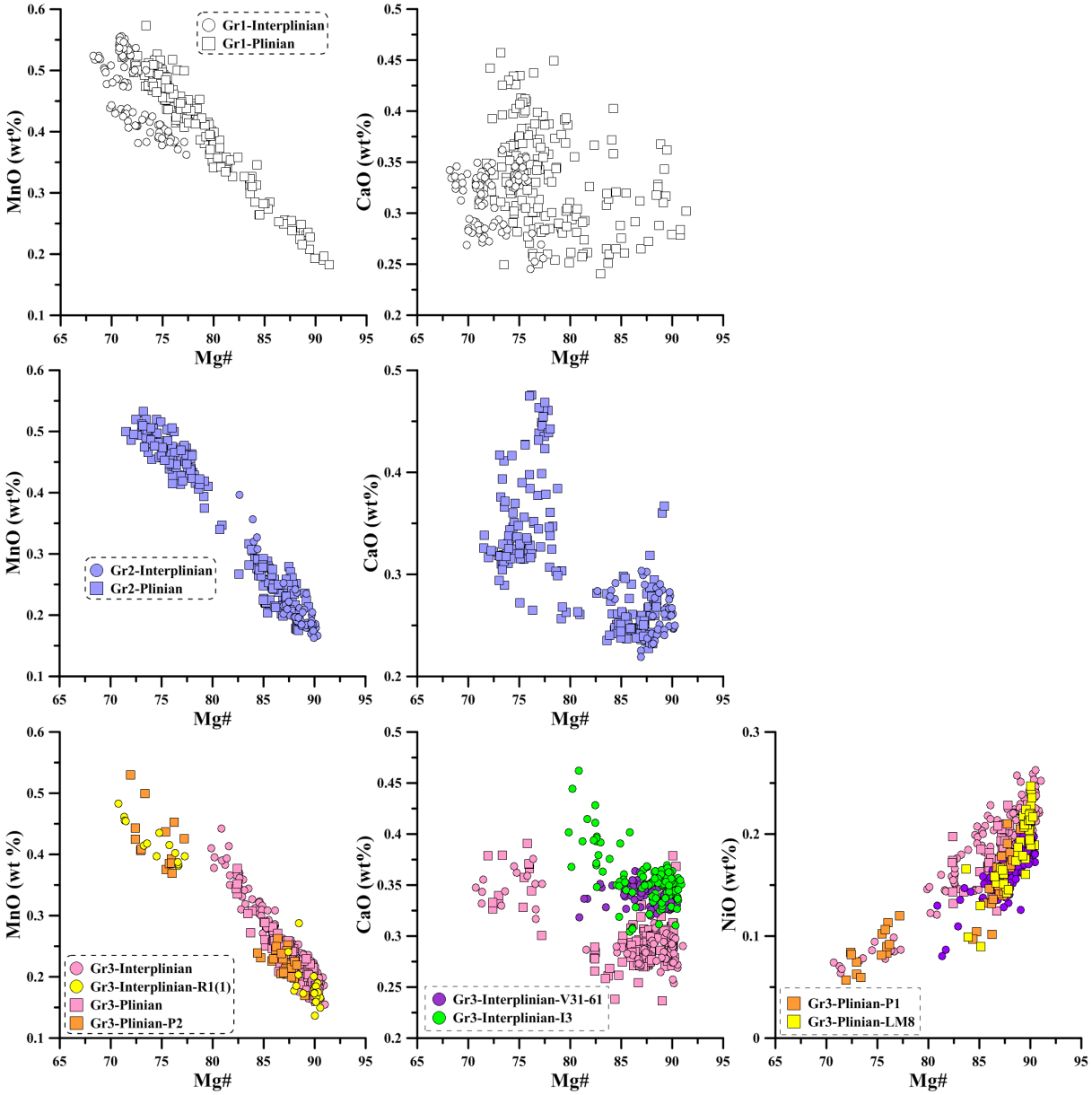

Figure 6.7 Comparative plots of minor elements in Plinian and inter-Plinian olivine phenocrysts.

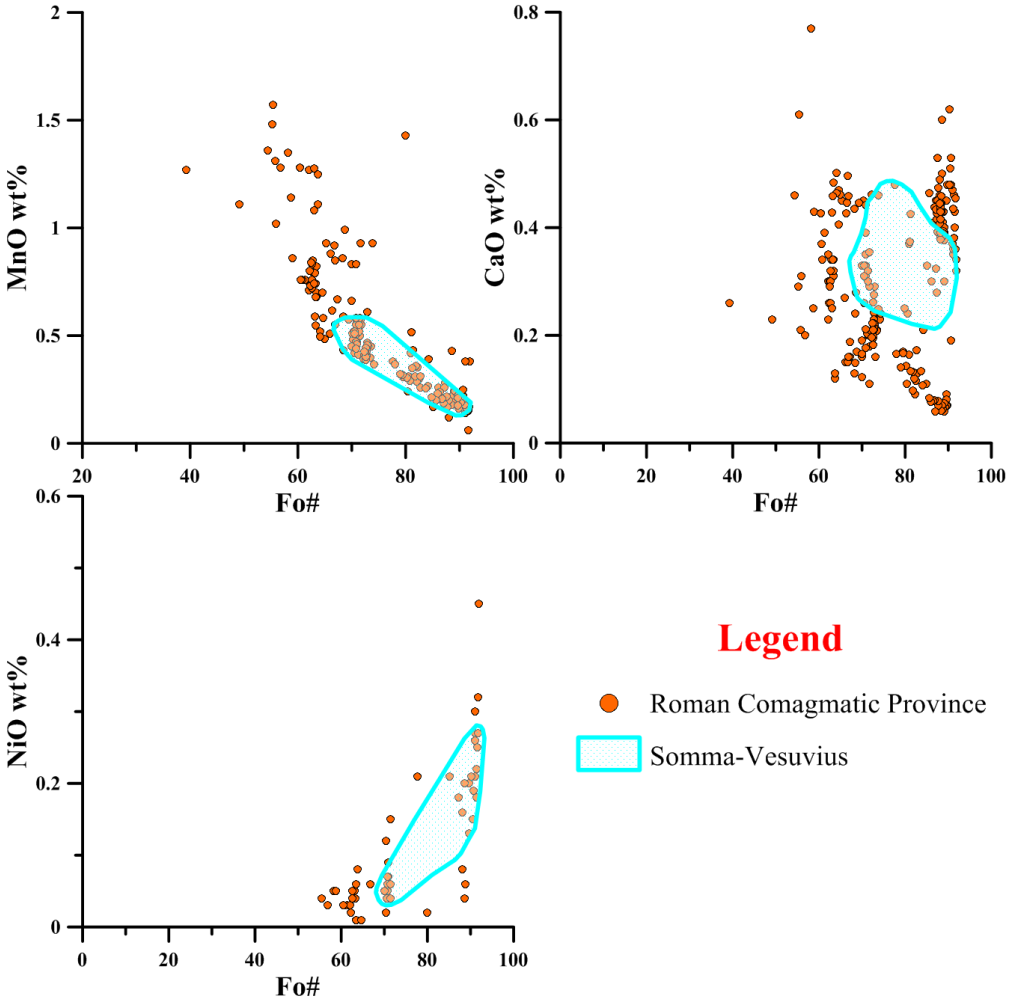

Figure 6.8 Comparative major/minor elements plots (oxide element in wt% versus Fo#) for Somma-Vesuvius olivine phenocrysts (light blue polygons) in comparison to those from other volcanoes of the Roman Comagmatic Province. Data for olivines belonging to the RCP were collected from different authors (Aurisicchio et al., 1988; Barnekow, 2000; Conticelli, 1998; Conticelli et al., 1997; Cortés et al., 2007; De Fino et al., 1986; Di Battistini et al., 1998; Kamenetsky et al., 1995; Melluso et al., 1996; Metrich, 2001; Perini and Conticelli, 2002; Renzulli et al., 2001; Santo, 2000).

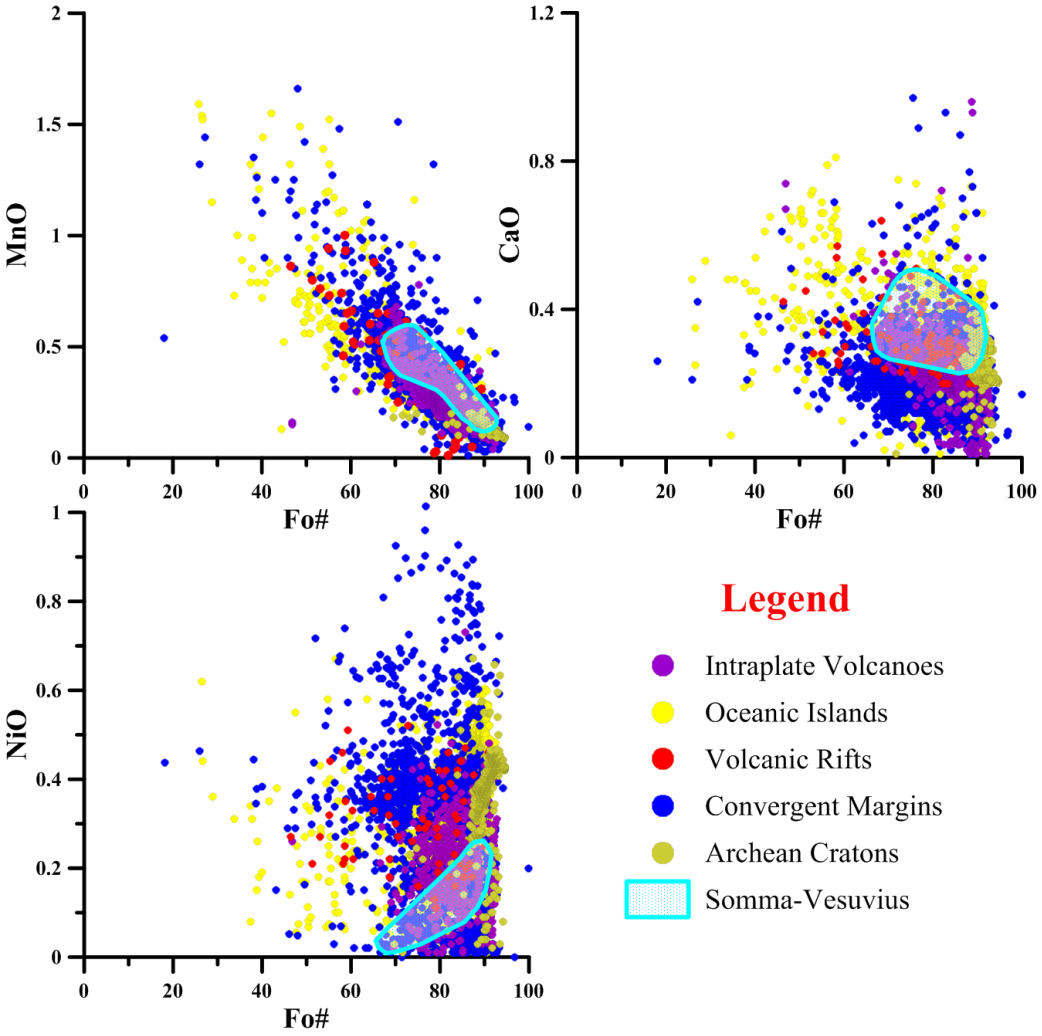

Figure 6.9 Comparative minor elements plots (oxides in weight % versus Fo#) for Somma-Vesuvius olivine phe no crysts (light blue polygons) relative to those from other tectonic settings (symbols differently coloured, see legend). The major/minor elements data for olivines belonging to different tectonic settings are prevalently from database of the Max Planck Institute of Chemistry Mainz (1999) (available online in the mineral section at http://georoc.mpch-mainz.gwdg.de/georoc/ with the name "OLIVINES 1") and from Sobolev et al., 2007.

6.5 Somma-Vesuvius olivines: trace elements

Representative LA-ICPMS trace elements analyses in Somma-Vesuvius olivine phenocrysts together with their corresponding EMPA major/minor elements oxides are listed in tables 6.3 and 6.4. Fo values calculated from both EPMA and LA-ICPMS data are presented to demonstrate that the analyses represent the same areas of zoned phenocrysts, however EPMA data are used to represent phenocrysts compositions as the accuracy of this technique is better for major elements

The data are plotted on Figures 6.10, 6.11, and 6.12. Overall, the majority of trace elements are characterized by clear trends of increasing concentrations with decreasing Fo. The exceptions are Cr (decreasing) and Sc (relatively constant).

Similarly to the observations on the behaviour of minor elements, trace elements in olivnes from Plinian eruptions are similar and display less inter-sample variability than olivines from inter-Plinian eruptions. However intra-sample variability is larger within Plinian eruptions, resulting in inter-Plinian olivines plotting generally inside the field defined by Plinian olivines. The implications of this will be discussed in Chapter 7.

Within Group 1, the inter-Plinian olivines are generally more evolved than the Plinian olivines, resulting in little overlap between their compositions. Overall, the inter-Plinian olivine compositions follow the trend defined by Plinian olivines, however sample I2 is characterised by somewhat lower Cu and Na contents, whereas sample SCL12 olivines have somewhat lower V and Ti contents (Fig. 6.10). Within the Plinian trend, olivines from the Sarno eruption have higher Al values at Fo 91-84, higher Li, Ti, V, Cr and Cu values at Fo 84-72, and lower Na, Sc and Ti values at Fo 88-72 ; The Novelle olivines population has higher Ti, Cr and Cu andlower Al, Sc, Ti, and V values at Fo 88-73.

Within Group 2, the Interplinian olivines are restricted to the more primitive compositions (Fo < 84). There are no obvious offsets between the Plinian and inter-Plinian olivine compositions (Fig. 6.11). The two inter-Plinian samples have somewhat different Li, Sc, V and Zn values. Within Plinian olivines the more primitive Plinian Ottaviano olivines population displays slightly higher Li, Na, Cr, Cu and Zn and lower Sc values at Fo 88-80. The more evolve Ottaviano olivines population shows somewhat higher Al, Sc, Ti, Cr, Co, Cu and Zn and lower Sc, Ti and Co values at Fo 80-72. The more primitive Avellino olivines population displays slightly lower Li, Na and Al and higher Sc and Co values at Fo 88-82, whereas the more evolve population exhibits lower Sc and Ti at Fo 77-74.

Group 3 is characterized by the broadest inter-sample trace elements variability (Fig. 6.12). Among the Plinian olivines, the Pompeii population reveals the widest range of trace element

compositions compared to both the Pollena and the Renaissance (AD 1631) populations. In detail, the Pollena olivine population is characterized by somewhat lower Al, Sc and V values at Fo ~ 90, and by several higher Sc and Cr values at Fo 90-86. The Renaissance eruption is also characterized by slightly higher Li, Na and lower Al, Sc, Ti, V and Cu values at Fo 88-80. The inter-Plinian olivine population is characterised by large inter-sample variations, however all inter-Plinian samples plot within the range of Plinian olivines. The olivine populations from samples S20(1), and I3 display mildly higher Li, Na, Al, and Cr, and lower Sc, Ti, V and Cu values at Fo 90-78. The V31 olivine population contains several phenocrysts with somewhat higher Na, Al, and Ti values, whereas the V61 population is characterised by several lower Sc and higher Ti and Cr values at Fo 90- 83.

6.6 Mineral inclusions

As it was observed in clinopyroxenes, mineral inclusions are also commonly present within the Somma-Vesuvius olivine phenocrysts. Approximately 113 were analysed by the electron microprobe and among the latter, around the 56 % were identified as apatites (10 - 15 μm in size), also present within clinopyroxene phenocrysts, which is a further indication that olivine and clinopyroxene co-crystallised during the evolution of Somma-Vesuvius magmas. The second most abundant phase is chromite-magnesiochromite which occur as micro-crystals ~ 10-15 μm in size.

Rare clinopyroxene and olivine mineral inclusions are also present; both occur as euhedral crystals with similar sizes to apatites. Clinopyroxenes range in composition from Mg# 83 to 79, and their major/minor elements chemistry is similar to the phenocryst populations described in the Chapter 5. Olivine inclusions range in compositions from Fo 81 to 53 and their major/minor elements chemistry matches the composition of the Somma-Vesuvius olivine phenocrysts. Representative inclusion analyses are reported in table 6.5.

age	> 33 Ka		> 33 Ka		22.03-19.3 Ka		~ 22.03 Ka - basal Sarno		~ 22.03 Ka - top Sarno	
sample	SCL12	SCL12	SCL14	SCL14	I2	I2	LM6	LM6	LM5	LM5
mount/grain	D7/74	D7/8	D92/124	D92/137	D89/32	D89/20	D30/102	D30/91	D4/9	D3/7
Instr. Technique	EMPA	EMPA	EMPA	EMPA	EMPA	EMPA	EMPA	EMPA	EMPA	EMPA
SiO_2	37.58	37.65	37.80	38.23	37.66	37.48	38.25	40.37	38.73	41.15
FeO	25.59	24.81	26.15	24.05	25.51	25.97	21.64	11.03	17.90	9.11
MnO	0.53	0.49	0.49	0.43	0.41	0.43	0.44	0.24	0.37	0.19
MgO	35.43	35.88	35.09	36.99	36.15	36.24	39.22	48.06	41.76	50.36
CaO	0.33	0.33	0.29	0.28	0.29	0.31	0.26	0.33	0.28	0.28
NiO	0.06	0.07	0.05	0.08	0.04	0.05	0.12	0.20	0.14	0.24
Total	99.50	99.22	99.85	100.07	100.05	100.46	99.94	100.30	99.20	101.36
cations*4/O	3.00	3.00	3.00	3.00	3.00	3.01	3.01	3.01	3.00	3.01
Fo#	71.17	72.05	70.52	73.27	71.64	71.33	76.36	88.59	80.62	90.79
Class	chrysolite	chrysolite	chrysolite	chrysolite	chrysolite	chrysolite	chrysolite	chrysolite	chrysolite	fayalite
Instr. Technique	LA-ICPMS	LA-ICPMS	LA-ICPMS	LA-ICPMS	LA-ICPMS	LA-ICPMS	LA-ICPMS	LA-ICPMS	LA-ICPMS	LA-ICPMS
Fo#	68.92	71.81	68.83	74.10	70.26	71.61	75.71	87.47	78.62	90.57
Ti^{47}	62	93	94	116	82	112	29	39	71	26
Al^{27}	136	197	149	169	145	183	122	127	180	120
Na^{23}	44	57	42	45	47	36	38	24	59	29
Cr^{53}	8	15	8	9	8	11	51	103	19	
Li^{7}	10.15	11.67	10.86	11.84	11.95	11.73	5.79	2.52	9.16	2.20
Sc^{45}	5.51	6.98	9.02	7.49	6.28	7.35	4.27	6.66	6.16	5.10
V^{51}	8.54	9.77	13.17	13.05	10.62	13.42	5.93	3.34	8.20	3.01
Co^{59}	221.03	204.60	199.66	191.62	209.19	213.52	217.34	169.01	232.12	126.52
Cu^{63}	5.97	6.44	4.15	3.13	3.72	3.59	6.29	2.31	5.50	1.87
Cu^{65}	8.54	8.30	6.53	5.31	5.40	5.14	7.83	3.72	7.75	3.50
Zn^{66}	300.45	285.35	339.63	323.12	292.63	291.84	197.20	84.18	215.79	60.19
Sr^{88}	0.00	0.00	0.00	0.00	0.04	0.00	0.02	0.01	0.02	0.01
Y^{89}	0.44	0.54	0.56	0.48	0.58	0.61	0.24	0.10	0.37	0.07
Zr^{90}	0.09	0.23	0.27	0.20	0.25	0.25	0.09	0.04	0.13	0.03
Dy^{163}	0.06	0.00	0.04	0.05	0.05	0.07	0.02	0.01	0.04	0.01
Er^{166}	0.06	0.09	0.09	0.04	0.08	0.10	0.03	0.01	0.05	0.01
Yb^{172}	0.10	0.12	0.16	0.11	0.18	0.17	0.08	0.03	0.10	0.02
Lu^{175}	0.04	0.04	0.04	0.02	0.03	0.04	0.01	0.01	0.02	0.00
age	~ 19.2 Ka - basal Novelle		~ 19.2 Ka - top Novelle		~ 8.9 Ka - basal Ottaviano		~ 8.9 Ka - top Ottaviano		~ 4.3 Ka - basal Avellino	
sample	LM4	LM4	LM3	LM3	LM1	LM1	LM2	LM2	LFL1	LFL1
mount/grain	D19/31	D19/11	D15/20	D14/7	D21/9	D23/112	D34/156	D35/76	D38/35	D38/44
Instr. Technique	EMPA	EMPA	EMPA	EMPA	EMPA	EMPA	EMPA	EMPA	EMPA	EMPA
SiO_2	37.53	39.10	37.29	40.24	37.66	38.04	36.71	39.72	38.57	40.22
FeO	23.22	17.48	24.00	10.54	24.24	22.65	23.63	13.38	20.62	12.28
MnO	0.50	0.36	0.50	0.23	0.51	0.47	0.49	0.25	0.45	0.22
MgO	37.45	42.42	37.02	48.44	36.83	38.29	37.54	46.11	39.82	47.09
CaO	0.32	0.29	0.42	0.31	0.29	0.32	0.31	0.29	0.42	0.26
NiO	0.10	0.13	0.08	0.21	0.06	0.08	0.09	0.20	0.08	0.16
Total	99.11	99.78	99.30	99.99	99.57	99.84	98.77	99.98	99.95	100.22
cations*4/O	3.01	3.00	3.01	3.01	3.00	3.00	3.02	3.01	3.00	3.00
Fo#	74.20	81.23	73.33	89.12	73.03	75.09	73.91	86.00	77.50	87.24
Class	chrysolite	chrysolite	chrysolite	chrysolite	chrysolite	chrysolite	chrysolite	chrysolite	chrysolite	chrysolite
Instr. Technique	LA-ICPMS	LA-ICPMS	LA-ICPMS	LA-ICPMS	LA-ICPMS	LA-ICPMS	LA-ICPMS	LA-ICPMS	LA-ICPMS	LA-ICPMS
Fo#	72.57	80.76	71.89	88.53	72.20	79.31	72.85	88.63	76.07	86.34
Ti^{47}	32	71	94	21	87	25	92	17	48	22
Al^{27}	102	146	192	97	191	81	206	96	127	63
Na^{23}	47	20	54	29	48	21	56	24	56	17
Cr^{53}	42	13	9	165	12		11	173	11	71
Li^{7}	9.81	3.88	8.81	2.71	9.78	2.11	10.63	4.35	7.43	2.24
Sc^{45}	4.40	6.15	6.58	5.27	6.50	4.04	6.07	5.11	4.55	5.73
V^{51}	6.57	5.37	10.56	2.67	9.57	2.33	9.33	2.27	5.24	3.47
Co^{59}	212.07	199.87	233.02	150.85	209.96	116.15	225.94	150.63	226.72	172.64
Cu^{63}	4.01	2.78	5.41	2.51	6.34	1.83	7.92	2.21	5.07	2.39
Cu^{65}	5.75	4.26	6.74	3.56	8.17	2.68	9.75	3.77	6.33	3.52
Zn^{66}	268.11	155.59	220.63	74.60	261.44	79.93	276.46	90.91	187.24	82.94
Sr^{88}	0.01	0.01	0.03	0.01	0.03	0.00	0.03	0.01	0.03	0.00
Y^{89}	0.37	0.16	0.49	0.08	0.45	0.06	0.49	0.08	0.39	0.07
Zr^{90}	0.08	0.06	0.14	0.02	0.18	0.03	0.19	0.02	0.08	0.02
Dy^{163}	0.04	0.01	0.06	0.01	0.04	0.00	0.04	0.01	0.04	0.01
Er^{166}	0.05	0.03	0.07	0.01	0.06	0.01	0.08	0.01	0.06	0.01
Yb^{172}	0.13	0.04	0.11	0.02	0.15	0.02	0.14	0.02	0.09	0.02
Lu^{175}	0.02	0.01	0.03	0.00	0.03	0.00	0.03	0.01	0.02	0.01

Table 6.3 Representative major/minor elements compositions from EMPA and trace elements compositions from LA- ICPMS of Somma-Vesuvius olivine phenocrysts belonging to the activity period comprised between 33 - 4.3 Ka. Major elements are reported from EMPA and Fo#s from both techniques (EMPA and LA-ICPMS) as basis of comparison; indeed, the EMPA measurements accuracy is typically < 5 % for major elements (Cousens et al., 1997), whereas the LA-ICPMS accuracy reaches values ~ 5 % (Jarvis and Williams, 1993).

age	~ 4.3 Ka - top Avellino		~ 3.5 Ka - Protohistoric		~ 2.8 Ka - Protohistoric		AD 79 - basal Pompeii		AD 79 - top Pompeii		AD 79-472	
sample	LFL2	LFL2	S12(1)b	S12(1)b	S16	S16	P1	P1	P2	P2	S20(1)	S20(1)
mount/grain	D44/60	D44/44	D83/49	D83/43	D77/91	D77/95	D50/85	D49/46	D43/138	D53/82	D73/49	D73/32
Instr. Technique	EMPA	EMPA	EMPA	EMPA	EMPA	EMPA	EMPA	EMPA	EMPA	EMPA	EMPA	EMPA
SiO_2	39.75	40.22	40.15	40.69	39.82	40.90	39.50	40.52	40.02	40.54	40.43	40.74
FeO	13.67	11.19	12.62	9.72	15.01	9.73	13.05	12.11	13.49	9.91	12.36	8.80
MnO	0.22	0.19	0.20	0.17	0.32	0.18	0.24	0.25	0.26	0.20	0.23	0.16
MgO	45.68	47.86	47.16	49.68	44.27	48.32	45.61	46.98	46.25	49.30	47.47	50.09
CaO	0.25	0.27	0.23	0.25	0.28	0.26	0.31	0.30	0.28	0.28	0.29	0.29
NiO	0.14	0.20	0.16	0.21	0.16	0.22	0.13	0.14	0.15	0.20	0.19	0.25
Total	99.70	99.97	100.53	100.75	99.85	99.64	98.84	100.31	100.45	100.47	100.99	100.38
cations*4/O	3.00	3.01	3.01	3.01	3.00	2.99	3.00	3.00	3.01	3.01	3.01	3.01
Fo#	85.62	88.41	86.95	90.11	84.02	89.85	86.17	87.36	85.94	89.87	87.26	91.03
Class	chrysolite	chrysolite	chrysolite	chrysolite	chrysolite	chrysolite	chrysolite	chrysolite	chrysolite	chrysolite	chrysolite	fayalite
Instr. Technique	LA-ICPMS	LA-ICPMS	LA-ICPMS	LA-ICPMS	LA-ICPMS	LA-ICPMS	LA-ICPMS	LA-ICPMS	LA-ICPMS	LA-ICPMS	LA-ICPMS	LA-ICPMS
Fo#	83.90	87.11	86.15	89.48	82.79	89.31	85.68	86.84	85.28	89.25	86.49	90.50
Ti^{47}	32	21	35	27	40	28	34	37	39	27	43	29
Al^{27}	79	85	107	110	92	108	73	73	91	82	88	97
Na^{23}	20	23	22	31	29	31	24	25	23	28	23	29
Cr^{53}	24	150	52	221	15	218	44	49	21	223	52	212
Li^{7}	2.74	2.66	2.90	2.83	8.99	4.49	3.33	3.52	3.44	3.01	4.45	3.94
Sc^{45}	6.21	5.68	6.19	5.09	4.74	4.84	5.45	5.24	6.03	4.68	5.68	4.35
V^{51}	4.19	3.70	3.78	2.64	2.43	2.16	2.44	2.22	2.85	2.06	2.72	1.65
Co^{59}	203.89	168.02	172.58	146.49	201.96	151.26	178.00	169.27	180.82	145.99	170.39	137.52
Cu^{63}	2.32	2.49	2.29	2.43	2.25	1.96	2.30	2.41	2.75	2.50	2.16	1.36
Cu^{65}	3.29	3.51	3.84	4.13	2.91	2.74	2.92	2.98	3.15	3.10	2.85	1.99
Zn^{66}	101.22	86.83	93.40	73.14	193.44	89.59	93.68	82.89	98.48	70.04	97.94	74.40
Sr^{88}	0.00	0.01	0.01	0.01	0.04	0.01	0.01	0.01	0.00	0.01	0.00	0.01
Y^{89}	0.10	0.08	0.10	0.08	0.15	0.07	0.10	0.10	0.11	0.07	0.10	0.07
Zr^{90}	0.03	0.02	0.03	0.03	0.04	0.03	0.04	0.03	0.07	0.02	0.04	0.04
Dy^{163}	0.01	0.01	0.01	0.01	0.02	0.01	0.01	0.01	0.01	0.01	0.01	0.01
Er^{166}	0.01	0.01	0.02	0.01	0.02	0.01	0.01	0.01	0.02	0.02	0.01	0.01
Yb^{172}	0.02	0.03	0.03	0.02	0.06	0.02	0.03	0.03	0.02	0.03	0.03	0.02
Lu^{175}	0.01	0.01	0.01	0.00	0.01	0.01	0.01	0.01	0.01	0.00	0.01	0.00
age	AD 472 - Pollena		AD 472-1139		AD 472-1139		AD 1631-Renaissance Erup.		AD 1760		AD 1834	
sample	LM8	LM8	R1(1)	R1(1)	I3	I3	R6	R6	V31	V31	V61	V61
mount/grain	D90/132	D57/9	D71/25	D71/61	D67/70	D67/83	D54/114	D54/119	D64/106	D63/43	D60/175	D60/152
Instr. Technique	EMPA	EMPA	EMPA	EMPA	EMPA	EMPA	EMPA	EMPA	EMPA	EMPA	EMPA	EMPA
SiO_2	40.45	40.29	38.03	40.89	40.54	40.67	39.02	40.32	39.10	40.44	40.60	40.73
FeO	12.15	12.42	24.15	9.15	10.72	9.18	16.63	10.46	17.56	10.01	9.32	9.29
MnO	0.22	0.21	0.41	0.15	0.24	0.16	0.34	0.23	0.40	0.22	0.20	0.19
MgO	47.15	46.43	37.07	49.12	48.33	49.46	43.46	48.50	42.99	49.23	49.47	49.40
CaO	0.28	0.29	0.33	0.27	0.36	0.35	0.28	0.33	0.34	0.33	0.35	0.34
NiO	0.15	0.16	0.08	0.26	0.20	0.22	0.17	0.18	0.08	0.18	0.18	0.17
Total	100.40	99.82	100.07	99.91	100.41	100.09	99.92	100.02	100.46	100.43	100.16	100.15
cations*4/O	3.00	3.00	3.00	3.00	3.00	3.00	3.01	3.01	3.01	3.01	3.01	3.00
Fo#	87.38	86.95	73.23	90.54	88.93	90.57	82.33	89.21	81.36	89.77	90.44	90.46
Class	chrysolite	chrysolite	chrysolite	fayalite	chrysolite	fayalite	chrysolite	chrysolite	chrysolite	chrysolite	fayalite	fayalite
Instr. Technique	LA-ICPMS	LA-ICPMS	LA-ICPMS	LA-ICPMS	LA-ICPMS	LA-ICPMS	LA-ICPMS	LA-ICPMS	LA-ICPMS	LA-ICPMS	LA-ICPMS	LA-ICPMS
Fo#	86.72	90.19	71.64	90.09	86.10	90.06	80.35	88.03	78.79	89.17	87.82	89.92
Ti^{47}	38	22	84	24	33	32	21	28	52	47	35	24
Al^{27}	69	69	167	92	96	110	65	52	122	120	102	78
Na^{23}	19	27	46	26	21	25	27	36	31	27	30	30
Cr^{53}	52	194	7		148	251	67	27	7	243	125	213
Li^{7}	2.38	3.14	9.59	2.37	3.18	2.85	6.11	9.89	6.32	2.60	3.45	2.91
Sc^{45}	6.15	4.33	5.63	4.71	4.96	5.12	4.01	5.76	4.19	5.85	5.44	4.83
V^{51}	2.89	1.51	9.66	2.82	2.38	2.64	2.64	2.20	4.25	2.99	2.84	1.95
Co^{59}	166.32	130.92	223.84	134.91	152.17	136.40	197.75	161.54	211.09	144.50	172.15	135.35
Cu^{63}	3.02	2.27	5.89	2.96	2.53	2.65	1.22	0.50	2.94	2.71	3.22	2.55
Cu^{65}	3.62	2.80	6.52	3.69	3.24	3.26	2.36	1.56	3.58	3.40	3.82	3.19
Zn^{66}	79.80	61.09	244.93	65.46	78.05	63.10	193.12	103.36	158.65	68.91	84.36	64.09
Sr^{88}	0.01	0.01	0.09	0.01	0.01	0.01	0.00	0.01	0.02	0.01	0.01	0.01
Y^{89}	0.09	0.07	0.46	0.07	0.07	0.07	0.14	0.13	0.20	0.08	0.11	0.06
Zr^{90}	0.03	0.02	0.16	0.03	0.02	0.03	0.03	0.06	0.04	0.03	0.03	0.02
Dy^{163}	0.01	0.01	0.05	0.01	0.01	0.01	0.01	0.02	0.02	0.01	0.01	0.01
Er^{166}	0.01	0.01	0.07	0.01	0.01	0.01	0.01	0.02	0.04	0.01	0.02	0.01
Yb^{172}	0.02	0.02	0.12	0.02	0.02	0.02	0.03	0.04	0.07	0.02	0.04	0.01
Lu^{175}	0.01	0.00	0.03	0.00	0.00	0.00	0.01	0.01	0.01	0.01	0.01	0.00

Table 6.4 Representative major/minor elements compositions from EMPA and trace elements compositions from LA- ICPMS of Somma-Vesuvius olivine phenocrysts belonging to the activity period comprised between 4.3 Ka and modern times. Major elements are reported from EMPA and Fo#s from both techniques (EMPA and LA-ICPMS) as basis of comparison; indeed, the EMPA measurements accuracy is typically < 5 % for major elements (Cousens et al., 1997), whereas the LA-ICPMS accuracy reaches values ~ 5 % (Jarvis and Williams, 1993).

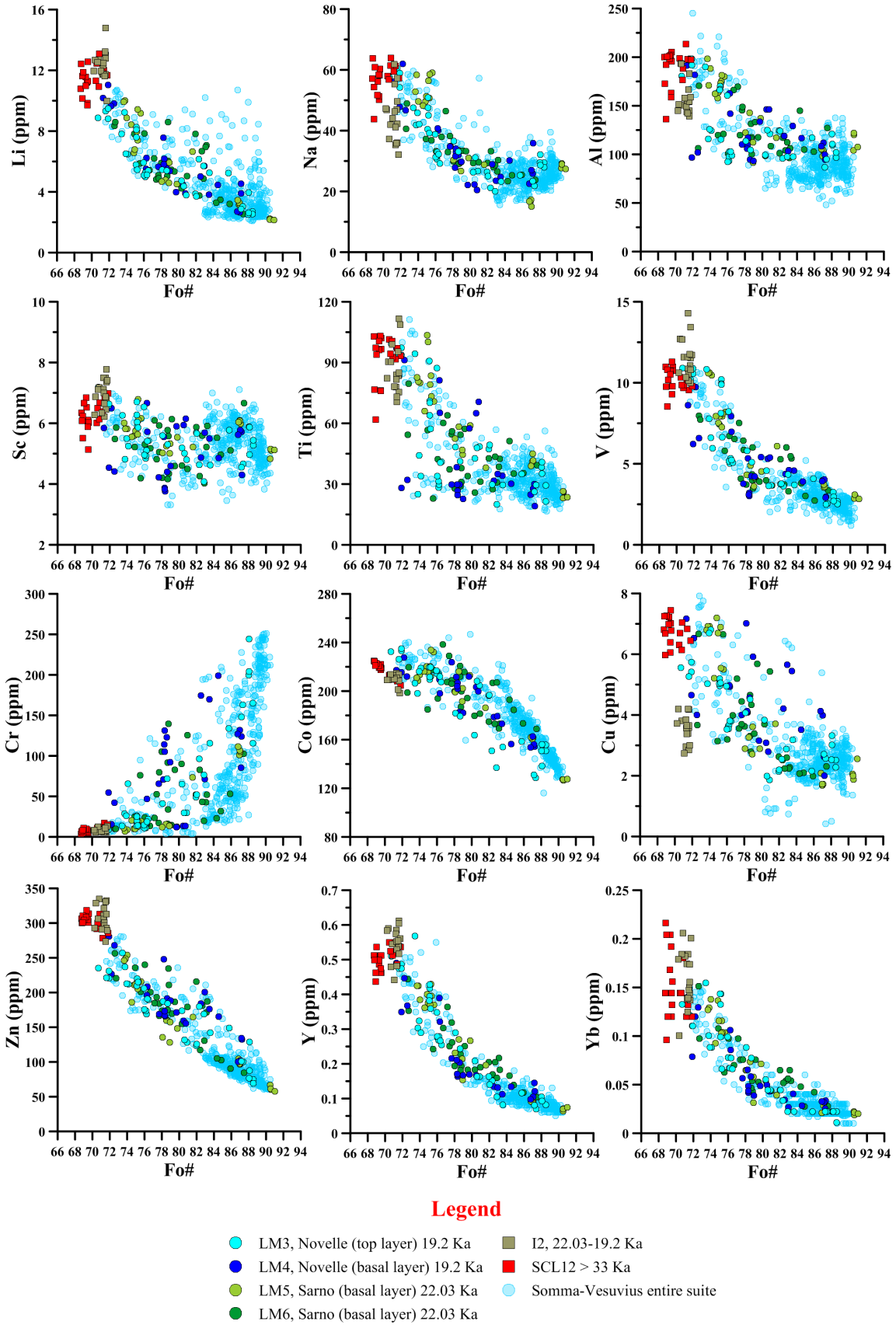

Figure 6.10 Representative plots of trace elements (ppm versus Fo#) in olivine phenocrysts belonging to Group 1 fol lowing Ayuso et al. (1998) geochemical subdivision of Somma-Vesuvius rocks.

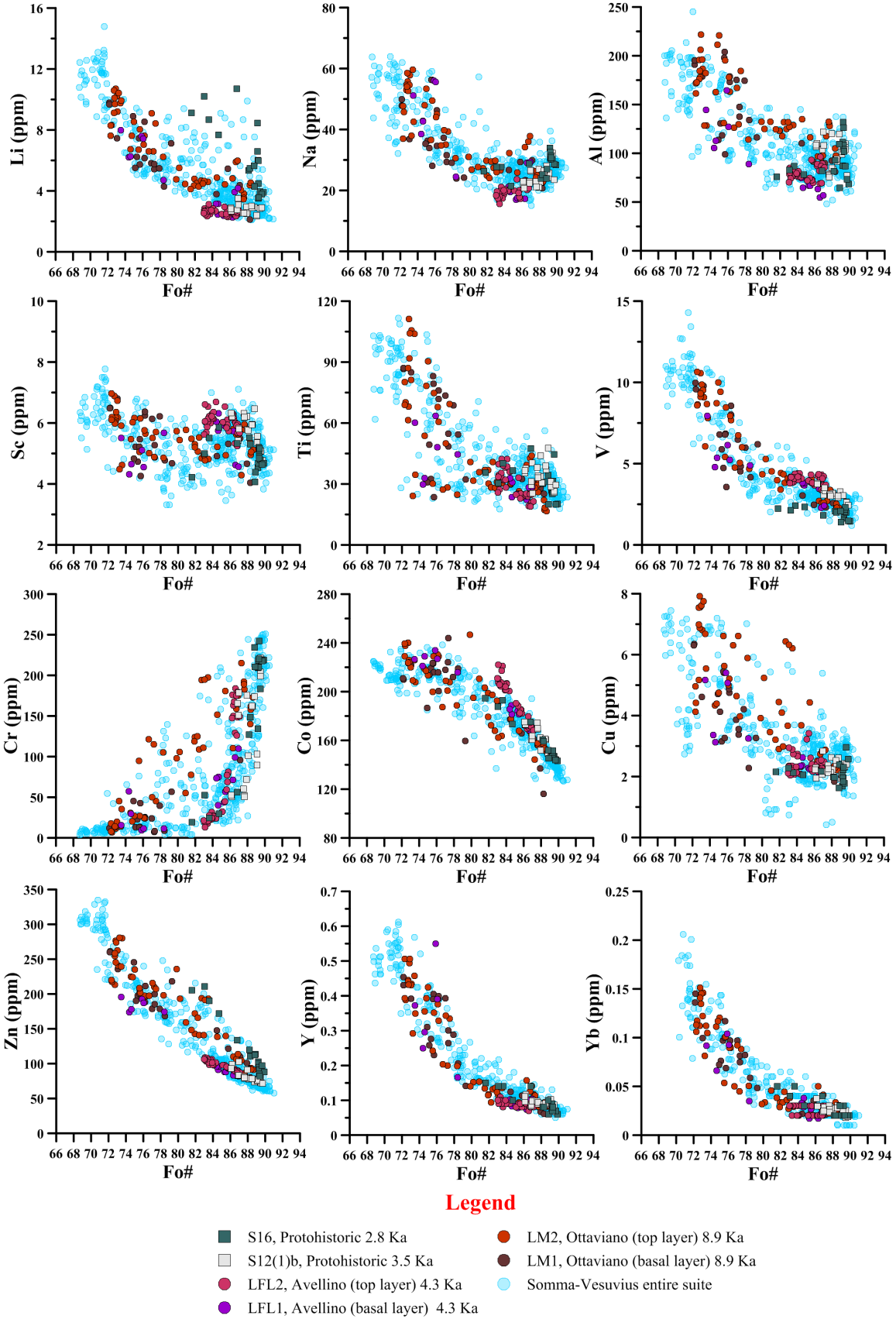

Figure 6.11 Representative plots of trace elements (ppm versus Fo#) in olivine phenocrysts belonging to Group 2 fol lowing Ayuso et al. (1998) geochemical subdivision of Somma-Vesuvius rocks

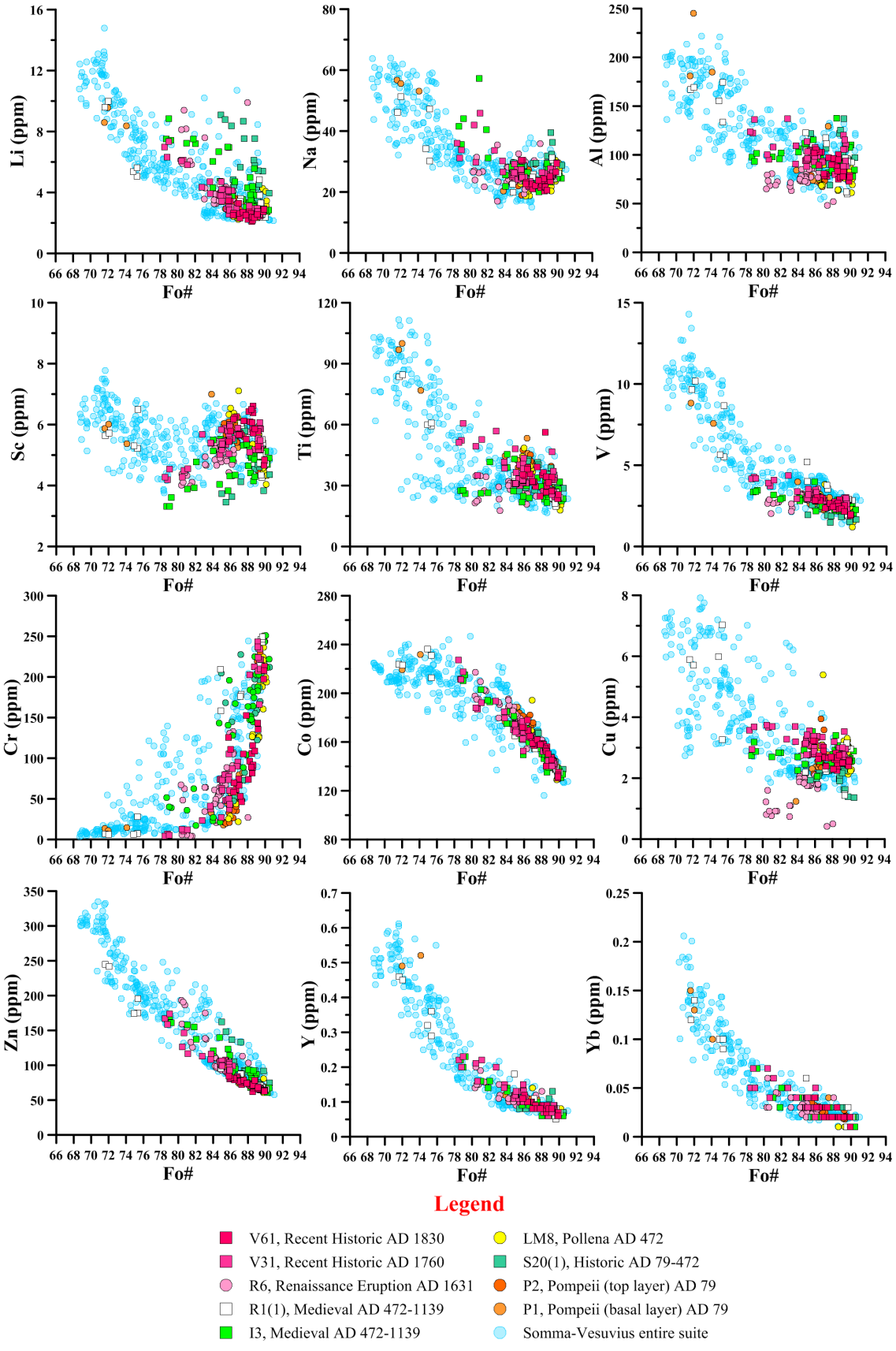

Figure 6.12 Representative plots of trace elements (ppm versus Fo#) in olivine phenocrysts belonging to Group 3 following Ayuso et al. (1998) geochemical subdivision of Somma-Vesuvius rocks.

sample	LM4	LM1	R1(1)	S16	R6	LFL2	SCL14	V31
mount/grain	D20/48	D21014	D71/65	D77/101	D54/96	D44/51	D92/122	D63/78
SiO_2	0.41	0.33	0.11	0.00	50.91	53.18	36.88	39.52
TiO_2	0.01	0.03	0.90	0.74	0.43	0.26	0.01	0.03
Al_2O_3	0.01	0.01	9.18	7.64	2.70	1.69	0.03	0.04
FeO*	0.91	0.61	22.59	24.60	4.03	3.50	29.02	11.07
MnO	0.05	0.06	0.36	0.38	0.07	0.08	0.55	0.22
MgO	0.29	0.35	11.96	10.72	15.86	17.59	33.41	47.66
CaO	54.08	54.39	0.01	0.01	23.88	23.62	0.31	0.33
K_2O	0.01	0.10	0.00	0.00	0.15	0.14	0.04	0.00
Na_2O	0.00	0.00	0.00	0.00	0.01	0.01	0.00	0.00
Cr_2O_3	0.02	0.00	54.91	55.06	0.37	0.22	0.00	0.02
NiO	0.00	0.02	0.12	0.06	0.04	0.04	0.00	0.20
P_2O_5	41.27	41.12	0.00	0.00	0.01	0.05	0.00	0.03
SO_3	0.02	0.01	0.00	0.00	0.00	0.00	0.01	0.00
SrO	0.36	0.51	0.04	0.06	0.00	0.00	0.00	0.07
BaO	0.14	0.15	0.01	0.00	0.00	0.00	0.05	0.00
Cl	0.48	0.77	0.01	0.01	0.02	0.00	0.00	0.00
total	98.07	98.46	100.20	99.27	98.48	100.38	100.30	99.19
class	apatite	apatite	cromite	cromite	diopside	diopside	hyalosiderite	chrysolite
Mg#			34.62	30.36	79.72	83.40	53.52	81.15
Mg# host					86.7	86.9	68.52	88.9
Wo					48.6	46.5		
En					44.9	48.2		
Fs					6.4	5.4		

Table 6.5 Representative (EMPA) major/minor elements compositions of mineral inclusions in olivine phenocrysts.

Chapter 7

Summary and conclusions

Explosive volcanism is commonly related to a process known as fragmentation of magma containing bubbles rich in gas phases. This process is activated by the brittle failure of the melt as its strength is overcame by viscous stresses related to bubble growth and ascending magma flow. Individual volcanoes often produce alternating effusive and explosive eruptions which cyclical dynamics remain unclear and are a subject of ongoing debate.

The Somma-Vesuvius, famous for its A.D. explosive 79 Pompeii eruption, generated a wide variety of eruptive events during the past 33 Ky, ranging from mild effusive (inter-Plinian) eruptions to highly disruptive (Plinian) phenomena. Over the last 3 decades, a large number of samples have been collected from the Somma-Vesuvius volcanic complex. As a result of this research effort, a large database of chemical analyses of various volcanic products from lavas to pumices and tephra is currently available (De Vivo et al., 2003). This allowed for detailed studies of magma compositions aimed at reconstructing magma differentiation processes and identifying parental and primary magma compositions. Currently there is no general consensus on whether the primary magma precursors to both eruptive styles were of a similar composition. At the same time, the compositions of mineral phases in Somma-Vesuvius volcanic products have received significantly less attention. Phenocrysts phases such as olivine and clinopyroxene occur early on the liquid line of descent and dominate fractional crystallization in the primitive Somma-Vesuvius magmas. At the later stages of crystallisation they are joined and/or replaced by feldspars, feldspathoids, biotite, apatite and oxides. This project characterized minor and trace elements in both olivine and clinopyroxene phenocrysts from representative lava, scoriae and pumice samples from the main Plinian eruptions and a range of inter-Plinian events over the last 33 Ky. The main aim of this work was to present new constraints on the factors leading to the different Somma-Vesuvius eruptive styles.

In order to achieve this goal, 14 pumice samples from Plinian pyroclastic deposits as well as 3 scoria and 8 lava samples from effusive flows were collected, and a representative number of olivine and clinopyroxene phenocrysts were selected under an optical microscope from each sample and analysed with an electron microprobe and by a LA-ICP mass-spectrometry, resulting in a large database containing 2127 EMP and 1259 LA-ICP-MS analyses.

The mineral compositions obtained were examined considering the following two factors: 1) eruptive style; and 2) age of the samples. Magmas from Plinian and inter-Plinian eruptions were

compared using the results of this study in conjunction with published data on lava chemistry. Further, the mineral compositions have been compared with those from other volcanoes of the Roman Comagmatic Province (RCP) and also from other tectonic settings such as Oceanic Islands, Volcanic Rifts, Mid-ocean Ridges and Supra-subduction Zones, in order to assess the extent of compositional variation among Somma-Vesuvius olivine and pyroxene phenocrysts. The above approach led to the following main observations:

I) All eruption products of Somma-Vesuvius, from very evolved pumices with MgO < 1 wt% to high-magnesian lavas, contain clinopyroxene and olivine phenocrysts. This observation is made in this study for the first time, and is an important contribution to building a better understanding of the Somma-Vesuvius magmatism.

II) All studied eruptive products contain a wide range of clinopyroxene and olivine compositions, from very magnesian crystals (Mg# > 90) down to significantly evolved compositions (Mg# ~ 70) (Chapters 5 and 6). Importantly, the range of clinopyroxene and olivine phenocrysts compositions in all Somma-Vesuvius eruptive products is effectively the same regardless of the composition of the magma at the moment of the eruption, or eruption style. Most samples display bimodal distributions of phenocrysts composition, having a more evolved and a more primitive groups with a gap at ~ Mg# 80. Several samples are characterised by a narrower, but still a very substantial range of compositions. Based on the data available, we conclude that the observed differences between samples most likely reflect non-representative sampling, rather than differences in the range of phenocryst compositions between eruptions. We thus conclude that our results argue for a similar range of phenocryst compositions in all eruptions.

III) Several observations support co-crystallisation of clinopyroxene and olivine during evolution of Somma-Vesuvius magmas as it has been also suggested by several studies (i.e., Cigolini, 2007; Joron et al., 1987; Lima et al., 2003, Marianelli et al., 1999; Pappalardo et al., 2010; Piochi et al., 2006a). Firstly, both minerals commonly contain mineral inclusions of apatite which is a relatively early crystallising phase at Somma-Vesuvius, based on the P_2O_5 contents of the eruption products (Fig. 5.9, Chapter 5). Secondly, inclusions of olivine in clinopyroxene and vice versa are common (Chapters 5 and 6). Thirdly, the average compositions of olivine and clinopyroxene phenocrysts in the samples correlate, suggesting their common origin. In samples with more magnesian phenocrysts compositions, there is little difference between Mg# of clinopyroxene and olivine. Whereas in samples dominated by more evolved compositions, clinopyroxene is more magnesian than olivine. This is consistent with the data on olivine-clinopyroxene equilibrium (Vrnr-zrur, 1992) at higher temperatures, when more magnesian phenocrysts are formed, both minerals have similar Mg#, whereas at lower temperature, when

more evolved composition crystallise, clinopyroxene is more magnesian than olivine.

IV) The fact that the range of phenocryst compositions is independent of the extent of melt evolution at the moment of eruption, and that olivine and clinopyroxene are found in melt that cannot crystallise these minerals (too low in MgO), suggest that in all Somma-Vesuvius magma these phenocrysts are incorporated from the cumulate piles within the magmatic system during the eruption. This explains the preservation of the phenocrysts in the magma, as fast quenching prevented their dissolution in evolved melts. A similar conclusion has been reached by Danyushevsky and Lima (2001) for the inter-Plinian eruptions within the 3rd cycle. These authors concluded that during the last period of inter-Plinian activity the compositon of erupted melt remained relatively constant, having ~ 3.5 – 4 wt% MgO, and that variations in magma compositions reflected the extent of clinopyroxene and olivine accumulation. The new data obtained in this study demonstrate that the same applies to all eruptions of Somma-Vesuvius within the last 33 Ky. This conclusion can be demonstrated by comparing the compositional trends of Somma-Vesuvius eruption products with the compositons of accumulated phenocrysts (Figs. 7.1, 7.2, 7.3). As can be seen on figure 7.1, some of the Group 3 high-magnesian lavas accumulated, on average, evolved low-MgO clinopyroxene compositions, whereas others,

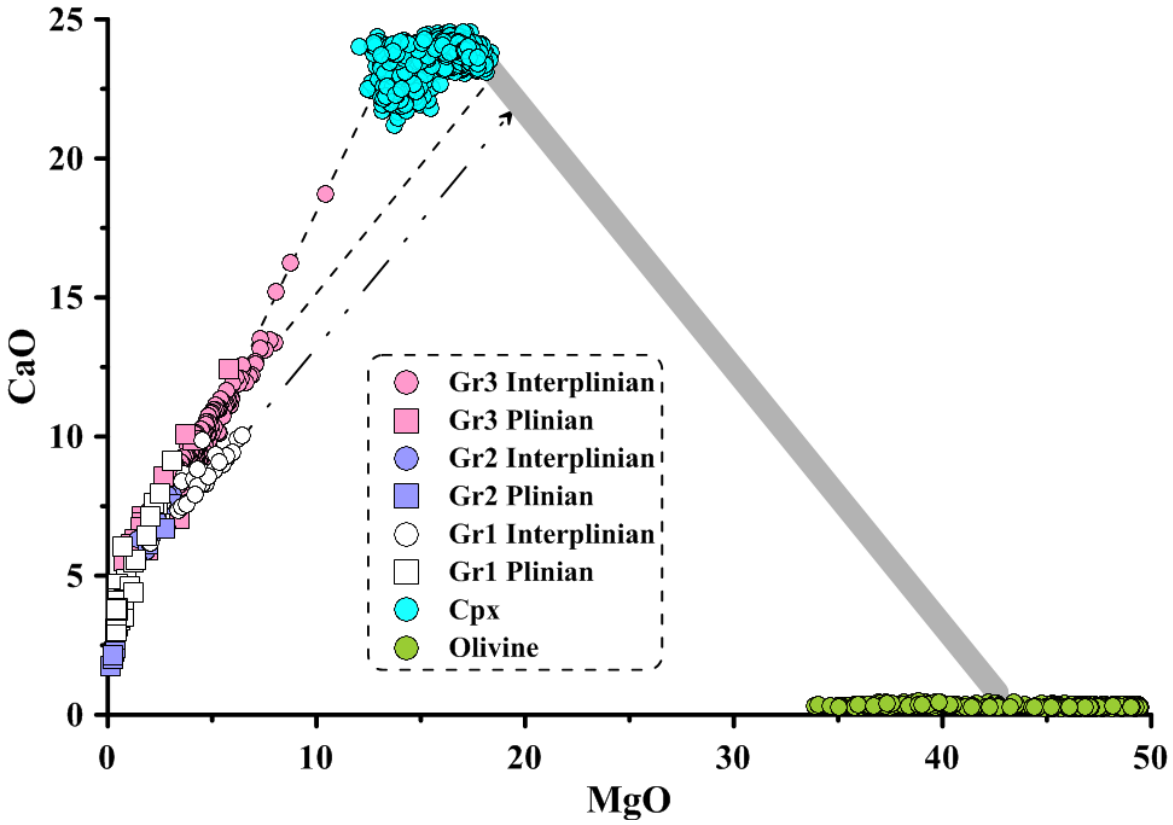

Figure 7.1 Dashed lines indicate the average composition of the accumulated clinopyroxenes in high-magnesian Group 3 lavas. It is clear that different lavas have different average clinopyroxene compositions, from more evolved, low MgO in the 3 samples with the highest MgO and CaO contents, to more primitive high-MgO. Dashed-dotted line shows the extrapolation of the trend of the magnesian Group 1 lavas, which suggests a higher proportion of olivine in the accumulated phenocrysts.

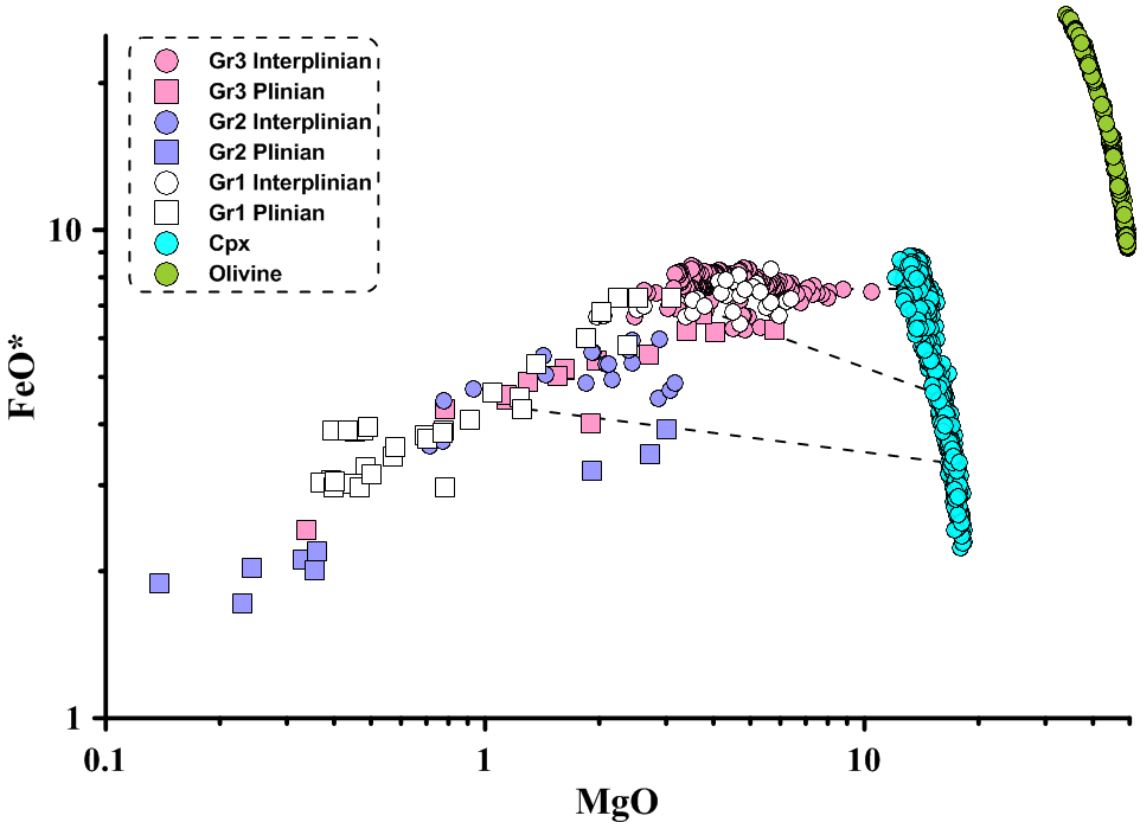

Figure 7.2 Dashed lines are the same as on figure 7.1.

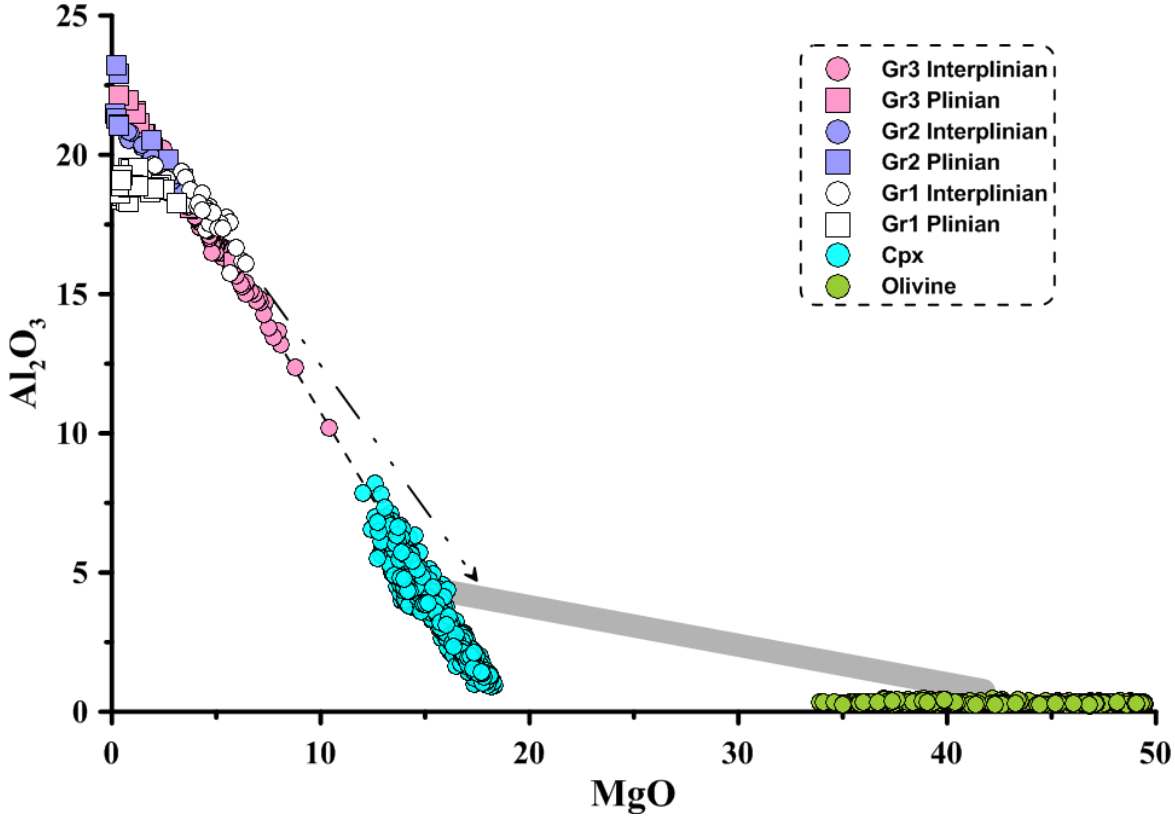

Figure 7.3 The dashed line indicate the average composition of the accumulated clinopyroxene in high-magnesian Group 3 lavas. It is clear that different lavas have different average clinopyroxene compositions. Dashed-dotted line shows the extrapolation of the trend of the magnesian Group 1 lavas, which suggests a higher proportion of olivine in the accumulated phenocrysts.

including the samples studied in this project, accumulated a more magnesian average composition. It is alo clear from Figure 7.1 that the amount of accumulate olivine in Group 3 lavas is very minor (< 1%), compared to clinopyroxene, and the trends of lava compositions point directly to the field of clinopyroxene compositions. This is consistent with our observations and published studies (i.e., Joron et al., 1987; Di Renzo et al., 2007) as clinopyroxene is much more abundant than olivine in Group 3 lavas. The trend of high-magnesian Group 1 lavas is not as steep on the CaO-MgO diagram, suggesting a larger proportion of olivine in those samples (up to 5% of the phenocryst population), which is also consistent with our observations. The fact that Somma-Vesuvius magmas accumulated on average different compositions of olivine and clinopyroxene phenocyrsts is supported by the FeO-MgO relationships (Fig. 7.2). The larger proportion of olivine in high-magnesian Group 2 lavas is also consistent with the Al_2O_3-MgO relationships (Fig. 7.3) and is consistent with other element abundances (not shown).

V) The data obtained suggest that there is no systematic differences between phenocryst compositions between Plinian and inter-Plinian eruptions, suggesting in turn that the magma compositions that fed both eruptive styles were similar.

VI) However, despite the overall similarity between phenocrysts populations in Somma-Vesuvius eruptions, some subtle differences exist:

- Based on the data obtained in this project, overall the average Mg# of accumulated phenocrysts increases with decreasing eruption age (Figs 5.10 and 6.5, Chapters 5 and 6);
- Increasing degree of Silica undersaturation with decreasing age (Ayuso et al., 1998; Fig. 5.9 in Chapter 5) correlated with increasing Sm/Lu values in clinopyroxenes of the same composition (Fig. 5.21 in Chapter 5), suggesting increasing extent of heavy REE fractionation in younger lavas;
- Clinopyroxenes with lower Mg# from the youngest Somma-Vesuvius eruptions have higher CaO contents than clinopyroxene from older eruptions;
- The largest range of variations in REE patterns in clinopyroxenes (differences in La/Sm and Sm/Lu values) is observered in high-Mg phenocrysts from the youngest eruptions (Group 3).

Taken together, these observations suggest the increasing role of assimilation of carbonates by Somma-Vesuvius magmas (Barberi and Leoni, 1980; Belkin et al., 1985; Gilg et al., 2001; Marziano et al., 2009) with decreasing age. As it has been shown by experimental studies (Marziano et al., 2007), carbonate assimilation results in increasing CaO content in

clinopyroxenes. This can also lead to more fractionated REE patterns and the larger localised variations in REE patterns, which are reflected by the compositions of clinopyroxene in younger lavas.

VII) The fact that phenocrysts within Plinian samples always display a somewhat larger range of compositions at a given Mg# compared to the inter-Plinian samples is likely explained by the fact that during more rigorous Plinian eruptions the phenocrysts are gathered from a larger area within the plumbing system.

The above results suggest the following conclusions:

I) a prevalently magmatic origin of olivine phenocrysts whose presence was previously ascribed by some authors (i.e., Barberi et al., 1981; Rosi and Santacroce, 1983) to magma reaction with the carbonate basement of the Campania Plain. The prevalent magmatic origin is also in agreement with the $^{3}He/^{4}He$ isotope ratios (Graham et al., 1993) measured for some olivines from recent historic eruptions (i.e., A.D. 1944) which are not modified considerably by crustal contamination and point a deeper crystallization.

II) Persisting multiple sites of crystallisation where magmas of variable extent of fractionation reside at any given time regardless of the type of eruptive activity. This aspect is in agreement with the presence of well-developed mush zones (Marsh 1995, 1998) located at different depths beneath the Volcano which was assumed by fluid and melt inclusions studies (i.e.; Belkin et al., 1985; Belkin and De Vivo, 1993a; Lima et al., 2003).

III) The increasing role of assimilation with decreasing age most likely reflect continuous propagation of the volcanic plumbing system beneath Somma-Vesuvius towards shallower depths, in response to increasing crustal temperatures under the volcano due to its continuous activity.

III) Chemically similar sources of parental magmas feeding the Somma-Vesuvius system, which does not appear to have changed over the last 33 Ky;

IV) A common composition of parental magmas for the Somma-Vesuvius Plinian and inter-Plinian eruptions.

Therefore, this study suggests that the magma residence times and the magma supply rate are the likely main factors controlling eruption style at Somma-Vesuvius. Further insights into these processes may be derived from the study of melt and fluid inclusions within the Somma-Vesuvius olivine and clinopyroxene phenocrysts, which is envisaged as a continuation to this project.

References

Agostinetti, N., and Amato, A., 2009, Moho depth and Vp/Vs ratio in peninsular Italy from teleseismic receiver functions: Journal of Geophysical Research, v. 114, p. 1-17.

Alvarez, W., 1976, A former continuation of the Alps: Geological Society of America Bulletin, v. 87, no. 6, p. 891-896.

Amato, A., Alessandrini, B., and Cimini, G., 1993, Teleseismic wave tomography of Italy: Seismic Tomography: Theory and Practice, p. 361-396.

Arrighi, S., Principe, C., and Rosi, M., 2001, Violent strombolian and subplinian eruptions at Vesuvius during post-1631 activity: Bulletin of Volcanology, v. 63, p. 126-150.

Auger, E., Gasparini, P., Virieux, J., and Zollo, A., 1999, Seismic evidence of an extended magmatic sill under Mt. Vesuvius: Science, v. 294, p. 1510-1512.

Aurisicchio, C., Gianfangna, A., and Federico, M., 1988, Clinopyroxene chemistry of the high-potassium suite from the Alban Hills, Italy: Mineralogy and Petrology.

Ayuso, R., De Vivo, B., Rolandi, G., Seal II, R., and Paone, A., 1998, Geochemical and isotopic Nd-Pb-Sr-O variations bearing on the genesis of volcanic rocks from Vesuvius, Italy: Journal of Volcanolgicy and Geothermal Research, v. 82, p. 53-78.

Barberi, F., Bizouard, H., Clocchiatti, R., Metrich, N., Santacroce, R., and Sbrana, A., 1981, The Somma-Vesuvius magma chamber; a petrological and volcanological approach: Bulletin Volcanologique, v. 44, no. 3, p. 295-315.

Barberi, F., Bizouard, H., and Varet, J., 1971, Nature of the clinopyroxene and iron enrichment in alkalic and transitional basaltic magmas: Contributions to Mineralogy and Petrology, v. 33, no. 2, p. 93-107.

Barberi, F., Innocenti, F., Lirer, L., Munno, R., Pescatore, T., and Santacroce, R., 1978, The Campanian Ignimbrite: a major prehistoric eruption in the Neapolitan area (Italy): Bulletin of Volcanology, v. 41, no. 1, p. 10-31.

Barberi, F., and Leoni, L., 1980, Methamorphic carbonate ejecta from Vesuvius plinian eruptions: evidence of the occurrence of shallow magma chambers: Bulletin of Volcanology, v. 43, p. 107-120.

Barnekow, P., 2000, Volcanic rocks from central Italy an oxygen isotopic microanalytical and geochemical study.

Barton, M., and Bergen, M., 1981, Green clinopyroxenes and associated phases in a potassium-rich lava from the Leucite Hills, Wyoming: Contributions to Mineralogy and Petrology, v. 77, no. 2, p. 101-114.

Barton, M., Varekamp, J., and Van Bergen, M., 1982, Complex zoning of clinopyroxenes in the lavas of Vulsini, Latium, Italy: evidence for magma mixing: Journal of Volcanology and Geothermal Research, v. 14, no. 3, p. 361-388.

Beccaluva, L., Bonatti, E., Dupuy, C., Ferrara, G., Innocenti, F., Lucchini, F., Macera, P., Petrini, R., Rossi, P. L., Serri, G., Seyler, M., Siena, F., Kastens, K., Mascle, J., Auroux, C., Broglia, C., Channell, J., Curzi, P., Emeis, K., Glacon, G., Hasegawa, S., Hieke, W., McCoy, F., McKenzie, J., Mascle, G., Mendelson, J., Mueller, C., Rehault, J. P., Robertson, A. H., Sartori, R., Sprovieri, R., and Torii, M., 1990, Geochemistry and mineralogy of volcanic rocks from ODP sites 650, 651, 655, and 654 in the Tyrrhenian Sea: Proceedings of the Ocean Drilling Program, Scientific Results, v. 107, p. 49-74.

Beccaluva, L., Di Girolamo, P., and Serri, G., 1991, Petrogenesis and tectonic setting of the Roman Volcanic Province, Italy: Lithos, v. 26, no. 3–4, p. 191-221.

Belkin, H., and De Vivo, B., 1993a, Fluid inclusion studies of ejected nodules fron plinian eruptions of Somma-Vesuvius: Journal of Volcanoly and Geothermal Research, v. 58, p. 89-100.

Belkin, H., De Vivo, B., Roedder, E., and Cortini, M., 1985, Fluid inclusion geobarometry from ejected Vesuvian mafic xenoliths: American Mineralogist, v. 70, p. 288-303.

Belkin, H., De Vivo, B., Török, K., and Webster, J., 1998, Pre-eruptive volatile content, melt-inclusion chemistry, and microthermometry of interplinian Vesuvius lavas (pre-A.D. 1631): Journal of Volcanology and Geothermal Research, v. 82.

Belkin, H., Kilburn, C., and De Vivo, B., 1993b, Sampling and major element chemistry of the Recent (A.D. 1631-1944) Vesuvius activity: Journal of Volcanology and Geothermal Research, v. 58, no. 1-4, p. 273-290.

Berrino, G., Corrado, G., and Riccardi, U., 1998, Sea gravity data in the Gulf of Naples: a contribution to delineating the structural pattern of the Vesuvian area: Journal of Volcanology and Geothermal Research, v. 82, no. 1, p. 139-150.

Bertagnini, A., Rita, D., and Landi, P., 1995, Mafic inclusions in the silica-rich rocks of the Tolfa-Ceriti-Manziana volcanic district (Tuscan Province, Central Italy): Chemistry and mineralogy: Mineralogy and Petrology, v. 54.

Bindi, L., Cellai, D., Melluso, L., Conticelli, S., Morra, V., and Menchetti, S., 1999, Crystal chemistry of clinopyroxene from alkaline undersaturated rocks of the Monte Vulture Volcano, Italy: Lithos.

Birle, J., Gibbs, G., Moore, P., and Smith, J., 1968, Crystal structures of natural olivines: American Mineralogist, v. 53, p. 807-824.

Blundy, J., and Cashman, K., 2008, Petrologic reconstruction of magmatic system variables and processes: Reviews in Mineralogy and Geochemistry, v. 69, no. 1, p. 179-239.

Bosellini, A., 2002, Dinosaurs "re-write" the geodynamics of the eastern Mediterranean and the paleogeography of the Apulia Platform: Earth-Science Reviews, v. 59, no. 1, p. 211-234.

Brocchini, Principe, C., Castradori, D., Laurenzi, M., and Gorla, L., 2001, Quaternary evolution of the southern sector of the Campanian Plain and early Somma-Vesuvius activity: insights from the Trecase 1 well: Mineralogy and Petrology, v. 73, no. 1, p. 67-91.

Brooks, C., and Printzlau, I., 1978, Magma mixing in mafic alkaline volcanic rocks: the evidence from relict phenocryst phases and other inclusions: Journal of Volcanology and Geothermal Research, v. 4, no. 3, p. 315-331.

Calvert, A., Sandvol, E., Seber, D., Barazangi, M., Roecker, S., Mourabit, T., Vidal, F., Alguacil, G., and Jabour, N., 2000, Geodynamic evolution of the lithosphere and upper mantle beneath the Alboran region of the western Mediterranean: Constraints from travel time tomography: Journal of Geophysical Research, v. 105, p. 10871-10898.

Cameron, M., and Papike, J., 1980, Crystal chemistry of silicate pyroxenes: Reviews in Mineralogy and Geochemistry, v. 7, no. 1, p. 5-92.

Capaldi, G., Gillot, P., Munno, R., Orsi, G., and Rolandi, G., 1985, The Sarno formation: the major plinian eruption of the Somma–Vesuvius: IAVCEI Scientific Assembly, Giardini-Naxos.

Caprarelli, G., 1993, Preliminary Sr and Nd isotopic data for recent lavas from Vesuvius volcano: Journal of Volcanology and Geothermal Research, v. 58, p. 377-381.

Carbonin, S., Dal Negro, A., Molin, G., Munno, R., Rossi, G., Lirer, L., and Piccirillo, E., 1984, Crystal chemistry of Ca-rich pyroxenes from undersaturated to oversaturated trachytic rocks, and their relationships with pyroxenes from basalts: Lithos, v. 17, p. 191-202.

Freda C., Gaeta, M., Karner, D.B., Marra, F., Renne, P.R., Taddeucci, J., Scarlato, P., Christensen, J.N., and Dallai, L., 2006, Eruptive history and petrologic evolution of the Albano multiple maar (Alban Hills, Central Italy): Bulletin of Volcanology, v. 68.

Carminati, E., Lustrino, M., and Doglioni, C., 2012, Geodynamic evolution of the central and western Mediterranean: Tectonics vs. igneous petrology constraints: Tectonophysics, v. 579, no. 0, p. 173-192.

Carminati, E., Wortel, M., Meijer, P., and Sabadini, R., 1998a, The two-stage opening of the western–central Mediterranean basins: a forward modeling test to a new evolutionary model: Earth and Planetary Science Letters, v. 160, no. 3, p. 667-679.

Catalano, R., Doglioni, C., and Merlini, S., 2001, On the Mesozoic Ionian Basin: Geophysical Journal International, v. 144, no. 1, p. 49-64.

Cavazza, W., Roure, F., and Ziegler, P., 2004, The Mediterranean area and the surrounding regions: Active processes, remnants of former Tethyan oceans and related thrust belts: The Transmed Atlas, p. 1-29.

Cellai, D., Conticelli, S., and Menchetti, S., 1994, Crystal-chemistry of clinopyroxenes from potassic and ultrapotassic rocks in central Italy: implications on their genesis: Contributions to Mineralogy and Petrology, v. 116.

Channell, J., D'Argenio, B., and Horvath, F., 1979, Adria, the African promontory, in Mesozoic Mediterranean palaeogeography: Earth-Science Reviews, v. 15, no. 3, p. 213-292.

Chester, D., Dibben, C., and Duncan, A., 2002, Volcanic hazard assessment in western Europe: Journal of Volcanology and Geothermal Research, v. 115, no. 3, p. 411-435.

Chiarabba, C., Jovane, L., and Di Stefano, R., 2005, A new view of Italian seismicity using 20 years of instrumental recordings: Tectonophysics, v. 395, no. 3, p. 251-268.

Cigolini, C., 2007, Petrography and termobarometry of high pressure ultramafic ejecta from Mount. Vesuvius, Italy: inferences on the deep feeding system: Periodico di Mineralogia, v. 76, no. 2-3, p. 5-24.

Cioni, R., Bertagnini, A., Santacroce, R., and Andronico, D., 2008, Explosive activity and eruption scenarios at Somma-Vesuvius (Italy): towards a new classification scheme: Journal of Volcanology and Geothermal Research, v. 178, no. 3, p. 331-346.

Cioni, R., Marianelli, P., and Santacroce, R., 1998, Thermal and compositional evolution of the shallow magma chambers of Vesuvius: Evidence from pyroxene phenocrysts and melt inclusions: Journal of Geophysical Research, v. 103, p. 18.

Cioni, R., Sulpizio, R., and Garruccio, N., 2003, Variability of the eruption dynamics during a subplinian event: the Greenish Pumice eruption of Somma–Vesuvius (Italy): Journal of Volcanology and Geothermal Research, v. 124, no. 1, p. 89-114.

Civetta, L., D'Antonio, M., De Lorenzo, S., Di Renzo, V., and Gasparini, P., 2004, Thermal and geochemical constraints on the deep magmatic structure of Mt. Vesuvius: Journal of Volcanology and Geothermal Research, v. 133, no. 1-4, p. 1-12.

Cocchi, L., Caratori Tontini, F., Carmisciano, C., and Marani, M., 2008, Tortonian-Pleistocenic oceanic features in the Southern Tyrrhenian Sea: magnetic inverse model of the Selli-Vavilov region: Marine Geophysical Research, v. 29, no. 4, p. 251-266.

Conticelli, S., 1998, The effect of crustal contamination on ultrapotassic magmas with lamproitic affinity: mineralogical, geochemical and isotope data from the Torre Alfina lavas and xenoliths, Central Italy: Chemical Geology, v. 149.

Conticelli, S., Bortolotti, V., Principi, G., Laurenzi, M. A., D'Antonio, M., and Vaggelli, G., 2007, Petrology, mineralogy and geochemistry of a mafic dike from Monte Castello, Elba Island, Italy: Ofioliti, v. 26, no. 2a, p. 249-262.

Conticelli, S., D'Antonio, M., Pinarelli, L., and Civetta, L., 2002, Source contamination and mantle heterogeneity in the genesis of Italian potassic and ultrapotassic volcanic rocks; Sr-Nd-Pb isotope data from Roman Province and southern Tuscany: Mineralogy and Petrology, v. 74, no. 2-4, p. 189-222.

Conticelli, S., Francalanci, L., Manetti, P., Cioni, R., and Sbrana, A., 1997, Petrology and geochemistry of the ultrapotassic rocks from the Sabatini Volcanic District, central Italy: the role of evolutionary processes in the genesis of variably enriched alkaline magmas: Journal of Volcanology and Geothermal Research, v. 75.

Cortés, J., Palma, J., and Wilson, M., 2007, Deciphering magma mixing: the application of cluster analysis to the mineral chemistry of crystal populations: Journal of Volcanology and Geothermal Research, v. 165, no. 3, p. 163-188.

Costa, F., Dohmen, R., and Chakraborty, S., 2008, Time scales of magmatic processes from modeling the zoning patterns of crystals: Reviews in Mineralogy and Geochemistry, v. 69, no. 1, p. 545-594.

Cousens, D. R., Rasch, R., and Ryan, C. G., 1997, Detection limits and accuracy of the electron and proton microprobe: Micron, v. 28, no. 3, p. 231-239.

Cundari, A., 1975, Mineral chemistry and petrogenetic aspects of the Vico lavas, Roman volcanic region, Italy: Contributions to Mineralogy and Petrology, v. 53.

Cundari, A., 1982, Petrology of Clinopyroxenite Ejecta from Somma Vesuvius and Their Genetic Implications: TMPM Tscherraaks Mineralogische und Petrographische Iitteilungen, v. 30, p. 17-35.

Cundari, A., and Salviulo, G., 1987, Clinopyroxenes from Somma-Vesuvius; implications of crystal chemistry and site configuration parameters for studies of magma genesis: Journal of Petrology, v. 28, no. 4, p. 727-736.

Dal Negro, A., Carbonin, S., Salviulo, G., Piccirillo, E., and Cundari, A., 1985, Crystal Chemistry and Site Configuration of the Clinopyroxene from Leucite–bearing Rocks and Related Genetic Significance: the Sabatini Lavas, Roman Region, Italy: Journal of Petrology, v. 26, no. 4, p. 1027-1040.

Dallai, L., Freda, C., and Gaeta, M., 2004, Oxygen isotope geochemistry of pyroclastic clinopyroxene monitors carbonate contributions to Roman-type ultrapotassic magmas: Contributions to Mineralogy and Petrology, v. 148.

De Astis, G., La Volpe, L., Peccerillo, A., and Civetta, L., 1997, Volcanological and petrological evolution of Vulcano island (Aeolian Arc, southern Tyrrhenian Sea): Journal of Geophysical Research, v. 102, p. 8021-8050.

De Fino, M., La Volpe, J., Peccerillo, A., Piccarreta, G., and Poli, G., 1986, Petrogenesis of Monte Vulture volcano (Italy): inferences from mineral chemistry, major and trace element data: Contributions to Mineralogy and Petrology, v. 92.

De Gori, P., Cimini, G., Chiarabba, C., De Natale, G., Troise, C., and Deschamps, A., 2001, Teleseismic tomography of the Campanian volcanic area and surrounding Apenninic belt: Journal of Volcanology and Geothermal Research, v. 109, no. 1–3, p. 55-75.

De Natale, G., Capuano, P., Troise, C., and Zollo, A., 1998, Seismicity at Somma-Vesuvius and its implications for the 3D tomography of the volcano: Journal of Volcanology and Geothermal Research, v. 82, no. 1, p. 175-197.

De Natale, G., Troise, C., Pingue, F., De Gori, P., and Chiarabba, C., 2001, Structure and dynamics of the Somma-Vesuvius volcanic complex: Mineralogy and Petrology, v. 73, p. 5-22.

De Vivo, B., Ayuso, R., Belkin, H., Fedele, L., Lima, A., Rolandi, G., Somma, R., and Webster, J., 2003, Chemistry, fluid/melt inclusions and isotopic data of lavas, tephra and nodules from> 25 ka to 1944 AD of the Mt: Somma-Vesuvius volcanic activity. Mt. Somma-Vesuvius Geochemical Archive. Dipartimento di Geofisica e Vulcanologia, Università di Napoli Federico II, Open File Report, p. 143.

De Vivo, B., Petrosino, P., Lima, A., Rolandi, G., and Belkin, H., 2010, Research progress in volcanology in the Neapolitan area, southern Italy: a review and some alternative views: Mineral Petrology, v. 99, p. 1-28.

De Vivo, B., and Rolandi, G., 2012, Vesuvius: volcanic hazard and civil defense: Rendiconti Lincei, v. 24.

De Vivo, B., Rolandi, G., Gans, P., Calvert, A., Bohrson, W., Spera, F., and Belkin, H., 2001, New constraints on the pyroclastic eruptive history of the Campanian volcanic Plain (Italy): Mineralogy and Petrology, v. 73, no. 1, p. 47-65.

Deer, W., Howie, R., and Zussman, J., 1966, An introduction to the rock-forming minerals, Longman.

Del Moro, A., Fulignati, P., Marianelli, P., and Sbrana, A., 2001, Magma contamination by direct wall rock interaction: constraints from xenoliths from the walls of a carbonate-hosted magma chamber (Vesuvius 1944 eruption): Journal of Volcanology and Geothermal Research, v. 112, no. 1, p. 15-24.

Delibrias, G., Di Paola, G., Rosi, M., and Santacroce, R., 1979, La storia eruttiva del complesso vulcanico Somma-Vesuvio ricostruita dalle successioni piroclastiche del Monte Somma: Rendiconti Società Italiana Mineralogia Petrologia, v. 35, p. 411-438.

Dewey, J., Helman, M., Turco, E., Hutton, D., and Knot, S., 1989, Kinematics of the western Mediterranean: Geological Society, Special Publications, v. 45, p. 265-283.

Dewey, J., Pitman, W., Ryan, W., and Bonnin, J., 1973, Plate tectonics and the evolution of the Alpine system: Geological Society of America Bulletin, v. 84, no. 10, p. 3137-3180.

Di Battistini, G., Montanini, A., Vernia, L., Bargossi, G., and Castorina, F., 1998, Petrology and geochemistry of ultrapotassic rocks from the Montefiascone Volcanic Complex (Central Italy): magmatic evolution and petrogenesis: Lithos, v. 43, no. 3, p. 169-195.

Di Renzo, V., Di Vito, M. A., Arienzo, I., Carandente, A., Civetta, L., D'Antonio, M., Giordano, F., Orsi, G., and Tonarini, S., 2007, Magmatic History of Somma-Vesuvius on the Basis of New Geochemical and Isotopic Data from a Deep Borehole (Camaldoli della Torre): Journal of Petrology, v. 48, no. 4, p. 753-784.

Di Stefano, R., Bianchi, I., Ciaccio, M., Carrara, G., and Kissling, E., 2011, Three-dimensional Moho topography in Italy: New constraints from receiver functions and controlled source seismology: Geochemistry Geophysics Geosystems, v. 12, no. 9, p. 1-15.

Di Vito, M., Isaia, R., Orsi, G., Southon, J., De Vita, S., D'Antonio, M., Pappalardo, L., and Piochi, M., 1999, Volcanism and deformation since 12,000 years at the Campi Flegrei caldera (Italy): Journal of Volcanology and Geothermal Research, v. 91, no. 2, p. 221-246.

Dilek, Y., 2006, Collision tectonics of Mediterranean region; causes and consequences: Special Paper - Geological Society of America, v. 409, p. 1-13.

Dobosi, G., 1989, Clinopyroxene zoning patterns in the young alkali basalts of Hungary and their petrogenetic significance: Contributions to Mineralogy and Petrology.

Donaldson, C., 1981, Olivine group, Mineralogy, Springer US, p. 325-330.

Donaldson C., 1990, Forsterite dissolution in superheated basaltic, andesitic and rhyolitic melts: Mineral Magazine, v. 54, p. 67-74.

Downes, M., 1974, Sector and oscillatory zoning in calcic augites from M. Etna, Sicily: Contributions to Mineralogy and Petrology, v. 47, p. 187-196.

Duda, A., and Schmincke, H., 1985, Polybaric differentiation of alkali basaltic magmas: evidence from green-core clinopyroxenes (Eifel, FRG): Contributions to Mineralogy and Petrology, v. 91, p. 340-353.

Edel, J., Dubois, D., Marchant, R., Hernandez, J., and Cosca, M., 2001, La rotation Miocene inferieur du bloc corso-sarde; nouvelles contraintes paleomagnetiques sur la fin du mouvement: Bulletin de la Societe Geologique de France, v. 172, no. 3, p. 275-283.

Edel, J., Montigny, R., and Thuizat, R., 1981, Late Paleozoic rotations of Corsica and Sardinia: new evidence from paleomagnetic and K-Ar studies: Tectonophysics, v. 79, no. 3, p. 201-223.

Faraone, D., Molin, G., and Zanazzi, P., 1988, Clinopyroxenes from Vulcano (Aeolian Islands, Italy): crystal chemistry and cooling history: Lithos.

Fedele, L., Zanetti, A., Morra, V., Lustrino, M., Melluso, L., and Vannucci, R., 2009, Clinopyroxene/liquid trace element partitioning in natural trachyte–trachyphonolite systems: insights from Campi Flegrei (southern Italy): Contributions to Mineralogy and Petrology, v. 158, no. 3, p. 337-356.

Ferguson, A., 1973, On hour-glass sector zoning in clinopyroxene: Mineralogical Magazine (London), v. 29, p. 321-325.

Ferrucci, F., Gaudiosi, G., Pino, N., Luongo, G., Hirn, A., and Mirabile, L., 1989, Seismic detection of a major Moho upheaval beneath the Campania volcanic area (Naples, Southern Italy): Geophysical Research Letters, v. 16, no. 11, p. 1317-1320.

Francalanci, L., Avanzinelli, R., Petrone, C., and Santo, A., 2004, Petrochemical and magmatological characteristics of the Aeolian Arc volcanoes, southern Tyrrhenian Sea, Italy: inferences on shallow level processes and magma source variations: Per Mineral, v. 73, p. 75-104.

Francalanci, L., Peccerillo, A., and Poli, G., 1987, Partition coefficients for minerals in potassium-alkaline rocks: data from Roman province (central Italy): Geochemical Journal, v. 21, no. 10.

Freda, C., Gaeta, M., Karner, D., Marra, F., Renne, P. R., Taddeucci, J., Scarlato, P., Christensen, J., and Dallai, L., 2006, Eruptive history and petrologic evolution of the Albano multiple maar (Alban Hills, Central Italy): Bulletin of Volcanology, v. 68.

Gaeta, M., Freda, C., Christensen, J., Dallai, L., Marra, F., Karner, D., and Scarlato, P., 2006, Time-dependent geochemistry of clinopyroxene from the Alban Hills (Central Italy): clues to the source and evolution of ultrapotassic magmas: Lithos, v. 86, no. 3, p. 330-346.

Gasparini, C., Iannaccone, G., Scandone, P., and Scarpa, R., 1982, Seismotectonics of the Calabrian arc: Tectonophysics, v. 84, no. 2–4, p. 267-286.

Giaccio, B., Isaia, R., Fedele, F., Di Canzio, E., Hoffecker, J., Ronchitelli, A., Sinitsyn, A., Anikovich, M., Lisitsyn, S., and Popov, V., 2008, The Campanian Ignimbrite and Codola tephra layers: two temporal/stratigraphic markers for the Early Upper Palaeolithic in southern Italy and eastern Europe: Journal of Volcanology and Geothermal Research, v. 177, no. 1, p. 208-226.

Giacomuzzi, G., Chiarabba, C., and De Gori, P., 2011, Linking the Alps and Apennines subduction systems: New constraints revealed by high-resolution teleseismic tomography: Earth and Planetary Science Letters, v. 301, no. 3, p. 531-543.

Gilg, H., Lima, A., Somma, R., Belkin, H., De Vivo, B., and Ayuso, R., 2001, Isotope geochemistry and fluid inclusion study of skarns from Vesuvius: Mineralogy and Petrology, v. 73, p. 145-176.

Gioncada, A., Mazzuoli, R., and Milton, A., 2005, Magma mixing at Lipari (Aeolian Islands, Italy): Insights from textural and compositional features of phenocrysts: Journal of Volcanology and Geothermal Research, v. 145, p. 97-118.

Grad, M., and Tiira, T., 2009, The Moho depth map of the European Plate: Geophysical Journal International, v. 176, no. 1, p. 279-292.

Graham, D., Allard, P., Kilburn, C., Spera, F., and Lupton, J., 1993, Helium isotopes in some historical lavas from Mount Vesuvius: Journal of Volcanology and Geothermal Research, v. 58, no. 1, p. 359-366.

Handy, M., Schmid, S., Bousquet, R., Kissling, E., and Bernoulli, D., 2010, Reconciling plate-tectonic reconstructions of Alpine Tethys with the geological–geophysical record of spreading and subduction in the Alps: Earth-Science Reviews, v. 102, no. 3, p. 121-158.

Hollister, L., and Gancarz, A., 1971, Compositional sector-zoning in clinopyroxene from the Narce area, Italy: American Mineralogist, v. 56, p. 959-979.

Holm, P., 1982, Mineral chemistry of perpotassic lavas of the Vulsinian district, the Roman Province, Italy: Mineralogical Magazine, v. 46, p. 379-386.

Huebner, J., 1980, Pyroxene phase equilibria at low pressure: Reviews in Mineralogy and Geochemistry, v. 7, no. 1, p. 213-288.

Jackson, S., Longerich, H., Dunning, G., and Freyer, B., 1992, The application of laser-ablation microprobe; inductively coupled plasma-mass spectrometry (LAM-ICP-MS) to in situ trace-element determinations in minerals: Can Mineral, v. 30, no. 4, p. 1049-1064.

Jarosewich, E., Nelen, J., and Norberg, J., 1979, Electron Microprobe Reference Samples for Mineral Analyses: Smithsonian Contributions Earth Science v. 22, p. 68-72.

Jarvis, K., and Williams, J., 1993, Laser ablation inductively coupled plasma mass spectrometry (LA-ICP-MS): a rapid technique for the direct, quantitative determination of major, trace and rare-earth elements in geological samples: Chemical Geology, v. 106, no. 3, p. 251-262.

Jochum, K., Nohl, U., Herwig, K., Lammel, E., Stoll, B., and Hofmann, A., 2005, GeoReM: A New Geochemical Database for Reference Materials and Isotopic Standards: Geostandards and Geoanalytical Research, v. 29, p. 333-338.

Joron, J., Metrich, N., Rosi, M., Santacroce, R., and Sbrana, A., 1987, Chemistry and petrography: Somma Vesuvius. CNR Monograph, p. 105-174.

Kamenetsky, V., Metrich, N., and Cioni, R., 1995, Potassic primary melts of Vulsini (Roman Province): evidence from mineralogy and melt inclusions: Contributions to Mineralogy and Petrology, v. 120.

Krijgsman, W., Hilgen, F., Raffi, I., Sierro, F., and Wilsonk, D., 1999, Chronology, causes and progression of the Messinian salinity crisis: Nature, v. 400, p. 652-655.

Landi, P., Bertagnini, A., and Rosi, M., 1999, Chemical zoning and crystallization mechanisms in the magma chamber of the Pomici di Base plinian eruption of Somma-Vesuvius (Italy): Contributions to Mineralogy and Petrology, v. 135, no. 2-3, p. 179-197.

Lavecchia, G., Creati, N., and Boncio, P., 2002, The Intra-montane Ultra-alkaline Province (IUP) of Italy: a brief review with considerations on the thickness of the underlying lithosphere: Bollettini Società Geologica Italiana, v. 1, p. 87-98.

Lavecchia, G., and Stoppa, F., 1996, The tectonic significance of Italian magmatism: an alternative view to the popular interpretation: Terra Nova, v. 8, p. 435-446.

Le Bas, M., 1962, The role of aluminum in igneous clinopyroxenes with relation to their parentage: American Journal of Science, v. 260, no. 4, p. 267-288.

Leterrier, J., Maury, R., Thonon, P., Girard, D., and Marchal, M., 1982, Clinopyroxene composition as a method of identification of the magmatic affinities of paleo-volcanic series: Earth and Planetary Science Letters, v. 59, no. 1, p. 139-154.

Leung, I., 1974, Sector-zoned titanaugites: morphology, crystal chemistry, and growth: American Mineralogist, v. 59, no. 1/2, p. 128-138.

Lima, A., Danyushevsky, L., De Vivo, B., and Fedele, L., 2003, A model for the evolution of Mt. Somma-Vesuvius magmatic system based on fluid and melt inclusions investigations, Amsterdam, Netherlands (NLD), Elsevier, Amsterdam, Melt inclusions in volcanic systems; methods, applications and problems.

Lima, A., De Vivo, B., Fedele, L., Sintoni, M., and Milia, A., 2007, Geochemical variations between the 79 A.D. and 1944 A. D. Somma- Vesuvius volcanic products: constraints on the evolution of the hydrothermal system based on fluid and melt inclusions: Chemical Geology, v. 237, p. 401-417.

Lindsley, D., 1980, Phase equilibria of pyroxenes at pressures > 1 atmosphere: Reviews in Mineralogy and Geochemistry, v. 7, no. 1, p. 289-307.

Lirer, L., Munno, R., Petrosino, P., and Vinci, A., 1993, Tephrostratigraphy of the AD 79 pyroclastic deposits in perivolcanic areas of Mt. Vesuvio (Italy): Journal of Volcanology and Geothermal Research, v. 58, no. 1, p. 133-149.

Lirer, L., Petrosino, P., Alberico, I., and Postiglione, I., 2001, Long-term volcanic hazard forecasts based on Somma-Vesuvio past eruptive activity: Bulletin of Volcanology, v. 63, no. 1, p. 45-60.

Ludden, J., Rui, F., Gauthier, F., Stix, J., Lang, S., Francis, D., Machado, N., and Wu, G., 1995, Applications of LAM-ICP-MS analysis to minerals: Canadian Mineralogist v. 33, p. 419-434.

Lustrino, M., Duggen, S., and Rosenberg, C., 2011, The Central-Western Mediterranean: Anomalous igneous activity in an anomalous collisional tectonic setting: Earth-Science Reviews, v. 104, no. 1, p. 1-40.

Lustrino, M., Melluso, L., and Morra, V., 2000, The role of lower continental crust and lithospheric mantle in the genesis of Plio–Pleistocene volcanic rocks from Sardinia (Italy): Earth and Planetary Science Letters, v. 180, no. 3, p. 259-270.

Marianelli, P., Metrich, N., Santacroce, R., and Sbrana, A., 1995, Mafic magma batches at Vesuvius: a glass inclusion approach to the modalities of feeding stratovolcanoes: Contributions to Mineralogy and Petrology, v. 120, no. 2, p. 159-169.

Marianelli, P., Métrich, N., and Sbrana, A., 1999, Shallow and deep reservoirs involved in magma supply of the 1944 eruption of Vesuvius: Bulletin of Volcanology, v. 61, no. 1-2, p. 48-63.

Marra, F., Taddeucci, J., Freda, C., Marzocchi, W., and Scarlato, P., 2004, Recurrence of volcanic activity along the Roman Comagmatic Province (Tyrrhenian margin of Italy) and its tectonic significance: Tectonics, v. 23, no. 4, p. 1-15.

Marsh, B., 1996, Solidification fronts and magmatic evolution: Mineralogical Magazine, v. 60, no. 398, p. 5-40.

Marsh, B., 1998, On the interpretation of crystal size distributions in magmatic systems: Journal of Petrology, v. 39, p. 553-599.

Marziano, G., Gaillard, F., and Pichavant, M., 2007, Limestone assimilation by basaltic magmas: an experimental re-assessment and application to Italian volcanoes: Contributions to Mineralogy and Petrology, v. 155, p. 719-738.

Marziano, I., Gaillard, F., Scaillet, B., Pichavant, M., and Chiodini, G., 2009, Role of non-mantle CO (sub 2) in the dynamics of volcano degassing; the Mount Vesuvius example: Geology (Boulder), v. 37, no. 4, p. 319-322.

Marzocchi, W., Sandri, L., Gasparini, P., Newhall, C., and Boschi, E., 2004, Quantifying probabilities of volcanic events: the example of volcanic hazard at Mount Vesuvius: Journal of Geophysical Research: Solid Earth (1978–2012), v. 109, no. B11.

Max-Planck-Institut, 2013, Max Planck Institute database for references materials of geological and environmental interest, Volume 2013.

Max Planck Institute of Chemistry Mainz, 1999, GEOROC "Geochemistry of Rocks of the Oceans and Continents", Volume 2012: Germany.

McDonough, W., and Sun, S., 1995, The composition of the Earth: Chemical Geology, v. 120, no. 3, p. 223-253.

Melluso, L., Morra, V., and Di Girolamo, P., 1996, The Mt. Vulture volcanic complex (Italy): evidence for distinct parental magmas and for residual melts with melilite: Mineralogy and Petrology.

Melson, W., Vallier, T., Wright, T., Byerly, G., and Nelen, J., 1976, Chemical diversity of abyssal volcanic glass erupted along Pacific, Atlantic and Indian Ocean sea-floor spreading center: AGU monograph, v. 19, p. 351-367.

Metrich, N., 2001, Crystallization Driven by Decompression and Water Loss at Stromboli Volcano (Aeolian Islands, Italy): Journal of Petrology, v. 42, p. 1471-1490.

Middlemost, E., 1994, Naming materials in the magma/igneous rock system: Earth-Science Reviews, v. 37, no. 3, p. 215-224.

Milia, A., Torrente, M., Russo, M., and Zuppetta, A., 2003, Tectonics and crustal structure of the Campania continental margin: relationships with volcanism: Mineralogy and Petrology, v. 79, p. 33-47.

Ministero Ambiente, 2013, Geoportale Nazionale.

Mongelli, F., Zito, G., Della Vedova, B., Pellis, G., Squarci, P., and Taffi, L., 1991, Geothermal regime of Italy and surrounding seas: Exploration of the deep continental crust, p. 381-394.

Morimoto, N., 1988, Nomenclature of pyroxenes: Mineralogy and Petrology, v. 39, no. 1, p. 55-76.

Nakamura, Y., 1973, Origin of sector-zoning of igneous clinopyroxenes: American Mineralogist, v. 58, p. 986-990.

Nazzareni, S., Molin, G., Peccerillo, A., and Zanazzi, P., 1998, Structural and chemical variations in clinopyroxenes from the island of Alicudi (Aeolian Arc) and their implications for conditions of crystallization: European Journal of Mineralogy, v. 10, p. 291-300.

Nisbet, E., and Pearce, J., 1977, Clinopyroxene composition in mafic lavas from different tectonic settings: Contributions to Mineralogy and Petrology, v. 63, no. 2, p. 149-160.

Nunziata, C., 2011, Low shear-velocity zone in the Neapolitan-area crust between the Campi Flegrei and Vesuvio volcanic area: Terra Nova, v. 22, no. 3, p. 208-217.

Oldow, J., Ferranti, L., Lewis, D., Campbell, J., D'Argenio, B., Catalano, R., Pappone, G., Carmignani, L., Conti, P., and Aiken, C., 2002, Active fragmentation of Adria, the north African promontory, central Mediterranean orogen: Geology, v. 30, no. 9, p. 779-782.

Paone, A., 1998, Modellizzazione dei processi metallogenetici associati a vulcanismo di tipo alcalino. Potenziale della provincia vulcanica Napoletana: Thesis, Università degli Studi di Napoli “Federico II".

Paone A., 2006, The geochemical evolution of the Mt. Somma-Vesuvius volcano: Mineralogy and Petrology, v. 87, no. 1-2, p. 53-80.

Paone, A., Ayuso, R., and De Vivo, B., 2001, A metallogenic survey of alkalic rocks of Mt. Somma-Vesuvius volcano: Mineralogy and Petrology, v. 73, no. 1-3, p. 201-233.

Pappalardo, L., and Mastrolorenzo, G., 2010, Short residence times for alkaline Vesuvius magmas in a multi-depth supply system; evidence from geochemical and textural studies: Earth and Planetary Science Letters, v. 296, no. 1-2, p. 133-143.

Pappalardo, L., Piochi, M., and Mastrolorenzo, G., 2004, The 3800 yr BP-1944 A.D. magma plumbing system of Somma-Vesuvius: constraints on its behaviour and present state through a review of isotope data: Annales Geophysicae, v. 47, p. 1363-1375.

Pasqual, D., Molin, G., Zanazzi, P., and Crisci, G., 1998, Clinopyroxene from Lipari; comparison with analogues from other Aeolian islands, Italy: The Canadian Mineralogist, v. 36, no. 1, p. 97-105.

Patacca, E., Sartori, R., and Scandone, P., 1990, Tyrrhenian basin and Apenninic arcs: kinematic relations since late Tortonian times: Memorie della Società Geologica Italiana, v. 45, no. 1, p. 425-451.

Pe-Piper, G., 1984, Zoned pyroxenes from shoshonite lavas of Lesbos, Greece: inferences concerning shoshonite petrogenesis: Journal of Petrology, v. 25, p. 453-472.

Peccerillo, A., 1985, Roman comagmatic province (central Italy): Evidence for subduction-related magma genesis: Geology, v. 13, no. 2, p. 103-106.

Peccerrillo A., 1999, Multiple mantle metasomatism in central-southern Italy; geochemical effects, timing and geodynamic implications: Geology (Boulder), v. 27, no. 4, p. 315-318.

Peccerillo A., 2003, Plio-Quaternary magmatism in Italy: Episodes, v. 26, no. 3, p. 222-226.

Peccerillo, A., and Perugini, D., 2003, Introduzione alla petrografia ottica, Morlacchi Editore.

Perini, G., and Conticelli, S., 2002, Crystallization conditions of leucite-bearing magmas and their implications on the magmatological evolution of ultrapotassic magmas: the Vico Volcano, Central Italy: Mineralogy and Petrology, v. 74.

Perini, G., Conticelli, S., Francalanci, L., and Davidson, J., 2000, The relationship between potassic and calc-alkaline post-orogenic magmatism at Vico volcano, central Italy: Journal of Volcanology and Geothermal Research, v. 95, no. 1, p. 247-272.

Piochi, M., Ayuso, R., De Vivo, B., and Somma, R., 2006a, Crustal contamination and crystal entrapment during polybaric magma evolution at Mt Somma Vesuvius volcano, Italy: geochemical and Sr isotope evidence: Lithos, v. 86, p. 303-329.

Piochi, M., De Vivo, B., and Ayuso, R., 2006b, The magma feeding system of Somma-Vesuvius (Italy) strato-volcano: new inferences from a review of geochemical and Sr, Nd, Pb and O isotope data, Volcanism in the Campania Plain, p. 181-202.

Piochi, M., Pappalardo, L., and De Astis, G., 2004, Geochemical and isotopical variations whithin the Campanian Comagmatic Province: implications on magma source composition: Annales Geophysicae, v. 47, p. 1485-1499.

Piromallo, C., and Morelli, A., 2003, P wave tomography of the mantle under the Alpine-Mediterranean area: Journal of Geophysical Research, v. 108, no. 2065, p. 1925-1928.

Poldervaart, A., and Hess, H., 1951, Pyroxenes in the crystallization of basaltic magma: The Journal of Geology, p. 472-489.

Protezione Civile, 2013, Somma-Vesuvius evacuation plan.

Rahman, S., 1975, Some aluminous clinopyroxenes from Vesuvius and Monte Somma, Italy: Mineralogical Magazine, v. 40, p. 43-52.

Rehault, J., Boillot, G., and Mauffret, A., 1984, The Western Mediterranean Basin geological evolution: Marine Geology, v. 55, no. 3–4, p. 447-477.

Rehault, J., Moussat, E., and Fabbri, A., 1987, Structural evolution of the Tyrrhenian back-arc basin: Marine Geology, v. 74, no. 1, p. 123-150.

Reimer, P., Baillie, M., Bard, E., Bayliss, A., Beck, J., Bertrand, C., Blackwell, P., Buck, C., Burr, G., and Cutler, K., 2004, IntCal04 terrestrial radiocarbon age calibration, 0-26 cal kyr BP: Radiocarbon, v. 46, p. 1029-1058.

Renzulli, A., Serri, G., Santi, P., Mattioli, M., and Holm, P., 2001, Origin of high-silica liquids at Stromboli volcano (Aeolian Islands, Italy) inferred from crustal xenoliths: Bulletin of Volcanology, v. 62, p. 400-419.

Rolandi, G., 1997, The eruptive history of Somma-Vesuvius: Cortini M., De Vivo B., Volcanism and Archeology in Mediterranean Area. Reserch Signpost. Trivandrum, p. 77-88.

Rolandi, G., 2010, Volcanic hazard at Vesuvius: An analysis for the revision of the current emergency plan: Journal of Volcanology and Geothermal Research, v. 189, no. 3, p. 347-362.

Rolandi, G., Barrella, A., and Borrelli, A., 1993a, The 1631 eruption of Vesuvius: Journal of Volcanology and Geothermal Research, v. 58, no. 1, p. 183-201.

Rolandi, G., Bellucci, F., Heitzler, M., Belkin, H., and De Vivo, B., 2003a, Tectonic controls on the genesis of the Ignimbrites from the Campanian volcanic Zone, southern Italy, Ignimbrites of the Campanian Plain v. Special Issue.

Rolandi, G., Maraffi, S., Petrosino, P., and Lirer, L., 1993b, The Ottaviano eruption of Somma-Vesuvio (8000 y BP): a magmatic alternating fall and flow-forming eruption: Journal of Volcanology and Geothermal Research, v. 58, no. 1, p. 43-65.

Rolandi, G., Mastrolorenzo, G., Barrella, A., and Borrelli, A., 1993c, The Avellino plinian eruption of Somma-Vesuvius (3760 yBP): the progressive evolution from magmatic to hydromagmatic style: Journal of Volcanology and Geothermal Research, v. 58, no. 1, p. 67-88.

Rolandi, G., Munno, R., and Postiglione, A., 2004, The 472 AD eruption of Somma volcano: Journal of Volcanology and Geothermal Research, v. 129, p. 289-318.

Rolandi, G., Paone, A., Di Lascio, M., and Stefani, G., 2008, The 79 AD eruption of Somma: the relationship between the date of the eruption and the southeast tephra dispersion: Journal of Volcanology and Geothermal Research, v. 169, no. 1, p. 87-98.

Rolandi, G., Petrosino, P., and McGeehin, J., 1998, The interplinian activity at Somma–Vesuvius in the last 3500 years: Journal of Volcanology and Geothermal Research, v. 82, no. 1–4, p. 19-52.

Rosenbaum, G., and Lister, G., 2004, Neogene and Quaternary rollback evolution of the Tyrrhenian Sea, the Apennines, and the Sicilian Maghrebides: Tectonics, v. 23, no. 1, p. TC1013.

Rosenbaum, G., Lister, G., and Duboz, C., 2002, Reconstruction of the tectonic evolution of the western Mediterranean since the Oligocene: Journal of the Virtual Explorer, v. 8, p. 107-130.

Rosi, M., Principe, C., and Vecci, R., 1993, The 1631 Vesuvius eruption. A reconstruction based on historical and stratigraphical data: Journal of Volcanology and Geothermal Research, v. 58, no. 1, p. 151-182.

Rosi, M., and Santacroce, R., 1983, The AD 472 “Pollena” eruption: volcanological and petrological data for this poorly-known, Plinian-type event at Vesuvius: Journal of Volcanology and Geothermal Research, v. 17, no. 1, p. 249-271.

Rosi, M., and Sbrana, A., 1987, Campi Flegrei, CNR Quad: Ric. Sci, v. 114, no. 9, p. 175.

Santacroce, R., 1987, Somma Vesuvius. Quaderni de La Ricerca Scientifica, Consiglio Nazionale delle Ricerche, Rome.

Santacroce, R., Cioni, R., Marianelli, P., and Sbrana, A., 2005, Understanding Vesuvius and preparing for its next eruption: Cultural responses to the volcanic landscape, p. 27-55.

Santacroce, R., Cioni, R., Marianelli, P., Sbrana, A., Sulpizio, R., Zanchetta, G., Donahue, J., and Joron, J., 2008, Age and whole rock-glass compositions of proximal pyroclastics from the major explosive eruptions of Somma-Vesuvius: a review as a tool for distal tephrostratigraphy: Journal of Volcanolgicy and Geothermal Research, v. 177, p. 1-18.

Santacroce, R., Rosi, M., Cristofolini, R., and La Volpe, L., 2003, Italian active volcanoes: Episodes v. 26, p. 227-234.

Santacroce, R., and Sbrana, A., 2003a, Geological map of Vesuvius: SELCA Firenze.

Santacroce, R., 2003b, Geological map of Vesuvius at scale 1: 15,000 SELCA editor, Florence.

Santo, P., 2000, Volcanological and geochemical evolution of Filicudi (Aeolian Islands, south Tyrrhenian Sea, Italy): Journal of Volcanology and Geothermal Research, v. 96, p. 79-101.

Sartori, R., Torelli, L., Zitellini, N., Carrara, G., Magaldi, M., and Mussoni, P., 2004, Crustal features along a W–E Tyrrhenian transect from Sardinia to Campania margins (Central Mediterranean): Tectonophysics, v. 383, no. 3, p. 171-192.

Scaillet, B., Pichavant, M., and Cioni, R., 2008, Upward migration of Vesuvius Magma Chamber over the past 20,000 years: Nature, v. 455, p. 216-220.

Scandone, R., Bellucci, F., Lirer, L., and Rolandi, G., 1991, The structure of the Campanian Plain and the activity of the Neapolitan volcanoes (Italy): Journal of Volcanology and Geothermal Research, v. 48, no. 1, p. 1-31.

Schmid, S., Bernoulli, D., Fügenschuh, B., Matenco, L., Schefer, S., Schuster, R., Tischler, M., and Ustaszewski, K., 2008, The Alpine-Carpathian-Dinaridic orogenic system: correlation and evolution of tectonic units: Swiss Journal of Geosciences, v. 101, no. 1, p. 139-183.

Schmid, S., Fügenschuh, B., Kissling, E., and Schuster, R., 2004, Tectonic map and overall architecture of the Alpine orogen: Eclogae Geologicae Helvetiae, v. 97, no. 1, p. 93-117.

Séranne, M., 1999, The Gulf of Lion continental margin (NW Mediterranean) revisited by IBS: an overview: Geological Society of London, v. 156, p. 15-36.

Serretti, P., and Morelli, A., 2011, Seismic rays and traveltime tomography of strongly heterogeneous mantle structure: application to the Central Mediterranean: Geophysical Journal International, v. 187, p. 1708-1724.

Serri, G., Innocenti, F., and Manetti, P., 1993, Geochemical and petrological evidence of the subduction of delaminated Adriatic continental lithosphere in the genesis of the Neogene-Quaternary magmatism of central Italy: Tectonophysics, v. 223, no. 1, p. 117-147.

Shore, M., and Fowler, A., 1996, Oscillatory zoning in minerals; a common phenomenon: The Canadian Mineralogist, v. 34, no. 6, p. 1111-1126.

Siebert, L., Simkin, T., and Kimberly, P., 2010, Volcanoes of the world, Berkeley, CA, United States (USA), University of California Press, Berkeley, CA, Volcanoes of the world.

Sigurdsson, H., Cashdollar, S., and Sparks, S., 1982, The Eruption of Vesuvius in A.D. 79: Reconstruction from Historical and Volcanological Evidence: American Journal of Archaeology, v. 86, no. 1, p. 39-51.

Simkin, T., and Siebert, L., 1984, Explosive eruptions in space and time; durations, intervals, and a comparison of the world's active volcanic belt, Washington, DC, United States (USA), National Academy Press, Washington, DC, Explosive volcanism; inception, evolution, and hazards.

Simkin, T., and Smith, J. V., 1970, Minor element distribution in olivine: Journal of Geology, v. 78, p. 304-325.

Smith, A. G., 1971, Alpine deformation and the oceanic areas of the Tethys, Mediterranean, and Atlantic: Geological Society of America Bulletin, v. 82, no. 8, p. 2039-2070.

Sobolev, A., Hofmann, A., Kuzmin, D., Yaxley, G., Arndt, N., Chung, S., Danyushevsky, L., Elliott, T., Frey, F., Garcia, M., Gurenko, A., Kamenetsky, V., Kerr, A., Krivolutskaya, N., Matvienkov, V., Nikogosian, I., Rocholl, A., Sigurdsson, I., Sushchevskaya, N., and Teklay, M., 2007, The amount of recycled crust in sources of mantle-derived melts: Science (New York, N.Y.), v. 316, no. 5823, p. 412-417.

Somma, R., Ayuso, R., De Vivo, B., and Rolandi, G., 2001, Major, trace element and isotope geochemistry (Sr-Nd-Pb) of interplinian magmas from Mt. Somma-Vesuvius (southern Italy): Mineralogy and Petrology, v. 73, no. 1-3, p. 121-143.

Spakman, W., and Wortel, R., 2004, A tomographic view on Western Mediterranean geodynamics: The Transmed Atlas: The Mediterranean Region from Crust to Mantle, p. 31-52.

Stampfli, G., and Borel, G., 2002, A plate tectonic model for the Paleozoic and Mesozoic constrained by dynamic plate boundaries and restored synthetic oceanic isochrons: Earth and Planetary Science Letters, v. 196, no. 1, p. 17-33.

Stampfli, G., Mosar, J., Marquer, D., Marchant, R., Baudin, T., and Borel, G., 1998, Subduction and obduction processes in the Swiss Alps: Tectonophysics, v. 296, no. 1, p. 159-204.

Stewart, M., and Pearce, T., 2004, Sieve-textured plagioclase in dacitic magma: Interference imaging results: American Mineralogist, v. 89, no. 2-3, p. 348-351.

Streck, M., 2008, Mineral textures and zoning as evidence for open system processes: Reviews in Mineralogy and Geochemistry, v. 69, no. 1, p. 595-622.

Streck, M., Leeman, W., and Chesley, J., 2007, High-magnesian andesite from Mount Shasta: A product of magma mixing and contamination, not a primitive mantle melt: Geology, v. 35, no. 4, p. 351-354.

Sulpizio, R., Zanchetta, G., Paterne, M., and Siani, G., 2003, A review of tephrostratigraphy in central and southern Italy during the last 65 ka: Il Quaternario, v. 16, no. 1, p. 91-108.

Taylor, S., and McLennan, S., 2005, The evolution of continental crust, Blackwell Scientific Publications, v. 15, p. 44-49.

Thompson, R., 1973, Oscillatory and sector zoning in augite from a Vesuvian lava: Carnegie Institute of Washington v. 71, p. 463-470.

Tiberi, C., Diament, M., Lyon Caen, H., and King, T., 2001, Moho topography beneath the Corinth Rift area (Greece) from inversion of gravity data: Geophysical Journal International, v. 145, no. 3, p. 797-808.

Tomiya, A., and Takahashi, E., 2005, Evolution of the Magma Chamber beneath Usu Volcano since 1663: a Natural Laboratory for Observing Changing Phenocryst Compositions and Textures: Journal of Petrology, v. 46.

Trigila, R., and De Benedetti, A., 1993, Petrogenesis of Vesuvius historical lavas constrained by Pearce element ratios analysis and experimental phase equilibria: Journal of Volcanology and Geothermal Research, v. 58, no. 1–4, p. 315-343.

Trincardi, F., and Zitellini, N., 1987, The rifting of the Tyrrhenian Basin: Geo-marine letters, v. 7, no. 1, p. 1-6.

Turco, E., and Schettino, A., 2011, Tectonic history of the western Tethys since the Late Triassic: Geological Society of America Bulletin, v. 123, no. 1-2, p. 89-105.

Turco, E., Schettino, A., Pierantoni, P., and Santarelli, G., 2006, Chapter 2 The Pleistocene extension of the Campania Plain in the framework of the southern Tyrrhenian tectonic evolution: morphotectonic analysis, kinematic model and implications for volcanism, in Vivo, B. D., ed., Developments in Volcanology, Volume Volume 9, Elsevier, p. 27-51.

Vaggelli, G., Belkin, H., De Vivo, B., and Trigila, R., 1992, Silicate-melt inclusions in recent Vesuvius lavas (AD 1631-1944). I: Petrography and microthermometry: European Journal of Mineralogy, v. 4, no. 5, p. 1113-1124.

Vaggelli, G., De Vivo, B., and Trigila, R., 1993, Silicate-melt inclusions in recent Vesuvius lavas (1631–1944): II. Analytical chemistry: Journal of Volcanology and Geothermal Research, v. 58, no. 1–4, p. 367-376.

Vance, J., 1962, Zoning in igneous plagioclase; normal and oscillatory zoning: American Journal of Science, v. 260, no. 10, p. 746-760.

Vernon, R., 2004, A practical guide to rock microstructure, Cambridge University Press.

Villemant, B., 1988, Trace element evolution in the Phlegrean Fields (Central Italy): fractional crystallization and selective enrichment: Contributions to Mineralogy and Petrology, v. 98.

Villemant, B., Trigila, R., and De Vivo, B., 1993, Geochemistry of Vesuvius volcanics during 1631–1944 period: Journal of Volcanology and Geothermal Research, v. 58, no. 1–4, p. 291-313.

Vitale, S., and Ciarcia, C., 2013, Tectono-stratigraphic and kinematic evolution of the southern Apennines/Calabria–Peloritani Terrane system (Italy): Tectonophysics, v. 583.

Vrnr-zrur, D., 1992, Experimental investigation of Fe-Mg distribution between olivine and clinopyroxene: Implications for mixing properties of Fe-Mg in clinopyroxene and garnet-clinopyroxene thermometry American Mineralogist, v. 77, p. 774-783.

Washington, H., 1906, The Roman comagmatic region, Carnegie institution of Washington, v. 57.

Webster, J., Raia, F., De Vivo, B., and G, R., 2001, The behavior of chlorine and sulfur during differentiation of the Mt. Somma-Vesuvius magmatic system: Mineralogy and Petrology, v. 73, no. 1, p. 177-200.

Wilson, M., and Bianchini, G., 1999a, Tertiary-Quaternary magmatism within the Mediterranean and surrounding regions: Geological Society of London, Special Publications, v. 156, p. 141-168.

Wilson, M., and Bianchini, G., 1999b, Tertiary-Quaternary magmatism within the Mediterranean and surrounding regions: (special publication) Geological Society of London, v. 156, p. 141-168.

Wortel, M., and Spakman, W., 2000, Subduction and slab detachment in the Mediterranean-Carpathian region: Science, v. 290, no. 5498, p. 1910-1917.

Wortmann, U., Weissert, H., Funk, H., and Hauck, J., 2001, Alpine plate kinematics revisited: the Adria problem: Tectonics, v. 20, no. 1, p. 134-147.

Zeck, H., 1999, Alpine plate kinematics in the western Mediterranean: a westward-directed subduction regime followed by slab roll-back and slab detachment: Geological Society, London, Special Publications, v. 156, no. 1, p. 109-120.

Zollo, A., Gasparini, P., Virieux, J., Le Meur, H., De Natale, D., Biella, G., Boschi, E., Capuano, P., De Franco, R., Dell'Aversana, P., De Matteis, R., Guerra, I., Iannaccone, G., Mirabile, L., and Vilardo, G., 1996, Seismic Evidence for a Low-Velocity Zone in the Upper Crust Beneath Mount Vesuvius: Science, v. 274, p. 592-594.

Zuccaro, G., Baratta, A., Petrazzuoli, S., and Iannello, D., 2008, Structural vulnerability to possible pyroclastic flows consequent to the eruption of volcano Vesuvius: Journal of Volcanology and Geothermal Research, v. 178, p. 416-453.